RATE-DEPENDENT DEFORMATION BEHAVIOR OF POSS-FILLED AND PLASTICIZED POLY(VINYL CHLORIDE)

by

Sharon Yu-Wen Soong

Master of Science in Chemical Engineering Practice
Department of Chemical Engineering
Massachusetts Institute of Technology, Cambridge, MA, 2005
Bachelor of Science in Chemical Engineering
Department of Chemical Engineering
National Taiwan University, Taipei, Taiwan, 2002

Submitted to the Department of Chemical Engineering
in partial fulfillment of the requirement for the degree of

DOCTOR OF PHILOSOPHY IN CHEMICAL ENGINEERING

at the

MASSACHUSETTS INSTITUTE OF TECHNOLOGY

JUNE 2007

Signature of Author: _____
Department of Chemical Engineering
May 17, 2007

Certified by: _____
Robert E. Cohen
St. Laurent Professor of Chemical Engineering
Thesis Supervisor

Certified by: _____
Mary C. Boyce
Gail E. Kendall Professor of Mechanical Engineering
Thesis Supervisor

Accepted by: _____
William M. Deen
Carbon P. Dubbs Professor of Chemical Engineering
Chairman, Committee for Graduate Students

Rate-Dependent Deformation Behavior of POSS-Filled and Plasticized Poly(vinyl chloride)

by

Sharon Yu-Wen Soong

Submitted to the Department of Chemical Engineering on May 17, 2007
in partial fulfillment of the requirements for the degree of
Doctor of Philosophy in Chemical Engineering

Abstract

Polymers are known to exhibit strong time-dependent mechanical behavior. In different temperatures or frequency regimes, the rate sensitivities of polymers change as various primary and secondary molecular mobility mechanisms are accessed. The incorporation of nanoparticles can potentially alter the molecular level structure of polymer, offering the opportunity to tailor the rate-dependent mechanical deformation and failure behavior of the polymer.

This study focuses on polyhedral oligomeric silsesquioxanes (POSS) enhanced polymeric systems. POSS are hybrid organic-inorganic nano-scale molecules which consist of a silica cage with functional groups attached to the cage corners. Various binary and ternary polymer blends were produced by incorporating methacryl-POSS ($C_{56}H_{88}O_{28}Si_8$) (mPOSS) and dioctyl phthalate (DOP) into poly(vinyl chloride) (PVC) through melt blending. mPOSS was found to be miscible with PVC up to 15 wt% added. Both mPOSS and DOP plasticize PVC and reduce the α-transition temperature. While mPOSS also reduces the secondary (β) transition temperatures in PVC, DOP was found to restrict the β-relaxation motions. The rate-dependent yield and postyield behavior was characterized in compression testing over a wide range of strain rate (10^{-4}/s to ~4000/s). Due to the geometric and size distinctions between the two molecules, mPOSS and DOP have different influences on PVC local molecular motions, resulting in dissimilar mechanical behavior. A clear rate-dependent sensitivity transition in yield was observed in the pure PVC and PVC/mPOSS blends in the intermediate strain rate regime, which is attributed to the need for stress-assisted activation of β-motions at high strain rates. A transition in rate sensitivity was also identified in high DOP content compounds; this transition is due to the α-transition.

The potential of using POSS as a plasticizer for PVC was evaluated. Through the use of ternary compositions, the proportion of mPOSS in PVC was increased substantially. The T_g of appropriately formulated ternary PVC/mPOSS/DOP compounds can be reduced to near room temperature, and these materials exhibit desirable ductile behavior.

A constitutive model was used to predict the large deformation behavior of the PVC compounds. The two-process model is shown to capture the rate-sensitivity transitions in yield and the large deformation stress-strain behavior at low and high strain rates.

Thesis Supervisors: Robert E. Cohen, St. Laurent Professor of Chemical Engineering
Mary C. Boyce, Gail E. Kendall Professor of Mechanical Engineering

Acknowledgement

Many people deserve credits for the accomplishment of this dissertation. First and foremost, I would like to acknowledge my two wonderful thesis advisors, Prof. Cohen and Prof. Boyce. They not only provided me valuable guidance and advices for my research at MIT, but also taught me a lot in life. They are always positive, knowledgeable, enthusiastic, and encouraging, even when the experimental results were confusing or when the funding was gone. I appreciate them letting me complete the Master degree through Chemical Engineering Practice School. I gained tremendous amount of experience in many ways because of the program. I am also thankful for the opportunities they gave me in participating in the DYFP conference in Holland and the DYMAT conference in France, given I only had posters to present in both cases. MIT is a great environment for Ph.D. research, and having them both as advisors definitely has made my graduate studying more educational and enjoyable. I also want to acknowledge my thesis committee members, Prof. McKinley and Prof. Hammond, for giving me their time and many helpful feedbacks throughout my doctorate study. This research is funded by various organizations and sources, including DURINT Polymer Nanocomposite, Du Pont-MIT Alliance, Gilliland Fellowship, Chyn Duog Shiah Memorial Fellowship, and Institute for Soldier Nanotechnologies at MIT, and I am appreciative for all the financial supports.

I would like to thank many talented graduate students, postdocs, and scientists from the Cohen Research Group, the Boyce Research Group, and ISN whom I worked with and learned from. I thank Dr. Yonathan T., Dr. Roger A., Dr. Ed K., Dr. LaShaunda J., Dr. Greg P., and Prof. Russell G. for bringing me up to speed in lab when I first started at MIT as a youngling; Dr. Adam M. and Dr. Sai S. for bridging me to the mechanical engineering world and helping me with the high rate testing and constitutive modeling regarding the rate-dependent study; Ben W. and Dr. Rajdeep S. for working on the multilayer project together during the first year, even though it didn't work out at the end; Ben W., Ryan B., Kirill T., Shawna L., Eric V., Erik A., Joe L., Dr. Katia B., Dr. Daeyeon L., Dr. Chungxia H., Dr. Prem P., and Dr. Alex H. for the helpful discussions about research; Dr. Sai for being not only a good company but also a good photographer in the two European conferences and the Purdue combat-testing trip we went together. I also want to acknowledge Prof. Wayne Cheng and his postdoc, Dr. Bow S., at Purdue University for the collaboration in moderate strain rate compression testing; Peter M. from MIT Central Machine Shop for granting me some urgent specimen orders; lab manager Dr. Steve K. at ISN for helping me with equipment setup and maintenance.

Without the supports from my beloved family and friends, I would not have the courage to move half an earth away from home, not to mention being able to complete my doctorate degree at MIT. My parents, my brother, my little aunt, and my cousins, have always been there for me. I am extremely thankful for the freedom and trust my awesome parents have given me, as much as the faith they have in me. They are always supportive of my decisions, and encouraging me to live up my life. I am thankful for having my little aunt in Florida, who is very kind and very much like a second mom to me. My brother is always there for me when I want to be silly and childish. For that, I am extremely grateful.

My friends in Boston have made my life both enjoyable and content for the past five years.

Todd, Cindy, Gregg, Wilson, Jake, Theis, Kris, Jane, Erik, Kirill, Marco, Sinead, Bridget, Guille, and Leggy are the people who lent me thermo homework when I was desperate, coded with me when I sucked at Matlab, visited me when Boston was buried in blizzard, brought me soup when I was sick, took a walk with me when I was aggravated by everything, showed up with chocolate when I was low, and opened his or her arms when I needed a good cry. Some we came to Boston together, some we studied quals and celebrated passing together, some we spent every important occasion together, some we worked in Switzerland together, and some we simply go through life and laugh at the ups and downs together. I am extremely grateful for having my two best friends back home, Jenny and Helen, in my life. They pulled me up many times when life was difficult; they traveled far distances to visit me when I needed a friend and a hug the most; they shared my laughs and tears on the phone; and most importantly, they made me feel that I never left home. The five weeks of having Jenny here in Boston and the 1860 miles Helen and I drove will forever in my memory. My friends who are still in Florida, Chris and John, you guys are just joy.

My grandpa Wen-Hu was the person who told me that girls are no different than boys when I was only 7. My aunt Teresa was the person who taught me Sesame Street and gave me a head start in English when I was 10. My mom was the person who stopped me from giving up high school for culinary school when I was 15. My friend Alex was the person who inspired me to pursue education in the United States when I was 17. Prof. L. J. Chen in ChemE at NTU was the person who encouraged and convinced me to go to MIT when I was 22. My dad was the person who called me everyday and kept me going during my first semester at MIT. Without them, I would not be writing this acknowledgement.

At the end, I would like to thank my grandma Pei-Mei and my mom's cookbooks, my precious Trek, Lindt, L.A. Burdick, that 1500 pieces Mona Lisa puzzle at the warehouse, Ben & Jerry's, Red Sox, Pats, Charles river, J. K. Rowling, and Jack Bauer. In one way or another, I was given a lift of spirit, a moment of peace, a smile, a relief, or faith.

TABLE OF CONTENTS

LIST OF FIGURES

LIST OF TABLES

Chapter 1: Introduction

1.1. Fillers Enhanced Polymeric Materials

Polymer systems have extremely wide and diverse applications due to their unique attributes: low density, low cost, ease of processing and production, and often ductile and transparent nature. Polymeric materials have been filled with a variety of compounds in order to improve the properties of interest, such as heat resistance, mechanical strength, impact resistance, gas permeability, and electrical conductivity. Additives for polymers may be organic or inorganic, synthetic or natural, and in forms of fibers, particles, platelets, or whiskers. The size of additives also ranges from micron-scale to nano-scale.

To enhance the mechanical properties of polymer, two types of additives are commonly considered: fillers or plasticizers. Fillers are generally rigid and much larger in size than the polymer chain. Reinforcement by the conventional fillers like glass fibers and calcium carbonate is in the length scale of micron. Incorporating rigid fillers in a polymer matrix generally increases the mechanical modulus and strengthens the polymer structure; however the toughness of polymer may be jeopardized as a trade-off. Rubber particles are also important fillers for polymer toughening. However, the discussion here primarily concerns filler particles that are significantly stiffer than the polymer matrix. Plasticizers are molecular in nature, with length scale less than 1 nm. Commonly used plasticizers such as phthalate esters are added to neat polymers in order to increase the toughness, soften the material, and reduce the glass transition temperature. As a result, the modulus and mechanical strength are lowered as a compromise.

Interesting material behavior has been observed when the filler size is decreased from the micron-scale to the nano-scale. Figure 1-1 [1] shows the interparticle spacing (d_{space}) as a function of particle volume fraction (φ) in a composite system where the spherical particle size ranges from 1 μm to 1 nm. The highlighted gray area denoted R_g indicates the normal range for the radius of gyration of polymer chains, where 5 nm<R_g<20 nm. When particle size is at 1 μm (1000 nm), the interparticle spacing is maintained at more than an order of magnitude higher than R_g until the volume fraction φ exceeds 0.4. With the particle size reduced to 100 nm, the interparticle spacing still remains reasonably larger than R_g with φ less than 0.2. However,

further reducing the particle size to 10 nm causes a significant change. At φ=0.02, the interparticle spacing is only 20 nm, which is in close approximation to R_g. Thus, a substantial portion of the material volume will be in the 'interphase' region with only a very low loading of nanofiller. Depending on the interaction between the filler and the matrix, tremendous differences in properties may be observed with a very small amount of additives. Furthermore, composites with nano-sized fillers are also likely to have dissimilar properties than composites with micron-scale fillers.

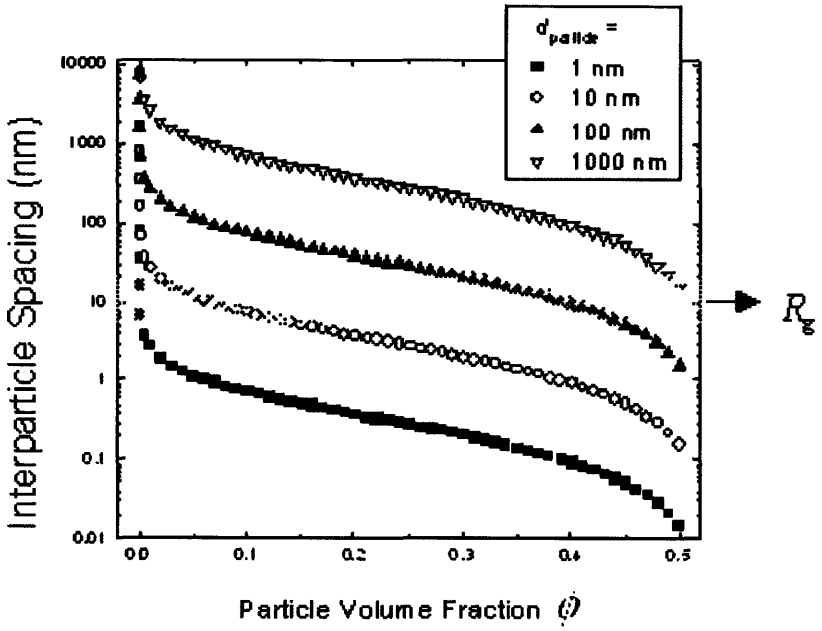

Figure 1-1. Interparticle spacing as a function of particle volume fraction for spherical particles on a simple cubic lattice. Data are platted for four different particle sizes. [1]

In recent years significant progress has been made in the syntheses and characterizations of various polymer-nanocomposite systems based on the understanding of basic principles that determine their properties. Nano-scale fillers have been studied extensively [2,3] with processing techniques continuously improving each year. In general, to qualify as a "nanocomposite", the material should consist of a nanometer-scale filler phase in combination with another phase, and the filler should have at least one dimension in the range of 1-100 nm [3]. Classified by the dimensionality of the nanofiller, there are a few types of nanocomposites: zero-dimensional (nanoparticle, e.g. polyhedral oligomeric silsesquioxane (POSS), carbon black and

fumed silica), one-dimensional (nanofiber, e.g. alumina nanofibers and single and multi-walled carbon nanobubes), two-dimensional (nanolayer, e.g. clay layered silicates), and three-dimensional (interpenetrating network) [4]. The nano-scale filler phase in the material often has properties that are significantly different from their macroscale counterparts. When organic and inorganic materials are mixed on a nanometer-length, the exhibited properties are often superior to conventional composites, such as mechanical strength, stiffness, thermal and oxidative stability, barrier properties, as well as other unique properties. Nanocomposites also often lack property trade-offs that are typically found in conventional polymer composites. Therefore, applications of nanocomposites have been seen in countless areas including aerospace, automotive, electronics, and biotechnology.

Table 1-1. Summary of polymer nanocomposite trends. [3]

	Crystalline	Amorphous	
Elastic modulus	Increase w/volume fraction Increase or no change with decrease of size	Increase w/volume fraction Increase w/decrease size	Good interaction
	Increase w/volume fraction Increase w/decrease size Greater increase than for good interaction	Increase w/volume fraction Increase w/decrease size	Poor interaction
Yield stress/strain	Increase w/volume fraction Increase w/decrease size	N/A	Good Interaction
	Decrease with addition of particles	Decrease with addition of particles	Poor interaction
Ultimate stress strain	Increase w/decrease size No unified result for change in Vf	Nano—micro after 20% weight	Good interaction
	Lower than pure for small volume fractions	Decrease with addition of particles	Poor interaction
Density/volume	Increased volume as size decreases	Increased volume as size decreases	Good interaction
	N/A	N/A	Poor interaction
Strain-to-failure	Decrease with addition of particles	Increase with addition of particles Increase w/decrease size	Good interaction
	Decrease with addition of particles	Increase with addition of particles	Poor interaction
Tg	Decrease with addition of particles	Increase w/decrease size	Good interaction
	N/A	Level until 0.5%, drops off level from 1–10%	Poor interaction
Crystallinity	No major effect	N/A	Good interaction
	No major effect	N/A	Poor interaction
Viscoelastic	Increase w/volume fraction Increase w/decrease size	Increase w/volume fraction nano less regular	Good interaction
	N/A	Decrease with addition of particles—drop at 1% with rise following	Poor interaction

Different trends in the mechanical properties have been observed in various polymer nanocomposite systems. The interaction between the nanofiller and matrix, and the microstructure of the system are both crucial factors in determining the mechanical properties of

the nanocomposite [3,5-8]. In general, when good dispersion is achieved and no aggregation is observed in the system, the elastic modulus tends to increase with increasing nanofiller content and decreasing particle size [9-12]. The yield stress tends to increase with increasing filler volume fraction for composite systems with good filler-matrix interaction; however, the pattern changes when the interaction is poor [10-12]. Jordan et al. [3] summarized the currently observed trends in the mechanical behavior of polymer nanocomposites, as shown in Table 1-1; however, they were not able to identify any universal patterns for the mechanical behavior of polymer nanocomposites.

1.2. Polyhedral Oligomeric Silsesquioxane (POSS)

The term "silsesquioxane" refers to chemical structures with the empirical formula $RSiO_{1.5}$, where R is hydrogen or any alkyl, alkylene, aryl, arylene, or organic functional derivatives of the above. The silsesquioxanes include random structures such as ladder, cage, and partial cage, as shown in Figure 1-2 [13]. The structure, preparation, properties, and applications of silsesquioxanes were reviewed by Baney et al. in 1995 [13]. The ladder-like polysilsesquioxanes (structure (b) in Figure 1-2) have applications in various areas such as photoresist coatings, interlayer dielectrics and protective coatings, optical fiber coatings, magnetic recording media, gas separation membranes, and binders for ceramics [13,14].

Silsesquioxanes with specific cage structures (structures (c)-(f) in Figure 1-2) have attracted more attention than others, and these polyhedral oligomeric silsesquixane have been abbreviated as POSS. POSS has received much interest due to its hybrid organic-inorganic structure which consists of a silica cage with functional groups attached at the cage corners. With diameter ranging from 1-3 nm, POSS nanoparticles can be viewed as the smallest particle of silica [14]. As the interest in POSS derivatives has increased, POSS with various reactive and/or inert function groups are now commercially available.

POSS can be incorporated into polymeric materials through copolymerization, grafting, or physical blending. The former two cases require at least one reactive functional group at the cage corner. The selection of the function groups is especially crucial for physical blending, since

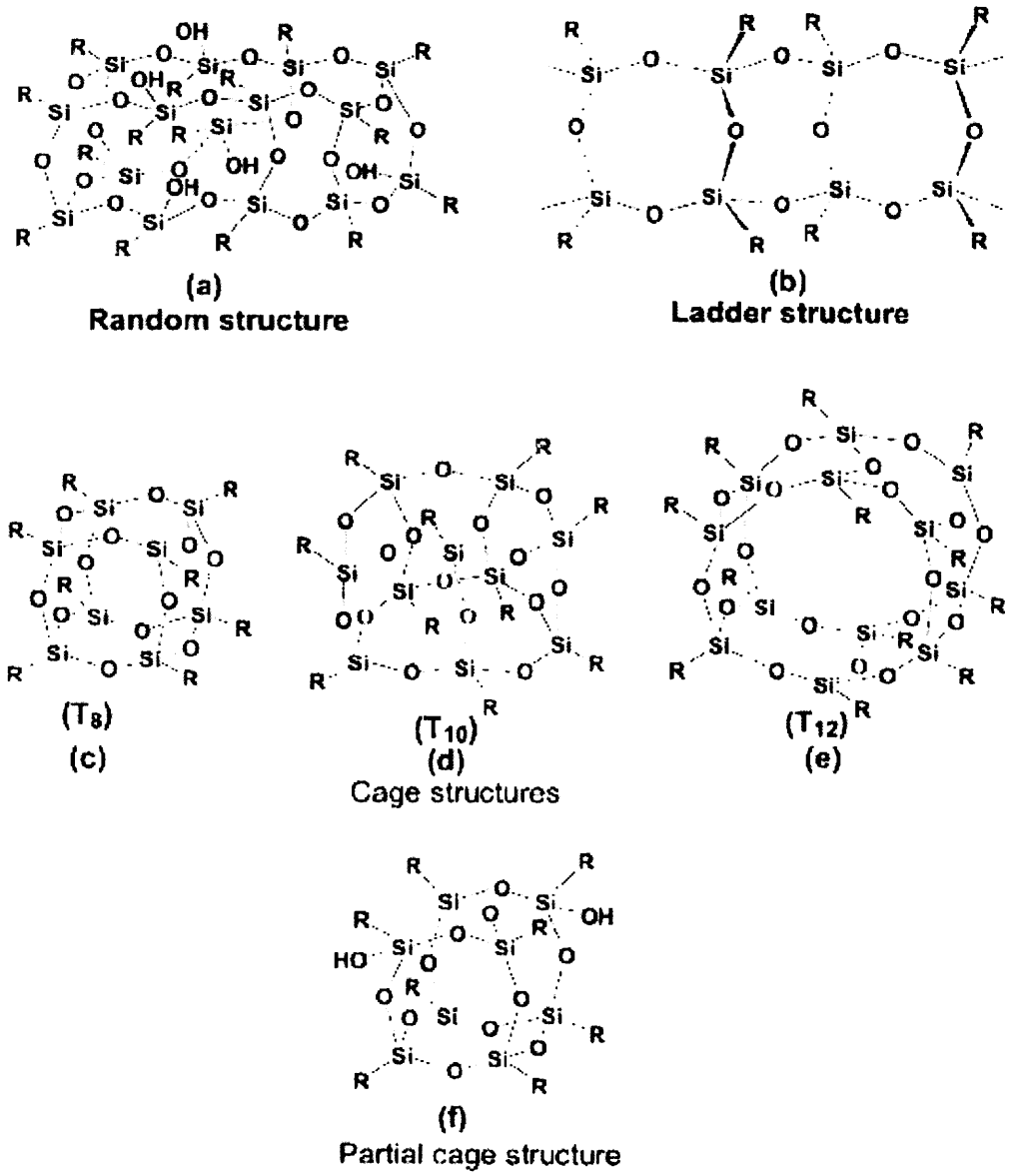

Figure 1-2. Structures of silsesquioxanes [13].

POSS is known to phase separate and form crystalline particles within the polymer matrix. With reactive functional groups, POSS can be covalently attached to the polymer backbones through copolymerization or grafting, and dramatic property improvements have been observed, such as increased glass transition temperature (T_g) [15-17], improved thermoxidative stability [18-20], and nanoscale reinforcement of the polymer matrix [16,17,21-27]. Other novel applications of polymer-POSS nanocomposites include shape memory material [28], atomic oxygen resistant

nanocomposites for space application [29], and photoresist for low and high voltage patterning applications [30].

The relationship between structure and properties of polymer-POSS nanocomposites has also been a research focus [21]. Waddon and Coughlin [31] studied the crystal structure of POSS using X-ray diffraction and electron microscopy. Capaldi el al. [32] conducted atomistic simulations to investigate the influence of blending POSS into polyethylene (PE) matrix. The effect of POSS molecules on the polymer structure was studied by Baker et al. [33] through combination of modeling and mass spectroscopy. Kopesky and coworkers [34,35] compared and contrasted the thermomechanical properties of poly(methyl methacrylates) (PMMA) containing POSS in the form of blends and copolymers. The influence of POSS on the rheological properties varies based on the type of POSS cage and whether POSS molecules were covalently attached to the PMMA backbone. Improvement in PMMA toughness was observed in various strain rates when a mixture of two distinct POSS species – one miscible, one immiscible – was incorporated into PMMA [35]. Haddad and Mather et al. [16,28,36-38] focused on the synthesis and characterization of POSS macromers and polymers, and developed blocky and random POSS-norbronyl copolymers

1.3. Rate-Dependent Deformation Behavior of Amorphous Polymers

1.3.1. Polymer Stress-Strain Behavior

The stress-strain behavior of polymers has been well-documented. Figure 1-3 shows a representative true stress-true strain[1] curve of poly(vinyl chloride) (PVC) in quasi-static uniaxial

---

[1] True stress and true strain provide a more accurate measure of the material properties than engineering stress and engineering strain during deformation. While engineering stress and strain are defined using the original sample geometry before deformation, the true stress and true strain are based on the current specimen geometry. True stress (σ_{true}) and true strain (ε) can be approximated from engineering stress (σ_{eng}) and engineering strain (e):

$$\varepsilon = \ln(1+e)$$
$$\sigma_{true} = \sigma_{eng}(1+e)$$

compression. During the loading, the material initially deforms elastically where the chain segments can rotate reversibly with respect to one another. As the stress increases, more local rotation and sliding of polymer chain segments are enabled. Eventually, the material accumulates enough localized events, where it yields in plastic deformation and "flows" without further increase in stress. The relative maximum in the stress-strain curve, or the stress level that is required for plastic deformation, is considered to be the polymer's yield point. Following the yield point, the polymer goes through "strain softening", where the chain rotation can be generated with a lower stress. During the process of plastic deformation, the macromolecules are performing large rotations of the whole chain to reach the strain values. The displacement motions are analogous to the intermolecular motions happen above the glass transition (α-transition) temperature [39,40]. Thus, the plastic flow of a given polymer corresponds to its specific α-transition motions at the considered temperature. With increasing plastic deformation, the polymer chains orient and align preferentially in directions that allow maximum stretch. At the end, a "strain hardening" is observed.

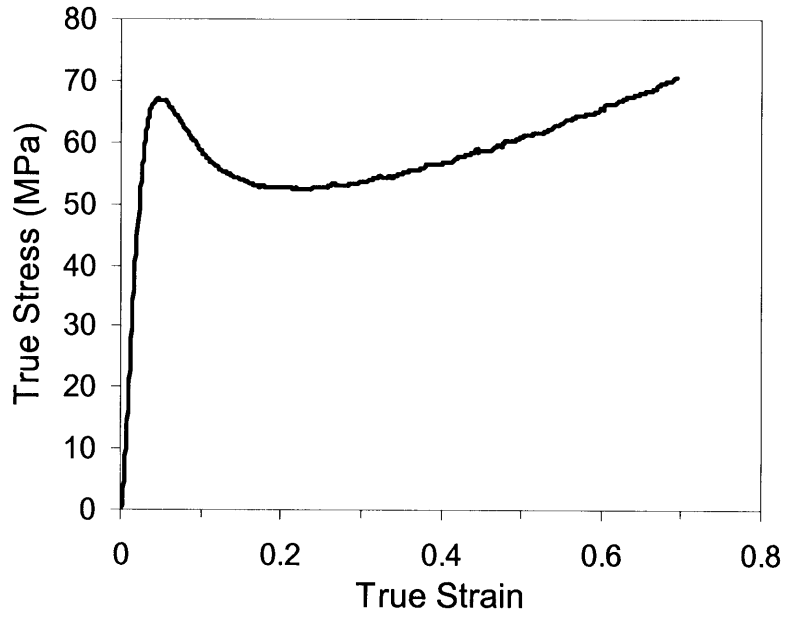

Figure 1-3. True stress-true strain behavior of poly(vinyl chloride) (PVC) in uniaxial compression at a strain rate of $3x10^{-4}/s$.

The stress-strain behavior of polymers illustrated above is strongly time-dependent. Generally, the yield stress required for plastic deformation and the initial elastic modulus increases with decreasing temperature or increasing strain rate. A transition in the rate dependence of the yield behavior over a wide range of temperature (-50 to 150 °C) and strain rate (10^{-5} to 10^{-1}/s) has been observed in various glassy polymers including poly(methyl methacrylate) (PMMA) [41-44], polycarbonate (PC) [45,46], and poly(vinyl chloride) (PVC) [45,47,48]. These studies revealed that two rate processes are involved in activating inelastic deformation. As the temperature is reduced and/or the strain rate is increased, in order for the material to yield, an additional stress is required to activate the secondary (β) process that is related to polymer local relaxation motions.

1.3.2. Polymer Viscoelastic Behavior-Relaxation Processes

There are many types of relaxation processes that can occur in polymers. The viscoelastic transitions of a typical amorphous polymer are illustrated in Figure 1-4 [49] and Figure 1-5 [50]. When considering amorphous polymers, a significant changeover in the mechanical properties happens at the glass-to-rubber transition temperature. At the glass transition temperature, the intermolecular motionss of polymer main chains are enabled and the modulus of polymer decreases dramatically. Furthermore, at temperatures below the glass transition temperature, more gradual secondary transitions (β, γ, ...) have been observed in various amorphous polymers. At the temperature and frequency where these motions are enabled, a specific energy is dissipated, which is accompanied by a decrease in the mechanical modulus.

Secondary transitions are generally caused by motions involving the side groups, one or a small number of the repeat units (local chain motions), or the entire molecule (Johari-Goldstein) [51,52]. Examples for these molecular motions include ring flip, side group rotations, cooperative motions among repeat units, and transition between unequivalent conformations. A secondary transition, for example, β, can also involve more than one motional process, and it is attributed to different motions in different polymers. For instances, the β-transition in polycarbonate (PC) involves the phenyl ring motions[53,54], the motions performed by the ester groups are associated with the β-transition in PMMA[55], and the β-relaxation in PVC is due to movements of small segments of the main chain [56].

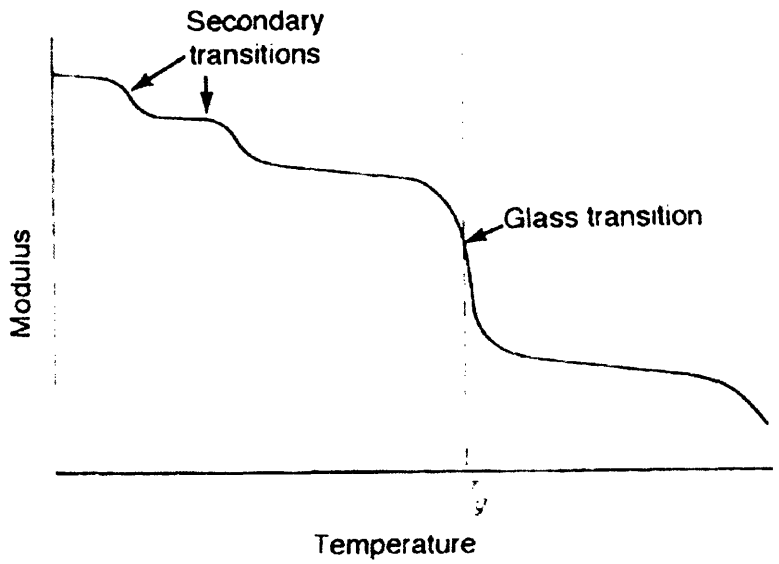

Figure 1-4. Temperature dependence of modulus in a typical polymer. [49]

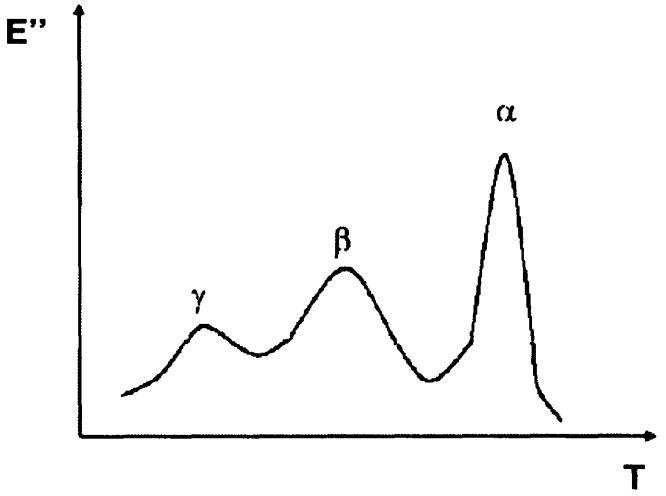

Figure 1-5. A typical example of temperature dependence of the mechanical loss modulus, showing α, β, and γ transitions. [50]

The true occurrence of the glass to rubber transition is determined by techniques which exam the polymer samples at rest, such as thermal measurements and spectroscopic techniques. Glass transition temperatures determined by the above techniques are generally denoted as T_g. When the techniques involve agitations of the sample, like dynamic mechanical testing and dielectric measurements, the temperature corresponding to the glass transition is often referred as T_α, which has a different numerical value compared to T_g. For example, when choosing T_α as the

temperature at which the loss modulus goes through its maximum, at a testing frequency of 1 Hz, T_α is 10 °C higher than the T_g measured by differential scanning calorimetry at a 20 °C /min heating rate. Figure 1-6 shows another example of the discrepancy in relaxation transition measurement between the dielectric measurement and the dynamic mechanical measurement.

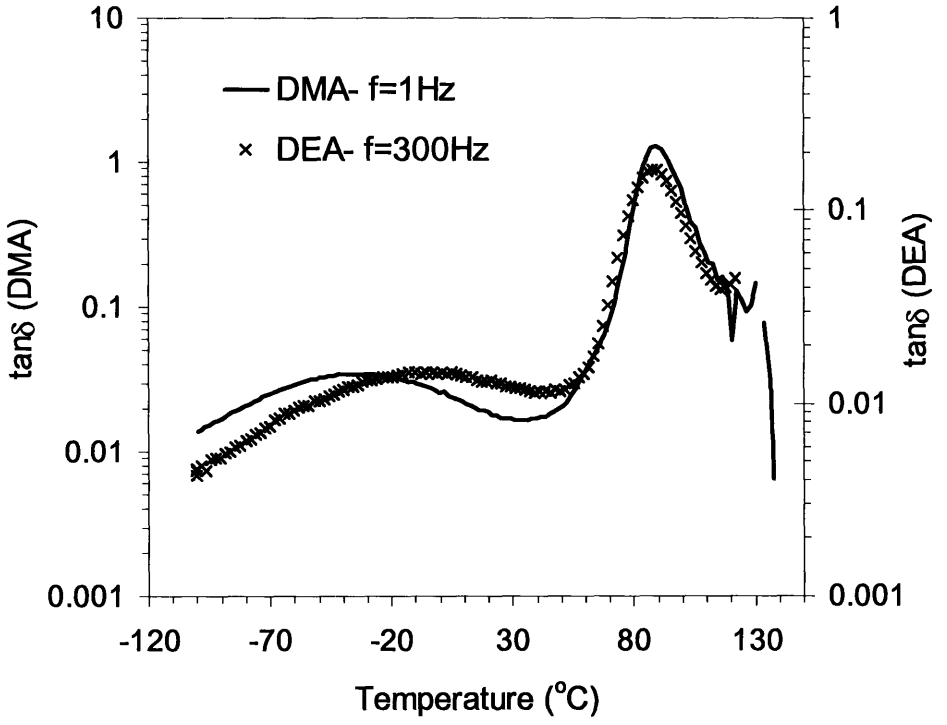

Figure 1-6. Discrepancy between dynamic mechanical measurement and dielectric measurement. Showing tanδ curves of PVC.

The temperatures of various relaxation transitions vary correspondingly with the frequency which the polymer is subjected to. The temperature dependence of the process frequency can be presented in a relaxation map, as shown in Figure 1-7. In a relaxation map, the logarithm of the frequency is plotted as a function of the inverse of the absolute temperature. Since the α-transition is characterized by the cooperative chain segment motions, its temperature dependence of the frequency can be described by the modified Willams-Landel-Ferry (WLF) model:

$$\log(f_T / f_{Tg}) = [C_g^1 (T - T_g)]/[C_g^2 + (T - T_g)] \quad (1\text{-}1)$$

where T_g is the glass transition temperature, f_{Tg} refers to the frequency at T_g, C_g^1 is related to the free volume fraction at T_g, and C_g^2 is related to the thermal expansion of the free volume at T_g. In the case of the secondary transitions such as β and γ, the temperature dependence of the frequency can be described by the Arrhenius law:

$$f_T = f_o \exp(-E_a / RT) \quad (1\text{-}2)$$

where f_o is a preexponential factor, E_a refers to the activation energy of the considered relaxation process, and R is the universal gas constant. Figure 1-7 clearly shows that a higher transition temperature is observed when a higher frequency is experienced. Note that a lower process transition temperature corresponds to a smaller activation energy and a faster shift in transition temperature with a change in frequency.

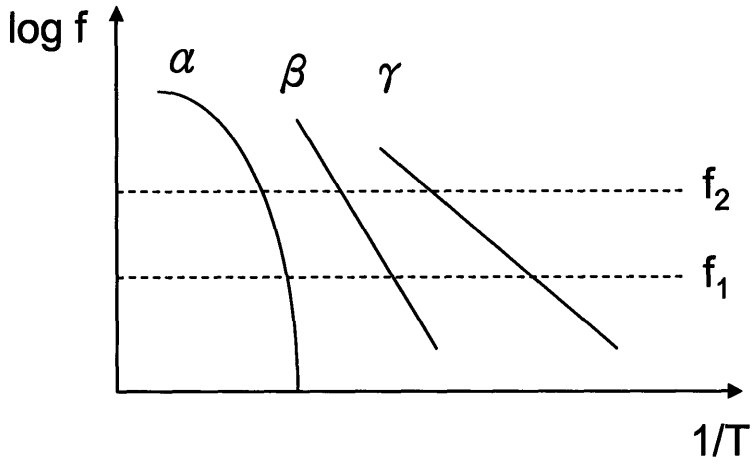

Figure 1-7. A typical example of relaxation map with α, β, and γ transitions [50].

1.3.3. Rate-Dependence of Polymer Mechanical Behavior

The rate-dependent mechanical behavior have been well documented for various amorphous polymers including polycarbonate (PC) [46,47,57-59], poly(methyl methacrylate) (PMMA) [41-44,57,58] , poly(vinyl chloride) (PVC) [45,47,48,59-61], and polystyrene (PS) [44].

Eyring's theory is perhaps the first model that is used to describe rate-dependent plastic flow in amorphous, glassy polymers [62]. Erying's general theory considers that the deformation of a polymer is a rate activated process that involves the polymer chain segments at one equilibrium state overcoming a potential barrier and transitioning to another equilibrium state. The theory results in a model describing the shear strain rate ($\dot{\gamma}$) as a function of shear stress (τ):

$$\dot{\gamma} = \dot{\gamma}_o \exp(-\frac{Q}{RT})\sinh(\frac{\Omega\tau}{RT}) \tag{1-3}$$

where $\dot{\gamma}_o$ is a lumped parameter related to material properties, Q is the activation energy required for the transition, R is the universal gas constant, T is the absolute temperature, and Ω is the activation volume. With assumption based on physical understandings of the plastic flow[2], Eq. (1-3) can be written as:

$$\dot{\gamma} = \frac{\dot{\gamma}_o}{2}\exp(\frac{-Q+\Omega\tau}{RT}) \tag{1-4}$$

Rearranging Eq. (1-4), shear stress (τ) can be expressed as a function of shear strain rate ($\dot{\gamma}$):

$$\frac{\tau}{T} = A'\left[\ln(2C'\dot{\gamma}) + \frac{Q}{RT}\right] \tag{1-5}$$

where $A' = \frac{R}{\Omega}$ and $C' = \frac{1}{\dot{\gamma}_o}$ are lumped model parameters. This model predicts a linear relationship between the shear stress and the logarithm of the shear strain rate.

---

[2] Using the definition of hyperbolic sine, Eq. (1-3) can be rewritten as:

$$\dot{\gamma} = \frac{\dot{\gamma}_o}{2}\exp(\frac{-Q+\Omega\tau}{RT}) - \frac{\dot{\gamma}_o}{2}\exp(\frac{-Q-\Omega\tau}{RT})$$

The first term represents the forward process of the plastic transition, and the second term captures the reverse/backward process. The second term has been shown to be non-negligible only in the unloading or low stresses conditions. In the work presented here, the stresses (τ) in loading are assumed to be sufficiently high and unloading is not an interest. When $\Omega\tau >> RT$, the second term can be approximated to zero and omitted. This simplification then gives rise to Eq. (1-4).

Bauwen-Crowet et al. applied the Eyring theory to the rate-dependent yield behavior of amorphous polymers [45,47]. In order to express the tensile yield stress (σ_e) as a function of the axial strain rate ($\dot{\varepsilon}$), Eq. (1-5) was rewritten as:

$$\frac{\sigma_e}{T} = A\left[\ln 2C\dot{\varepsilon} + \frac{Q}{RT}\right] \tag{1-6}$$

where A and C are again lumped parameters with values different from A' and C' of Eq. (1-5). Eq. (1-6) was used by Bauwen-Crowet et al. to predict the rate-dependent yield behavior of PC in tension. The yield data of PC and the Eyring model predictions are presented in Figure 1-8, with corresponding parameter values shown in Table 1-2.

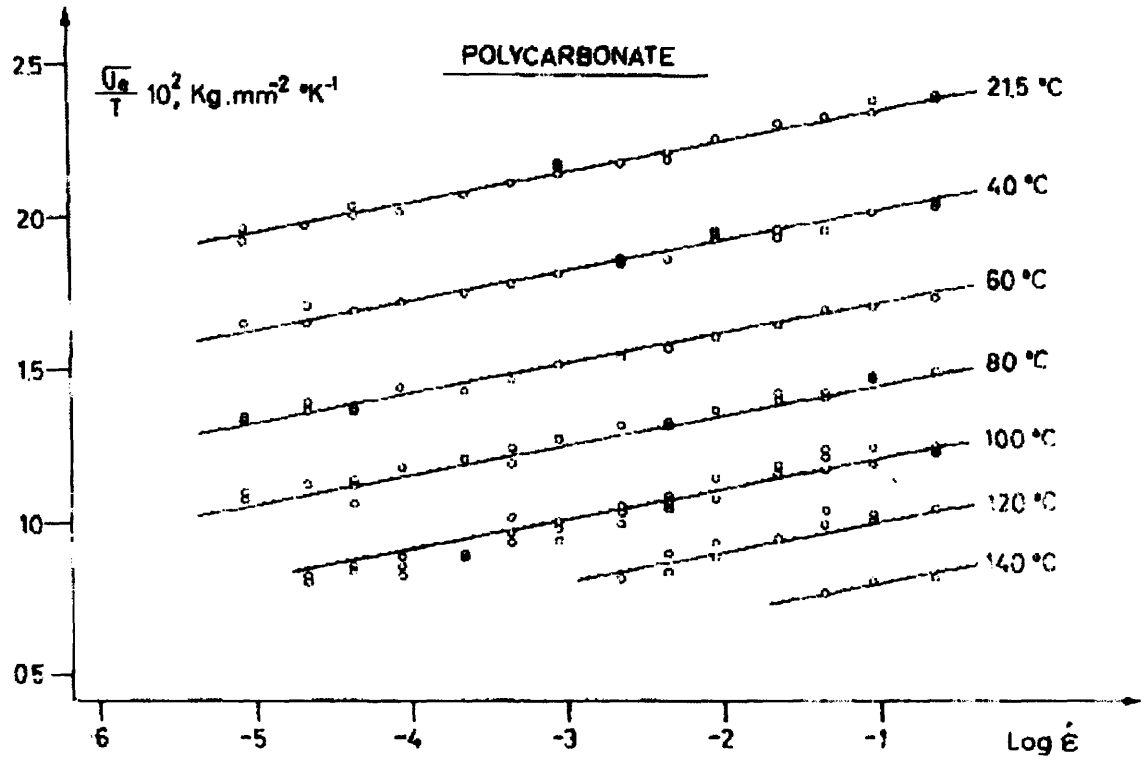

Figure 1-8.Tensile yield data of PC presented by Bauwens-Crowet et al. [45]. The set of parallel curves were calculated from Eq. (1-5).

Table 1-2. Eyring model parameters for the PC data of Figure 1-8.

A	4.16×10^{-4}	$kg/mm^2\text{-}^oK$
Q	75.5	kcal/mol
C	10^{-31}	Sec

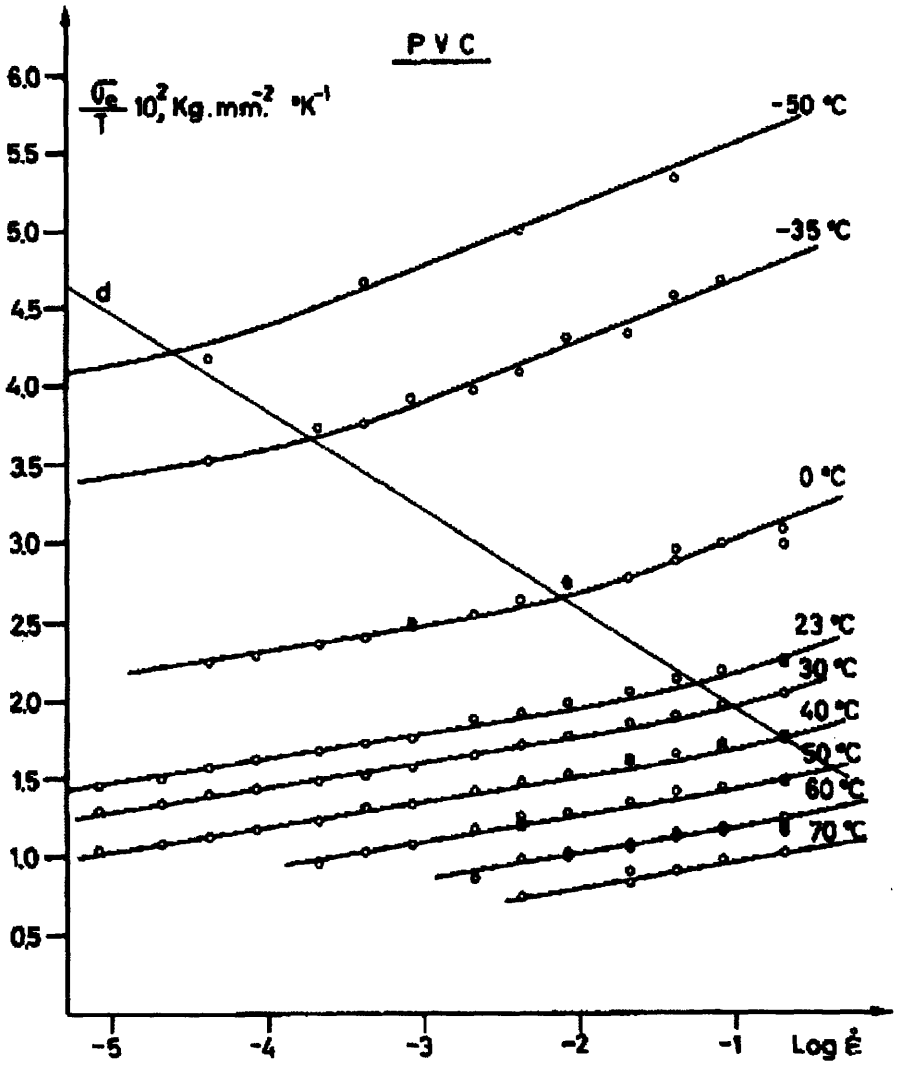

Figure 1-9. Tensile yield data of poly(vinyl chloride) presented by Bauwens-Crowet et al. [45]. The set of parallel curves was calculated from Eq. (1-6).

The rate-dependent yield behavior of PVC from -50 to 70 °C over a range in strain rate of 10^{-5} to 10^{-1}/s is shown in Figure 1-9 (Bauwen-Crowet et al. [45]). In the case of PVC, within the

temperature and strain rate studied, a clear transition in rate dependency was observed and marked as line *d*. This transition in rate sensitivity was attributed to the local β-relaxation motions of the polymer chains by the researchers. Below the indicated line *d*, the molecular motions governing yield mainly correspond to the main-chain α-relaxation motions, commonly associated with the glass transition. Above line *d*, the β-motions associated with local relaxation movements of small groups along the chain become important, and a nonnegligible stress is required to activate β-motions to enable yield. The intersection of each σ_y/T curve with *d* reveals the character of the frequency or rate dependence of the β-transition temperature.

To capture the transition in rate-dependence, Bauwens-Crowet et al. took the β-process into account and explained the yield data using the Ree-Eyring theory [63,64]. The Ree-Eyring theory simply allows multiple rate-activated processes to be acting in tandem, and in this simplified two-process equation, the polymer total yield stress is derived to be the sum of the α- and β-contributions:

$$\frac{\sigma_e}{T} = \frac{\sigma_\alpha}{T} + \frac{\sigma_\beta}{T} = A_\alpha \sinh^{-1}\left[C_\alpha \dot{\varepsilon} \exp\left(\frac{Q_\alpha}{RT}\right)\right] + A_\beta \sinh^{-1}\left[C_\beta \dot{\varepsilon} \exp\left(\frac{Q_\beta}{RT}\right)\right] \qquad (1\text{-}7)$$

where T is the absolute temperature, $\dot{\varepsilon}$ is the strain rate, Q_i (i=α, β) is the activation energy, R is the universal gas constant, and A_i and C_i are lumped parameters. Here the approximation seen in footnote 2 can be applied to the first term, since the α-process is considered to be in a high enough stress over the entire range of interest. However, the assumption is not valid for the β-process since the stress level of the β-process is much lower. Eq. (1-7) can be rewritten as:

$$\frac{\sigma_e}{T} = \frac{\sigma_\alpha}{T} + \frac{\sigma_\beta}{T} = A_\alpha \left[\ln 2C_\alpha \dot{\varepsilon} + \frac{Q_\alpha}{RT}\right] + A_\beta \sinh^{-1}\left[C_\beta \dot{\varepsilon} \exp\left(\frac{Q_\beta}{RT}\right)\right] \qquad (1\text{-}8)$$

The predicted yield behavior calculated from Eq. (1-8) is shown as the paralleled curves in Figure 1-9, and the constant values are presented in Table 1-3. Note that the activation energy for the β-process (Q_β) is only approximately one quarter of the value of the α-process activation energy (Q_α).

Table 1-3. Ree-Eyring model parameters for the PVC data of Figure 1-9.

A_α	7×10^{-4}	kg/mm^2-°K
Q_a	70.5	kcal/mol
C_α	10^{-38}	sec
A_β	10.1×10^{-4}	kg/mm^2-°K
Q_β	14	kcal/mol
C_β	4.26×10^{-10}	sec

The parallel curves shown in Figure 1-9 can be shifted along the *d* line and generate a master curve over a wide range of strain rate for a specific temperature. Figure 1-10 shows the master curve of tensile yield stress reduced to 0 °C for PVC, where the transition can be clearly observed. From Figure 1-10 it is possible to extrapolate the yield stress value of PVC to rates that were not accessible experimentally at the time.

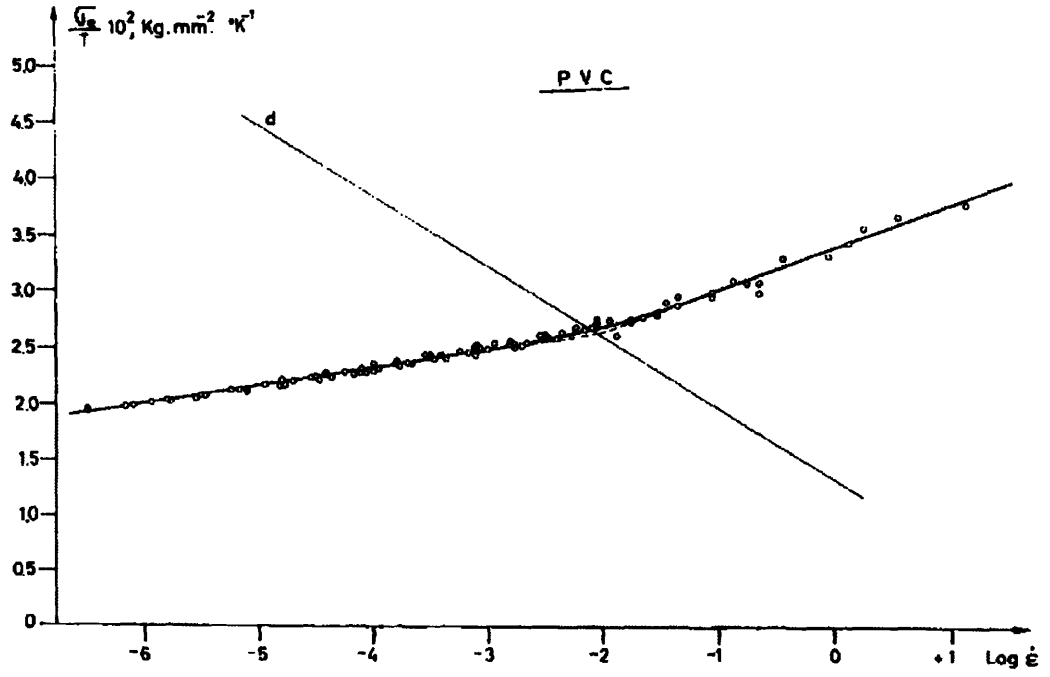

Figure 1-10. Master curve of tensile yield stress reduced to 0 °C for PVC [45].

The rate-dependent stress-strain behavior of PVC at 70 ^{0}C under three different strain rates in tension was investigated by Bauwens et al. [47], shown in Figure 1-11. The PVC was tested at a temperature near its glass-to-rubbery transition, and glassy material behavior with a well-defined yield point was observed at the highest strain rate ($4.16x10^{-5}$/s). With decreasing strain rate, the elastic modulus and the stress level decrease, and the PVC transitions from glassy to rubbery with gradually disappearing yield point. Since the PVC was tested at a temperature near the glass transition, the observed glassy-to-rubbery transition with decreasing strain rate is attributed to the α-relaxation process.

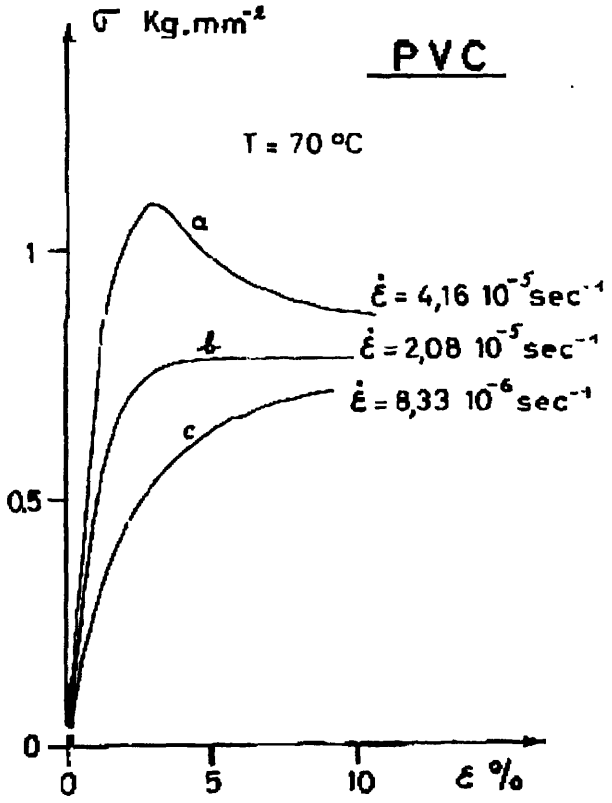

Figure 1-11. Rate-dependent stress-strain behavior of PVC in tension near the glass transition temperature [47] .

Earlier studies on polymer rate-dependent mechanical behavior were limited by the experimental techniques. Due to the lack of ability in high strain rate mechanical testing, characterizations in compression and tension could only be done at strain rates less than 1/s. Testing temperatures were often manipulated, as seen in Figure 1-9, in order to capture the transition in rate sensitivity.

With the development and advances in high rate mechanical testing techniques, researches can now capture the rate-dependent behavior of materials over a truly wide range of strain rates (10^{-6}/s to ~6000/s). Recently the rate-dependent elastic-plastic deformation of PC and PMMA was investigated by Mulliken and Boyce [57,58] over the strain rate range of 10^{-3} to 3000/s and a constitutive model was developed to predict the rate-dependent mechanical behavior. Both PC and PMMA were found to exhibit increased rate sensitivity of yield under the same strain rate/temperature conditions as the β-transition.

The aims of this study were to investigate the effect of incorporating POSS on the elastic and plastic deformation behavior of PVC at different strain rates, to understand the rate-dependency of PVC/POSS systems utilizing constitutive modeling, to compare and contrast the influence of POSS as nanofiller for PVC to conventional small molecule additive, and to explore the possible novel applications of PVC/POSS nanocomposites.

1.4. References

1. Kopesky, E. T., "Thermomechanical Properties of Polyhedral Oligomeric Silsesquioxane-Poly(methyl methacrylate) Nanocomposites", PhD Thesis, Massachusetts Institute of Tehnology, Cambridge, MA, **2005**.

2. Fischer, H., "Polyner Nanocomposites: From Fundamental Research to Specific Applications", *Mat. Sci. Eng., C* **2003**, *23*, 763-772.

3. Jordan, J.; Jacob, K. I.; Tannenbaum, R.; Sharaf, M. A.; Jasiuk, I., "Experimental Trends in Polymer Nanocomposites - A Review", *Mat. Sci. Eng., A* **2005**, *393*, 1-11.

4. Schmidt, D.; Shah, D.; Giannelis, E. P., "New Advances in Polymer/Layered Silicate Nanocomposites", *Curr. Opin. Solid State Mater. Sci.* **2002**, *6*, 205-212.

5. Akita, H.; Kobayashi, H., "Studies on Molecular Composite. III. Nano Composites Consisting of Poly(p-phenylene benzobisthiazole) and Thermoplastic Polyamide", *J. Polym. Sci.: Part B: Polym. Phys.* **1999**, *37*, 209-218.

6. Sarvestani, A. S.; Picu, C. R., "Network Model for the Viscoelastic Behavior of Polymer Nanocomposites", *Polymer* **2004**, *45*, 7779-7790.

7. Luo, J. J.; Daniel, I. M., "Characterization and Modeling of Mechanical Behavior of Polymer/Clay Nanocomposites", *Compos. Sci. Technol.* **2003**, *63*, 1607-1616.

8. Sheng, N.; Boyce, M. C.; Parks, D. M.; Rutledge, G. C.; Abes, J. I.; Cohen, R. E., "Multiscale Micromechanical Modeling of Polymer/Clay Nanocomposites and the Effective Clay Particle", *Polymer* **2004**, *45*, 487-506.

9. Vollenberg, P. H. T.; Heikens, D., "Particle-Size Dependence of the Young Modulus of Filled Polymers. 1. Preliminary Experiments", *Polymer* **1989**, *30*, 1656-1662.

10. Chan, C.-M.; Wu, J. S.; Li, J. X.; Cheung, Y. K., "Polypropylene/Calcium Carbonate Nanocomposites", *Polymer* **2002**, *43*, 2981-2992.

11. Shelley, J. S.; Mather, P. T.; DeVries, K. L., "Reinforcement and Environmental Degradation of Nylon-6/Clay Nanocomposites", *Polymer* **2001**, *42*, 5849-5858.

12. Zhang, Y. Q.; Lee, J. H.; Jang, H. J.; Nah, C. W., "Preparing PP/Clay Nanocomposites Using a Swelling Agent", *Compos. PART B - Eng.* **2004**, *35*, 133-138.

13. Baney, R. H.; Itoh, M.; Sakakibara, A.; Suzuki, T., "Silsesquioxanes", *Chem. Rev.* **1995**, *95*, 1409-1430.

14. Li, G.; Wang, L.; Ni, H.; Pittman Jr., C. U., "Polyhedral Oligomeric Silsesquioxane (POSS) Polymers and Copolymers: A Review", *J. Inorg. Organomet. Polym.* **2002**, *11*, 123-154.

15. Xu, H.; Kuo, S.-W.; Lee, J.-S.; Chang, F.-C., "Preparations, Thermal Properties, and Tg Increase Mechanism of Inorganic/Organic Hybrid Polymers Based on Polyhedral Oligomeric Silsesquioxanes", *Macromolecules* **2002**, *35*, 8788-8793.

16. Mather, P. T.; Jeon, H. G.; Romo-Uribe, A.; Haddad, T. S.; Lichtenhan, J. D., "Mechanical Relaxation and Microstructure of Poly(norbonyl-POSS) Copolymers", *Macromolecules* **1999**, *32*, 1194-1203.

17. Fu, B. X.; Namani, M.; Lee, A., "Influence of Phenyl-Trisilanol Polyhedral Silsesquioxane on Properites of Epoxy Network Glasses", *Polymer* **2003**, *44*, 7739-7747.

18. Zheng, L.; Farris, R. J.; Coughlin, E. B., "Novel Polyolefin Nanocomposites: Synthesis and Characterizations of Metallocene-Catalyzed Polyolefin Polyhedral Oligomeric Silsesquioxane Copolymers", *Macromolecules* **2001**, *34*, 8034-8039.

19. Yei, D.-R.; Kuo, S.-W.; Su, Y.-C.; Chang, F.-C., "Enhanced Thermal Properties of PS Nanocomposites Formed from Inorganic POSS-Treated Montmorillonite", *Polymer* **2004**, *45*, 2633-2640.

20. Fina, A.; Tabuani, D.; Carniato, F.; Frache, A.; Boccaleri, E.; Camino, G., "Polyhedral Oligomeric Silsesquioxanes (POSS) Thermal Degradation", *Thermochim. Acta* **2006**, *440*, 36-42.

21. Philips, S. H.; Haddad, T. S.; Tomczak, S. J., "Development in Nanoscience: Polyhedral Oligomeric Silsesquioxane (POSS)-Polymers", *Curr. Opin. Solid State Mater. Sci.* **2004**, *8*, 21-29.

22. Fu, B. X.; Hsiao, B. S.; White, H.; Rafailovich, M.; Mather, P. T.; Jeon, H. G.; Philips, S. H.; Lichtenhan, J. D.; Schwab, J., "Nanoscale Reinforcement of Polyhedral Oligomeric Silsesquioxane (POSS) in Polyunrethane Elastomer", *Polym. Int.* **2000**, *49*, 437-440.

23. Fu, B. X.; Hsiao, B. S.; Pagola, S.; Stephens, P.; White, H.; Rafailovich, M.; Sokolov, J.; Mather, P. T.; Jeon, H. G.; Philips, S. H.; Lichtenhan, J. D.; Schwab, J., "Structural Development During Deformation of Polyurethane Containing Polyhedral Oligomeric Silsesquioxanes (POSS) Molecules", *Polymer* **2001**, *42*, 599-611.

24. Lee, A.; Lichtenhan, J. D., "Viscoelastic Responses of Polyhedral Oligosilsesquioxane Reinforced Epoxy Systems", *Macromolecules* **1998**, *31*, 4970-4974.

25. Lee, A.; Lichtenhan, J. D., "Thermal and Viscoelastic Property of Epoxy-Clay and Hybrid Inorganic-Organic Epoxy Nanocomposites", *J. Appl. Polym. Sci.* **1999**, *73*, 1993-2001.

26. Strachota, A.; Kroutilove, I.; Kovarova, J.; Matejke, L., "Epoxy Networks Reinforced with Polyhedral Oligomeric Silsesquioxane (POSS). Thermomechanical Properties", *Macromolecules* **2004**, *37*, 9457 - 9464.

27. Zeng, J.; Kumar, S.; Iyer, S.; Gonzalez, R. I., "Reinforcement of Poly(ethylene terephthalate) Fibers with Polyhedral Oligomeric Silsesquioxanes (POSS)", *High Perform. Polym.* **2005**, *17*, 403-424.

28. Jeon, H. G.; Mather, P. T.; Haddad, T. S., "Shape Memory and Nanostructure in Poly(norbornyl-POSS) Copolymers", *Polym. Int.* **2000**, *49*, 453-457.

29. Gonzalez, R. I.; Philips, S.; Hoflund, G. B., "In Situ Oxygen-Atom Erosion Study of Polyhedral Oligomeric Silsesquioxane-Siloxane Copolymer", *J. Spacecraft Rockets* **2000**, *37*, 463-467.

30. Ali, M. A.; Gonsalves, K. E.; Agrawal, A.; Jeyakumar, A.; Henderson, C. L., "A New Nanocomposite Resist for Low and High Voltage Electron Beam Lithography", *Electron. Eng* **2003**, *70*, 19-29.

31. Waddon, A. J.; Coughlin, E. B., "Crystal Structure of Polyhedral Oligomeric Silsesquioxane (POSS) Nano-Materials: A Study by X-ray Diffraction and Electron Microscopy", *Chem. Mater.* **2003**, *15*, 4555-4561.

32. Capaldi, F. M.; Rutledge, G. C.; Boyce, M. C., "Structure and Dynamics of Blends of Polyhedral Oligomeric Silsesquioxanes and Polyethylene by Atomistic Simulation", *Macromolecules* **2005**, *38*, 6700-6709.

33. Baker, E. S.; Gidden, J.; Fee, D. P.; Kemper, P., R.; Anderson, S. E.; Bowers, M. T., "3-Dimensional Structureal Characterization of Cationized Polyhedral Oligomeric Silsesquioxanes (POSS) with Styryl and Phenylethyl Capping Agents", *Int. J. Mass Spectrom.* **2003**, *227*, 205-216.

34. Kopesky, E. T.; Haddad, T. S.; Cohen, R. E.; McKinley, G. H., "Thermomechanical Properties of Poly(methyl methacrylate)s Containing Tethered and Untethered Polyhedral Oligomeric Silsesquioxanes", *Macromolecules* **2004**, *37*, 8992-9004.

35. Kopesky, E. T.; McKinley, G. H.; Cohen, R. E., "Toughened Poly(methyl methacrylate) Nanocomposites by Incorporating Polyhedral Oligomeric Silsesquioxanes", *Polymer* **2006**, *47*, 299-309.

36. Haddad, T. S.; Viers, B.; Philips, S., "Polyhedral Oligomeric Silsesquioxane (POSS)-Styrene Macromers", *J. Inorg. Organomet. Polym.* **2002**, *11*, 155-164.

37. Haddad, T. S.; Mather, P. T.; Jeon, H. G.; Philips, S. *Material Research Society Symposia Proceedings* **2000**, 628.

38. Kim, B.-S.; Mather, P. T., "Amphiphilic Telechelics Incorporating Polyhedral Oligosilsesquioxane. 1. Synthesis and Characterization", *Macromolecules* **2002**, *35*, 8378-8384.

39. Zhou, Q.-Y.; Argon, A. S.; Cohen, R. E., "Enhanced Case-II Diffusion of Diluents into Glassy Polymers Undergoing Plastic Flow", *Polymer* **2001**, *42*, 613-621.

40. Monnerie, L.; Halary, J. L.; Kausch, H.-H., "Deformation, Yield and Fracture of Amorphous Polymers: Relation to the Secondary Transitions", *Adv. Polym. Sci.* **2005**, *187*, 215-364.

41. Roetling, J. A., "Yield Stress Behaviour of Polymethylmethacrylate", *Polymer* **1965**, *6*, 311-317.

42. Bauwens-Crowet, C., "The Compression Yield Behaviour of Polymethyl Methacrylate over a Wide Range of Temperatures and Strain Rates", *J. Mater. Sci.* **1973**, *8*, 968-979.

43. Lefebvre, J. M.; Escaig, B., "Plastic Deformation of Glassy Amorphous Polymers: Influence of Strain Rate", *J. Mater. Sci.* **1985**, *20*, 438-448.

44. Swallowe, G. M.; Lee, S. F., "A Study of the Mechanical Properties of PMMA and PS at Strain Rates of 10^{-4} to 10^{3} over the Temperature Range 293-363 K", *J. Phys. IV France* **2003**, *110*, 33-38.

45. Bauwens-Crowet, C.; Bauwens, J. C.; Homes, G., "Tensile Yield-Stress Behavior of Glassy Polymers", *J. Polym. Sci., Part A-2* **1969**, *7*, 735-742.

46. Bauwens, J. C., "Relation between the Compression Yield Stress and the Mechanical Loss Peak of Bisphenol-A-Polycarbonate in the β-Transition Range", *J. Mater. Sci.* **1972**, *7*, 577-584.

47. Bauwens, J. C.; Bauwens-Crowet, C.; Homes, G., "Tensile Yield-Stress Behavior of Poly(vinyl chloride) and Polycarbonate in the Glass Transition Region", *J. Polym. Sci., Part A-2* **1969**, *7*, 1745-1754.

48. Bauwens, J. C., "Relation Between the Compression Yield Stress of Poly(vinyl chloride) and the Loss Peak in the β-Transition Range", *J. Polym. Sci.* **1971**, *33*, 123-133.

49. Ward, I. M.; Hardley, D., "An Introduction to the Mechanical Properties of Solid Polymers", John Wiley and Sons, New York, **1993**.

50. Monnerie, L.; Laupretre, F.; Halary, J. L., "Investigation of Solid-State Transitions in Linear and Crosslinked Amorphous Polymers", *Adv. Polym. Sci.* **2005**, *187*, 35-213.

51. Ngai, K. L.; Paluch, M., "Classification of Secondary Relaxation in Glass-Formers Based on Dynamic Properties", *J. Chem. Phys.* **2004**, *120*, 857-873.

52. Ngai, K. L.; Capaccioli, S., "Relation between the Activation Energy of the Johari-Goldstein β Relaxation and Tg of Glass Formers", *Phys. Rev. E.* **2004**, *69*, 031501.

53. Schaefer, J.; Stejskal, E. O.; McKay, R. A., "Molecular Motion in Polycarbonate by Dipolar Rotational Spin-Echo ^{13}C NMR", *Macromolecules* **1984**, *17*, 1479-1489.

54. Steger, T. R.; Schaefer, J.; Stejskal, E. O.; McKay, R. A., "Molecular Motion in Polycarbonate and Modified Polycarbonate", *Macromolecules* **1980**, *13*, 1127-1132.

55. Schmidt-Rohr, K.; Kulik, A. S.; Beckham, H. W.; Ohlemacher, A.; Pawelzik, U.; Boeffel, C.; Spiess, H. W., "Molecular Nature of the β Relaxation in Poly(methyl methacrylate) Investigated by Multidimensional NMR", *Macromolecules* **1994**, *27*, 4733-4745.

56. Flores, R.; Perez, J., "Mechanical Spectroscopy of the β Relaxation in Poly(vinyl chloride)", *Macromolecules* **1995**, *28*, 7171-7179.

57. Mulliken, A. D.; Boyce, M. C., "Mechanics of the Rate-Dependent Elastic-Plastic Deformation of Glassy Polymers from Low to High Strain Rates", *Int. J. Solids Struct.* **2006**, *43*, 1331-1356.

58. Mulliken, A. D.; Boyce, M. C. *SEM X International Congress and Exposition on Experimental and Applied Mechanics* **2004**, Paper No 197.

59. Siviour, C. R.; Walley, S. M.; Proud, W. G.; Field, J. E., "The High Strain Rate Compressive Behaviour of Polycarbonate and Polyvinylidene Difluoride", *Polymer* **2005**, *46*, 12546-12555.

60. Soong, S. Y.; Mulliken, A. D.; Cohen, R. E.; Boyce, M. C., "Rate-Dependent Deformation Behavior of POSS-Filled and Plasticized Poly(vinyl chloride)", *Macromolecules* **2006**, *39*, 2900-2908.

61. Povolo, F.; Schwartz, G.; Hermida, E. B., "Temperature and Strain Rate Dependence of the Tensile Yield Stress of PVC", *J. Appl. Polym. Sci.* **1996**, *61*, 109-117.

62. Eyring, H., "Viscosity, Plasticity, and Diffusion as Examples of Absolute Reaction Rates", *J. Chem. Phys.* **1936**, *4*, 283-291.

63. Ree, T.; Eyring, H., "Theory for Non-Newtonian Flow I. Solid Plastic System", *J. Appl. Phys.* **1955**, *26*, 793.

64. Ree, T.; Eyring, H., Rheology, Vol. II, Chap. III, Academic Press, New York, **1958**.

Chapter 2: Miscibility and Thermomechanical Properties of POSS-Filled and Plasticized Poly(vinyl chloride)

[Part of this work has been published previously, in slightly different form, in "Rate-Dependent Deformation Behavior of POSS-Filled and Plasticized Poly(vinyl chloride)" by S.Y. Soong, R.E. Cohen, M.C. Boyce, and A.D. Mulliken, *Macromolecules* **2006**, *39*, 2900-2908 [1].]

2.1. Introduction

Polyhedral oligomeric silsesquioxanes (POSS) can be incorporated into a homopolymer matrix by either chemically attaching the POSS cages onto the polymer backbones or by direct physical blending. As mentioned in Chapter 1, covalently attaching POSS to the polymer backbones can lead to improve physical and mechanical properties, such as increased glass transition temperature (T_g) [2,3], improved thermoxidative stability [4], and higher storage modulus at low temperature [3], due to reinforcement at the molecular level [5]. Compared to chemically grafted POSS-polymer systems, relatively few studies have been conducted regarding the physically blended POSS-polymer nanocomposites. Physically blended POSS-polymer systems imply that there are no covalent POSS-polymer linkages; therefore crystallization or aggregation of POSS is likely to occur and limits the miscibility of POSS in polymer. When POSS crystallizes or aggregates in the polymer system, the aggregates can act like stiff fillers [6,7].

Fu et al. studied a few non-reactive POSS-polymer nanocomposite systems. Their work includes the influence of phenyl-trisilanol-POSS on the thermomechanical properties and curing of epoxy-amine networks [8], the rheological behavior of octamethyl-POSS filled ethylene-propylene (EP) copolymer [9], and the crystallization in isotactic polypropylene (iPP) containing octamethyl-POSS [10].

Fina et al. [11] studied the influence of the functional group chain length of POSS on the properties of polypropylene (PP), and a good dispersion was found particularly at low loadings of POSS functionalized with longer organic chains.

Kopesky et al. [7,12,13] studied the rheological and thermomechanical properties of various POSS filled poly(methyl methacrylate) (PMMA) systems, including cyclohexyl-POSS, isobutyl-POSS, methacryl-POSS, and modified (hydrogenated) methacryl-POSS. Both the cyclohexyl- and isobutyl-POSS are in the form of crystals, while the methacryl-POSS is a non-crystallizable cage mixture. They showed that cyclohexyl-POSS or isobutyl-POSS can be blended into PMMA, producing nanocomposites with excellent dispersion up to a volume fraction of 0.01. At higher volume fraction, the POSS was found to aggregate and crystallize into larger particles. Selection of the non-crystallizable methacryl-POSS increases the miscibility of POSS in PMMA. It was found that when POSS was molecularly well dispersed in PMMA, it behaved like a plasticizer. The unmodified methacryl-POSS showed better compatibility with PMMA than the hydrogenated type. At a loading of 0.2 volume fraction, the unmodified methacryl-POSS/PMMA composite appeared to be transparent while the hydrogenated methacryl-POSS/PMMA one appeared to be opaque. A larger reduction in T_g was also observed in the first case. Significant phase separation was observed in wide-angle x-ray analysis for both the unmodified and modified methacryl-POSS/PMMA nanocomposites when the loading is above a 0.2 volume fraction.

Incorporation of POSS was also shown to affect the high rate mechanical behavior of a homopolymer. Mulliken and Boyce showed that when 5 wt % of the trisilanophenyl-POSS was incorporated into polycarbonate (PC), the effect POSS on the α-transition region was insignificant, but the POSS enhances the mobility of the β-motions significantly and therefore reduces the resistance in high rate deformation [14].

2.2. Experimental Section

2.2.1. Materials

The poly(vinyl chloride) used in this study was custom-made by Scientific Polymer Products, Inc. (Ontario, NY) with an approximate molecular weight of 90,000 g/mol. Methacryl-POSS was obtained from Hybrid Plastics (Fountain Valley, CA). It is a non-crystallizable mixture of 8-, 10-,

12-, and 14-corner POSS cages, with 10-corner cages having the highest weight fraction (T_{10} = 47.5 wt%; T_{12} = 27.3 wt%;T_{14} = 21.4 wt%; T_8 = 3.8 wt% as measured by NMR [7,12]).

Methacryl-POSS appears in the form of a light brown heavy oil at room temperature. Figure 2-1 shows the chemical structure of a 10-corner methacryl-POSS molecule. Methacryl-POSS had a density of 1.19 g/cm^3 [12,13].

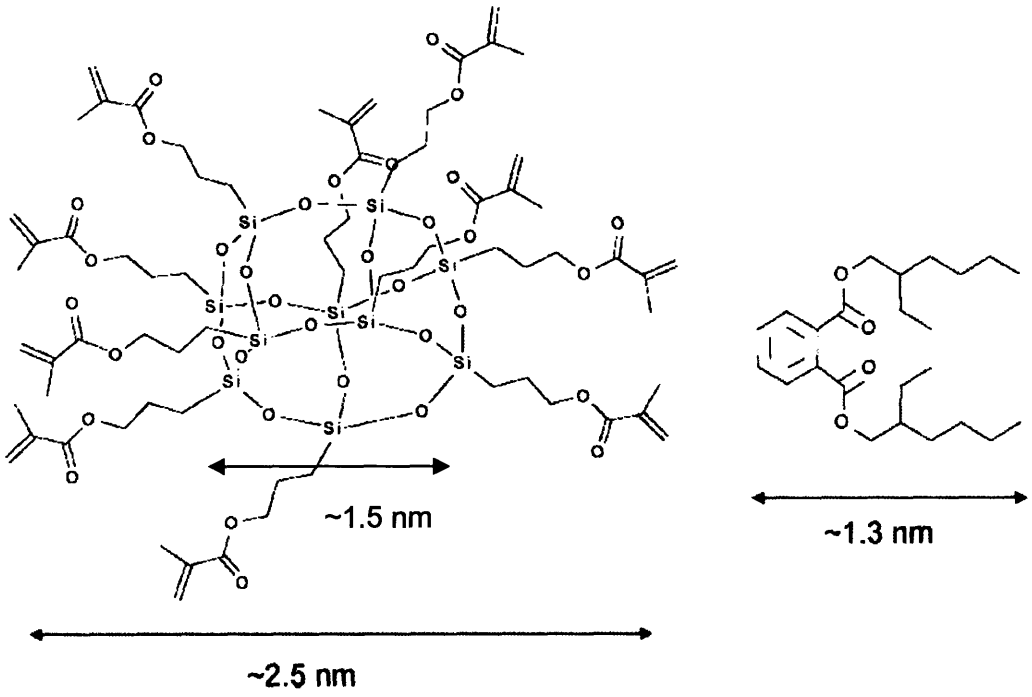

Figure 2-1. Molecular structures of a 10-corner cage methacryl-POSS molecule and a DOP molecule.

2.2.2. Blend Preparation

Neat PVC; 10, 15, and 20 wt % of methacryl-POSS in PVC; and 5, 10, 15, and 20 wt % of dioctyl phthalate (DOP, Sigma-Aldrich) in PVC were prepared for this study. After a targeted percentage of methacryl-POSS or DOP was mixed into PVC powders, the mixture was then melt-blended for 1 min in a lab scale extruder (DACA Instruments) at 180 °C. The PVC used in all of the polymer blends contained 3 wt % of thermal stabilizer (Thermolite 890S, Atofina) to minimize degradation. While some thermal and thermomechanical analyses were performed on direct polymer extrudates, most of the extruded polymer strands were pelletized and then

compression molded into different specimen geometries for various testing. Figure 2-2 shows the schematic of the experimental procedures from blend preparation to sample characterization.

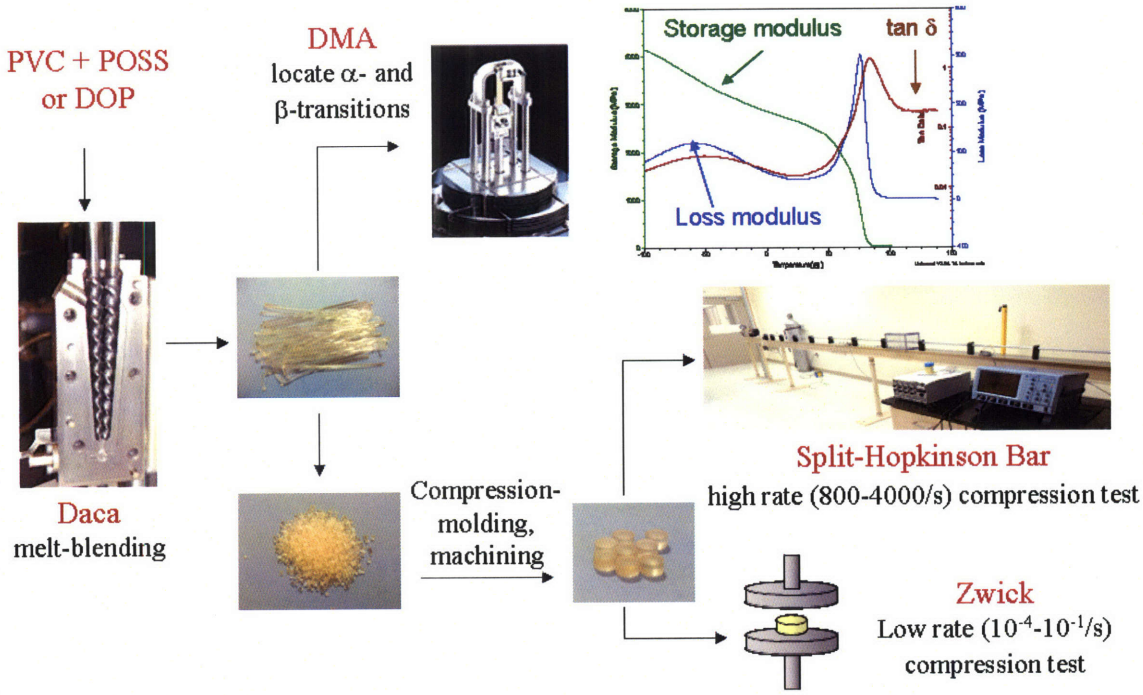

Figure 2-2. Schematic of blend and specimen preparation and mechanical characterization.

2.2.3. Differential Scanning Calorimetry (DSC)

The thermal analysis was performed on TA Instruments Q1000 DSC. Materials tested were the polymer extrudates from DACA. Samples were heated at 10 °C/min and then cooled at the same rate. Data were collected on the second heating ramp. The glass transition temperatures (T_g) were identified as the inflection points in the heat flow vs. temperature curves using the TA Universal Analysis software.

2.2.4. Dynamic Mechanical Analysis

Dynamic mechanical analysis (DMA) was performed on a TA Instruments Q800 DMA to observe and investigate the α- and β-transitions of the materials in this study. Storage modulus and loss modulus were measured as a function of temperature by the equipment. The storage modulus in viscoelastic solids measures the stored energy, representing the elastic portion that is in phase with the loading. The loss modulus measures the energy dissipated as heat, representing

the viscous portion that is out of phase with the loading. For example, for a strain controlled sinusoidal loading, the strain can be described as:

$$\varepsilon(t) = \varepsilon_o \sin \omega t \tag{2-1}$$

where t is the time, ε_0 is the amplitude of the strain, and ω is the oscillating frequency. The stress response can then be written in two components as:

$$\sigma(t) = \sigma_o \sin(\omega t + \delta) = \sigma_o \cos\delta \sin \omega t + \sigma_o \sin\delta \cos \omega t \tag{2-2}$$

where σ_0 is the amplitude of the responding stress and δ is the phase lag of the viscous response. Eq. (2-2) can be rewritten as:

$$\sigma(t) = \varepsilon_o G' \sin \omega t + \varepsilon_o G'' \cos \omega t \tag{2-3}$$

where

$$G' = \frac{\sigma_o \cos\delta}{\varepsilon_o} \tag{2-4}$$

and

$$G'' = \frac{\sigma_o \sin\delta}{\varepsilon_o} \tag{2-5}$$

G' is known as the storage modulus and *G"* is known as the loss modulus. The corresponding tan δ, which is the ratio of the loss modulus and the storage modulus, was calculated using TA Universal Analysis software. A typical example of polymer responses in DMA through its glass transition is illustrated in Figure 2-3. The storage modulus (G_1) of polymer changes dramatically through its glass transition, where transition peaks are seen in the loss modulus (G_2) and tan δ curves.

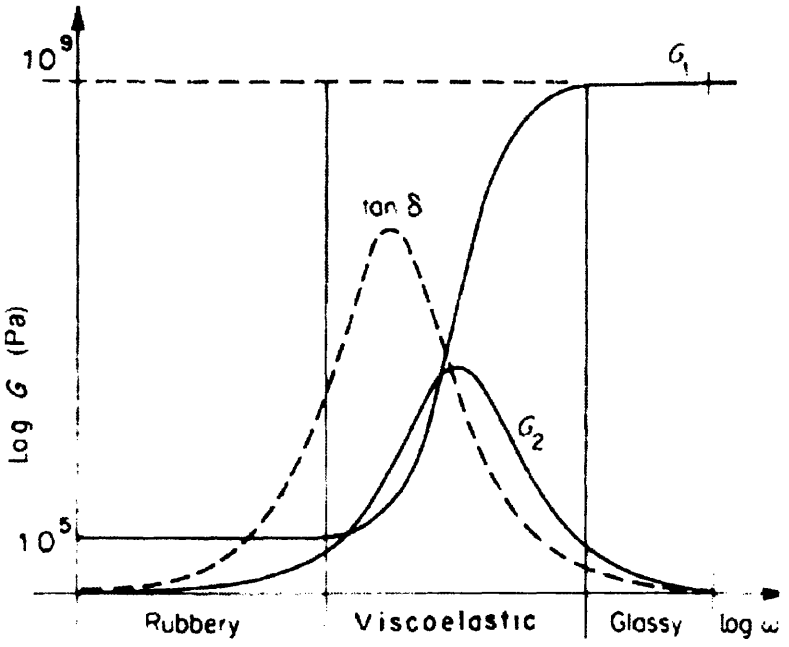

Figure 2-3. Schematic of the storage modulus (G_1), loss modulus (G_2), and tan δ curves of a polymer through its glass transition [15].

Cylindrical polymer samples extruded from DACA with a diameter of 2.5 mm and a length of 15 mm were tested in the single cantilever mode in DMA with a fixed displacement of 25 μm. The testing temperature ranged from -140 °C to 140 °C with a 2 °C/min heating rate at frequencies of 1, 10, and 100 Hz. The particular frequencies of these tests were converted to corresponding average strain rates, giving a range in strain rate of $5x10^{-3}$ to $5.8x10^{-1}/s^3$. Since the storage and loss modulus are frequency-dependent, converting the frequencies to corresponding strain rates allows us to relate the DMA data to the compression testing results. The same tests were repeated at least three times for each blend composition using three different specimens.

---

[3] The frequency ω of each test is converted to a strain rate by examining one-quarter of the sinusoidal loading cycle. The time duration of this quarter cycle is known from the test frequency, and the maximum strain amplitude achieved during this time is measured during the test. It is assumed that the increase in strain over this time is approximately linear, and an average strain rate can be calculated: $\dot{\varepsilon} = strain / time = 4\varepsilon_o\omega$, *where* ε_o is the maximum strain amplitude achieved at one quarter of the loading cycle. The value of ε_o in each test was calculated using TA Universal Analysis Software.

2.3. Results

2.3.1. Miscibility

Figure 2-4 shows the images of PVC with various methacryl-POSS contents. All PVC/mPOSS blends with POSS content below 15 wt % were transparent, while the 20 wt % POSS sample is opaque. Miscibility of the PVC/POSS blends was further examined using transmission electron microscopy (TEM). Figure 2-5a shows a micrograph of 15 wt % POSS in PVC, and it appears to be a homogeneous and miscible system. Figure 2-5b shows a micrograph of 20 wt % POSS in PVC, revealing a second phase of submicron-sized aggregates throughout the sample. Since methacryl-POSS appears to be heavy oily liquid at room temperature, the POSS aggregates were squeezed and deformed during microtoming, resulting in the long elliptic morphology seen in Figure 2-5b. Additional evidence of POSS aggregation in the 20 wt % blend is seen in DMA results and will be discussed later. All of the PVC/DOP blends in this study are transparent and homogeneous.

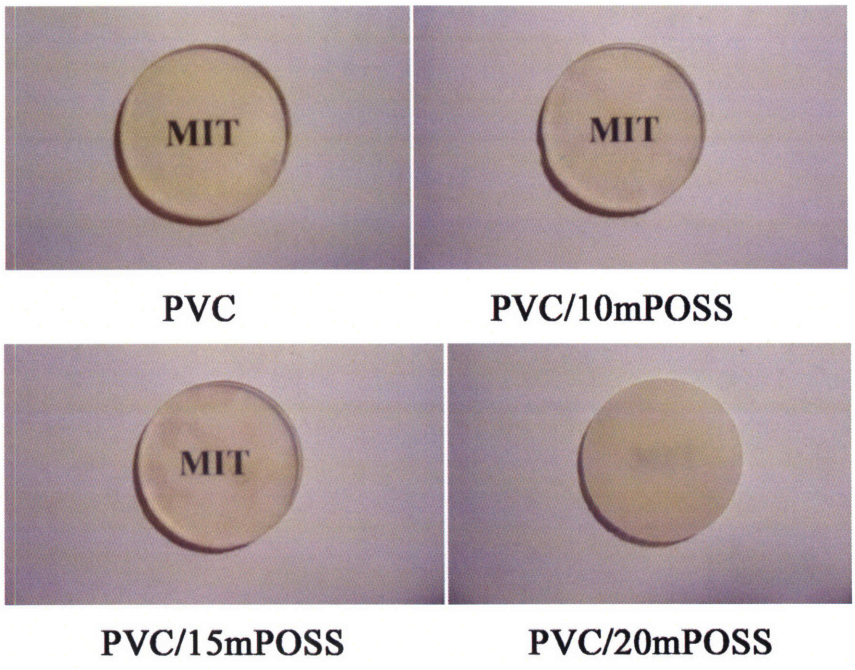

Figure 2-4. Images of compression molded disks of PVC with 10, 15, and 20 wt % methacryl-POSS.

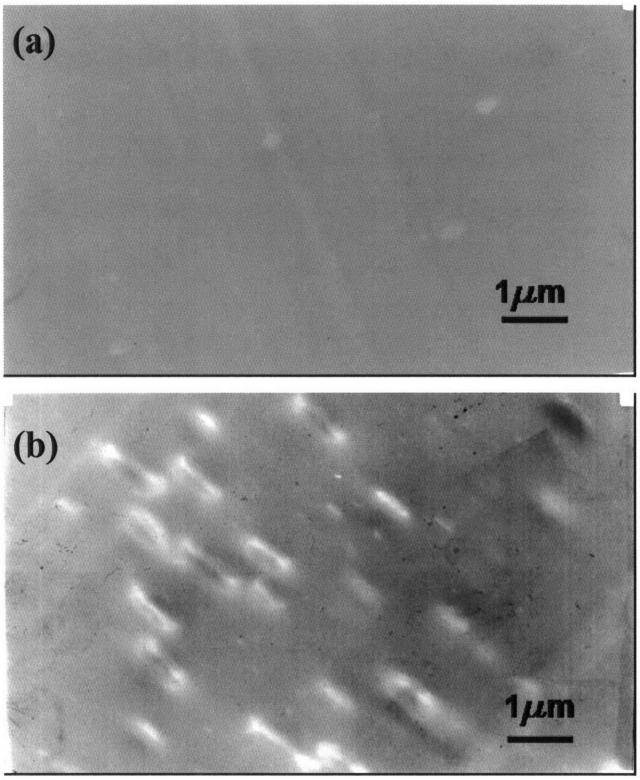

Figure 2-5. Transmission electron micrographs of the PVC/POSS blends: 15 wt % methacryl-POSS (a) and 20 wt % methacryl-POSS (b).

2.3.2. Differential Scanning Calorimetry (DSC)

Figure 2-6 and Figure 2-7 show the DSC results of PVC/DOP and PVC/mPOSS blends, respectively. The neat PVC has a glass transition temperature (T_g) of 71.84 °C in the DSC analysis. The addition of DOP decreases the glass transition temperature monotonically. The transition temperature range also broadens with the increasing DOP content. With 20 wt% DOP added, the inflection point became difficult to identify.

Broad and gradual transitions were also observed in the DSC curves for PVC/mPOSS blends, and exact inflection points of PVC/mPOSS blends were found difficult to identify. An additional small inflection point was observed at near -50 °C in the 20 wt% POSS blend. This is attributed to the aggregated methacryl-POSS, which has a T_g of -55 °C [13]. Due to the broad transition observed in DSC, the glass transition temperatures mentioned in later chapters refer to the α-transition temperatures measured in DMA, unless noted otherwise.

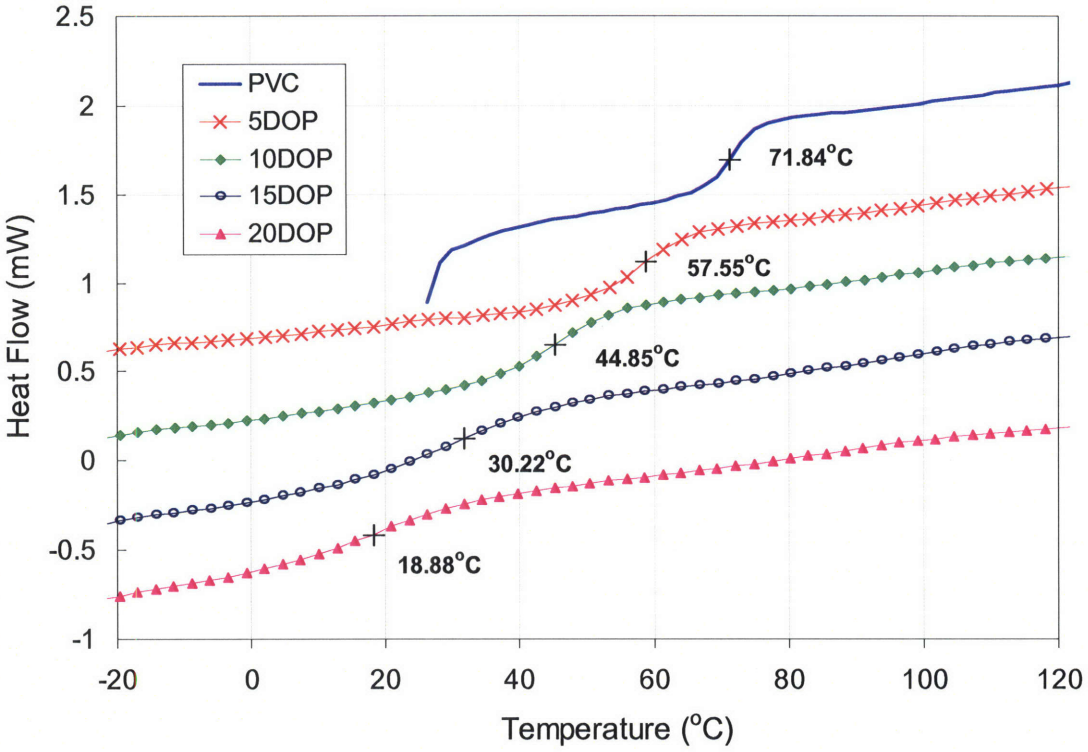

Figure 2-6. DSC curves (exotherm down) of PVC/DOP blends at 10 °C/min heating rate.

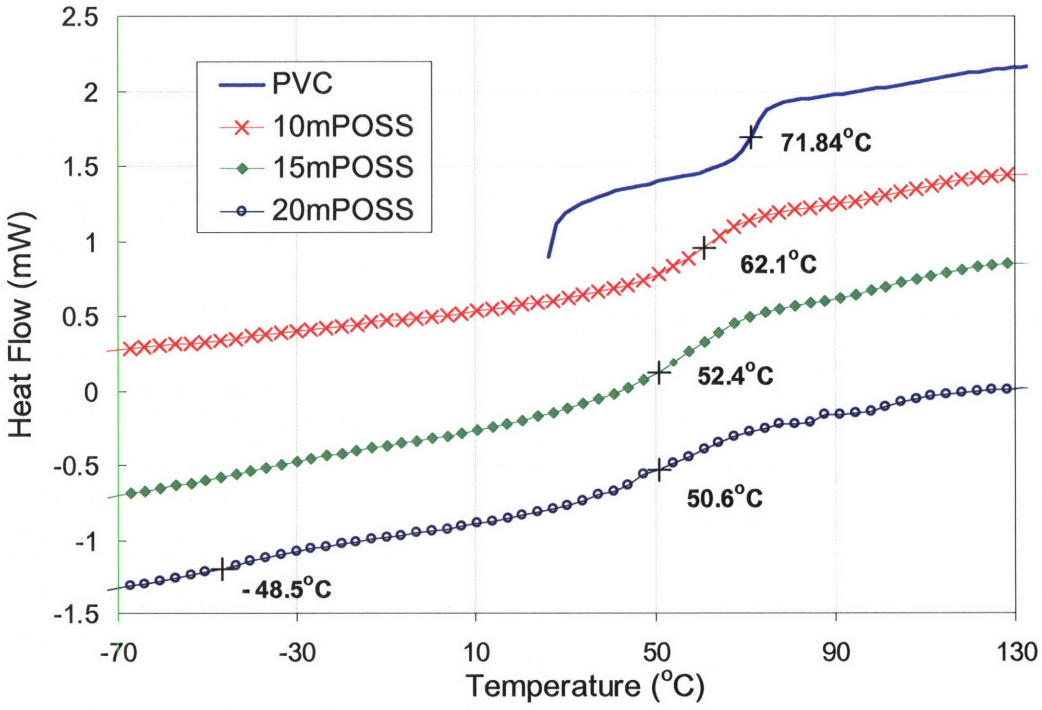

Figure 2-7. DSC curves (exotherm down) of PVC/mPOSS blends at 10 °C/min heating rate.

2.3.3. Dynamic Mechanical Analysis (DMA)

Storage modulus, loss modulus, and tan δ curves of neat PVC at a converted strain rate of 0.005/s (1 Hz) are shown in Figure 2-8. As temperature is increased and PVC goes through the β-transition, the storage modulus gradually decreases from 4.2 to 3.0 GPa, and a broad transition peak appears in the loss modulus and tan δ. At the α-transition, the storage modulus drops sharply from 2.5 GPa to 5.0 MPa, and a narrower and more intense peak can be seen in the loss modulus and tan δ. On the basis of the peak values of tan δ at 0.005/s strain rate, PVC has a β-transition temperature of -50 °C and an α-transition temperature of 85 °C. Both the α-transition and the β-transition are known to be rate-dependent. By testing the material at higher frequencies in the DMA, the strain rate experienced by the sample is increased. The rate dependent DMA data will be discussed in the next chapter.

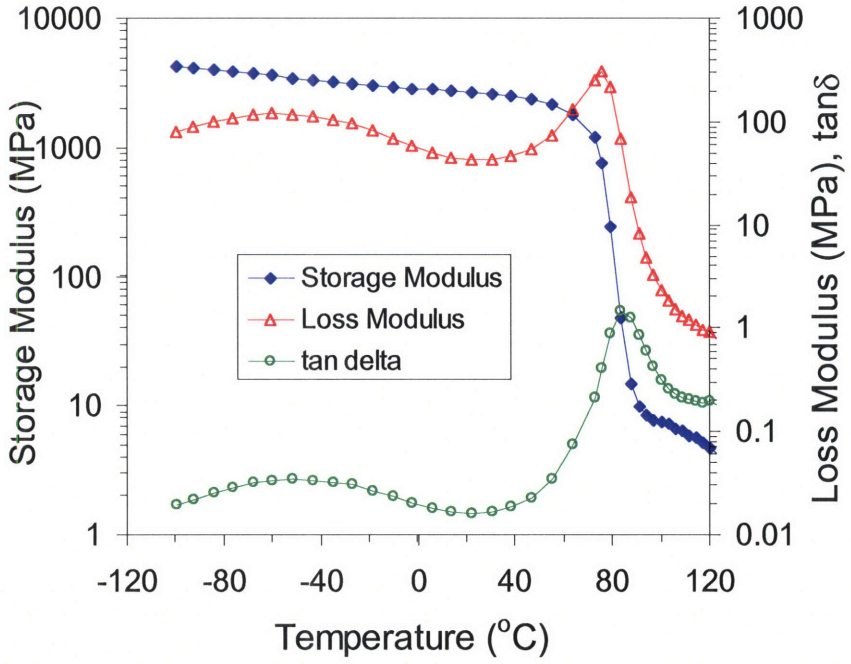

Figure 2-8. PVC storage modulus, loss modulus, and tan δ curves as a function of temperature at 1 Hz (0.005/s).

PVC/mPOSS. Figure 2-9 shows the storage and loss modulus curves for 5, 10, 15, and 20 wt% methacryl-POSS in PVC. The α-transition temperature decreases monotonically for 5, 10 and 15 wt% blends, suggesting that free volume increases in the PVC upon addition of POSS molecules.

Thus, the POSS is acting as a plasticizer. A small inflection in the storage modulus and a bump in loss modulus were observed near -45 °C in the 20 wt% blend, which are consistent with the small inflection observed in the 20 wt% methacryl-POSS DSC curve near -48.5 °C (Figure 2-7. DSC curves (exotherm down) of PVC/mPOSS blends at 10 °C/min heating rate.). Thus, the observation of a bump at -45 °C in the DMA is attributed to the aggregated POSS pools in the 20 wt% blend. The maximum amount of this methacryl-POSS that could be incorporated into PVC homogeneously through melt-blending is somewhere between 15 and 20 wt%. Therefore, the α-transition temperature no longer decreases with increasing POSS concentration at concentration greater than 15 wt% POSS. The β-transition temperature shifts to a lower temperature, and the β-peak lowers and broadens when methacryl-POSS was added. Therefore, the POSS has a plasticizing effect on the β-transition as well as the α-transition due to the liberating effect of free volume on the local motions.

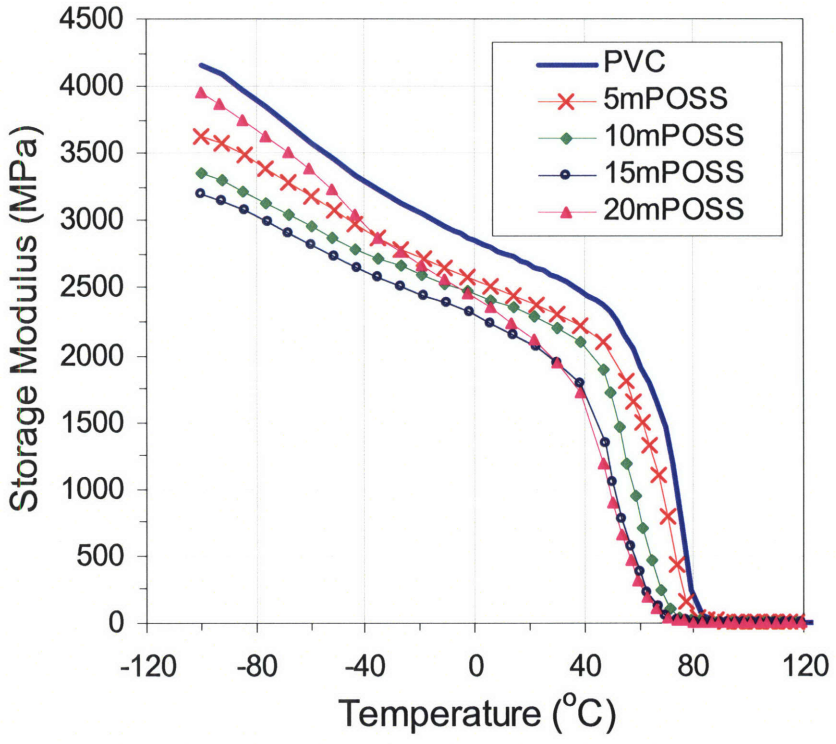

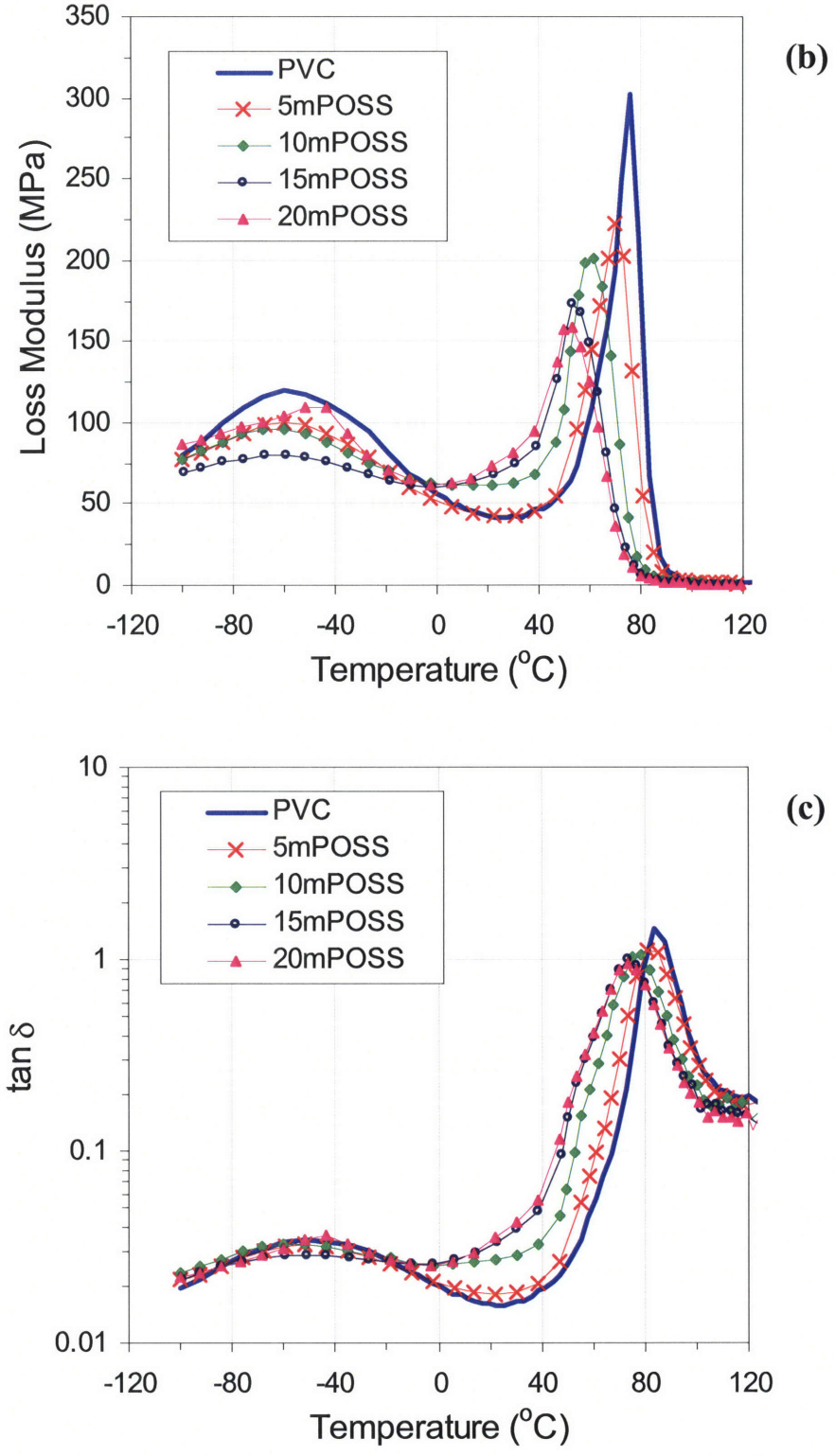

Figure 2-9. Storage modulus (a), loss modulus (b), and tan δ (c) of PVC/mPOSS blends as a function of temperature at 1 Hz (0.005/s).

PVC/DOP. Figure 2-10 shows the storage and loss modulus curves of 5, 10, 15, and 20 wt% DOP in PVC. The α-transition temperature decreases monotonically with the addition of DOP up to 20 wt%, and the α-transition peak also broadens. In the case of the 20 wt% DOP compound, the storage modulus dropoff begins at approximately -20 °C and reaches fully rubbery behavior at around 40 °C. The β-transition is heavily suppressed with increasing DOP content, as evidenced by the dramatic reduction in the magnitude of the β-transition loss modulus peak. Only a very small hump was seen near -70 °C in the loss modulus of the 10 wt% blend, and the peak becomes unrecognizable when DOP concentration is at or above 15 wt%. Furthermore, the storage modulus of the 5 and 10 wt% DOP blend (Figure 2-10a) were slightly higher than the pure PVC in the temperature range between the β- and α-transitions.

Such unexpected mechanical behavior has been observed in slightly plasticized PVC in the glassy state below the glass transition temperature. An increase in modulus, a decrease in creep compliance, and a decrease in impact strength have been documented in PVC containing relatively low concentrations of plasticizers (typically less than 15 wt%) [16-19], and this mechanical behavior is termed "antiplasticization". The decreasing intensity of the β-peak has been observed in many PVC-plasticizer systems since the late 1960s [16-23]. As the plasticizer content increases, the β-peak gradually decreases and ultimately vanishes. The suppression of β-motions is explained by localized interactions between the plasticizer molecules and the PVC repeat units. Vilics et al. [17] proposed that a strong affiliation is established between the aromatic rings of the plasticizer and the PVC backbones, thereby hindering the local short segmental motions (β). Such interaction continues to hinder these local motions even when the temperature exceeds the β-transition temperature and therefore results in a higher modulus at temperatures between the β- and α-transitions. In the case of PVC/DOP, the interaction that hinders the β-motions is the strong hydrogen-bonding between the carbonyl group (>C=O) of DOP and the PVC repeat unit (-[CH_2CHCl]-) [24]. This antiplasticization effect will be further studied and discussed in Chapter 5.

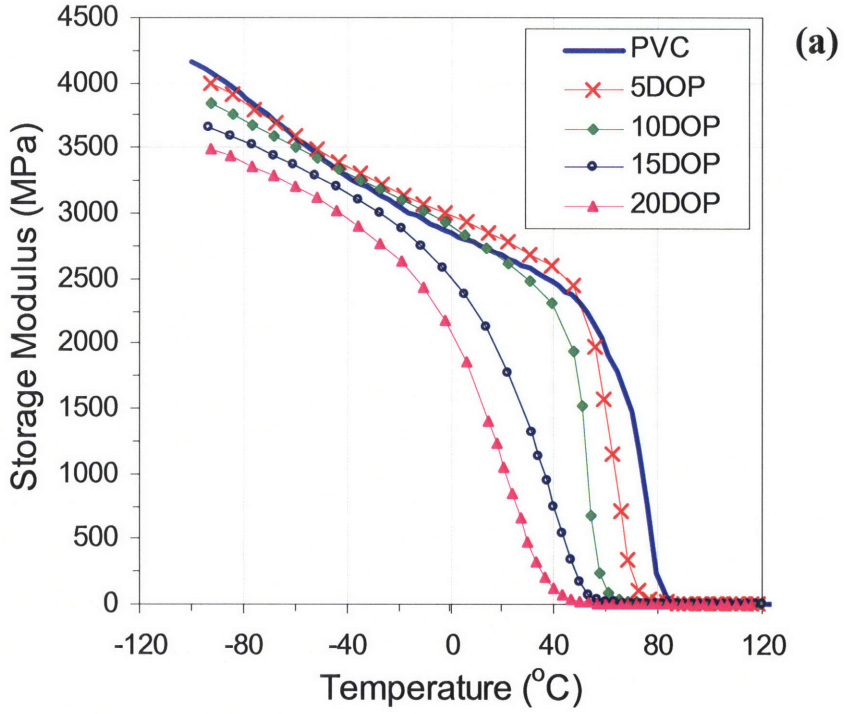
(a)
PVC
5DOP
10DOP
15DOP
20DOP
Storage Modulus (MPa)
4500
4000
3500
3000
2500
2000
1500
1000
500
0
-120
-80
-40
0
40
80
120
Temperature (°C)

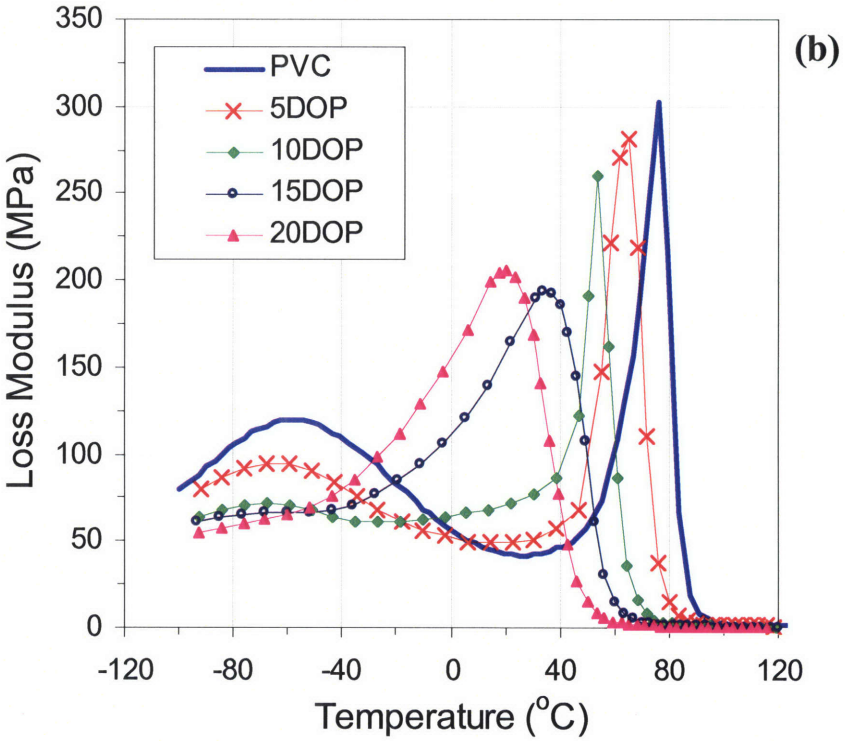
(b)
PVC
5DOP
10DOP
15DOP
20DOP
Loss Modulus (MPa)
350
300
250
200
150
100
50
0
-120
-80
-40
0
40
80
120
Temperature (°C)

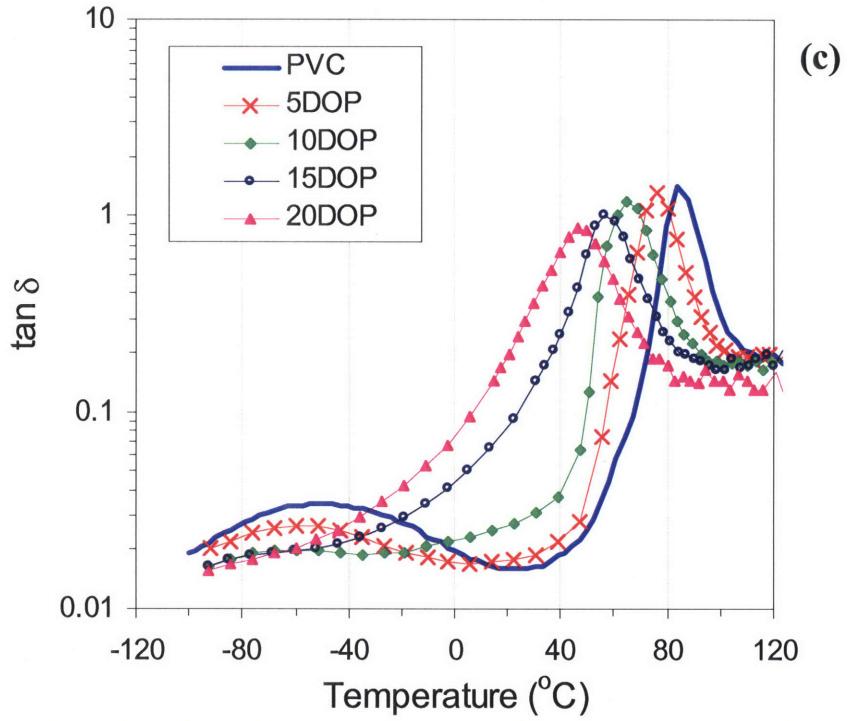

Figure 2-10. Storage modulus (a), loss modulus (b), and tan δ (c) of PVC/DOP blends as a function of temperature at 1 Hz (0.005/s).

mPOSS vs DOP. Unlike DOP, the methacryl-POSS does not restrict the β-motions in PVC and therefore does not "antiplasticize" the PVC. The methacryl-POSS molecule is larger than the DOP molecule, and its bulky, quasi-spherical structure restricts the molecule from such close affiliation with the PVC backbone. The β-motions of the PVC/mPOSS blends are not hindered as in the case of PVC/DOP. It is seen in Figure 2-9b that the loss modulus β-peak is reduced in the case of PVC/mPOSS blends, partially due to the decreasing PVC weight fraction and partially due to the POSS plasticizing the local β-process. The α- and β-transition temperatures were identified by the α- and β-peak values of the tan δ curves. The methacryl-POSS is able to reduce both the α- and β-transition temperatures in the PVC while the DOP reduces the α-transition temperature but restricts the β-motions.

2.4. Conclusions

Methacryl-POSS and DOP were incorporated into PVC through a melt-blending process, and the thermomechanical behavior of these materials was characterized using DSC and DMA. It was found that methacryl-POSS can be incorporated into PVC and result in homogeneous and transparent nanocomposites up to 15 wt% POSS. Above 15 wt%, material becomes opaque and submicron-sized methacryl-POSS aggregates were observed in the blend under TEM.

Both methacryl-POSS and DOP plasticize the PVC. Within the homogeneous regime, T_g (α-transition) decreases monotonically with increasing POSS content. The β-transition temperature shifts slightly to a lower temperature, and the peak becomes broader with the addition of methacryl-POSS. In the case of PVC/DOP blends, a larger reduction was observed in the α-transition temperature and the α-peak broadens with increasing DOP content. However, for the β-transition, the peak vanishes and becomes barely recognizable when the DOP concentration is above 10 wt%. The significant suppression of the β-transition peak is attributed to the molecular interaction between the carbonyl group of DOP and the PVC repeat unit. This interaction attracts the DOP molecules along the PVC main chain and hinders the local β-motions, resulting in an antiplasticization of the β-transition when DOP is added. The difference between incorporating methacryl-POSS and DOP into PVC in the β-transition is explained by the differences in molecular size and shape of POSS and DOP. The bulkiness and quasi-spherical shape restrict POSS molecules from approaching the PVC backbone.

2.5. References

1. Soong, S. Y.; Cohen, R. E.; Boyce, M. C.; Mulliken, A. D., "Rate-Dependent Deformation Behavior of POSS-Filled and Plasticized Poly(vinyl chloride)", *Macromolecules* **2006**, *39*, 2900-2908.

2. Xu, H.; Kuo, S.-W.; Lee, J.-S.; Chang, F.-C., "Preparations, Thermal Properties, and Tg Increase Mechanism of Inorganic/Organic Hybrid Polymers Based on Polyhedral Oligomeric Silsesquioxanes", *Macromolecules* **2002**, *35*, 8788-8793.

3. Mather, P. T.; Jeon, H. G.; Romo-Uribe, A.; Haddad, T. S.; Lichtenhan, J. D., "Mechanical Relaxation and Microstructure of Poly(norbonyl-POSS) Copolymers", *Macromolecules* **1999**, *32*, 1194-1203.

4. Zheng, L.; Farris, R. J.; Coughlin, E. B., "Novel Polyolefin Nanocomposites: Synthesis and Characterizations of Metallocene-Catalyzed Polyolefin Polyhedral Oligomeric Silsesquioxane Copolymers", *Macromolecules* **2001**, *34*, 8034-8039.

5. Philips, S. H.; Haddad, T. S.; Tomczak, S. J., "Development in Nanoscience: Polyhedral Oligomeric Silsesquioxane (POSS)-Polymers", *Curr. Opin. Solid State Mater. Sci.* **2004**, *8*, 21-29.

6. Capaldi, F. M.; Rutledge, G. C.; Boyce, M. C., "Structure and Dynamics of Blends of Polyhedral Oligomeric Silsesquioxanes and Polyethylene by Atomistic Simulation", *Macromolecules* **2005**, *38*, 6700-6709.

7. Kopesky, E. T.; Haddad, T. S.; Cohen, R. E.; McKinley, G. H., "Thermomechanical Properties of Poly(methyl methacrylate)s Containing Tethered and Untethered Polyhedral Oligomeric Silsesquioxanes", *Macromolecules* **2004**, *37*, 8992-9004.

8. Fu, B. X.; Namani, M.; Lee, A., "Influence of Phenyl-Trisilanol Polyhedral Silsesquioxane on Properites of Epoxy Network Glasses", *Polymer* **2003**, *44*, 7739-7747.

9. Fu, B. X.; Gelfer, M. Y.; Hsiao, B. S.; Philips, S. H.; Viers, B.; Blanski, R.; Ruth, P., "Physical Gelation in Ethylene-Propylene Copolymer Melts Induced by Polyhedral Oligomeric Silsesquioxane (POSS) Molecules", *Polymer* **2003**, *44*, 1499-1506.

10. Fu, B. X.; Yang, L.; Somani, R. H.; Zong, S. X.; Hsiao, B. S.; Philips, S.; Blanski, R.; Ruth, P., "Crystallization Studies of Isotactic Polypropylene Containing Nanostructured Polyhedral Oligomeric Silsesquioxane Molecules under Quiescent and Shear Conditions", *J. Polym. Sci.: Part B: Polym. Phys.* **2001**, *39*, 2727-2739.

11. Fina, A.; Tabuani, D.; Carniato, F.; Frache, A.; Boccaleri, E.; Camino, G., "Polyhedral Oligomeric Silsesquioxanes (POSS) Thermal Degradation", *Thermochim. Acta* **2006**, *440*, 36-42.

12. Kopesky, E. T., "Thermomechanical Properties of Polyhedral Oligomeric Silsesquioxane-Poly(methyl methacrylate) Nanocomposites", PhD Thesis, Massachusetts Institute of Tehnology, Cambridge, MA, **2005**.

13. Kopesky, E. T.; Haddad, T. S.; McKinley, G. H.; Cohen, R. E., "Miscibility and Viscoelastic Properties of Acrylic Polyhedral Oligomeric Silsesquioxane-Poly(methyl methacrylate) Blends", *Polymer* **2005**, *46*, 4743-4752.

14. Mulliken, A. D.; Boyce, M. C., "Polycarbonate and a Polycarbonate-POSS Nanocomposite at High Rates of Deformation", *J. Eng. Mater. Technol.* **2006**, *128*, 545-550.

15. Ward, I. M.; Hardley, D., "An Introduction to the Mechanical Properties of Solid Polymers", John Wiley and Sons, New York, **1993**.

16. Kinjo, N.; Nakagawa, T., "Antiplasticization in the Slightly Plasticized Poly(vinyl chloride)", *Polym. J.* **1973**, *4*, 143-153.

17. Vilics, T.; Schneider, H. A.; Manoviciu, V.; Manoviciu, I., "A DMA Study of the Suppression of the β-Transition in Slightly Plasticized PVC Blends", *J. Therm. Anal.* **1996**, *47*, 1141-1153.

18. Pezzin, G.; Ajroldi, G.; Garbuglio, C., "Dynamic-Mechanical Study of the Secondary Transition of Poly(vinyl chloride)", *J. Appl. Polym. Sci.* **1967**, *2*, 2553-2565.

19. Sundgren, N.; Bergman, G.; Shur, Y. J., "Antiplasticization and Transition to Marked Nonlinear Viscoelasticity in Poly(vinyl chloride) (PVC)/Poly-ε-caprolactone (PCL) Blends", *J. Appl. Polym. Sci.* **1978**, *22*, 1255-1265.

20. Dubault, A.; Bokobza, L.; Gandin, E.; Halary, J. L., "Effects of Molecular Interactions on the Viscoelastic and Plastic Behaviour of Plasticized Poly(vinyl chloride)", *Polym. Int.* **2003**, *52*, 1108-1118.

21. Elicegui, A.; del Val, J. J., "A Study of Plasticization Effects in Poly(vinyl chloride)", *Polymer* **1997**, *38*, 1647-1657.

22. Elicegui, A.; del Val, J. J.; Millan, J. L.; Mijangos, C., "α and β Relaxation Processes in Internally Plasticized Poly(vinyl chloride)", *J. Non-Cryst. Solids* **1998**, *235*, 623-627.

23. Bergman, G.; Bertilsson, H.; Shur, Y. J., "Antiplasticization and Transition to Marked Nonlinear Viscoelasticity in Poly(vinyl chloride)/Acrylonitrile-Butadiene Copolymer Blends", *J. Appl. Polym. Sci.* **1977**, *21*, 2953-2961.

24. Garnaik, B.; Sivaram, S., "Study of Polymer-Plasticizer Interaction by ^{13}C CP/MAS NMR Spectroscopy: Poly(vinyl chloride)-Bis(2-ethylhexyl) Phthalate System", *Macromolecules* **1996**, *29*, 185-190.

Chapter 3: Rate-Dependent Mechanical Properties of POSS-Filled and Plasticized Poly(vinyl chloride)

[Part of this work has been published previously, in slightly different form, in "Rate-Dependent Deformation Behavior of POSS-Filled and Plasticized Poly(vinyl chloride)" by S.Y. Soong, R.E. Cohen, M.C. Boyce, and A.D. Mulliken, *Macromolecules* **2006**, *39*, 2900-2908 [1].]

3.1. Introduction

3.1.1. Effect of Nanoparticles on Rate-Dependent Mechanical Behavior

The transition observed in the rate-dependent mechanical behavior of many glassy polymer is related to the local β-relaxation motions of the material. A transition in rate sensitivity of the yield behavior has been observed in various homopolymers, including poly(methyl methacrylate) (PMMA) [2-5], polycarbonate (PC) [6,7], and poly(vinyl chloride) (PVC) [6,8,9]. As the temperature is reduced and/or the strain rate is increased, an additional stress is required to activate the secondary (β) process in order for the material to yield.

As nanoparticles are incorporated into a polymer, the molecular level modifications offer opportunities to tailor the rate-dependent mechanical deformation and failure behavior of the polymer. Polymer nanocomposites have drawn much attention due to the potential for improvement in properties including modulus, strength, toughness, thermal stability, and gas permeability. Research regarding α- and β-relaxation processes of polymer nanocomposites has been conducted to understand the influence of nanoparticles on polymeric molecular motions [10-12].

Böhning et al.[10,11] showed that incorporating a low content of SiC nanoparticles in PC has no effect on the α-transition; however, the β-transition is broadened and the activation energy of the β-transition is reduced with increasing nanoparticle concentration [11]. Kuila et al. [12] showed that the α- and β-transition temperatures and the melting point of poly(3-hexylthiophene) were increased when montmorillonite clay particles are incorporated into the polymer system and the 1% clay content polymer nanocomposite exhibits the maximum thermal stability. Mulliken et al. [13] demonstrated that the incorporation of TriSilanolPhenyl-POSS in PC, while having little

influence on the α-regime, enhances the mobility of the β-motions significantly and therefore reduces the resistance to high rate elastic and plastic deformation. Kopesky et al. [14] observed toughening in PMMA in slow-speed tension when different POSS nanoparticles were incorporated into PMMA.

This Chapter focuses on the rate-dependent deformation behavior of polymer compounds comprised of polyhedral oligomeric silsesquioxanes (POSS) blended with PVC.

3.1.2. Split-Hopkinson Pressure Bar

The split-Hopkinson pressure bar system has been the primary testing method for obtaining material mechanical properties in homogenous deformation at high strain rates. The theory of high strain rate testing using a split-Hopkinson pressure bar apparatus has been well documented, and examples can be found in ref. [15-17].

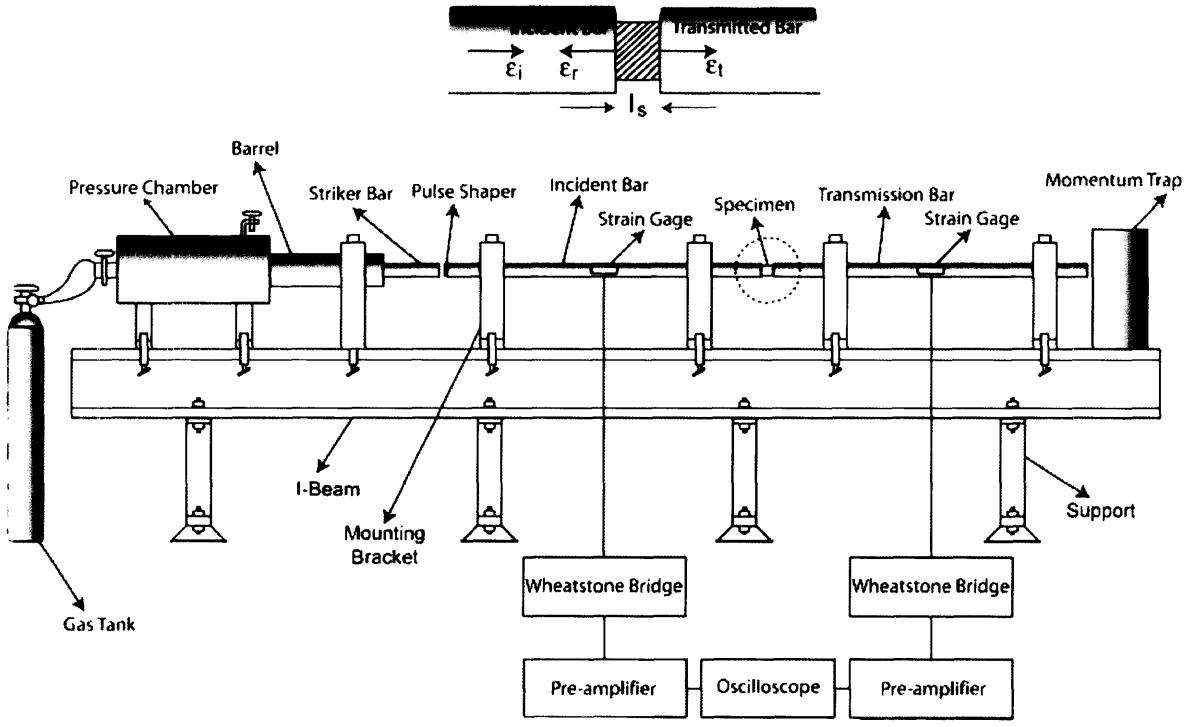

Figure 3-1. Schematic of a split-Hopkinson pressure bar apparatus (courtesy of O. Samudrala).

Figure 3-1 shows the schematic of a typical split-Hopkinson pressure bar system. This apparatus consists of two long pressure bars, an incident bar and a transmission bar, and a short striker bar. The specimen is positioned between the incident bar and the transmission bar. A typical test is initiated when high pressure gas is release from the pressure chamber, causing the striker bar to eject from the barrel. When the striker bar impacts the incident bar, it produces a compressive stress wave that travels through the incident bar until the specimen surface is reached. Due to the mismatch of material properties at the interface of incident bar and specimen, a portion of the wave is reflected back to the incident bar while the remaining transmits through the specimen and travels down the transmission bar. Corresponding strains of the three compressive stress pulses of interest – the incident, the reflected, and the transmitted – are recorded by the strain gages mounted on the bars during the test. An example of recorded strain signals of polycarbonate (PC) is shown in Figure 3-2.

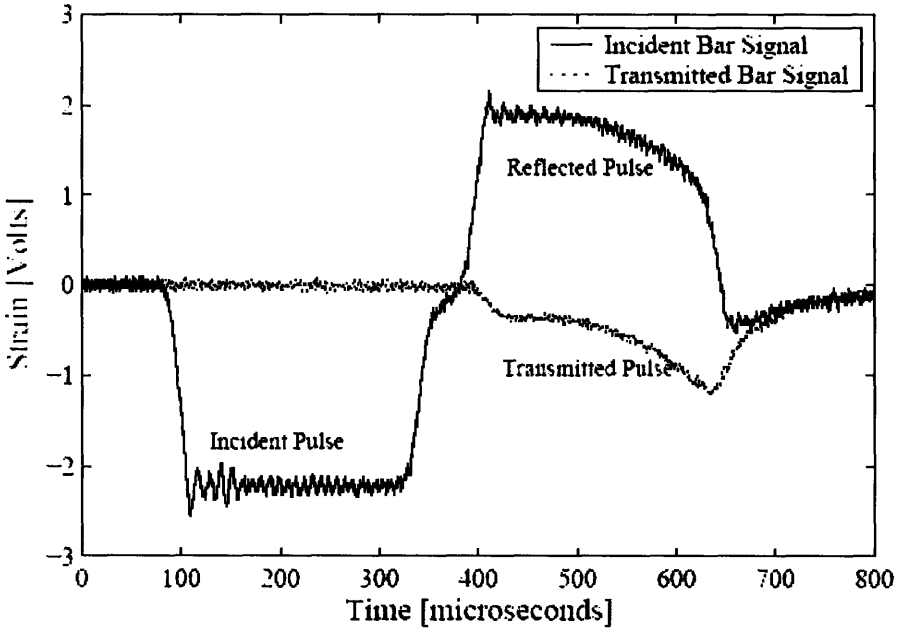

Figure 3-2. Strain gage signals collected from a split-Hopkinson bar test (PC).

To analyze the pulse signals and acquire the corresponding stress-strain behavior, significant conditions in the system geometry and bar materials must be met in order to obtain accurate data using theory to reduce the signals acquired during testing with the split-Hopkinson pressure bar.

Those system conditions and corresponding data reduction conditions include: 1. High aspect ratio bars such that the wave propagation is one-dimensional; 2. Bar material and geometry selection such that the strains in the pressure bars are only elastic strains; 3. Friction, radial inertia, and longitudinal inertia can be neglected; 4. Stress waves recorded at the gage locations are identical to the stress waves experienced at the interface between the bar and the specimen; and 5. The specimen is in dynamic equilibrium.

With the assumption that wave propagation is one-dimensional, a general equation of motion for wave propagation can be written as:

$$\frac{\partial^2 u}{\partial x^2} = \frac{1}{c^2}\frac{\partial^2 u}{\partial t^2} \tag{3-1}$$

where u is the displacement along the x-direction, t is time, and $c = \sqrt{E/\rho}$ is the acoustic wave speed in an elastic medium. Assuming the conditions mentioned above are true, Eq. (3-1) will lead to the simplified final stress and strain rate equations:

$$\dot{\varepsilon} = \frac{2c\varepsilon_r}{l_s} \tag{3-2}$$

$$\sigma = \frac{A_b E \varepsilon_t}{A_s} \tag{3-3}$$

where ε_r is the corresponding tensile strain of the reflective pulse, ε_t is the corresponding compressive strain of the transmitted pulse, l_s is the length of the specimen, A_b is the cross-sectional area of the bar, and A_s is the cross-sectional area of the specimen. In practice, the strain is obtained through numerical integration of Eq. (3-2).

Since there is no standard method for the split-Hopkinson bar test, nor a standard design, the experiment faces many issues. These issues include: proper choice of the bar material, axial alignment of the striker and pressure bars, optimization of the electronic settings for data acquisition, accounting for the effects of friction and wave dispersion, and last but not least, the

selection of proper specimen geometry. More detailed discussions on split-Hopkinson pressure bar can be found in ref. [15-18].

3.2. Experimental Section

3.2.1. Uniaxial Compression Testing

Uniaxial compression tests were performed over a wide range of strain rates (from 10^{-4}/s to nearly 4000/s) using four pieces of equipment including a Zwick mechanical tester, two split Hopkinson pressure bar apparatus, and a MTS machine. Extruded polymer strands from DACA were pelletized, compression-molded into disks, and then machined into right circular specimens for compression testing. Specimen dimensions were modified to suit different compression testing apparatus; however the ratio of diameter to height was maintained at 2 to 1. All specimens tested in compression deformed uniformly until the final strains were reached, as shown in Figure 3-3.

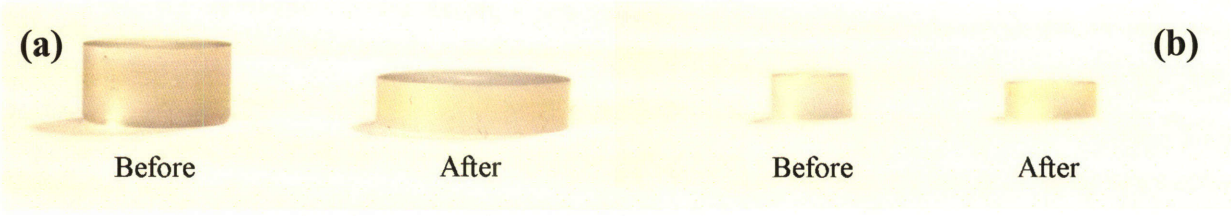

Figure 3-3. Images of specimens before and after compression testing: low rate compression testing (a) and high rate compression testing (b).

Low Rate Compression Testing. Low rate compression testing (10^{-4}/s to 10^{-1}/s) was accomplished on a Zwick mechanical tester (Zwick Roell Group). All specimens were machined to right circular cylinders with diameter of 9 mm and height of 4.5 mm. To reduce friction, thin Teflon films were placed between specimen and compression platens, and WD-40 lubricant was sprayed between Teflon films and platens. During low rate compression tests, a constant engineering strain rate was applied to a final true compressive strain of -0.70.

Moderate Rate Compression Testing. Moderate strain rate compression testing was performed on a MTS machine (1/s to 50/s) and a long split Hopkinson pressure bar (150/s to 600/s) in

collaboration with Professor Wayne Chen at Purdue University. Specimens for MTS machine were machined to right circular cylinders with diameter of 9 mm and height of 4.5mm; specimens for long split Hopkinson pressure bar were machined to right circular cylinders with diameter of 5.08 mm and height of 2.54 mm. Specimens of both the MTS machine and the long Hopkinson pressure bar were lubricated with a thin layer of petroleum jelly on both surfaces prior to testing to reduce friction. Copper pulse shapers were used in the long Hopkinson pressure bar testing.

High Rate Compression Testing. High strain rate compression testing (700/s to 4000/s) was conducted on a split Hopkinson pressure bar apparatus located at MIT. It was designed in cooperation with and built by Physics Applications, Inc. (Dayton, OH). This particular instrument is described in Mulliken and Boyce [18-20]. Specimens for high rate testing were machined to smaller right circular cylinders with diameter 5 mm and height 2.5 mm to meet the particular requirements of this test. Specimens were lubricated with a thin layer of petroleum jelly on each surface prior to testing. In the case of high rate testing, samples were tested under true strain rates at yield from 700/s to 4000/s.

3.2.2. Tensile Testing

Uniaxial tensile tests were also performed on the Zwick mechanical tester. All specimens were tested at a constant engineering strain rate of 10^{-3}/s until final failure. Extensometers were employed to determine the tensile strains. Pelletized materials were compression-molded into dog-bone-shaped specimens with gauge length of 25.4 mm, thickness of 1.6 mm, and width of 4.2 mm.

3.3. Results

3.3.1. Dynamic Mechanical Analysis

As mentioned in the previous chapter, both the α- and β-transitions are rate dependent and the locations of both transition peaks shift to higher temperatures with increasing strain rate. By testing the material at higher frequencies in the DMA, the strain rate experienced by the sample is increased, which enabled us to characterize the rate-dependent behavior of α- and β-transitions.

Figure 3-4 shows the shifting of the α-peak and the β-peak in storage and loss modulus curves for PVC. Since the β-transition has a much lower activation energy (~14.4 kcal/ mol) when compared to the α-transition (~66 kcal/mol) in PVC, the β-transition peak in loss modulus shifts faster than the α-transition. Based on the loss modulus curve, the β-peak shifted from -60 °C at 1 Hz to -20 °C at 100 Hz, whereas the α-peak shifted from 76 °C at 1 Hz to 83 °C at 100 Hz. Wider α- and β-transition peaks are also observed at higher strain rates.

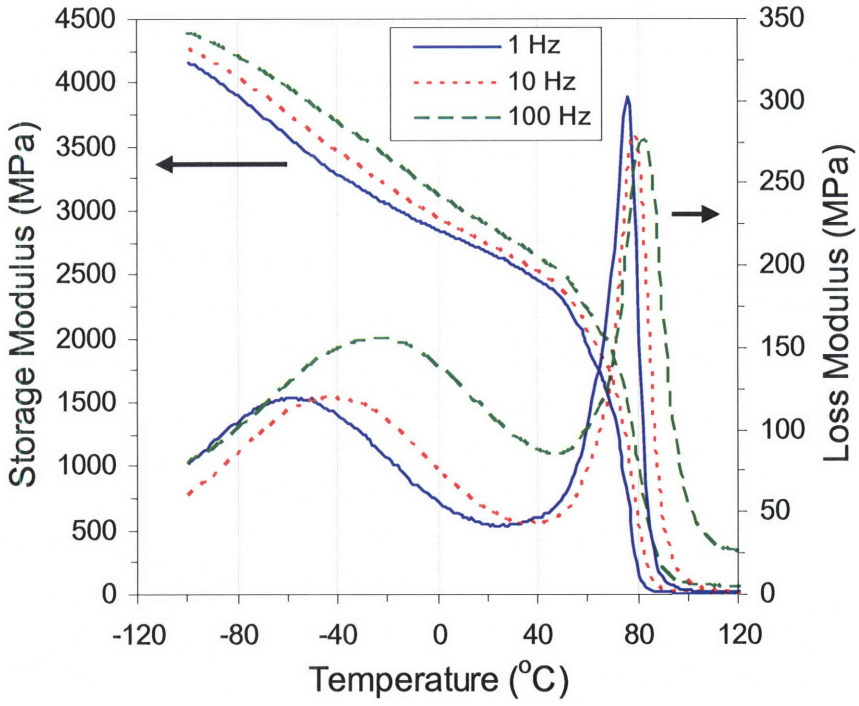

Figure 3-4. Storage and loss modulus curves of PVC as a function of temperature at 1, 10, and 100 Hz (corresponding to strain rate ranges from $5x10^{-3}$ to $5.8x10^{-1}$/s).

Figure 3-5 summarizes the rate dependency of α-transition of all blends. Incorporating either methacryl-POSS or DOP lowers the α-transition temperature. The α-transition temperature shifts to higher temperatures with increasing strain rate. The α-transition of PVC shifts approximately 3.8 °C per decade increase in strain rate.

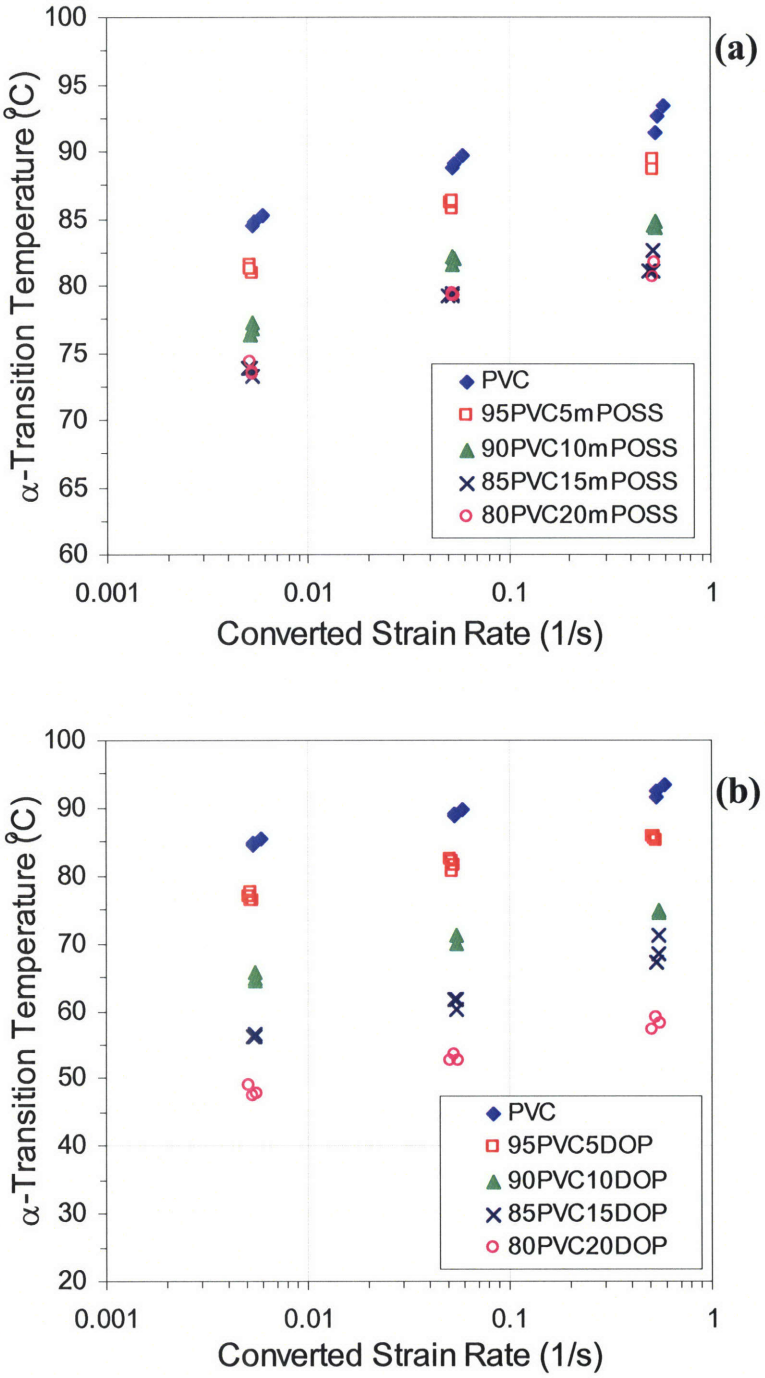

Figure 3-5. α-Transition temperature of PVC/mPOSS (a) and PVC/DOP (b) as a function of converted strain rate (tan δ peak value in DMA).

Table 3-1. Shifting of α- and β-transition temperatures (tan δ peak value in DMA).

	α (°C/decade strain rate)	β (°C/decade strain rate)
PVC	3.8	19.5
5 wt% mPOSS	3.9	18.3
10 wt% mPOSS	3.9	18.5
15 wt% mPOSS	4.0	18.0
5 wt% DOP	4.4	-
10 wt% DOP	4.8	-
15 wt% DOP	5.1	-
20 wt% DOP	5.1	-

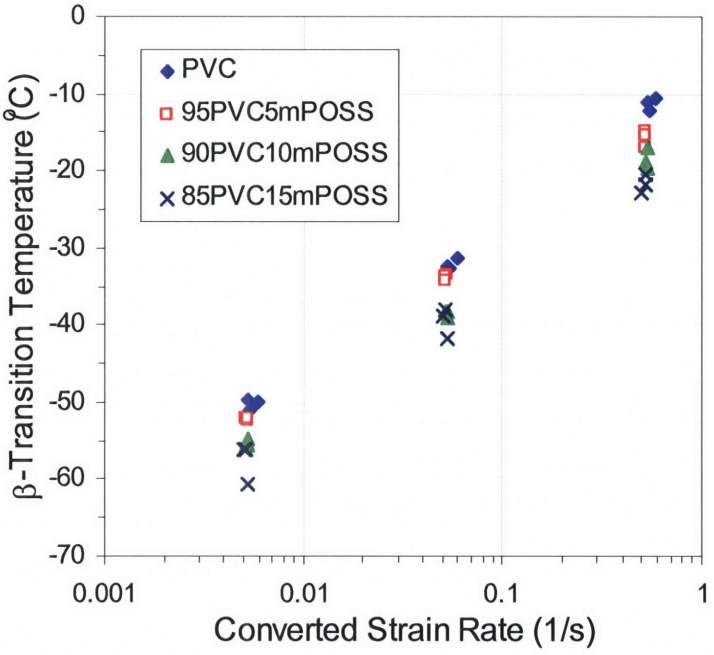

Figure 3-6. β-Transition temperature of PVC/mPOSS as a function of converted strain rate (tan δ peak value in DMA).

Table 3-1 shows that within the DMA testing range the shifting rate of the α-transition temperature in all blends ranges from 3.8 to 5.1 °C per decade increase in strain rate. The rate

dependence of the β-transition of PVC/POSS blends is shown in Figure 3-6. The β-transition temperature is lowered approximately 7 °C when 10 or 15 wt% methacryl-POSS is added. The β-peak shifting rate of the two blends remains approximately the same as neat PVC. The β-peak values in tan δ suggests that β-transition shifts nearly 17.4 °C per decade increase in strain rate, which indicates that β-transition is more sensitive to the change in strain rate than the α-transition. The β-process becomes significant in the mechanical behavior when its rapid shifting with strain rate causes the β-transition to move into the experimental window of deformation rate at the testing temperature. PVC/DOP data are not included in Figure 3-6 since the β-motions are suppressed and the β-peaks cannot be clearly identified when DOP content is higher than 10 wt%.

3.3.2. Uniaxial Compression Testing

Compression testing was conducted using the Zwick machine at MIT, the MTS machine and long split Hopkinson bar at Purdue University, and the split Hopkinson bar at MIT for low to high strain rate testing. All specimens were tested to large strains, capturing the elastic, initial yield, and post-yield behavior. Deformation was homogeneous in all compression tests; no cracks or other fracture events were observed.

Rate Dependence of Stress-Strain Behavior. Figure 3-7 to 3-10 show the compression true stress-true strain curves for PVC, PVC with 15 wt% POSS, PVC with 20 wt% DOP, and PVC with 40 wt% DOP, respectively, at tested strain rates. The rate-dependent behavior is clearly seen in these figures, where the initial yield stress increases with an increase in strain rate. Similar glassy polymer stress-strain behavior was observed in compression testing for PVC, all PVC/methacryl-POSS blends and PVC/DOP blends with DOP content less than 15 wt%. With increasing strain rate, PVC with 20 wt% DOP exhibited a transition from rubbery to glassy (Figure 3-9). DMA revealed the PVC/20 wt% DOP material to have an α-transition at 45 °C at a converted strain rate of 0.005/s based on the tan δ curve. Therefore, a rubberlike deformation behavior was expected and found in low rate compression testing (Figure 3-9). In the case of high rate compression tests, the α-transitions shift to higher temperatures (a linear extrapolation of Figure 3-5b estimates an α-transition temperature of 76 °C at 2000/s), and glassy polymer deformation behavior was observed again.

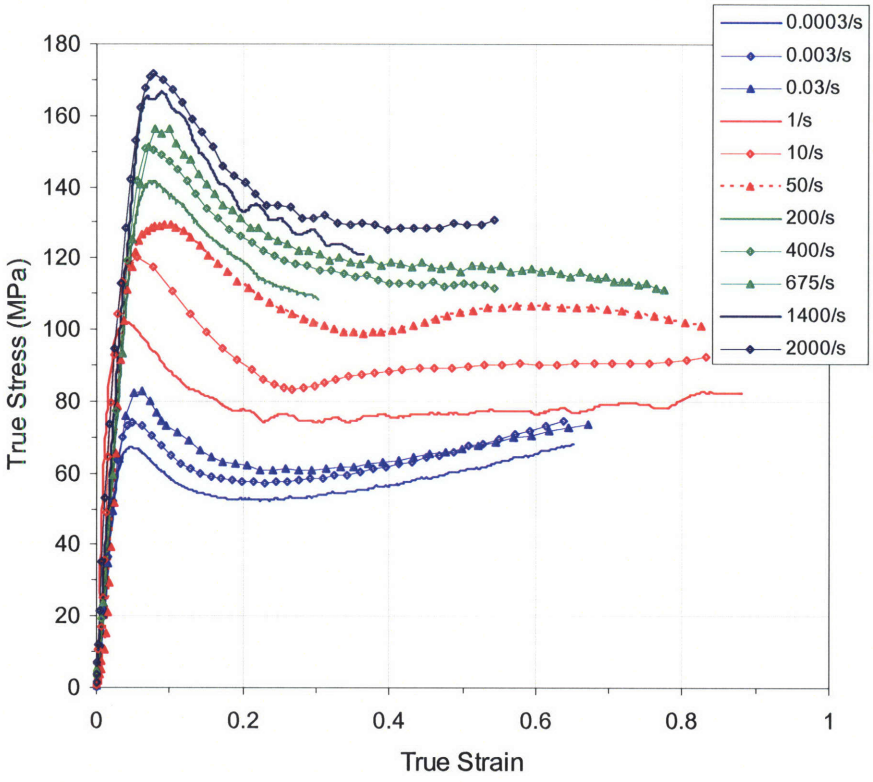

Figure 3-7. True stress-true strain curves of PVC under different strain rates (10^{-4}-2000/s) in uniaxial compression testing.

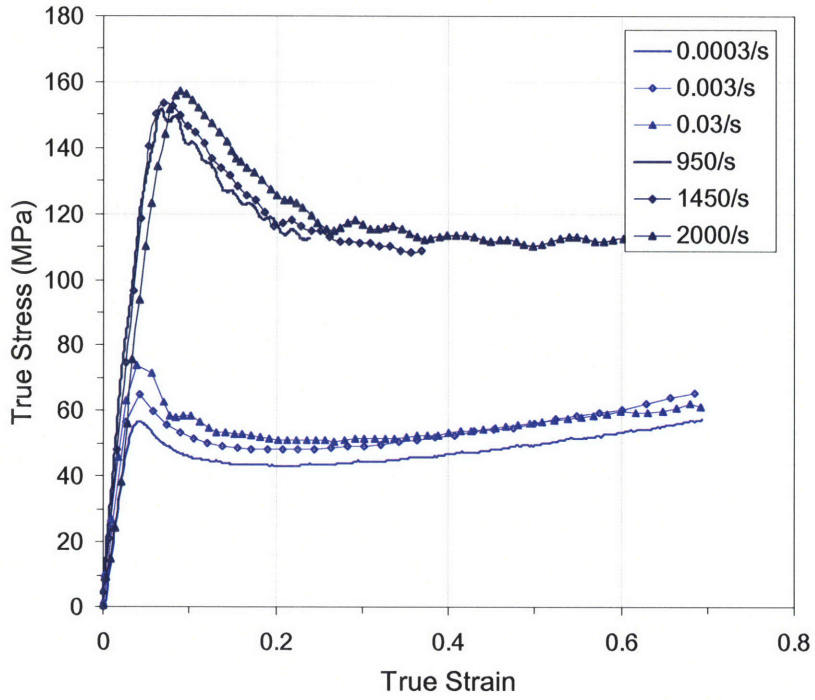

Figure 3-8. True stress-true stain curves of 85 wt% PVC/15 wt% mPOSS under different strain rates (10^{-4}-2000/s) in uniaxial compression testing.

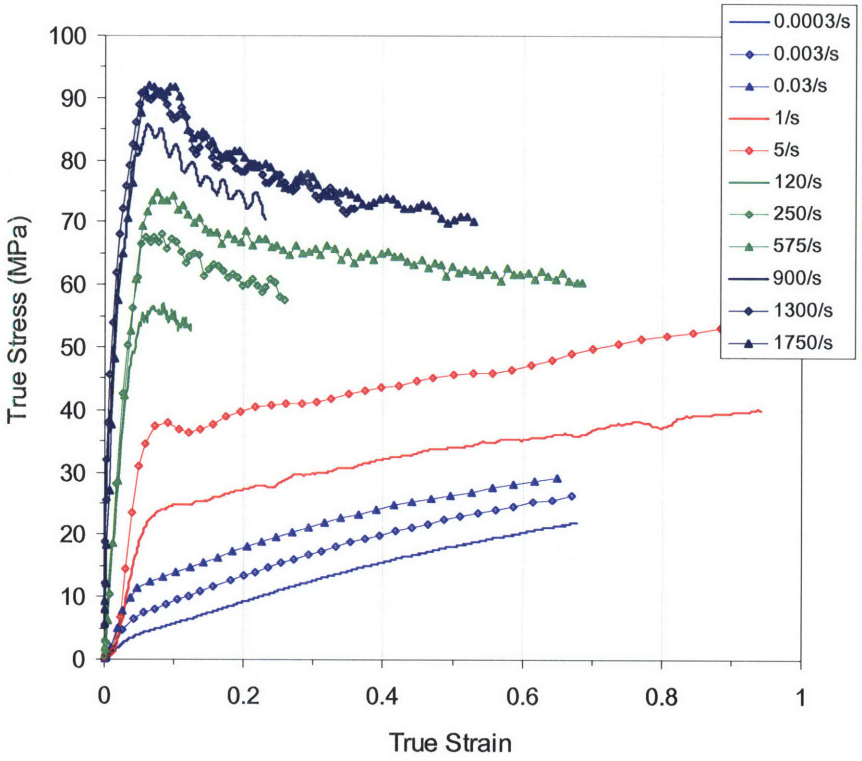

Figure 3-9. True stress-true strain curves of 80 wt% PVC/20 wt% DOP under different strain rates (10^{-4}-2000/s) in uniaxial compression testing.

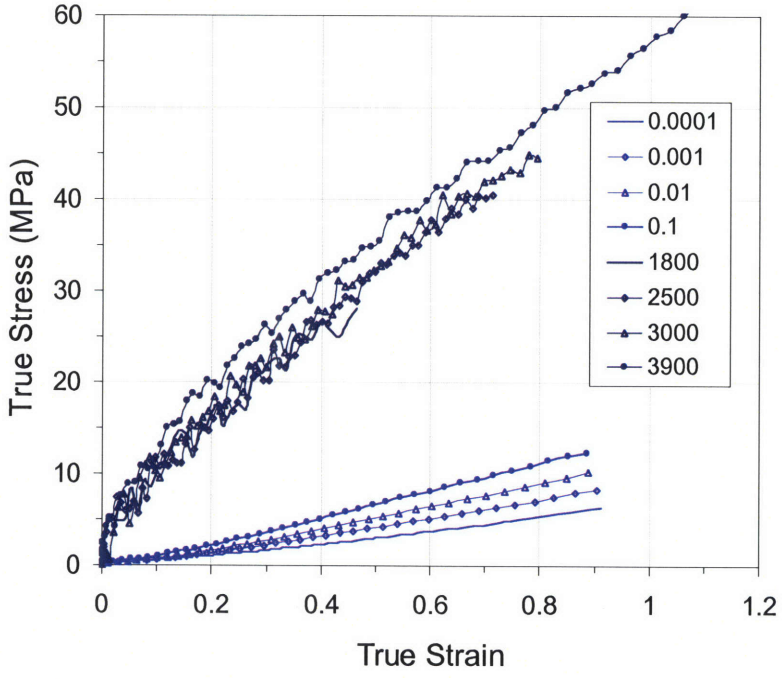

Figure 3-10. True stress-true strain curves of 60 wt% PVC/40 wt% DOP under different strain rates (10^{-4}-4000/s) in uniaxial compression testing.

Yield stress as a function of strain rate is shown in Figure 3-11 for all of the PVC/mPOSS and PVC/DOP blends. The neat PVC yield stress increases linearly with the logarithm of strain rate in the low strain rate regime. As strain rate increases into the high rate regime, the yield stress again increases approximately linearly with the logarithm of strain rate. However, the rate dependence is much greater in this high rate regime. At strain rates beyond the transition point, an additional stress is necessary to activate the β-process in order to yield the material.

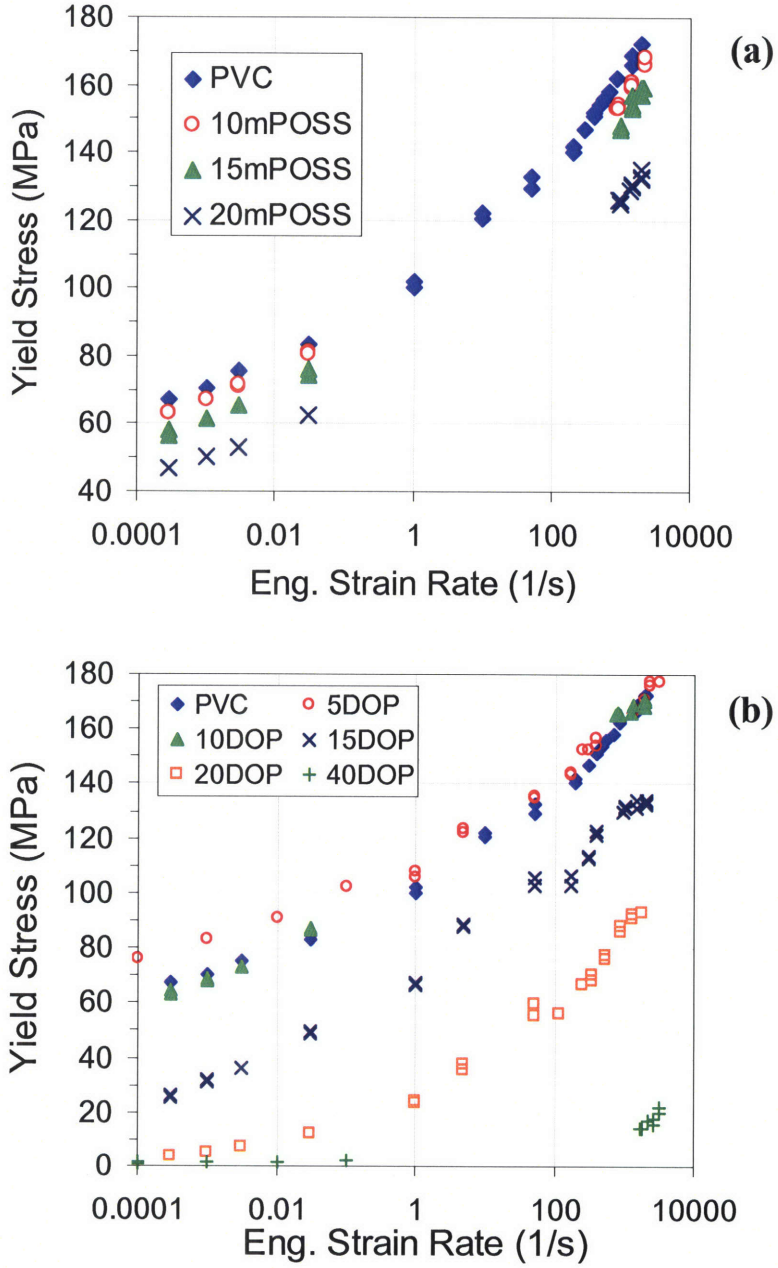

Figure 3-11. Yield stress as a function of strain rate: PVC/mPOSS (a) and PVC/DOP (b).

Figure 3-11a shows the effect of methacryl-POSS on yield stress in PVC. The yield strength decreases with an increase in POSS content due to the plasticizing effect of the POSS and the corresponding increased chain mobility. Rate-sensitivity transitions were also observed in the POSS-filled PVC materials and again this observation correlates with the rate dependence of the β-transition observed in the DMA. The yield stress deceased monotonically with increasing POSS concentration up to 15 wt%, and a larger reduction in the yield stress was observed due to the existence of POSS aggregates in the 20 wt% POSS blend. The rate dependence of yield stress on DOP addition is shown in Figure 3-11b. Antiplasticization was observed in the PVC/DOP blends. A higher yield stress was found in PVC/5 wt% DOP in the low rate regime, and the addition of 10 wt% DOP does not appear to alter the yield stress when compared to the neat PVC. This observation results from the compensating effects of plasticizing the α-motions, acting to decrease the resistance, and antiplasticizing the β-motions, which tends to increase the resistance. More detailed discussions regarding the antiplasticization phenomenon will appear in Chapter 5. Since the local β-motions were restricted from the low rate regime to the high rate regime, no distinct rate-sensitivity transition in yield stress was observed in PVC/DOP blends with DOP content from 5 to 15 wt%.

Two distinct yield stress rate sensitivities are observed in the 20 wt% DOP-modified materials; however, it is the rate dependence of the α-regime that governs this behavior. The yield strength of the 20 wt% DOP compound is less sensitive to the strain rate in the low rate regime because the material is rubbery; in the high rate regime, this blend behaves like a glassy polymer again; hence, the transition in overall magnitude with the yield stress in the PVC/DOP is a transition from rubbery to leathery to glassy behavior as we go from low rates to very high rates.

Stress-Strain Dependence on Additive Concentration. The effect of methacryl-POSS and DOP on the entire true stress-true strain behavior of PVC at both low and high strain rates is shown in Figure 3-12 and Figure 3-13, respectively. The addition of POSS reduces the yield strength and the flow stress of PVC in both the low strain rate (0.0003/s) and the high strain rate (2000/s) compression tests. More substantial reductions in the true stress-true strain curves were observed in the case of PVC/DOP blends, and the influence of DOP appears to be different in the low (0.001/s) and high (2000/s) strain rates.

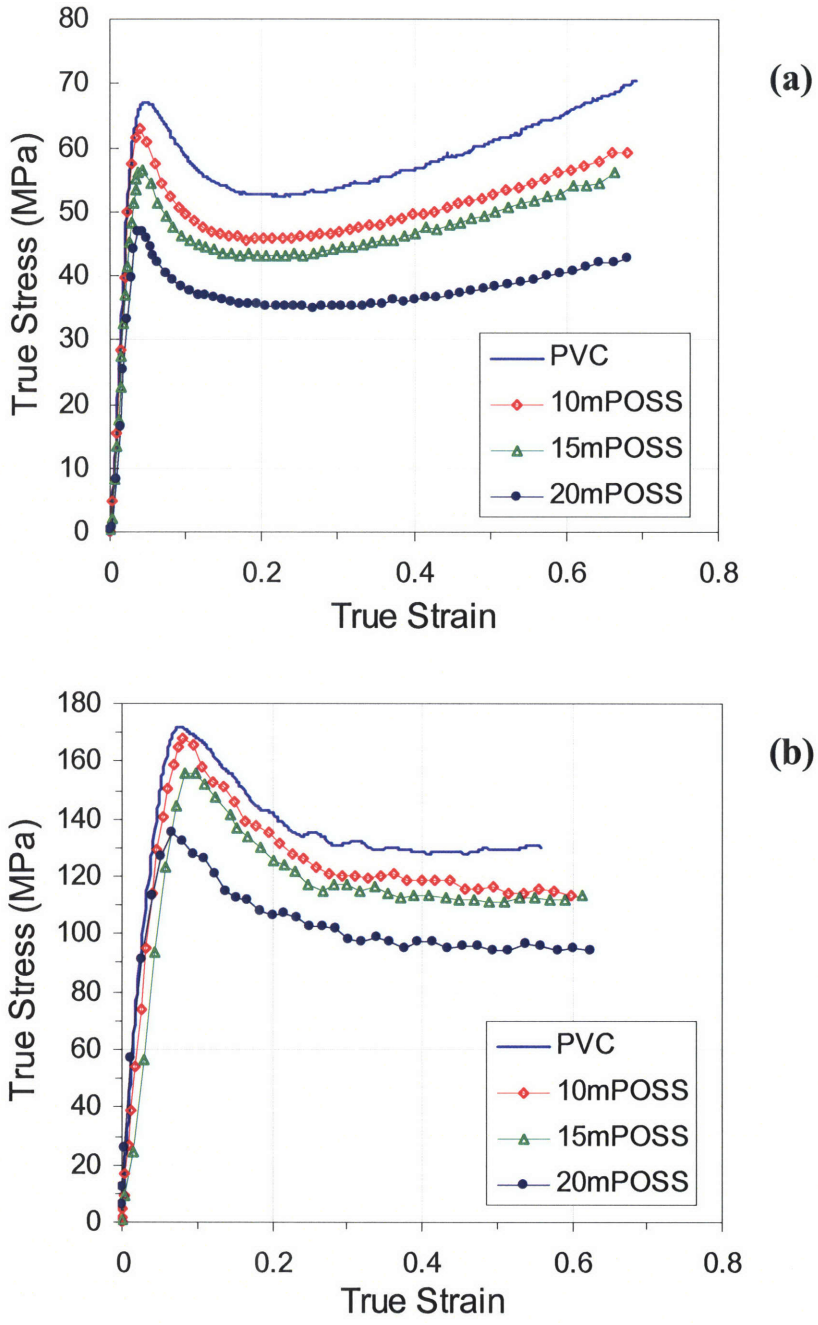

Figure 3-12. Effect of methacryl-POSS on true stress-true strain behavior in uniaxial compression testing: $\dot{\varepsilon}$ =0.0003/s (a) and $\dot{\varepsilon} \approx$2000/s (b).

A more substantial antiplasticization effect in yield was observed in slightly plasticized PVC at 0.001/s than at 2000/s. The yield strength of 5 wt% DOP is much higher than neat PVC at the low rate and it becomes approximately the same at the high rate. The yield strength of the 10

wt% DOP blend is nearly identical to the neat PVC in both the low and high strain rates. However, both the 5 and 10 wt% DOP compounds exhibit dramatic postyield strain softening, and hence their flow stresses are reduced significantly at all strain rates.

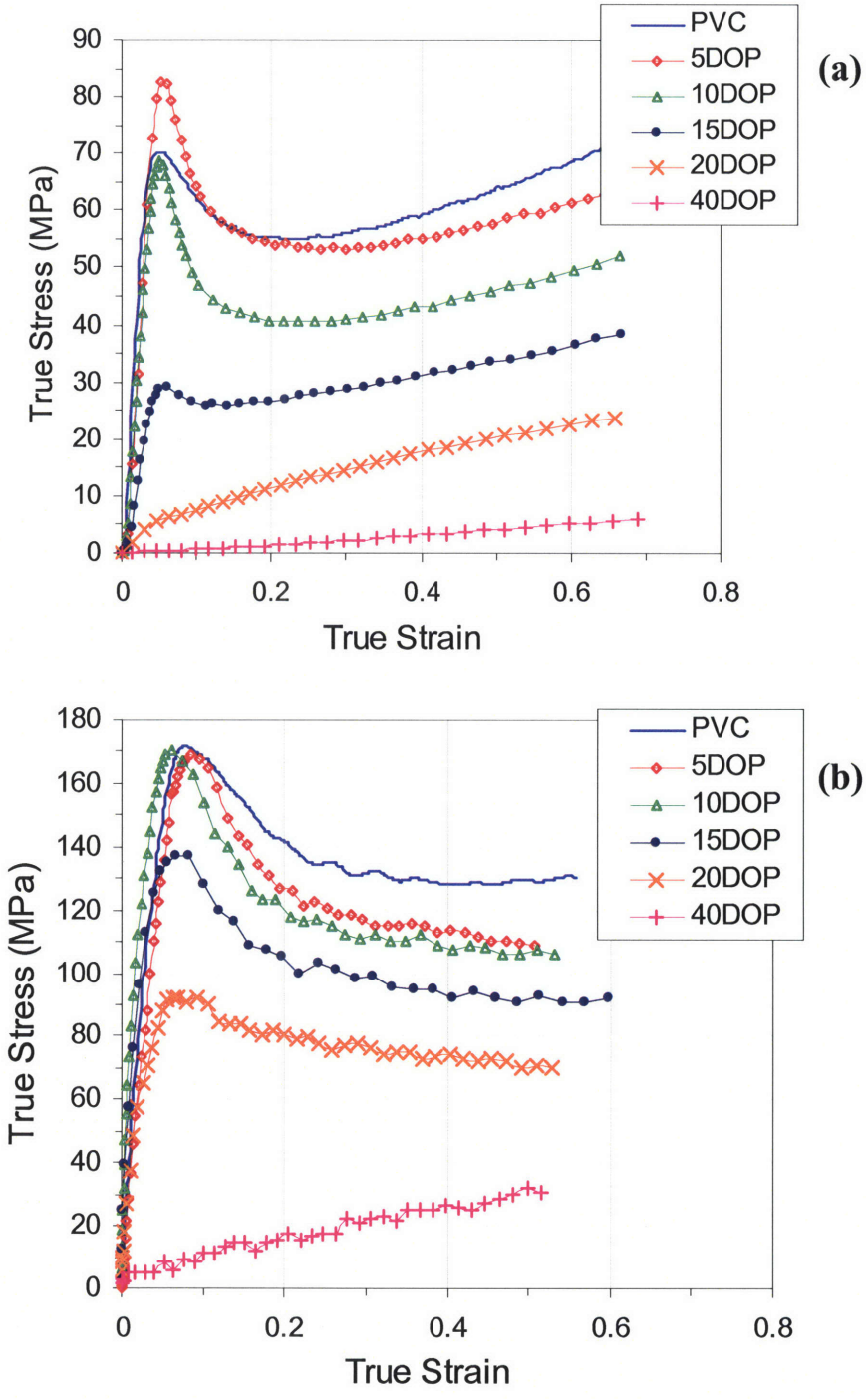

Figure 3-13. Effect of DOP on true stress-truie strain behavior in uniaxial compression testing: $\dot{\varepsilon}$ =0.001/s (a) and $\dot{\varepsilon} \approx$ 2000/s (b).

Previous publications have shown that a polymer undergoing active plastic deformation at temperature well below T_g is locally in a state that is equivalent to an elevated temperature close to T_g without deformation [21]. This explains the postyield stress-strain behavior of the 5 and 10 wt% DOP compounds. Prior to plastic deformation, the yield stresses of the 5 and10 wt% DOP blend reflect the combined effect of plasticized α-motions and antiplasticized β-motions, which appear to be higher than and approximately equal to the yield stress of neat PVC, respectively. During active plastic deformation, the materials are locally brought to a state that is effectively in the T_g, where the originally restricted β-motions are liberated in addition to the liberation of the main-chain motions. Therefore, the large reduction between the yield stress and the flow stress in the 5 and 10 wt% DOP compounds is not only due to the conventional strain softening but also due to effectively entering the T_g regime during active plastic deformation. This increased postyield strain softening during plastic strain of materials very near their T_g has been observed in other polymers (see, e.g., [22]). Additional discussions related to the antiplasticization are included in Chapter 5.

In the low strain rate compression tests, the material behavior changes from glassy to rubbery with increasing DOP content. However, in the high strain rate compression tests, PVC/DOP blends all behave like glassy polymers.

3.3.3. Tensile Testing

Tensile tests were performed at a strain rate of 0.001/s to evaluate the tensile toughness and modulus (Figure 3-14) of the materials. Figure 3-14a shows the true stress-true strain curves of PVC/mPOSS compounds in tensile testing. Neat PVC shows brittle behavior, and all specimens fail before reaching the yield point. Although adding methacryl-POSS softens PVC and reduces the modulus, all samples are still brittle and none are able to reach the yield point. In the case of DOP-filled PVC (Figure 3-14b), specimens are brittle when 10 wt% DOP is added. However, 15 wt% DOP samples exhibit a dramatic increase in tensile toughness, and the strain at break is increased to 65% true strain. 20 wt% DOP samples again are rubbery in the tensile tests and fail at 60% true strain.

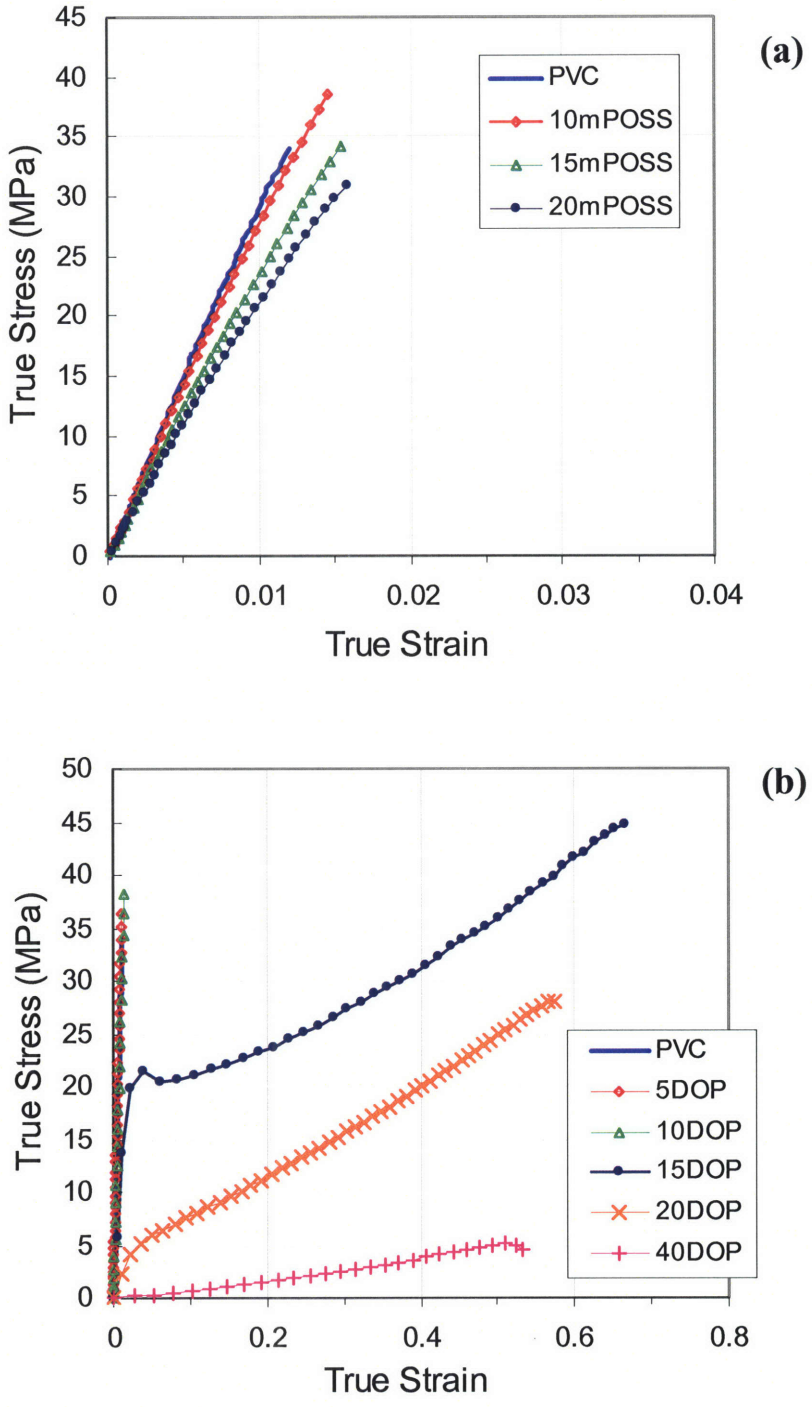

Figure 3-14. True stress-true strain curves in tensile testing: PVC/mPOSS (a) and PVC/DOP (b).

3.4. Conclusions

The rate-dependent α- and β-transitions of PVC, PVC/methacryl-POSS, and PVC/DOP blends were characterized in DMA. Both the α- and β-transitions of PVC shift to higher temperatures with increasing strain rate, shifting 3.8 and 17.4 °C per decade increase in strain rate for the α- and the β-transitions, respectively. No significant change in the shifting rate of the α-peak or the β-peak was found in the PVC/POSS blends. In the case of DOP, the same trends in the shifting of the α-transition temperature with increasing DOP content were observed; however the β-peaks become barely recognizable when the DOP concentration is above 10 wt%.

Compression testing was conducted on four different pieces of apparatus, including a Zwick mechanical tester at MIT for low rate regime (10^{-4}/s – 0.1/s), a MTS machine at Purdue University for low to moderate rate regime (1/s – 50/s), a long split Hopkinson pressure bar at Purdue University for moderate to high rate regime (120/s – 600/s), and last but not least, a split Hopkinson pressure bar at MIT for high rate regime (800/s – 4000/s). Since the methacryl-POSS plasticizes PVC, the compression yield stress of PVC decreases monotonically with increasing POSS concentration. In the case of PVC/DOP, the antiplasticization of β-motions compensated for the plasticization of α-motions in 5 and 10 wt% DOP blend leading to a higher and no real change in yield stress when compared to neat PVC. The yield stress decreases beyond 10 wt% DOP added.

A clear rate-sensitivity transition is observed in the compression yield data of pure PVC and PVC/mPOSS blends between the low rate (<1/s) and the high rate (>500/s) regimes. This transition is attributed to the need for stress-assisted activation of β-motions at high strain rates, which provides a significant increase in the barrier to plastic flow and hence the increased rate-sensitivity of yield. A transition in rate sensitivity is also observed in the DOP blends; this transition is due to the rubbery-to-leathery-to-glassy transition as one goes from the low-to-moderate- to-high strain rates.

Adding DOP also increases the tensile toughness of PVC. While the modulus decreases from 3000 to 1000 MPa with 15 wt% DOP added, the strain at break increased from 1% to 65% true strain. Unlike DOP, the POSS-filled materials remain brittle in tensile tests.

3.5. References

1. Soong, S. Y.; Cohen, R. E.; Boyce, M. C.; Mulliken, A. D., "Rate-Dependent Deformation Behavior of POSS-Filled and Plasticized Poly(vinyl chloride)", *Macromolecules* **2006**, *39*, 2900-2908.

2. Roetling, J. A., "Yield Stress Behaviour of Polymethylmethacrylate", *Polymer* **1965**, *6*, 311-317.

3. Bauwens-Crowet, C., "The Compression Yield Behaviour of Polymethyl Methacrylate over a Wide Range of Temperatures and Strain Rates", *J. Mater. Sci.* **1973**, *8*, 968-979.

4. Lefebvre, J. M.; Escaig, B., "Plastic Deformation of Glassy Amorphous Polymers: Influence of Strain Rate", *J. Mater. Sci.* **1985**, *20*, 438-448.

5. Swallowe, G. M.; Lee, S. F., "A Study of the Mechanical Properties of PMMA and PS at Strain Rates of 10^{-4} to 10^{3} over the Temperature Range 293-363 K", *J. Phys. IV France* **2003**, *110*, 33-38.

6. Bauwens-Crowet, C.; Bauwens, J. C.; Homes, G., "Tensile Yield-Stress Behavior of Glassy Polymers", *J. Polym. Sci., Part A-2* **1969**, *7*, 735-742.

7. Bauwens, J. C., "Relation between the Compression Yield Stress and the Mechanical Loss Peak of Bisphenol-A-Polycarbonate in the β-Transition Range", *J. Mater. Sci.* **1972**, *7*, 577-584.

8. Bauwens, J. C.; Bauwens-Crowet, C.; Homes, G., "Tensile Yield-Stress Behavior of Poly(vinyl chloride) and Polycarbonate in the Glass Transition Region", *J. Polym. Sci., Part A-2* **1969**, *7*, 1745-1754.

9. Bauwens, J. C., "Relation Between the Compression Yield Stress of Poly(vinyl chloride) and the Loss Peak in the β-Transition Range", *J. Polym. Sci.* **1971**, *33*, 123-133.

10. Bohning, M.; Goering, H.; Fritz, A.; VBrzezinka, K. W.; Turky, G.; Schonhals, A.; Schartel, B., "Dielectric Study of Molecular Mobility in Poly(propylene-graft-maleic anhydride)/Clay Nanocomposites", *Macromolecules* **2005**, *38*, 2764-2774.

11. Bohning, M.; Goering, H.; Hao, N.; Mach, R.; Schonhals, A., "Polycarbonate/SiC Nanocomposites - Influence of Nanoparticle Dispersion on Molecular Mobility and Gas Transport", *Polym. Adv. Technol.* **2005**, *16*, 262-268.

12. Kuila, B. K.; Nandi, A. K., "Physical, Mechanical, and Conductivity Properties of Poly(3-hexylthiophene)-Montmorillonite Clay Nanocomposites Produced by the Solvent Casting Method", *Macromolecules* **2004**, *37*,

13. Mulliken, A. D., "Mechanics of Amorphous Polymers and Polymer Nanocomposites during High Rate Deformation", PhD Thesis, Massachusetts Institute of Technology, Cambridge, MA, **2006**.

14. Kopesky, E. T.; McKinley, G. H.; Cohen, R. E., "Toughened Poly(methyl methacrylate) Nanocomposites by Incorporating Polyhedral Oligomeric Silsesquioxanes", *Polymer* **2006**, *47*, 299-309.

15. Davies, E., "A Critical Study of the Hopkinson Pressure Bar", *Philos. T. Roy. Soc. A* **1948**, *240*, 375-457.

16. Gray, G.; Blumenthal, W., ASM Handbook, 8, "Split-Hopkinson Pressure Bar Testing of Soft Materials", American Society of Metals, **2000**.

17. Kolsky, H., "An Investigation into the Mechanical Properties of Materials at Very High Rates of Loading", *Proc. Phys. Soc., B* **1949**, *62*, 676-701.

18. Mulliken, A. D., "Low to High Strain Rate Deformation of Amorphous Polymers: Experiments and Modeling", Master Thesis, Massachusetts Institute of Technology, Cambridge, MA, **2004**.

19. Mulliken, A. D.; Boyce, M. C. *SEM X International Congress and Exposition on Experimental and Applied Mechanics* **2004**, Paper No 197.

20. Mulliken, A. D.; Boyce, M. C., "Mechanics of the Rate-Dependent Elastic-Plastic Deformation of Glassy Polymers from Low to High Strain Rates", *Int. J. Solids Struct.* **2006**, *43*, 1331-1356.

21. Zhou, Q.-Y.; Argon, A. S.; Cohen, R. E., "Enhanced Case-II Diffusion of Diluents into Glassy Polymers Undergoing Plastic Flow", *Polymer* **2001**, *42*, 613-621.

22. Dupaix, R. B.; Boyce, M. C., "Finite Strain Behavior of Poly(ethylene terephthalate) (PET) and poly(ethylene terephthalate)-glycol (PETG)", *Polymer* **2005**, *46*, 4827-4838.

Chapter 4: Polyhedral Oligomeric Silsesquioxane as a Novel Plasticizer for Poly(vinyl chloride)

[Part of this work has been published previously, in slightly different form, in "Polyhedral Oligomeric Silsesquioxane as a Novel Plasticizer for Poly(vinyl chloride)" by S.Y. Soong, R.E. Cohen, and M.C. Boyce, *Polymer* **2007**, *48*, 1410-1418 [1].]

4.1. Introduction

Poly(vinyl chloride) (PVC) is the third most consumed polymeric material worldwide, with wide applications in areas including construction, tubing, medical devices and electronics packaging [2]. Due to the brittle nature of the neat PVC, it is often compounded with plasticizers to enhance its flexibility and toughness for various applications, and the most commonly used plasticizers for PVC are phthalate esters. Since dioctyl phthalate (DOP) was introduced in the 1930s, it has been the most widely used plasticizer. However, it is known that conventional low molecular weight organic plasticizers for PVC, such as DOP, are somewhat volatile, leading to plasticizer loss and unwanted deterioration of the material properties over the course of time. Furthermore, phthalate esters recently have been scrutinized for environmental and health related problems due to the leaching of plasticizer from the PVC matrix [3,4].

Many studies have been conducted to reduce the leaching and migration of plasticizers from the PVC materials [2]. Several alternative plasticizers and polymeric (oligomeric) plasticizers have been suggested to replace phthalate esters used in PVC [2,5,6]; surface modification techniques, such as crosslinking or coating the PVC surface, have also been developed to prevent leaching and improve the mechanical properties of plasticized PVC [2,7]. In our previous work, we have investigated the rate-dependent mechanical behavior of polyhedral oligomeric silsesquioxanes (POSS)-incorporated and DOP-plasticized PVC [8]. POSS has a hybrid organic/inorganic structure, which consists of a silica cage in the center with functional groups attached at the cage corners.

The experimental results showed that the methacryl-POSS is miscible with PVC up to 15 wt%, and it reduces the glass transition temperature (T_g), yield stress, and modulus of the PVC.

Furthermore, unlike DOP and most of the other commonly employed small molecule plasticizers, it does not result in antiplasticization [9] when incorporated in the polymer. Due to the hybrid organic/inorganic structure, POSS is also more stable and less volatile compared to the low molecular weight plasticizers. Unfortunately, its limited miscibility precludes the use of methacryl-POSS alone as a satisfactory plasticizer for PVC. Although the PVC/methacryl-POSS blends exhibited an increase in compliance over that of the neat PVC, the blends still failed in a brittle manner in tension at an engineering strain of 2% [8], as shown in the previous chapter. Here we explored the possibility of using a combination of methacryl- POSS and DOP as the plasticizer for PVC. First, a small amount of DOP was premixed into the PVC, and methacryl-POSS is then added. As will be shown, the small amount of DOP enhances the miscibility of POSS in PVC, achieving a wide range of tailorable mechanical properties including tensile ductility.

4.2. Experiment Section

4.2.1. Materials

The same PVC, methacryl-POSS, and DOP used in previous studies were again utilized here. Various PVC/mPOSS and PVC/DOP binary blends and PVC/mPOSS/DOP ternary blends were prepared through melt blending using a lab scale extruder (DACA Instruments). PVC powders were first premixed with DOP, and then methacryl-POSS was added. The mixture was then processed at 180 °C in DACA with a cycling time of 1 minute to achieve a homogeneous batch.

4.2.2. Dynamic Mechanical Analysis

The thermomechanical behavior of the materials was characterized using TA instruments Q800 DMA over a temperature range from -120 °C to 120 °C with a 2 °C per minute heating rate at a frequency of 1 Hz. Cylindrical polymer samples with a diameter of 2.5 mm and a length of 15 mm were tested in the single cantilever mode in DMA with a fixed displacement of 25 μm. Storage modulus and loss modulus were measured as a function of temperature and the corresponding tan δ value was calculated by the TA Universal Analysis software.

4.2.3. Tensile and Compression Testing

The uniaxial tensile testing was performed on Zwick mechanical tester with a constant engineering strain rate of 10^{-3}/s until final failure. Extensometers were employed for the tensile strain measurement. Sample preparation and dimensions and testing procedures were described in Chapter 3, and at least three specimens were tested for each blend to ensure the repeatability.

The rate-dependent mechanical behavior of the ternary blends was characterized in uniaxial compression testing. The uniaxial compression testing was performed at low rates (10^{-4}/s to 0.1/s) and high rates (800/s to 4000/s) using the Zwick mechanical tester and the split Hopkinson pressure bar apparatus at MIT, respectively. The equipment, sample preparation and dimensions, and testing procedures were the same as described in Chapter 3.

4.2.4. Accelerated Test for Plasticizer Loss

The loss of volatile plasticizers from PVC compounds has been measured in various accelerated testing schemes [10-12]. Here, we have held the compounds for two weeks in a vacuum oven at 85 °C to monitor this phenomenon. All of the plasticized binary and ternary blends were first pelletized and tested in one batch in order to minimize the experimental error due to any vacuum or temperature variations in the oven. The sample weight was measured before and after the vacuum oven treatment, and the percent weight loss of each PVC blend was calculated.

4.3. Results

4.3.1. Dynamic Mechanical Analysis

PVC/mPOSS/5 wt% DOP. Previous research in our laboratories has shown that methacryl-POSS plasticizes PVC [8]. However, methacryl-POSS was found to be miscible in the PVC only up to 15 wt% with a reduction in α-transition temperature (T_g) of 10.8 °C. With methacryl-POSS concentration above 15 wt%, the material became opaque and sub-micron sized POSS aggregates were observed in the transmission electron microscopy images (Figure 2-4).

Ternary blends containing 5 wt% DOP in PVC with addition of 15 wt%, 20 wt% and 25 wt% methacryl-POSS were prepared for this study. The addition of 5 wt% DOP increases the amount

of POSS that can be incorporated into the compound in a miscible manner up to 25 wt%. Figure 4-1 shows the images of the compression molded tensile specimens of various transparent ternary blends.

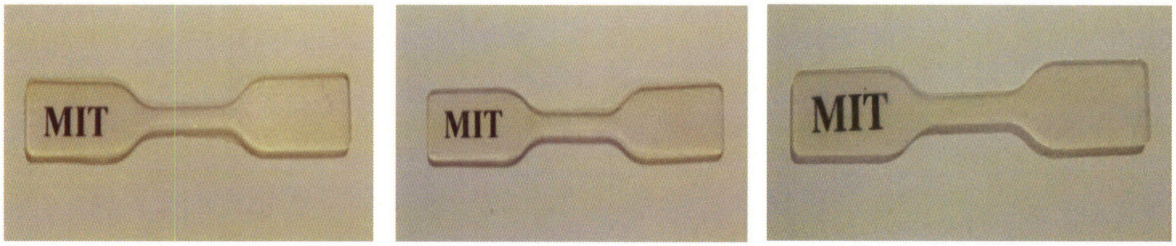

Figure 4-1. Images of PVC ternary blends with 5 wt% DOP and various methacryl-POSS contents. Compounds are transparent up to 25 wt% POSS added.

Figure 4-2 shows the storage modulus, loss modulus, and tan δ curves for the 95 wt% PVC/5 wt% DOP and the ternary PVC/mPOSS/5 wt% DOP blends. With increasing methacryl-POSS content, the PVC is further plasticized. The addition of 25 wt% methacryl-POSS reduces the α-transition temperature of the PVC/5 wt% DOP from 77 °C to 59 °C based on the tan δ peak value in DMA at 1 Hz. The addition of methacryl-POSS also broadens the α-transition peak; the 25 wt% addition of the POSS increases the FWHM[4] of the α-transition loss modulus from a width of 18 °C to a width of 65 °C. Although the α-transition temperature of the 70 wt% PVC/25 wt% mPOSS/5 wt% DOP blend is 59 °C based on the tan δ peak value, the α-transition occurs over a very broad temperature range (from -40 °C to 60 °C) (Figure 4-2). Therefore, the material is in the leathery regime at room temperature with a storage modulus value around 1000 MPa.

Less distinguishable β-transition peaks and wider α-peak shoulders on the lower temperature side were also observed in both the loss modulus and the tan δ curves with increasing POSS

---

[4] FWHM (full width at half maximum) here is defined as the breadth (duration of temperature) of the transition peak at half of its maximum peak value.

concentration. The observation of the shoulder results from the merging of the β-transition peak into the α-peak when the material is more plasticized and exhibits a lower α-transition temperature.

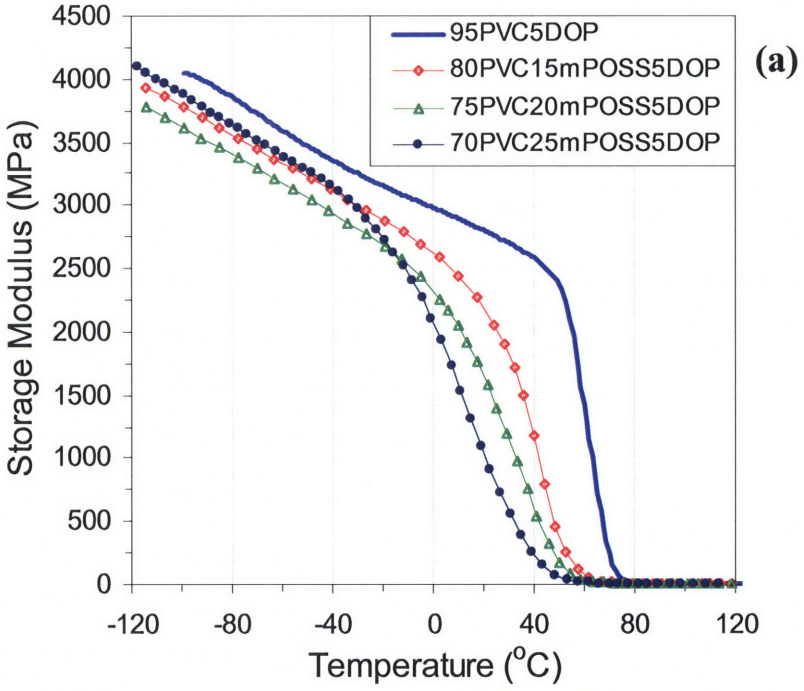

(a)

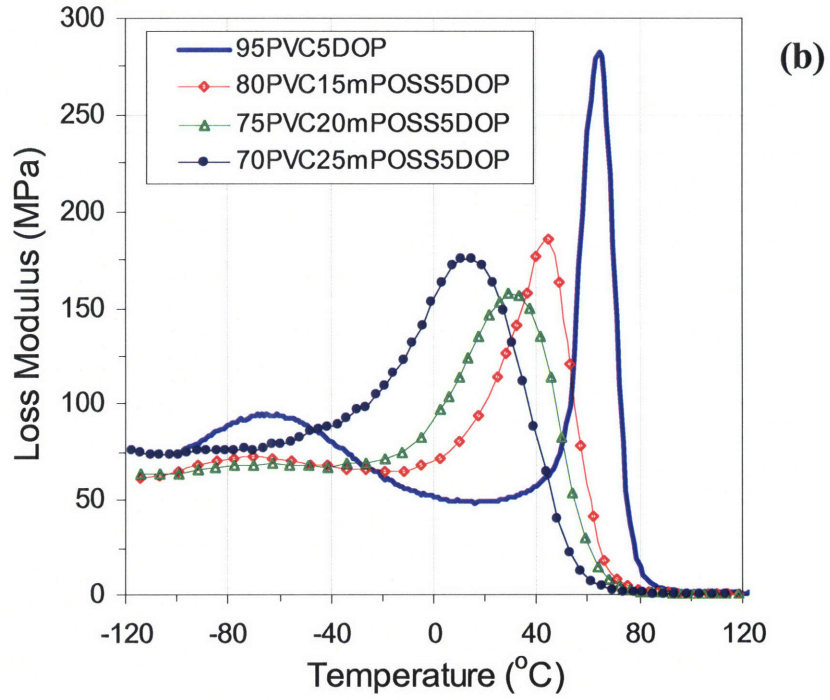

(b)

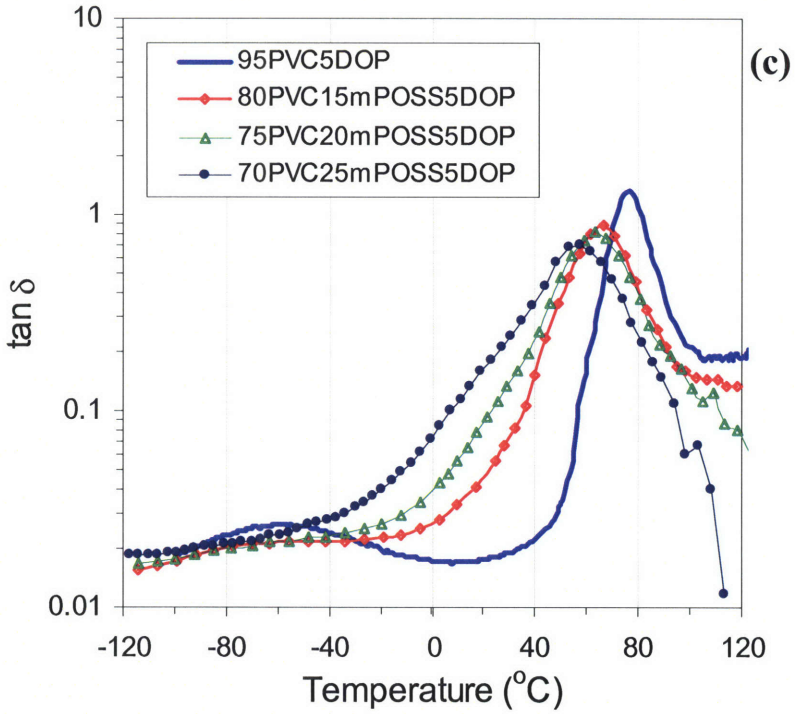

Figure 4-2. Storage modulus (a), loss modulus (b), and tan δ (c) of PVC/mPOSS/5 wt% DOP blends as a function of temperature at 1 Hz.

60 wt% PVC/mPOSS/DOP. Two heavily plasticized PVC blends containing 40 wt% of plasticizer (60 wt% PVC/40 wt% DOP and 60 wt% PVC/20 wt% mPOSS/20 wt% DOP) were prepared and characterized. Figure 4-3 shows the storage modulus, loss modulus, and tan δ curves of the two materials as a function of temperature at 1 Hz. The peak values of the tan δ curves indicate that the α-transition temperatures of the 60 wt% PVC/40 wt% DOP and the 60 wt% PVC/20 wt% mPOSS/20 wt% DOP are 5.6 °C and 25.6 °C, respectively. The onset of the broad α-transition of both compounds occurs at a much lower temperature, near -60 °C.

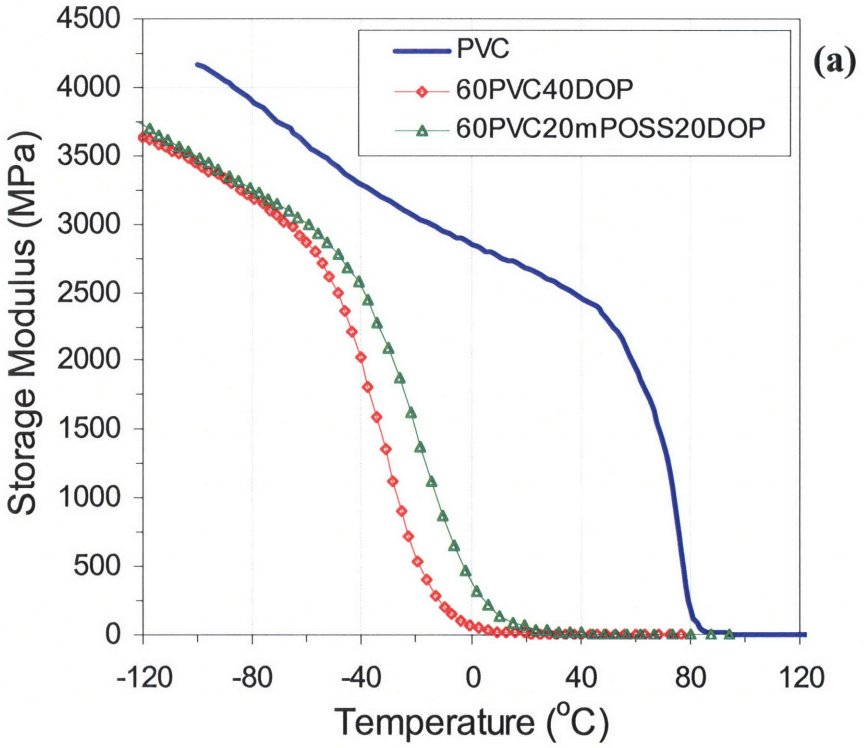
(a)
PVC
60PVC40DOP
60PVC20mPOSS20DOP
Storage Modulus (MPa)
4500
4000
3500
3000
2500
2000
1500
1000
500
0
-120
-80
-40
0
40
80
120
Temperature (°C)

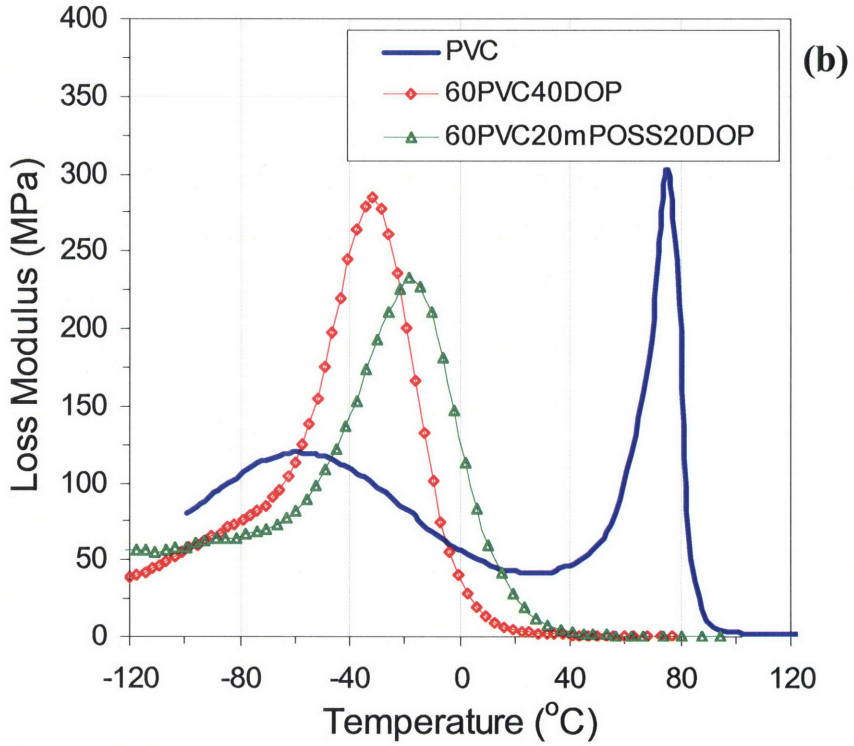
(b)
PVC
60PVC40DOP
60PVC20mPOSS20DOP
Loss Modulus (MPa)
400
350
300
250
200
150
100
50
0
-120
-80
-40
0
40
80
120
Temperature (°C)

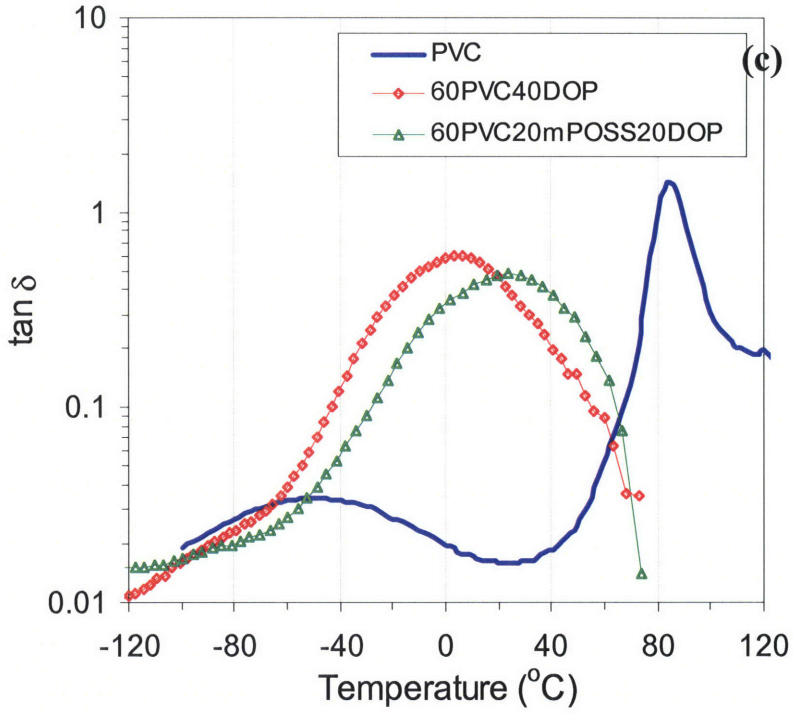

Figure 4-3. Storage modulus (a), loss modulus (b), and tan δ (c) of PVC, 60 wt% PVC/40 wt% DOP, and 60 wt% PVC/20 wt%mPOSS/20 wt% DOP blends as a function of temperature at 1 Hz.

DOP vs. mPOSS as Plasticizers. Table 4-1 summarizes the compositions, the α-transition temperatures (T_gs)[5], and the FWHM[6] of all the PVC blends prepared. Incorporating DOP and/or methacryl-POSS in PVC reduces T_g. Figure 4-4a and Figure 4-4b show the T_g as a function of plasticizer content on a basis of grams of plasticizer in per gram of compound (weight fraction) and moles of plasticizer in per mole of compound, respectively. DOP appears to be a more effective plasticizer than methacryl-POSS when compared on the basis of weight fraction of the plasticizer in the compound (Figure 4-4a).

---

[5] α-Transition temperature is based on the tan δ peak value at 1 Hz measured in DMA.

[6] FWHM is defined as the FWHM of the loss modulus transition peak at1 Hz in DMA.

If the effect of the methacryl-POSS or DOP is evaluated on a basis of moles of plasticizer in the compound (Figure 4-5), both plasticizers have essentially the same influence on T_g. Furthermore, the T_gs of the ternary blends show a linear combination of the plasticizing influence of the two molecules when considered on the basis of the molar amount of plasticizer per gram of compound. Figure 4-5 shows the linear regression curve that was constructed from the T_gs of various PVC blends, and it can be used to anticipate the T_g of all other homogeneous binary and ternary blends that can be produced with this system of components.

Table 4-1. α-Transition temperature (T_g) and FWHM of all PVC blends.

	PVC (wt%)	mPOSS (wt%)	DOP (wt%)	T_g (°C)	FWHM (°C)
PVC	100	0	0	84.8	15
5DOP	95	0	5	76.9	18
10DOP	90	0	10	65.0	10
15DOP	85	0	15	56.2	57
20DOP	80	0	20	47.5	64
40DOP	60	0	40	5.6	40
5mPOSS	95	5	0	82.5	20
10mPOSS	90	10	0	77.3	22
15mPOSS	85	15	0	74.0	20
15mPOSS5DOP	80	15	5	66.1	40
20mPOSS5DOP	75	20	5	62.5	51
25mPOSS5DOP	70	25	5	59.3	65
20mPOSS20DOP	60	20	20	25.6	47

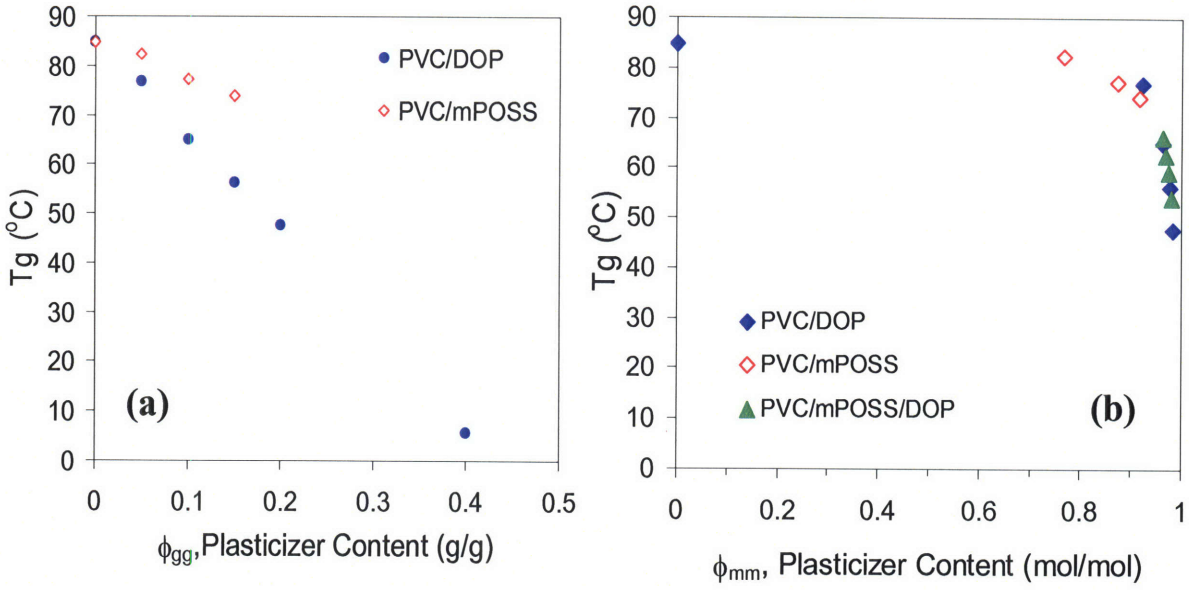

Figure 4-4. T_g as a function of the plasticizer content: on a basis of weight fraction (g/g) (a) and mole fraction (mol/mol) (b).

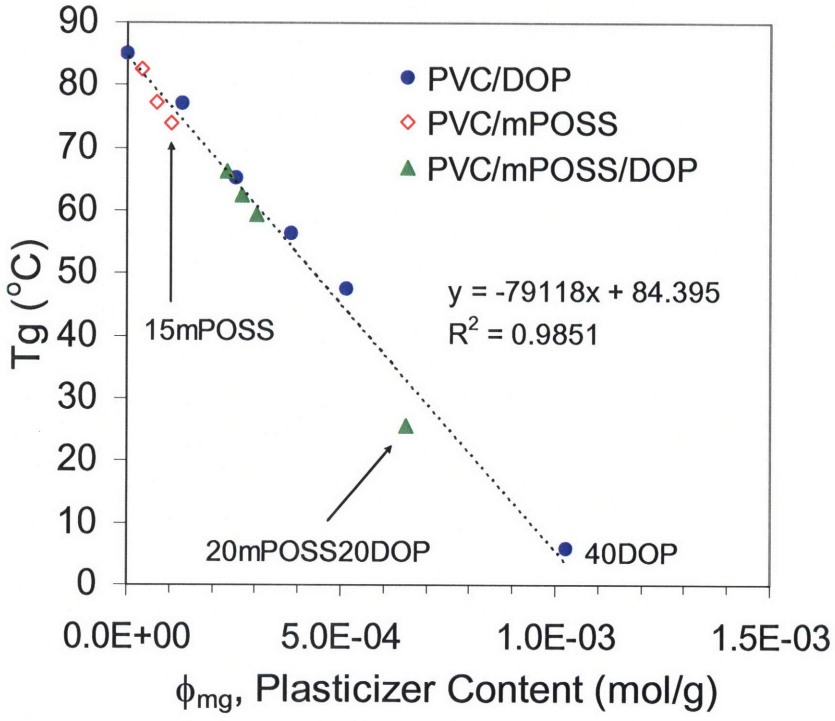

Figure 4-5. T_g as a function of the plasticizer content: on a basis of moles of plasticizer per gram of compound (mol/g).

4.3.2. Tensile Testing

Figure 4-6a shows the uniaxial tension true stress-true strain curves of the PVC ternary blends containing 5 wt% DOP and various amounts of methacryl-POSS at 10^{-3}/s constant engineering strain rate. The PVC/5 wt% DOP blend exhibits brittle behavior in tensile testing, where all specimens failed at a strain less than 5%. Incorporating 15 wt% methacryl-POSS in PVC containing 5 wt% DOP changed the tensile behavior from brittle to ductile and the strain at break was improved significantly to approximately 70% in true strain (nearly 100% in engineering strain).

Figure 4-6b shows the uniaxial tension true stress-true strain curves of heavily plasticized PVC containing 40 wt% of plasticizer. Both 60 wt% PVC/20 wt% mPOSS/20 wt% DOP and 60 wt%/40 wt% DOP exhibit rubbery behavior.

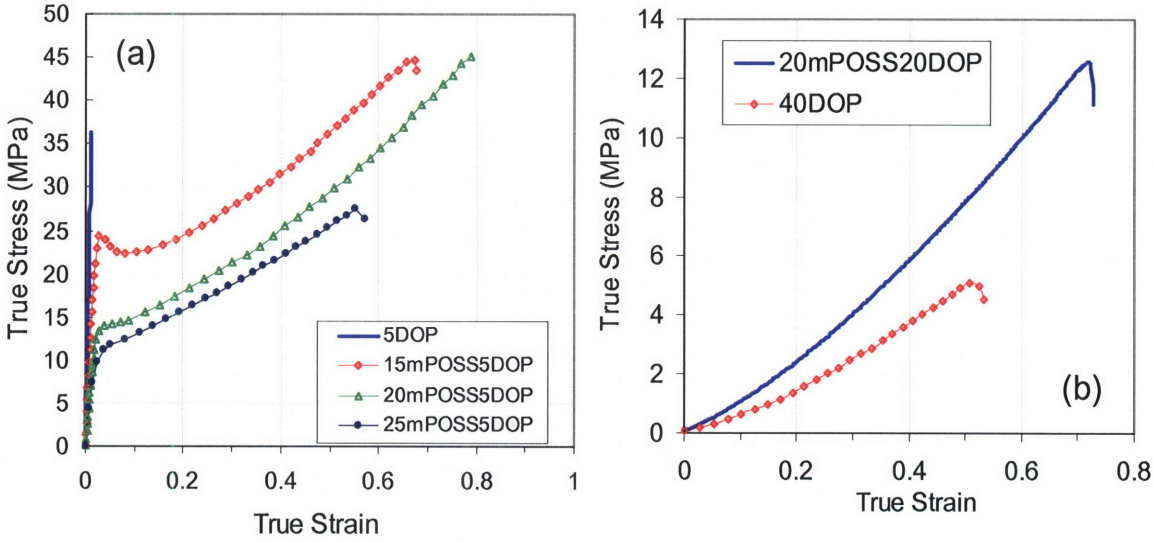

Figure 4-6. True stress-true strain curves in uniaxial tension at 0.001/s: compounds containing 5 wt% DOP with various mPOSS (a) and compounds containing 40 wt% plasticizer (b).

4.3.3. Uniaxial Compression Testing

PVC/mPOSS/5 wt% DOP. Figure 4-7 shows the uniaxial compression true stress-true strain curves of the ternary blends containing 5 wt% DOP at a strain rate of 10^{-3}/s. With the increasing amount of methacryl-POSS in PVC, the compounds become more plasticized. The materials

transition from glassy to leathery behavior with significant reductions in the yield stress and the flow stress.

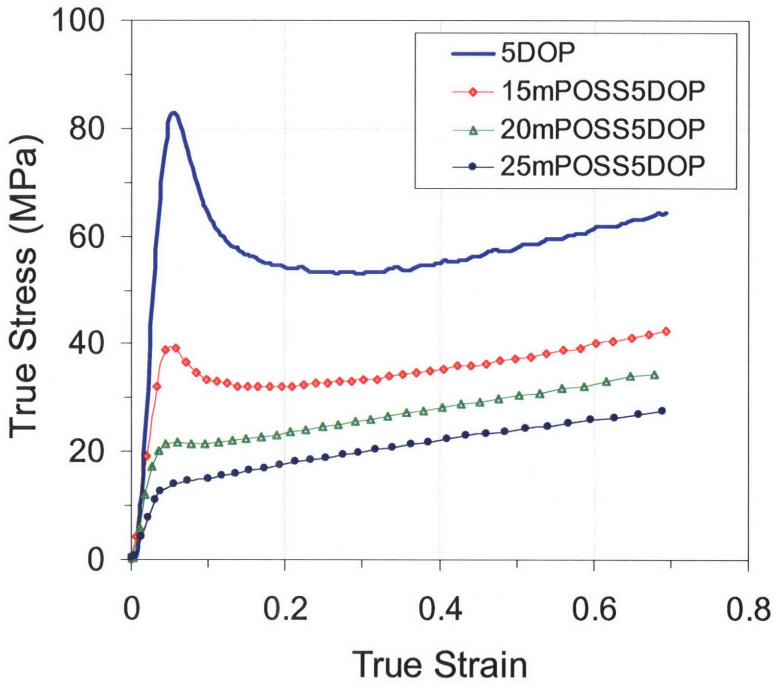

Figure 4-7. True stress-true strain curves of compounds containing 5 wt% DOP and various amounts of methacryl-POSS. Testing was done in uniaxial compression at 0.001/s.

Figure 4-8 shows the true stress-true strain curves of 70 wt% PVC/25 wt% mPOSS/5 wt% DOP under various strain rates. The material behavior transitions from leathery to glassy when the strain rate increases from low rate to high rate.

Figure 4-9 presents the yield stresses as a function of engineering strain rate for various PVC compounds containing 5 wt% DOP and different amounts of methacryl-POSS. The increasing amount of POSS in the ternary blend reduces the yield stress over a wide range of strain rate. PVC with 5 wt% DOP exhibits glassy mechanical behavior at all strain rates. Due to the antiplasticization effect in the 95 wt% PVC/5 wt% DOP blend, the rate sensitivity transition is not obvious in Figure 4-9. However, rate sensitivity transitions in the yield stress were observed in the ternary blends. Based on the DMA results and compression testing curves, the observed

transitions in rate sensitivity were attributed to the leathery to glassy transition (α-transition) of the compounds when the experienced strain rate was increased.

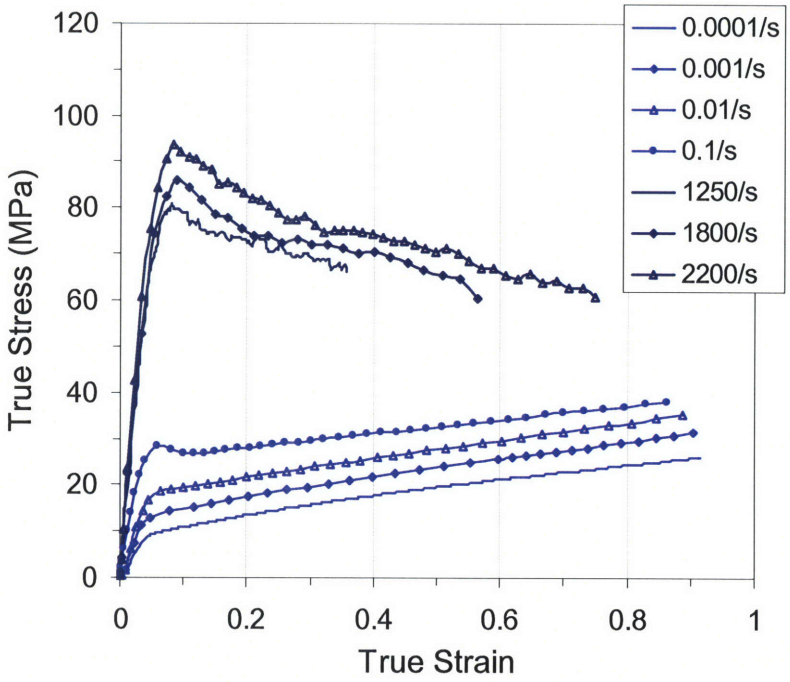

Figure 4-8. True stress-true strain curves of 70 wt% PVC/25 wt% mPOSS/5 wt% DOP under different strain rates (10^{-4}-2500/s) in uniaxial compression testing.

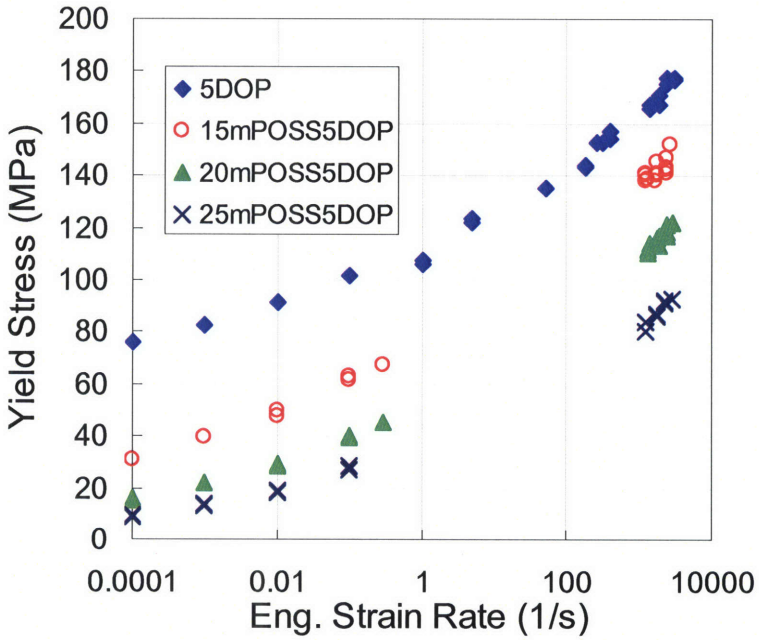

Figure 4-9. Yield stress as a function of engineering strain rate: PVC compounds containing 5 wt% DOP and various amounts of methacryl-POSS.

60 wt% PVC/mPOSS/DOP. Figure 4-10 presents the true stress-true strain curves of 60 wt% PVC/40 wt% DOP and 60 wt% PVC/20 wt% mPOSS/20 wt% DOP in uniaxial compression testing at a constant engineering strain rate of 10^{-3}/s. Both PVC compounds are heavily plasticized and exhibit rubbery behavior.

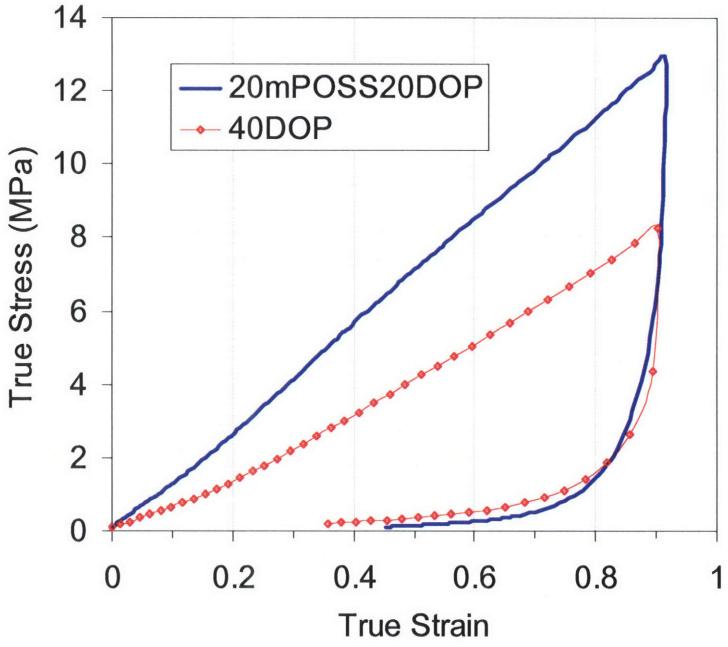

Figure 4-10. Uniaxial compression true stress-true strain curves of compounds containing 40 wt% plasticizer, at a nominal strain rate of 0.001/s.

Figure 4-11 shows the true stress-true strain curves of 60 wt% PVC/20 wt% mPOSS/20 wt% DOP over a wide range of strain rates. The material was seen to transition from rubbery in the low rate regime to leathery in the high rate regime.

Since the heavily plasticized PVC blends containing 40 wt% were rubbery, the true stress at -0.2 compressive true strain was taken to characterize the rate dependent yield behavior. Figure 4-12 shows the true stress at a true strain of -0.2 as a function of applied engineering strain rate. The true stress of both compounds increases linearly with the logarithm of strain rate in both the low rate and high rate regimes. The rate sensitivity of stress increases significantly and a clear transition is observed between the low rate and high rate regimes due to the rubbery to leathery transition.

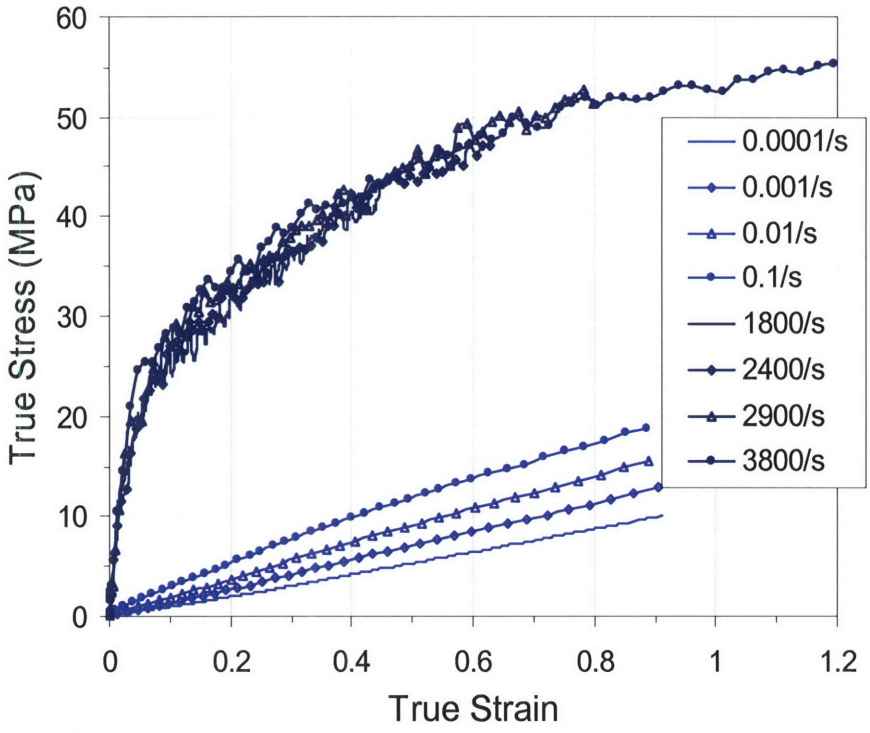

Figure 4-11. True stress-true strain curves of 60 wt% PVC/20 wt% mPOSS/20 wt% DOP under different strain rates (10^{-4}-4000/s) in uniaxial compression testing.

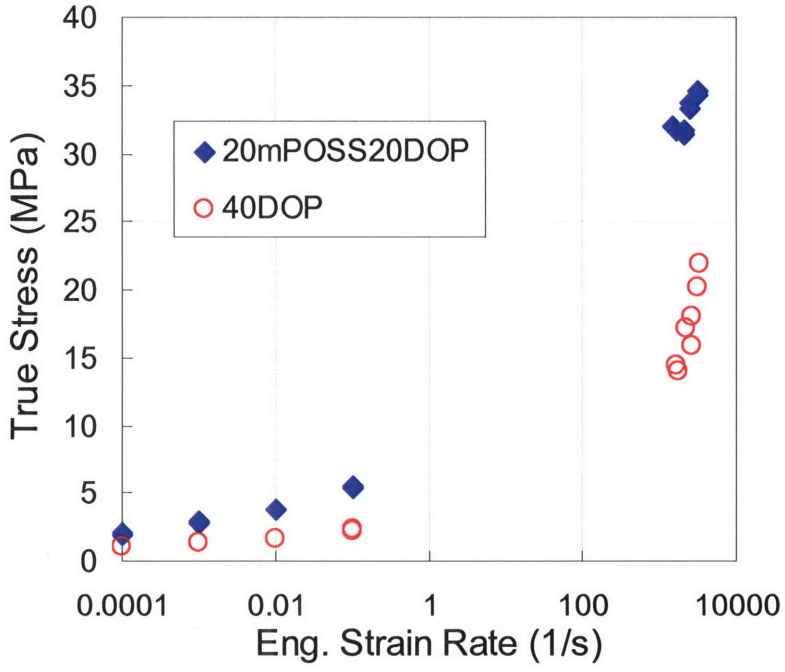

Figure 4-12. True stress at -0.2 true strain as a function of engineering strain rate: PVC compounds containing 40 wt% plasticizer.

4.3.4. Stability of the Plasticized Compounds

The stability of the plasticized compounds was evaluated by determining the percent weight loss of the sample pellets after being held in a vacuum oven at the 85 °C/two-week oven test. Figure 4-13 shows the percent weight loss of samples containing various loadings of methacryl-POSS or DOP in PVC as a function of the weight percent of the plasticizer. The weight loss is negligible in all of the PVC/methacryl-POSS blends. A 5% weight loss was observed in the PVC/20 wt% DOP blend and a 25% weight loss was observed in the PVC/40 wt% DOP blend. Assuming all the weight loss is attributed to the loss of DOP, more than 20% of the original DOP added in the PVC/20 wt% DOP blend and more than 50% of the initial amount of DOP in the PVC/40 wt% DOP blend was lost over the duration of our accelerated test.

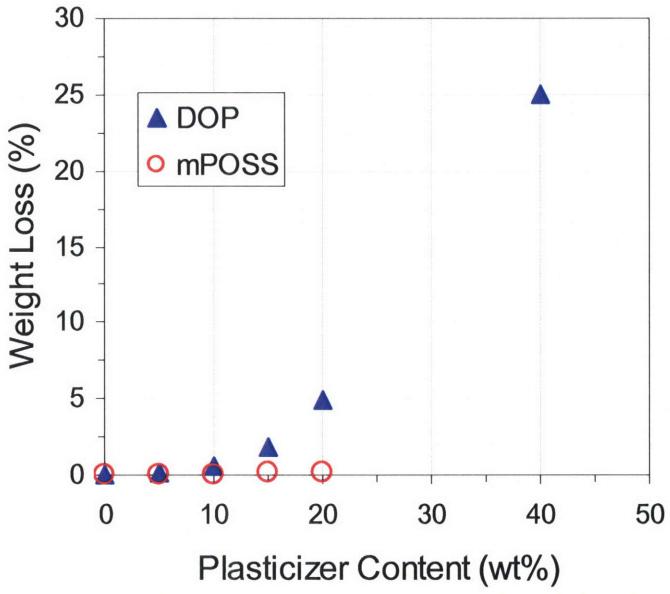

Figure 4-13. The percent weight loss of the PVC/mPOSS and the PVC/DOP blends as a function of the plasticizer content (wt%).

To compare the stability of methacryl-POSS and DOP on the basis of its effectiveness as a plasticizer, Figure 4-14 shows the percent weight loss as a function of the original reduction in T_g afforded by the added plasticizer. Due to the limited solubility of methacryl-POSS in PVC, the performance of PVC/methacryl-POSS blends is indistinguishable from that of the PVC/DOP blends in the limited range of overlap of the data.

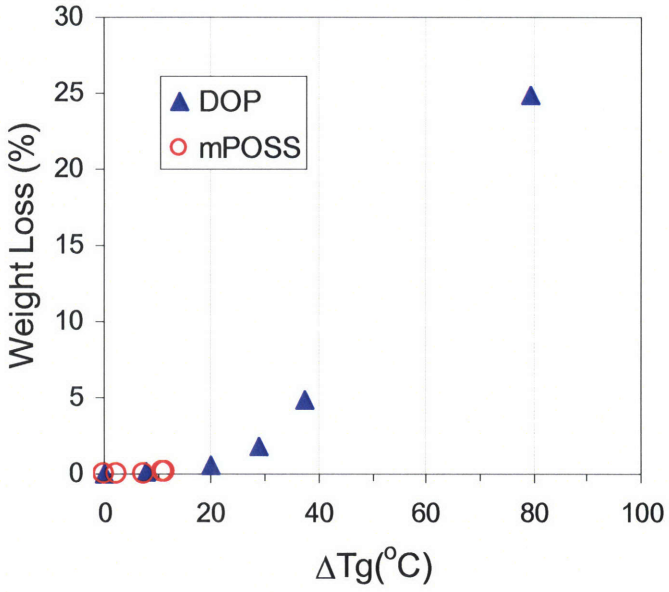

Figure 4-14. The percent weight loss of the PVC/mPOSS and the PVC/DOP blends as a function of the original reduction in T_g.

In order to evaluate the stability of the ternary blends compared to the PVC/DOP compounds, we considered the resulting increase in T_g that arises due to plasticizer loss; we denote this parameter as "T_g penalty" in Figure 4-15. Because of the observed molar character of the plasticization phenomenon, this parameter is a better measure of compound stability than weight loss. Since methacryl-POSS shows essentially no volatility in all of our oven tests, we assume that all the weight loss in any ternary blend can be attributed to the DOP. The expected regain in T_g (T_g penalty) was then calculated based on the loss of DOP using the linear regression equation (Figure 4-5). Figure 4-15 shows that the T_g penalty for the PVC/DOP blends, PVC/methacryl-POSS blends and PVC/methacryl-POSS/DOP blends all collapse into a single curve. Therefore, as in the case of Tg reduction, the stability of the various ternary compounds over the time frame of our accelerated test can be predicted from measurements on the two binary compounds. There is no synergistic effect of the methacryl-POSS on retention of DOP in the compounds tested. In all cases we expect that the formulated amount of methacryl-POSS would remain in the PVC indefinitely.

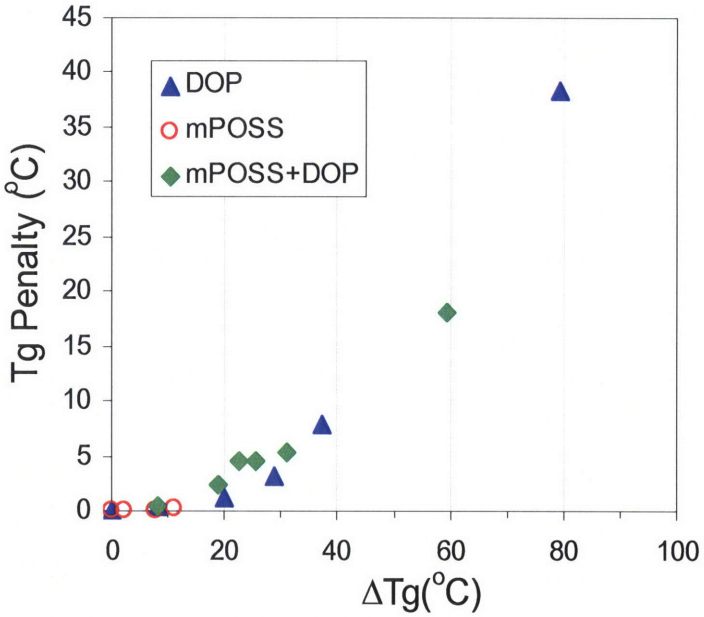

Figure 4-15. T_g penalty (calculated) due to the loss of DOP as a function of the original reduction in T_g.

4.4. Discussions

In this section we will discuss the potential of using methacryl-POSS and/or DOP as a plasticizer for PVC to engineer the mechanical properties of plasticized PVC blends possessing the same T_g.

4.4.1. Antiplasticization: DOP vs. Methacryl-POSS

Figure 3-10a shows the true stress-true strain curves of PVC/DOP blends in compression testing at a nominal strain rate of 10^{-3}/s. The yield stress of the 5 wt% DOP blend exceeded the yield stress of the neat PVC; such behavior is known as antiplasticization and has been well documented in PVC materials containing relatively low concentrations of plasticizer [9,13-15]. In the case of the 5 wt% DOP compound, antiplasticization is due to the strong affiliation between the aromatic rings of the plasticizer and the PVC backbones, which hinders the local short segmental motions (β-motions) [13,16]. The restricted β-motions in the 5 wt% DOP blend impose an additional resistance at the point of yield, resulting in a higher yield stress compared to neat PVC. However, a dramatic post-yield strain softening is observed in the 5 wt% DOP compound and its post-yield strain-softened flow stress falls beneath that of the neat PVC.

During steady plastic flow in a glassy polymer, the molecular mobility is locally enhanced to a level equal to that of the rubbery state [17]. Here we see that this effect also acts to locally liberate the antiplasticized β-motions in PVC as evidenced by the post-yield flow stress of the 5 wt% DOP blend falling beneath the neat PVC flow stress. The significant antiplasticization effect seen in the PVC/DOP compounds was not observed in the PVC/mPOSS blends, as shown in Figure 3-9a, where the initial yield stress of the PVC/POSS blends is always lower than that of the neat PVC. This observation is attributed to the differences in molecular size and shape of methacryl-POSS and DOP account for this behavior [8].

4.4.2. Same T_g, Different Mechanical Properties

Figure 4-16 shows the storage modulus and tan δ curves of the 95 wt% PVC/5 wt% DOP and 90 wt% PVC/10 wt% mPOSS blends. The two blends have nearly identical T_g based on the tan δ peak value; however, their room temperature mechanical properties are quite different. Due to the antiplasticization effect, the room temperature storage modulus (Figure 4-16) of the 5 wt% DOP is greater than that of the 10 wt% methacryl-POSS.

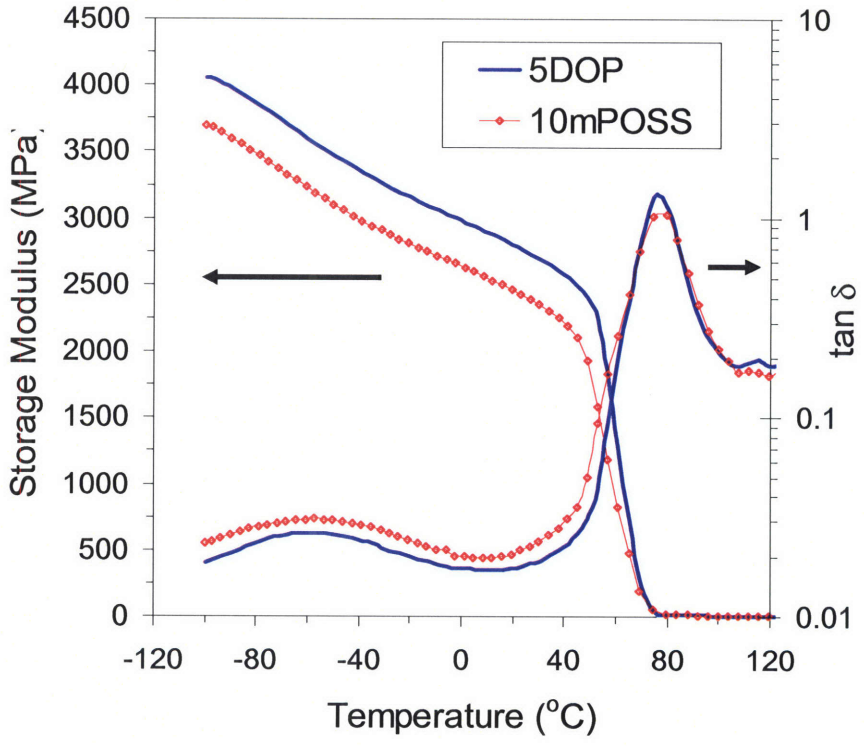

Figure 4-16. Storage modulus and tan δ curves of 95 wt% PVC/5 wt% DOP and 95 wt% PVC/10 wt% mPOSS as a function of temperature.

The results of the two blends in compression testing are shown in Figure 4-17. The initial yield stress of the 5 wt% DOP compound is much higher than the value exhibited by 10 wt% methacryl-POSS blend in the compression testing (Figure 4-17a) since the 5 wt% DOP blend has the extra barrier to yield due to the hindered β-motions. Interestingly, the post-yield strain-softened behavior of the two materials is nearly identical since the initially hindered β-motions of the PVC/5 wt% DOP material are locally liberated during active flow. The rate-dependent yield stress behavior of the two compounds is shown in Figure 4-17b. A clear rate-dependent transition in yield stress was observed in PVC/10 wt% mPOSS, whereas the transition is less significant in PVC/5 wt% DOP. The yield stress of the 5 wt% DOP blend is found to be higher than the 10 wt% methacryl-POSS one at low strain rates due to the antiplasticization caused by DOP.

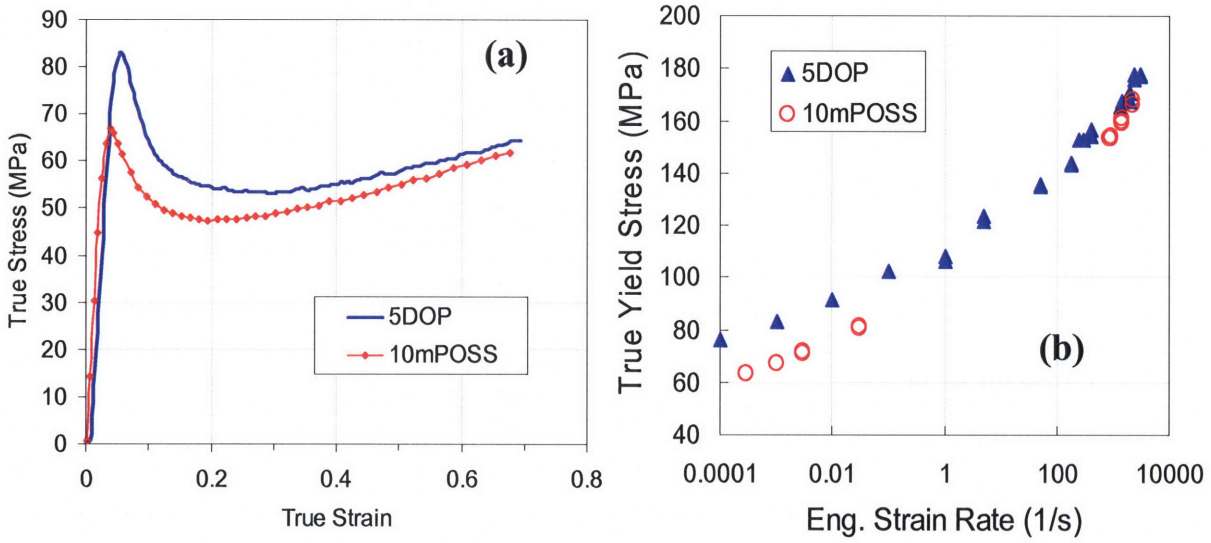

Figure 4-17. Compression behavior of 95 wt% PVC/5 wt% DOP and 90 wt% PVC/10 wt% mPOSS: true stress-true strain curves in compression testing at 0.001/s (a), and yield stress as a function of strain rate (b).

In a second example, we used the regression equation from Figure 4-5 to prepare a ternary blend that has the same T_g (56.2 °C) as the PVC/15 wt% DOP compound. We fixed the ternary compound to contain 10 wt% DOP and then backcalculated the amount of methacryl-POSS and PVC required to achieve the target T_g. The regression equation predicted that 17.5 wt%

methacryl-POSS with 10 wt% DOP in PVC should exhibit the same Tg as the PVC/15 wt% DOP blend.

Figure 4-18 shows the tan δ curves of the two blends. The two tan δ peak values are approximately equivalent, which confirms the prediction made by the regression equation. The results in compression testing are illustrated Figure 4-19a and Figure 4-19b. Although the T_gs of the two blends are nearly identical, their true stress-true strain curves are significantly different. While the PVC/15 wt% DOP compound still shows a near glassy polymer behavior, the ternary blend is leathery/nearly rubbery at room temperature in low rate compression testing. The distinction in mechanical behavior between the two blends is attributed to the different molecular level modifications offered by DOP and methacryl-POSS. Figure 4-19a suggests that the methacryl-POSS in the ternary blend created a broader transition and shoulder on the lower temperature side of the α-peak, and the onset of α-transition appears at a lower temperature compared to the DOP-plasticized PVC. Figure 4-19a also shows that the storage modulus of the ternary blend is significantly lower than the 15 wt% DOP compound when crossing the room temperature regime due to the breadth of the α-transition.

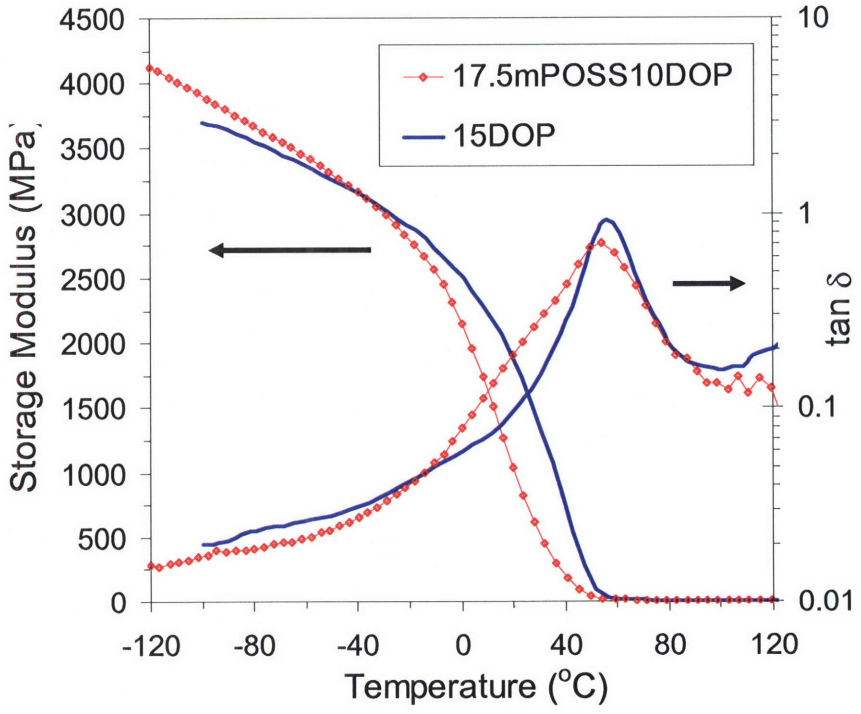

Figure 4-18. Storage modulus and tan δ curves of 85 wt% PVC/15 wt% DOP and 72.5 wt% PVC/17.5 wt% mPOSS/10 wt% DOP as a function of temperature.

Figure 4-19 demonstrates clearly the possibility to engineer a series of methacryl-POSS and DOP-plasticized PVC compounds that possess the same T_g but exhibit significantly different mechanical properties.

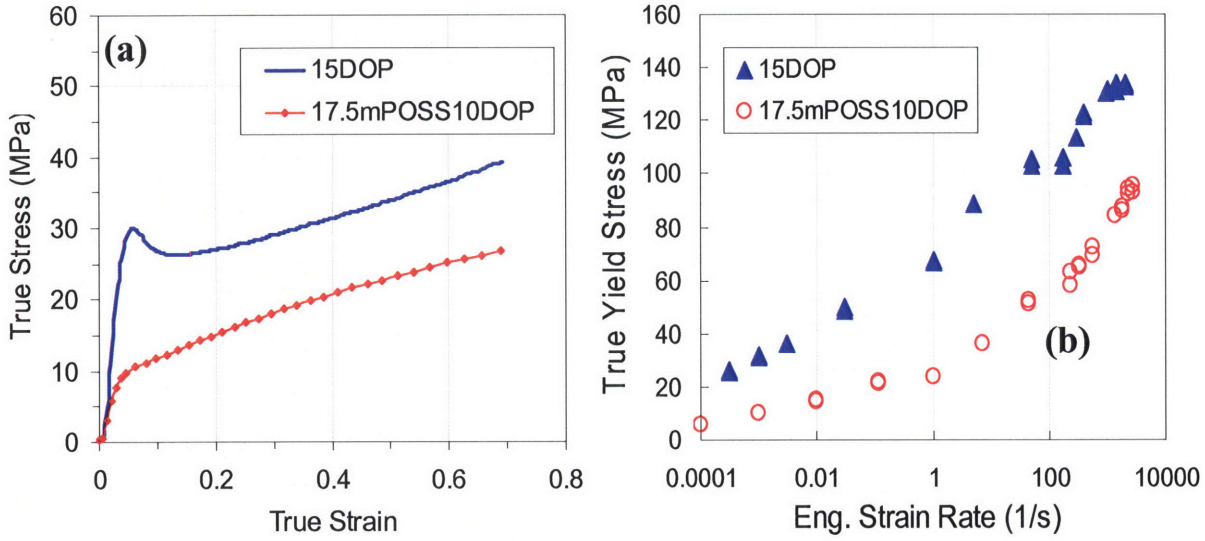

Figure 4-19. Compression behavior of 85 wt% PVC/15 wt% DOP and 72.5 wt% PVC/17.5 wt% mPOSS/10 wt% DOP: true stress-true strain curves in compression testing (a) and yield stress as a function of strain rate (b).

4.5. Conclusions

Previous research demonstrated that methacryl-POSS plasticizes PVC without causing antiplasticization, which is frequently observed when small organic plasticizers are used. However, using methacryl-POSS to plasticize PVC to room temperature-flexible compounds was not possible due to the miscibility limit [8]. In this study we demonstrate that the addition of a small amount of DOP increases the miscibility of methacryl-POSS in PVC substantially. With 5 wt% DOP added in the polymer blend, the amount of methacryl-POSS that can be incorporated into the compound was increased from 15 wt% to 25 wt%. The T_gs of the ternary PVC compounds can be reduced to near room temperature, and the material becomes leathery to nearly rubbery and exhibits ductile tensile behavior.

Comparing methacryl-POSS and DOP on a basis of moles of plasticizer added per gram of compound reveals that the two additives are equally effective in reducing the T_g of PVC. The

T_gs of methacryl-POSS, DOP, and POSS/DOP-plasticized PVC blends formed a linear relationship when plotted on this basis. The regression line can be used to anticipate the T_g of other homogeneous binary and ternary blends. The POSS/DOP-plasticized PVC did not show any synergistic effects in retaining the plasticizer in the PVC compounds through the duration of the oven tests conducted. However, the POSS/DOP-plasticized PVC demonstrated considerably different mechanical behavior in low rate compression and tensile experiments when compared to the DOP-plasticized PVC which has the same T_g. Such findings reveal the possibility of using POSS to engineer the material properties of plasticized PVC compounds.

4.6. References

1. Soong, S. Y.; Cohen, R. E.; Boyce, M. C., "Polyhedral Oligomeric Silsesquioxane as a Novel Plasticizer for Poly(vinyl chloride)", *Polymer* **2007**, *48*, 1410-1418.

2. Rahman, M.; Brazel, C. S., "The Plasticizer Market: An Assessment of Traditional Plasticizers and Research Trends to Meet New Challenges", *Prog. Polym. Sci.* **2004**, *29*, 1223-1248.

3. Tickner, J. A.; Schettler, T.; Guidotti, T.; McCally, M.; Rossi, M., "Health Risks Posed by Use of Di-2-Ethylhexyl Phthalate (DEHP) in PVC Medical Devices: A Critical Review", *Am. J. Ind. Med.* **2001**, *39*, 100-111.

4. Latini, G.; De Felice, C.; Verrotti, A., "Review: Plasticizers, Infant Nutrition and Reproductive Health", *Reprod. Toxicol.* **2004**, *19*, 27-33.

5. Krauskopf, L. G., "How About Alternatives to Phthalate Plasticizers?" *J. Vinyl. Addit. Techn.* **2003**, *9*, 159-171.

6. Lindstrom, A.; Hakkarainen, M., "Environmentally Friendly Plasticizers for Poly(vinyl chloride) - Improved Mechanical Properties and Compatibility by Using Branched Poly(butylene adipate) as a Polymeric Plasticizer", *J. Appl. Polym. Sci.* **2006**, *100*, 2180-2188.

7. Messori, M.; Toselli, M.; Pilati, F.; Fabbri, E.; Pasquali, L.; Nannarone, S., "Prevention of Plasticizer Leaching from PVC Medical Devices by Using Organic-Inorganic Hybrid Coatings", *Polymer* **2004**, *45*, 805-813.

8. Soong, S. Y.; Cohen, R. E.; Boyce, M. C.; Mulliken, A. D., "Rate-Dependent Deformation Behavior of POSS-Filled and Plasticized Poly(vinyl chloride)", *Macromolecules* **2006**, *39*, 2900-2908.

9. Kinjo, N.; Nakagawa, T., "Antiplasticization in the Slightly Plasticized Poly(vinyl chloride)", *Polym. J.* **1973**, *4*, 143-153.

10. Mrklic, Z.; Kovacic, T., "Thermogravimetric Investigation of Volatility of Dioctyl Phthalate from Plasticized Poly(vinyl chloride)", *Thermochim. Acta* **1998**, *322*, 129-135.

11. Storey, R. F.; Mauritz, K. A.; Cox, B. D., "Diffusion of Various Dialkyl Phthalate Plasticizers in PVC", *Macromolecules* **1989**, *22*, 289-294.

12. Marcilla, A.; Garcia, S.; Garcia-Quesada, J. C., "Study of the Migration of PVC Plasticizers", *J. Anal. Appl. Pyrolysis* **2004**, *71*, 457-463.

13. Vilics, T.; Schneider, H. A.; Manoviciu, V.; Manoviciu, I., "A DMA Study of the Suppression of the β-Transition in Slightly Plasticized PVC Blends", *J. Therm. Anal.* **1996**, *47*, 1141-1153.

14. Pezzin, G.; Ajroldi, G.; Garbuglio, C., "Dynamic-Mechanical Study of the Secondary Transition of Poly(vinyl chloride)", *J. Appl. Polym. Sci.* **1967**, *2*, 2553-2565.

15. Sundgren, N.; Bergman, G.; Shur, Y. J., "Antiplasticization and Transition to Marked Nonlinear Viscoelasticity in Poly(vinyl chloride) (PVC)/Poly-ε-caprolactone (PCL) Blends", *J. Appl. Polym. Sci.* **1978**, *22*, 1255-1265.

16. Garnaik, B.; Sivaram, S., "Study of Polymer-Plasticizer Interaction by ^{13}C CP/MAS NMR Spectroscopy: Poly(vinyl chloride)-Bis(2-ethylhexyl) Phthalate System", *Macromolecules* **1996**, *29*, 185-190.

17. Zhou, Q.-Y.; Argon, A. S.; Cohen, R. E., "Enhanced Case-II Diffusion of Diluents into Glassy Polymers Undergoing Plastic Flow", *Polymer* **2001**, *42*, 613-621.

Chapter 5: Antiplasticization

[Part of this work has been submitted to *Macromolecules* (**2007**), in slightly different form.]

5.1. Introduction

It is a common practice to compound brittle polymers with plasticizers to enhance their flexibility and toughness for various applications. However, the addition of a small amount of low molecular weight plasticizer can result in an anomalous "antiplasticization" effect on the mechanical and other physical properties of a polymer. Increases in modulus and yield stress, decreases in creep compliance and impact strength, and reductions in gas sorption and transport have been observed in many polymers including polycarbonate (PC) [1-6], poly(methyl methacrylate) (PMMA) [7], polysulfone (PSF) [8-10], and poly(vinyl chloride) (PVC) [7,11-19]. Previous studies also suggested that antiplasticization is time and temperature dependent [13,20].

The antiplasticization phenomenon has been attributed to the influence of the additive on hindering the local β-relaxation motions of the polymer [21,22]. Since PVC has no side group, it is suggested that its β-motions are due to the cooperative motions of the polymer main chain [19,23]. As the plasticizer content increases, decreasing intensity of the β-transition peak in the loss modulus curve has been observed in many PVC-plasticizer systems [14-16,19,24]. Vilics et al. [16] proposed that localized interactions are established between the aromatic rings of the plasticizer and the PVC backbone, thereby hindering the local segmental β-motions. Such a restriction on the β-motions continues when the temperature is greater than the β-transition temperature, resulting in a higher modulus and yield stress in the slightly plasticized polymers at temperatures between the β- and α-transitions. In the case of PVC and dioctyl phthalate (DOP) compounds, it is suggested that the interaction that hinders the β-motions is the strong hydrogen-bonding between the carbonyl group()C=O) of DOP and the PVC repeat unit (-[CH_2CHCl]-) [25,26].

Amorphous polymers are known for their thermodynamically nonequilibrium nature at the glassy state [27,28]. As a polymer is cooled at a finite rate from a melt state through the glass transition (T_g) into its glassy state, the mobility of the molecular chains decreases to a point

where equilibrium conformation and packing cannot be reached with respect to the temperature. Polymer molecules are essentially frozen in a nonequilibrium state with lower packing (higher "free volume") and greater disorder in the structure. With time, the polymer continues to gradually undergo molecular rearrangement/packing in order to reach the equilibrium state, which results in the observed physical aging behavior. Typically the aging of polymers results in increases in density, yield strength and modulus [27,28]. For example, Hasan et al. had demonstrated that the local free volume, yield stress and post-yield strain softening are sensitive to the thermomechanical history of the polymer [29,30]. Quenched (unaged) samples were found to have higher initial free volume and lower yield stress when compared to well-annealed (aged) samples. In both quenched and annealed samples, an increase in local free volume sites was observed to accompany the strain softening of the yield stress until both the quenched and annealed samples reached an identical steady state after sufficient inelastic strain. In this study, we investigate the effect of thermal treatment and inelastic straining on the antiplasticization of slightly plasticized PVC.

A transition in the rate sensitivity of polymer yield behavior has also been connected to the local β-relaxation process [31-34]. In general, the yield stress required for plastic deformation increases with increasing strain rate or decreasing temperature in an Arrhenius-like manner. However, as the strain rate increases beyond a particular magnitude, a transition in the rate dependence of the yield stress has been reported for various glassy polymers, such as PC [32,35-37], PMMA [33-36,38,39], and PVC [31,33,37,40]. Above the transition threshold, an additional stress is required to activate the β-process in order for the material to yield. Since both the rate-dependent behavior and the antiplasticization phenomenon of polymers are related to the local β-motions, compression testing over a wide range of strain rates is conducted here in order to investigate the influence of strain rate on the antiplasticization effect in slightly plasticized PVC.

5.2. Results and Discussions

5.2.1. Effect of Thermomechanical History on Antiplasticization

Physical aging is known to alter the microstructural states of glassy polymers [27,28]. Two different thermal treatments were conducted to observe the effect of thermal treatments on antiplasticization. Specimens were kept at 85 ^{0}C for 2 hours and then they were either cooled to room temperature immediately (quenching) or slowly over a period of time (annealing). Figure 5-1 shows the effect of thermal treatments on the stress-strain behavior of PVC. Annealing physically ages the samples and is seen to increase the initial yield stress and the amount of post-yield strain softening which occurs after yield; quenching from above the T_g acts to freeze in a more disordered, "higher free volume" state and results in a lower yield stress when compared to the annealed samples [30]. Both materials exhibit substantial strain softening after yield, resulting in very similar stress-strain behavior after sufficient inelastic strain. The inelastic straining immediately post-yield is considered to "rejuvenate" or "de-age" the structure, creating a more disordered, higher free volume state which gives the corresponding softening of the yield stress [30,41].

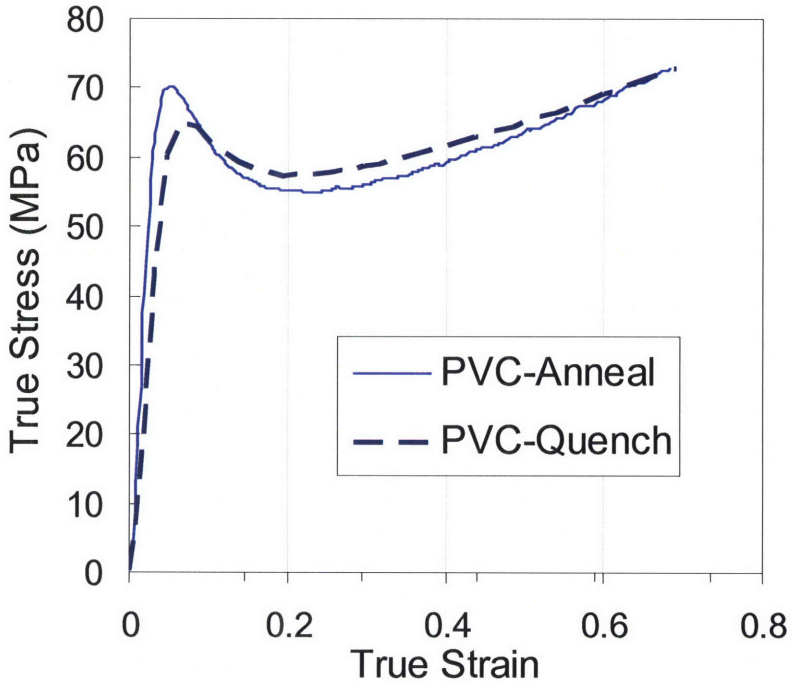

Figure 5-1. Effect of thermal treatments on PVC stress-strain behavior under uniaxial compression at 0.001/s strain rate.

Figure 5-2 shows the true stress-true strain curves of PVC and PVC with 5 wt% DOP after two different thermal treatments. Antiplasticization was observed in the annealed PVC/5 wt% DOP specimens as evidenced by the higher yield stress in the PVC/5 wt% DOP material, indicating the β-motions are hindered by the interactions between the DOP molecules and the PVC (as confirmed by dynamic mechanical analysis presented in Soong, et al. [40,42]). However, antiplasticization was not observed in the quenched samples (Figure 5-2).

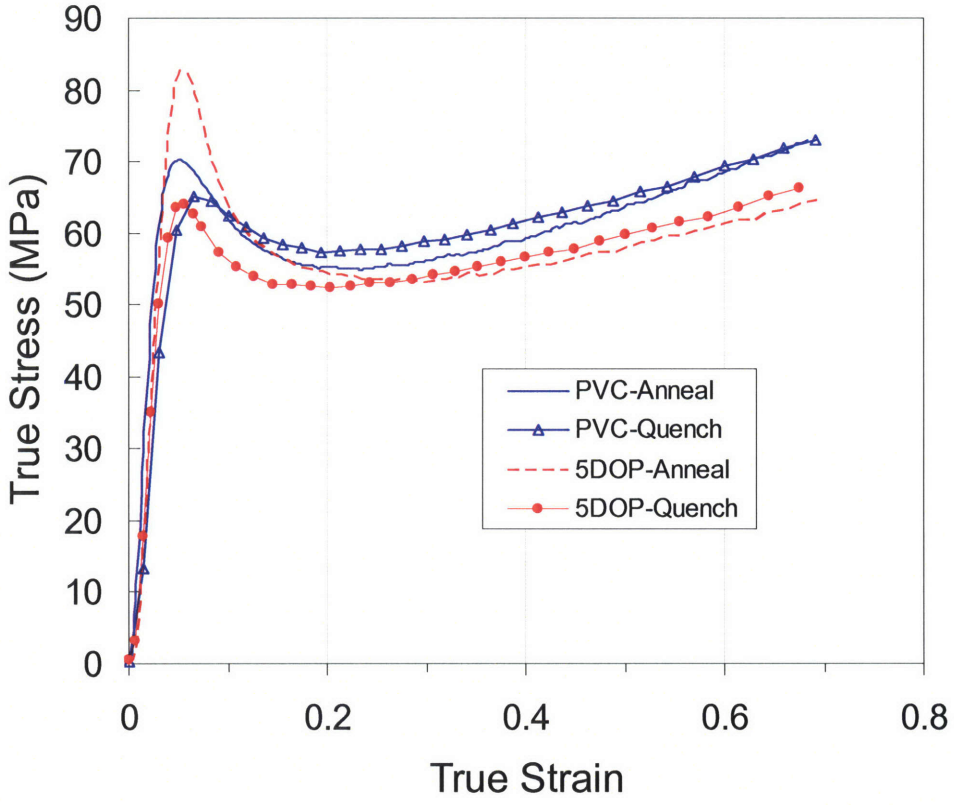

Figure 5-2. True stress-true strain curves of PVC and PVC/5 wt% DOP: annealing vs. quenching.

This observation suggests that the quenching treatment resulted in a more nonequilibrated, less packed microstructure whereby β-motion hindering interactions between DOP molecules and PVC repeat units were not fully established. Therefore the local β-motions were more liberated and mobile in the quenched polymer than in the physically-aged (annealed) material. After strain softening, both the annealed and quenched PVC/5 wt% DOP exhibit a lower flow stress when

compared to the neat PVC in Figure 5-2. This suggests that the increased structural disorder and free volume which accompanies inelastic straining [30,43,44] also liberates the β-motions in the slightly plasticized PVC during the post-yield plastic flow. Hence the flow stress of PVC/5 wt% DOP falls beneath the neat PVC flow stress. Therefore, the dramatic magnitude of strain softening observed in the annealed PVC/5 wt% DOP sample is a result of "liberating" the hindered β-motions in addition to the more typical rejuvenation effect of inelastic straining observed in amorphous polymers.

As discussed above, sufficient inelastic deformation is known to erase the initial thermomechanical history of polymer. In order to more definitively exam the effect of inelastic strain on antiplasticization, the annealed PVC and PVC/5 wt% DOP samples were first loaded in compression to a true strain of -0.15, unloaded, and then immediately reloaded until the true strain reached -0.7. Figure 5-3 shows the true stress-true strain curves of PVC and PVC with 5 wt% DOP in this two-cycle compression testing at 0.001/s. While the PVC with 5 wt% DOP material exhibited antiplasticization (a higher yield stress) in the first loading (c1), no antiplasticization was observed in the reloading curve (c2). This observation suggests that the initially restricted β-motions in PVC/5 wt% DOP were locally liberated due to the increase in local free volume generated by the inelastic deformation in the first loading step. Importantly, this result demonstrates that active plastic flow is not necessary to liberate the β-motions, but that the new structure (i.e., the increased disorder and higher local free volume) created by the inelastic strain provides the liberation of the formerly hindered β-motions. This result is fully consistent with the observation that the quenched PVC/5 wt% DOP material does not exhibit antiplasticization.

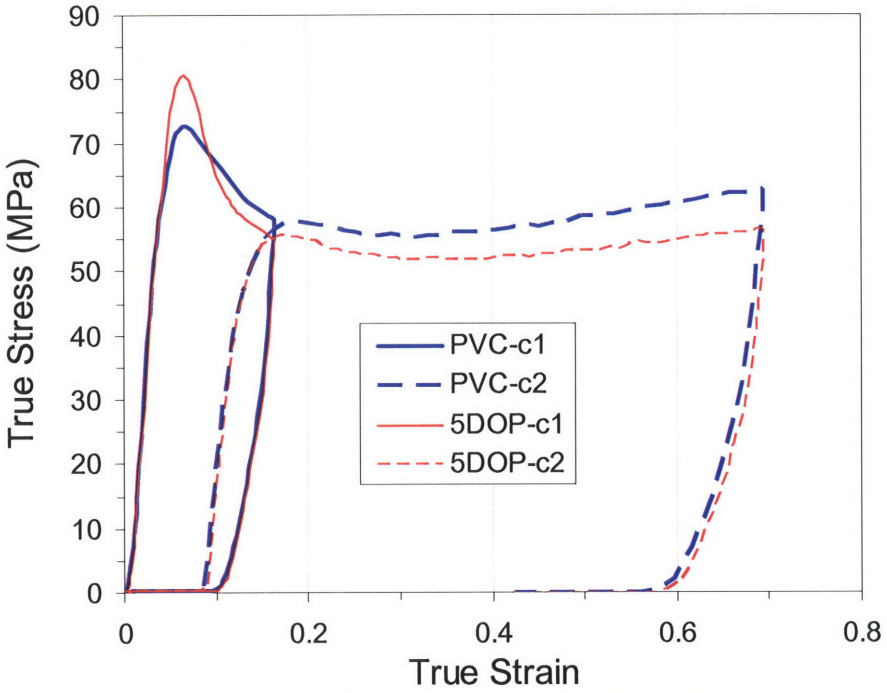

Figure 5-3. True stress-true strain curves of PVC and PVC with 5 wt% DOP under uniaxial compression at 0.001/s. Samples were compressed to a true strain of -0.15 (c1), unloaded, and then immediately reloaded to a true strain of -0.7 (c2).

To furthermore demonstrate the combined effect of thermal treatment and inelastic straining on the antiplasticization behavior, thermal treatments were applied to the specimens between the first loading (c1) and the second loading (c2). After being compressed to -0.15 true strain at a strain rate of 0.001, specimens were either annealed (slow-cooling) or quenched (fast-cooling) before the second loading process and the results are shown in Figure 5-4a and Figure 5-4b, respectively. After the heat treatments, the original specimen geometry was recovered and the sample heights returned to approximately the same as the initial values. The annealed specimens exhibited the same stress-strain behavior in c2 as in c1 where antiplasticization was observed in PVC/5 wt% DOP. On the contrary, the antiplasticization behavior was not found in the quenched sample. This observation agrees with the previous finding in the effect of thermal history on antiplasticization, which also suggests that thermal treatment erased the influence of inelastic straining.

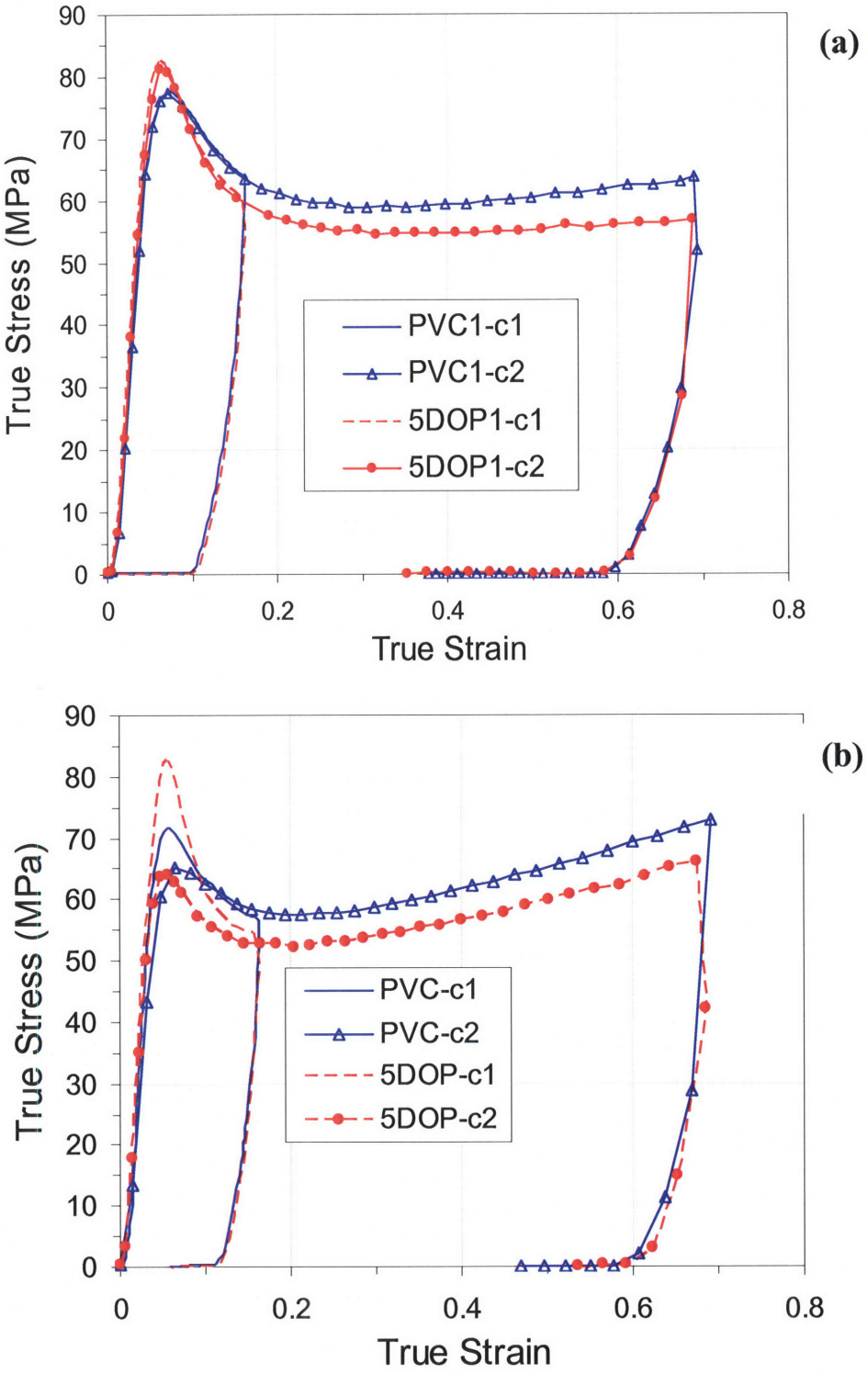

Figure 5-4. True stress-true strain curves of PVC and PVC with 5 wt% DOP under uniaxial compression at 0.001/s. Samples were compressed to -0.15 true strain (c1), unloaded, and two different thermal treatments were applied before reloading (c2): annealed (a) and quenched (b).

5.2.2. Rate-Dependency of Antiplasticization

Figure 5-5 presents the true stress-true strain curves of PVC and PVC with 5 wt% DOP at strain rates of 0.001/s, 1/s, 200/s, and 2000/s, and the yield data obtained from various compression strain rates are summarized in Figure 5-5b. Due to adiabatic heating at high strain rates, significant post-yield thermal softening was observed at 200/s and 2000/s in additional to the strain softening seen at low rates. More detailed discussions regarding the thermal softening at high strain rate compression testing were presented by Mulliken et al. [45]. For PVC, the yield stress increases linearly with the logarithm of strain rate in the low rate and high rate regimes. However the rate sensitivity is much greater in the high rate regime. Beyond the transition point, an additional stress is necessary to activate the β-process to enable global yield [40]. At low strain rates (<1/s), antiplasticization was seen in PVC with 5 wt% DOP. The strong affiliation established between DOP molecules and PVC backbones results in restricted local β-motions in PVC/5 wt% DOP; therefore a higher yield stress was required for the material to induce plastic deformation. When the strain rate is above 100/s, the β-process in neat PVC becomes important and a non-negligible stress is required to activate the β-process to cause yield. Hence, any influence of an "antiplasticization" effect on the yield stress disappears gradually with increasing strain rate since the β-motions are restricted in both the PVC and the PVC with 5 wt% DOP in the high rate deformation regime.

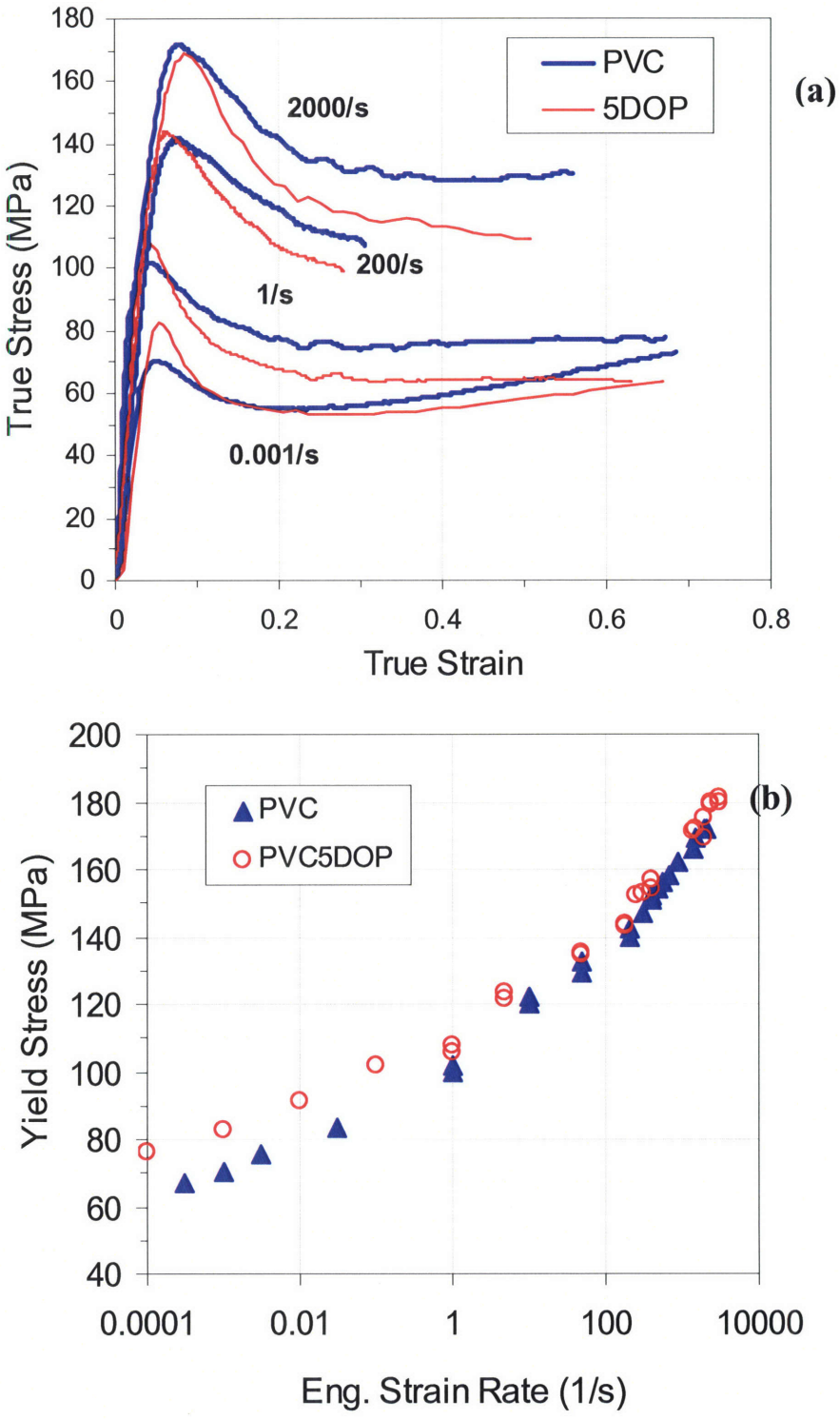

Figure 5-5. Rate-dependency of antiplasticization in PVC and PVC/5 wt% DOP under uniaxial compression: stress-strain behavior at various strain rates (a) and yield stress as a function of engineering strain rate (b).

5.3. Conclusions

The effects of thermomechanical history and strain rate on the antiplasticization phenomenon in slightly plasticized PVC were investigated in this study. The influence of thermal treatment was demonstrated by applying annealing or quenching to the PVC and PVC/5 wt% DOP specimens. Antiplasticization was seen in the annealed (aged) PVC/5 wt% DOP; however it was absent in the quenched samples. This observation suggests that quenching not only leads to a more non-equilibrated state than annealing, but the consequential higher free volume also locally liberates the β-motions and hence undoes the antiplasticization in PVC/5 wt% DOP. Inelastic straining also leads to an increase in the local free volume and erases the antiplasticization effect. While antiplasticization was seen in the form of a higher yield stress in the first compressive loading of PVC/5 wt% DOP, the post-yield strain softening was found to erase the antiplasticization effect and antiplasticization was not observed in the immediate reloading curve.

The mechanical behavior of PVC and PVC with 5 wt% DOP was characterized in compression testing over a wide range of strain rates (10^{-4}/s to 3000/s). A higher yield stress (antiplasticization) was observed in the low rate regime, and it gradually disappeared with the increasing strain rate. In the low rate regime, the local β-motions in PVC/5 wt% DOP material are restricted due to the strong interactions between the DOP molecules and PVC repeat units, whereas the β-motions are liberated in the neat PVC. As a result, an additional stress is required to activate the β-process and enable yield in the PVC/5 wt% DOP, but not in the neat PVC; hence, a higher yield stress was observed in the slightly plasticized PVC at low rates. As the strain rate is increased, the β-motions in neat PVC become less liberated. Beyond the transition point, an extra stress is necessary to activate the β-process in neat PVC to enable yield. Consequently, the antiplasticization due to the restricted β-motions disappears in the high rate regime since the β-motions must be stress-activated to yield both PVC and PVC/5 wt% DOP when deformed at high strain rates.

5.4. Reference

1. Bergquist, P.; Zhu, Y.; Jones, A. A.; Inglefield, P. T., "Plasticization and Antiplasticization in Polycarbonates: The Role of Diluent Motion", Macromolecules 1999, 32, 7925-7931.

2. Ngai, K. L.; Rendell, R. W.; Yee, A. F.; Plazek, D. J., "Antiplasticization Effects on a Secondary Relaxation in Plasticized Glassy Polycarbonates", Macromolecules 1991, 24, 61-67.

3. Robertson, R. E.; Yoynson, C. W., "Free Volume and the Annealing and Antiplasticizing of Bisphenol A Polycarbonate", J. Appl. Polym. Sci. 1972, 16, 733-738.

4. Jackson Jr., W. J.; Caldwell, J. R., "Antiplasticization. II. Characteristics of Antiplasticizers", J. Appl. Polym. Sci. 1967, 11, 211-226.

5. Jackson Jr., W. J.; Caldwell, J. R., "Antiplasticization. III. Characteristics and Properties of Antiplasticizable Polymers", J. Appl. Polym. Sci. 1967, 11, 227-244.

6. Robeson, L. M., "Secondary Loss Transitions in Antiplasticized Polymers", Polym. Lett. 1969, 7, 35-40.

7. Boughalmi, R.; Jarray, J.; Ben Cheikh Larbi, F.; Dubault, A.; Halary, J. L., "Molecular Analysis of the Mechanical Behavior of Plasticized Amorphous Polymers", Oil Gas Sci. Technol. 2006, 61, 725-733.

8. Maeda, Y.; Paul, D. R., "Effect of Antiplasticization on Gas Sorption and Transport. III. Free Volume Interpretation", J. Polym. Sci.: Part B: Polym. Phys. 1987, 25, 1005-1016.

9. Maeda, Y.; Paul, D. R., "Effect of Antiplasticization on Gas Sorption and Transport. I. Polysulfone", J. Polym. Sci.: Part B: Polym. Phys. 1987, 25, 957-980.

10. Vidotti, S. E.; Chinellato, A. C.; Hu, G.-H.; Pessan, L. A., "Effects of Low Molar Mass Additives on the Molecular Mobility and Transport Properties of Polysulfone", J. Appl. Polym. Sci. 2006, 101, 825-832.

11. Bergman, G.; Bertilsson, H.; Shur, Y. J., "Antiplasticization and Transition to Marked Nonlinear Viscoelasticity in Poly(vinyl chloride)/Acrylonitrile-Butadiene Copolymer Blends", J. Appl. Polym. Sci. 1977, 21, 2953-2961.

12. Elicegui, A.; del Val, J. J., "A Study of Plasticization Effects in Poly(vinyl chloride)", Polymer 1997, 38, 1647-1657.

13. Guerrero, S. J., "Antiplasticization and Crystallinity in Poly(vinyl chloride)", Macromolecules 1989, 22, 3480-3485.

14. Kinjo, N.; Nakagawa, T., "Antiplasticization in the Slightly Plasticized Poly(vinyl chloride)", Polym. J. 1973, 4, 143-153.

15. Sundgren, N.; Bergman, G.; Shur, Y. J., "Antiplasticization and Transition to Marked Nonlinear Viscoelasticity in Poly(vinyl chloride) (PVC)/Poly-e-caprolactone (PCL) Blends", J. Appl. Polym. Sci. 1978, 22, 1255-1265.

16. Vilics, T.; Schneider, H. A.; Manoviciu, V.; Manoviciu, I., "A DMA Study of the Suppression of the b-Transition in Slightly Plasticized PVC Blends", J. Therm. Anal. 1996, 47, 1141-1153.

17. Dubault, A.; Bokobza, L.; Gandin, E.; Halary, J. L., "Effects of Molecular Interactions on the Viscoelastic and Plastic Behavior of Plasticized Poly(vinyl chloride)", Polym. Int. 2003, 52, 1108-1118.

18. Pezzin, G.; Ajroldi, G.; Casiraghi, T.; Garbuglio, C.; Vittadini, G., "Dynamic-Mechanical and Tensile Properties of Poly(vinyl chloride). Influence of Thermal History and Crystallinity", J. Appl. Polym. Sci. 1972, 16, 1839-1849.

19. Pezzin, G.; Ajroldi, G.; Garbuglio, C., "Dynamic-Mechanical Study of the Secondary Transition of Poly(vinyl chloride)", J. Appl. Polym. Sci. 1967, 2, 2553-2565.

20. Mascia, L., "Antiplasticization of Poly(vinyl chloride) in Relation to Thermal Ageing and Non-linear Viscoelastic Behaviour", Polymer 1978, 19, 325-328.

21. Liu, Y.; Roy, A. K.; Jones, A. A.; Inglefield, P. T.; Ogden, P., "An NMR Study of Plasticization and Antiplasticization of a Polymeric Glass", Macromolecules 1990, 23, 968-977.

22. Quan, X.; Gancarz, I.; Koberstein, J. T.; Wignall, G. D., "Local Intermolecular Structure in an Antiplasticized Glass by Solid-State NMR", Macromolecules 1987, 20, 1434-1437.

23. Sefcik, M. D.; Schaefer, J.; May, F. L.; Raucher, D.; Dub, S. M., "Diffusivity of Gases and Main-Chain Cooperative Motions in Plasticized Poly(vinyl chloride)", J. Polym. Sci., Polym. Phys. Ed. 1983, 21, 1041-1054.

24. Dubault, A.; Bokobza, L.; Gandin, E.; Halary, J. L., "Effects of Molecular Interactions on the Viscoelastic and Plastic Behaviour of Plasticized Poly(vinyl chloride)", Polym. Int. 2003, 52, 1108-1118.

25. Garnaik, B.; Sivaram, S., "Study of Polymer-Plasticizer Interaction by 13C CP/MAS NMR Spectroscopy: Poly(vinyl chloride)-Bis(2-ethylhexyl) Phthalate System", Macromolecules 1996, 29, 185-190.

26. Gonzalez, N.; Fernandes-Berridi, M. J., "Application of Fourier Transform Infrared Spectroscopy in the Study of Interactions Between PVC and Plasticizers: PVC/Plasticizer Compatibility versus Chemical Structure of Plasticizer", J. Appl. Polym. Sci. 2005, 101,

27. Struik, L., "Physical Aging in Amorphous Polymers and Other Materials", Elsevier, New York, 1978.

28. Tant, M. R.; Wilkes, G. L., "An Overview of the Nonequilibrium Behavior of Polymer Glasses", Polym. Eng. Sci. 1981, 21, 874-895.

29. Hasan, O. A.; Boyce, M. C., "Energy Storage During Inelastic Deformation of Glassy Polymers", Polymer 1993, 34, 5085-5092.

30. Hasan, O. A.; Boyce, M. C.; Li, X. S.; Berko, S., "An Investigation of the Yield and Postyield Behavior and Corresponding Structure of Poly(methyl methacrylate)", J. Polym. Sci.: Part B: Polym. Phys. 1993, 31, 185-197.

31. Bauwens, J. C., "Relation Between the Compression Yield Stress of Poly(vinyl chloride) and the Loss Peak in the b-Transition Range", J. Polym. Sci. 1971, 33, 123-133.

32. Bauwens, J. C., "Relation between the Compression Yield Stress and the Mechanical Loss Peak of Bisphenol-A-Polycarbonate in the b-Transition Range", J. Mater. Sci. 1972, 7, 577-584.

33. Bauwens-Crowet, C.; Bauwens, J. C.; Homes, G., "Tensile Yield-Stress Behavior of Glassy Polymers", J. Polym. Sci., Part A-2 1969, 7, 735-742.

34. Roetling, J. A., "Yield Stress Behaviour of Polymethylmethacrylate", Polymer 1965, 6, 311-317.

35. Monnerie, L.; Halary, J. L.; Kausch, H.-H., "Deformation, Yield and Fracture of Amorphous Polymers: Relation to the Secondary Transitions", Adv. Polym. Sci. 2005, 187, 215-364.

36. Mulliken, A. D.; Boyce, M. C., "Mechanics of the Rate-Dependent Elastic-Plastic Deformation of Glassy Polymers from Low to High Strain Rates", Int. J. Solids Struct. 2006, 43, 1331-1356.

37. Bauwens, J. C.; Bauwens-Crowet, C.; Homes, G., "Tensile Yield-Stress Behavior of Poly(vinyl chloride) and Polycarbonate in the Glass Transition Region", J. Polym. Sci., Part A-2 1969, 7, 1745-1754.

38. Bauwens-Crowet, C., "The Compression Yield Behaviour of Polymethyl Methacrylate over a Wide Range of Temperatures and Strain Rates", J. Mater. Sci. 1973, 8, 968-979.

39. Swallowe, G. M.; Lee, S. F., "A Study of the Mechanical Properties of PMMA and PS at Strain Rates of 10-4 to 103 over the Temperature Range 293-363 K", J. Phys. IV France 2003, 110, 33-38.

40. Soong, S. Y.; Mulliken, A. D.; Cohen, R. E.; Boyce, M. C., "Rate-Dependent Deformation Behavior of POSS-Filled and Plasticized Poly(vinyl chloride)", Macromolecules 2006, 39, 2900-2908.

41. Oleynik, E. F., "High Performance Polymers", Hauser, Munich, 1990.

42. Soong, S. Y.; Cohen, R. E.; Boyce, M. C., "Polyhedral Oligomeric Silsesquioxane as a Novel Plasticizer for Poly(vinyl chloride)", Polymer 2007, 48, 1410-1418.

43. Hasan, O. A.; Boyce, M. C., "A Constitutive Model for the Nonlinear Viscoelastic Viscoplastic Behavior of Glassy Polymers", Polym. Eng. Sci. 1995, 35, 331-344.

44. Zhou, Q.-Y.; Argon, A. S.; Cohen, R. E., "Enhanced Case-II Diffusion of Diluents into Glassy Polymers Undergoing Plastic Flow", Polymer 2001, 42, 613-621.

45. Mulliken, A. D.; Soong, S. Y.; Boyce, M. C.; Cohen, R. E., "High-Rate Thermomechanical Behavior of Poly(vinyl chloride) and Plasticized Poly(vinyl chloride)", J. Phys. IV France 2006, 134, 217-223.

Chapter 6: Constitutive Modeling

[Part of this work has been published previously, in slightly different form, in "Rate-Dependent Deformation Behavior of POSS-Filled and Plasticized Poly(vinyl chloride)" by S.Y. Soong, R.E. Cohen, M.C. Boyce, and A.D. Mulliken, *Macromolecules* **2006**, *39*, 2900-2908 [1] and in "High-Rate Thermomechanical Behavior of Poly(vinyl chloride) and Plasticized Poly(vinyl chloride)" by A.D. Mulliken, S.Y. Soong, M.C. Boyce, and R.E. Cohen, *J. Phys. IV France* **2006**, *134*, 217-223 [2].]

6.1. Introduction

6.1.1. Constitutive Model – Mulliken and Boyce, 2004

The constitutive model for the rate-dependent elastic-plastic behavior of amorphous polymer proposed by Mulliken and Boyce [3,4] was employed to predict the strain rate dependence of the yield stress of the PVC/methacryl-POSS and PVC/DOP blends in uniaxial compression tests. The Mulliken and Boyce model may be considered as a revision of the three-dimensional rate-dependent thermoplastic model described by Arruda and Boyce [5-8]. The model proposed by Arruda and Boyce has demonstrated its ability to predict the stress-strain behavior of PC and PMMA at low and moderate strain rates (10^{-3}/s to 1/s), at temperatures from 20 °C to 90 °C, and in four states of deformation including plane strain compression, simple shear, uniaxial tension, and uniaxial compression. The Arruda and Boyce model was meant to simulate only the α-process. In order to capture the material behavior at high strain rates and low temperatures, this revised Mulliken and Boyce model considers the contribution of the β-process and its significance under those conditions. Using the experimental data of this study, predictive capabilities have been established within the framework of this model, which was developed by Mulliken and Boyce specifically for capturing the rate-dependent mechanical behavior of two other amorphous polymers, polycarbonate (PC) [7,8] and poly(methyl methacrylate) (PMMA) [6,9]. It was shown that both PC and PMMA exhibit an enhanced stiffness and strength under conditions of moderate and high strain rate related to restricted "β" molecular motions.

Figure 6-1 shows the 1-D rheological interpretation of the Mulliken and Boyce model. The model consists of three main components, each capturing a different molecular-level resistance to the macroscopic deformation. The model features *two* elastic-viscoplastic processes ("A"), α and

β, acting in tandem, along with a non-linear Langevin spring ("B") for strain hardening. The total stress of the material is the sum of the stress in these three components. The α-component captures the intermolecular resistance to large scale main chain motions, while the β-component captures the resistance to secondary local chain motions (for PVC, the β-motions are attributed to cooperative motions between neighboring repeat units). The β-process in this model is considered as its own elastic-viscoplastic component, which is in parallel with the existing "α" elastic-viscoplastic component. The β-component requires stress-assisted activation and becomes significant at low temperatures and high strain rates. The non-linear Langevin spring represents the back stress of entropic orientation hardening, which is developed from the alignment of polymer chains during increasing deformation.

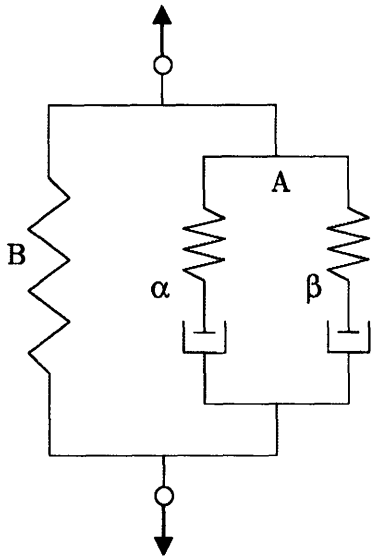

Figure 6-1. 1-D rheological interpretation of the proposed constitutive model by Mulliken and Boyce. [3,4]

Thermomechanical coupling is especially important at high rates of deformation where the testing condition can be considered adiabatic. The model takes into account the thermomechanical coupling through a conversion of the dissipative work of the viscoplastic dashpots into heat, leading to a temperature rise in the polymer. The resulting temperature rise alters the mechanical behavior of the polymer, as calculated through the thermal-activation

model of yield together with the temperature-dependent elastic constants and shear resistance, as well as thermal expansion effects.

Both the α- and β-components have unique material parameter definitions, and their relative contributions vary with the temperature and strain rate. In order to define the elasticity of the α- and β-component springs, an analytical decomposition of the storage modulus data (measured in DMA) is conducted, taking into account the unique rate and temperature dependencies of the α and β viscoelastic processes. Similarly, a component-wise split of the yield data in compression testing is used to calculate the activation parameters for the α- and β-component dashpots.

Kinematics. The kinematic framework of the Mulliken and Boyce model [3,4,10,11] follows the previous work of Bergstrom and Boyce (1998 [12], 2000 [13]), Boyce et al. (2000 [14]), and Boyce et al (2001[15]), except that the elastic-viscoplastic relationship is developed in duplicate to represent both the α- and β-components .

Here, we will show the formulation in a principal stretch frame. Upon loading, the total deformation gradient, as expressed as a stretch tensor in the principal stretch frame, is given by the diagonal tensor $\mathbf{\Lambda}$ where each diagonal component is the stretch ratio in a principal direction:

$$\mathbf{\Lambda}_{A\alpha} = \mathbf{\Lambda}_{A\beta} = \mathbf{\Lambda}_{B} = \mathbf{\Lambda} \tag{6-1}$$

The deformation gradients in element A may be decomposed into elastic and plastic components, via Kroner-Lee decomposition [16,17]:

$$\mathbf{\Lambda}_{A\alpha} = \mathbf{\Lambda}^{e}_{A\alpha}\mathbf{\Lambda}^{p}_{A\alpha} \tag{6-2}$$

$$\mathbf{\Lambda}_{A\beta} = \mathbf{\Lambda}^{e}_{A\beta}\mathbf{\Lambda}^{p}_{A\beta} \tag{6-3}$$

Assuming the plastic deformation is a volume-preserving process, i.e. $\det \mathbf{\Lambda}^{p}_{A\alpha} = \det \mathbf{\Lambda}^{p}_{A\beta} = 1$, thus all volume-changing deformation is elastic:

$$\det \mathbf{\Lambda}^{e}_{A\alpha} = \det \mathbf{\Lambda}^{e}_{A\beta} = J \tag{6-4}$$

The plastic deformation gradients $\mathbf{\Lambda}^{p}_{A\alpha}$ and $\mathbf{\Lambda}^{p}_{A\beta}$ are interpreted as the mapping of a material point in the reference configuration to the "relaxed configuration", obtained by elastic unloading to a stress-free state.

Next, the deformation rate in the body is expressed through the velocity gradient, **L**:

$$\mathbf{L} = \mathbf{L}_{A\alpha} = \mathbf{L}_{A\beta} = \frac{\partial v}{\partial x} = \dot{\mathbf{\Lambda}}_{A}\mathbf{\Lambda}_{A}^{-1} \tag{6-5}$$

Decomposing the velocity gradient into elastic and plastic components:

$$\mathbf{L}_{A\alpha} = \mathbf{L}^{e}_{A\alpha} + \mathbf{\Lambda}^{e}_{A\alpha}\mathbf{L}^{p}_{A\alpha}\mathbf{\Lambda}^{e-1}_{A\alpha} = \mathbf{L}^{e}_{A\alpha} + \tilde{\mathbf{L}}^{p}_{A\alpha} \tag{6-6}$$

$$\mathbf{L}_{A\beta} = \mathbf{L}^{e}_{A\beta} + \mathbf{\Lambda}^{e}_{A\beta}\mathbf{L}^{p}_{A\beta}\mathbf{\Lambda}^{e-1}_{A\beta} = \mathbf{L}^{e}_{A\beta} + \tilde{\mathbf{L}}^{p}_{A\beta} \tag{6-7}$$

where

$$\tilde{\mathbf{L}}^{p}_{A\alpha} = \tilde{\mathbf{D}}^{p}_{A\alpha} \tag{6-8}$$

$$\tilde{\mathbf{L}}^{p}_{A\beta} = \tilde{\mathbf{D}}^{p}_{A\beta} \tag{6-9}$$

$\tilde{\mathbf{D}}^{p}_{Ai}$ is a symmetric tensor (i=α, β) represents the rate of plastic stretching of the relaxed configuration, note that the rate of plastic spin of the relaxed configuration is zero since we are considering principle stretch conditions only.

$$\dot{\mathbf{\Lambda}}^{p}_{A\alpha} = \mathbf{\Lambda}^{e-1}_{A\alpha}\tilde{\mathbf{D}}^{p}_{A\alpha}\mathbf{\Lambda}_{A\alpha} \tag{6-10}$$

$$\dot{\mathbf{\Lambda}}^{p}_{A\beta} = \mathbf{\Lambda}^{e-1}_{A\beta}\tilde{\mathbf{D}}^{p}_{A\beta}\mathbf{\Lambda}_{A\beta} \tag{6-11}$$

The plastic portion of the deformation gradient $\mathbf{\Lambda}^{p}_{A\alpha}$ and $\mathbf{\Lambda}^{p}_{A\beta}$ can be obtained through integration of Eq. (6-10) and Eq. (6-11), and the elastic portion are then obtained via:

$$\mathbf{\Lambda}^{e}_{A\alpha} = \mathbf{\Lambda}_{A\alpha}\mathbf{\Lambda}^{p-1}_{A\alpha} \tag{6-12}$$

$$\mathbf{\Lambda}^{e}_{A\beta} = \mathbf{\Lambda}_{A\beta}\mathbf{\Lambda}^{p-1}_{A\beta} \tag{6-13}$$

The kinematics derived here are for cases of principal stretch conditions only. Constitutive laws can then be used to connect the rate of plastic stretching (shape change) and the stress in the deforming material for a material-specific model. Each rate of shape change is given as:

$$\widetilde{\mathbf{D}}^{p}_{A\alpha} = \dot{\gamma}^{p}_{\alpha}\mathbf{N}^{p}_{A\alpha} \tag{6-14}$$

$$\widetilde{\mathbf{D}}^{p}_{A\beta} = \dot{\gamma}^{p}_{\beta}\mathbf{N}^{p}_{A\beta} \tag{6-15}$$

where $\dot{\gamma}^{p}_{i}$ (i=α, β) is the plastic strain rate and $\mathbf{N}^{p}_{Ai}$ is a direction tensor. $\mathbf{N}^{p}_{Ai}$ is taken to be coaxial with the deviatoric stress acting on the α- or β-component of the intermolecular network A:

$$\mathbf{N}^{p}_{A\alpha} = \frac{\mathbf{T}'_{A\alpha}}{\left|\mathbf{T}'_{A\alpha}\right|} \tag{6-16}$$

$$\mathbf{N}^{p}_{A\beta} = \frac{\mathbf{T}'_{A\beta}}{\left|\mathbf{T}'_{A\beta}\right|} \tag{6-17}$$

Material Description and Constitutive Relations. The material model provides constitutive laws for the plastic strain rate, $\dot{\gamma}^{p}_{\alpha}$ and $\dot{\gamma}^{p}_{\beta}$, as well as the stress tensors, $\mathbf{T}_{A\alpha}$, $\mathbf{T}_{A\beta}$ and $\mathbf{T}_{B}$. For the linear elastic springs, the intermolecular contribution (element A) to the material stress is related to the deformation by constitutive laws:

$$\mathbf{T}_{A\alpha} = \frac{1}{J_\alpha}\mathcal{L}^e_\alpha\left[\ln \mathbf{\Lambda}^e_{A\alpha}\right] \tag{6-18}$$

$$\mathbf{T}_{A\beta} = \frac{1}{J_\beta}\mathcal{L}^e_\beta\left[\ln \mathbf{\Lambda}^e_{A\beta}\right] \tag{6-19}$$

where $\mathbf{T}_{Ai}$ (i=α, β) is the Cauchy true stress; J_i is the elastic volume change; $\mathcal{L}^e_i$ is the fourth-order modulus tensor; and $\ln \mathbf{\Lambda}^e_{Ai}$ is the Hencky strain. The material is assumed to be isotropic initially, and the elastic behavior of the material may be decomposed into α- and β-components. The modulus tensors can be derived from any two elastic constants that are component-specific, such as the shear modulus μ and bulk modulus κ:

$$\mathcal{L}^e_\alpha = 2\mu_\alpha I + \left(\kappa_\alpha - \frac{2}{3}\mu_\alpha\right)\mathbf{I}\otimes\mathbf{I} \tag{6-20}$$

$$\mathcal{L}^e_\beta = 2\mu_\beta I + \left(\kappa_\beta - \frac{2}{3}\mu_\beta\right)\mathbf{I}\otimes\mathbf{I} \tag{6-21}$$

where I and $\mathbf{I}$ are the forth-order and second-order identity tensors, respectively. The elastic constants, in this case μ_i and κ_i (i=α, β), are assumed to be both temperature and strain rate dependent.

The network (back) stress in the non-linear hardening component (element B) is taken to be deviatoric and is defined using the 8-chain interpretation of molecular alignment in the Arruda and Boyce model:

$$\mathbf{T}_B = \frac{c_R}{3}\frac{\sqrt{N}}{\lambda_{chain}}\mathcal{L}^{-1}\left(\frac{\lambda^p_{chain}}{\sqrt{N}}\right)\overline{\mathbf{B}}'_B \tag{6-22}$$

where $\lambda^p_{chain} = \sqrt{trace(\overline{\mathbf{B}}_B)/3}$ is the stretch on a chain in the eight-chain network; $\mathcal{L} = \mathcal{L}(\beta) \equiv \coth\beta - \frac{1}{\beta}$ is the Langevin function; $\overline{\mathbf{B}}'_B$ is the deviatoric part of the isochoric left Cauchy-Green tensor, $\overline{\mathbf{B}}_B = (\det\mathbf{\Lambda})^{-2/3}\mathbf{\Lambda}\mathbf{\Lambda}^T$; $\sqrt{N}$ is the limiting chain extensibility; and

$C_R \equiv nk\theta$ is the rubbery modulus, where n is the number of chains per unit volume, k is Boltzmann's constant, and θ is the absolute temperature. Note that the magnitude of this back stress increases asymptotically as the chain stretch reaches its limiting extensibility.

The total stress in the material is given as the sum of intermolecular stresses of α- and β-components and the network (back) stress:

$$\mathbf{T} = \mathbf{T}_{A\alpha} + \mathbf{T}_{A\beta} + \mathbf{T}_B \tag{6-23}$$

The effective equivalent shear stresses τ_α and τ_β are specified by:

$$\tau_\alpha = \sqrt{\frac{1}{2}\mathbf{T}'_{A\alpha}\mathbf{T}'_{A\alpha}} \tag{6-24}$$

$$\tau_\beta = \sqrt{\frac{1}{2}\mathbf{T}'_{A\beta}\mathbf{T}'_{A\beta}} \tag{6-25}$$

At last, two constitutive equations are assigned to the α and β viscoplastic behavior. When both the forward and backward processes are considered:

$$\dot{\gamma}^p_\alpha = 2\dot{\gamma}^p_{o,\alpha} \exp\left(-\frac{\Delta G_\alpha}{k\theta}\right) \sinh\left[\frac{\tau_\alpha\left(\dfrac{\Delta G_\alpha}{s_\alpha + \alpha_{p,\alpha} p}\right)}{k\theta}\right] \tag{6-26}$$

$$\dot{\gamma}^p_\beta = 2\dot{\gamma}^p_{o,\beta} \exp\left(-\frac{\Delta G_\beta}{k\theta}\right) \sinh\left[\frac{\tau_\beta\left(\dfrac{\Delta G_\beta}{s_\beta + \alpha_{p,\beta} p}\right)}{k\theta}\right] \tag{6-27}$$

where $\dot{\gamma}^p_{o,i}$ (i=α, β) is the preexponential factor, ΔG_i is the activation energy, k is the Boltzmann constant, θ is the absolute temperature, p is the pressure, $\alpha_{p,i}$ is the pressure coefficient, and s_i is an internal variable which captures the material's shear resistance [9]. When the equations above

are applied to glassy amorphous polymers, it is assumed that the stress in the α-process is sufficiently high such that the backward process may be neglected (see footnote 2 in Chapter 1, section 3). As a result, Eq. (6-26) may be simplified as:

$$\dot{\gamma}_{\alpha}^{p} \cong \dot{\gamma}_{o,\alpha}^{p} \exp\left[-\frac{\Delta G_{\alpha}}{k\theta}\left(1-\frac{\tau_{\alpha}}{s_{\alpha}+\alpha_{p,\alpha}p}\right)\right] \tag{6-28}$$

Such approximation is not appropriate for the β-process, where the backward process is considered non-negligible at low strain rates and moderate temperatures.

Following Argon [18], the initial shear resistance s_i (i=α, β) is related to the shear modulus μ_i and Poisson ratio υ_i:

$$s_{o,\alpha}(\theta,\dot{\varepsilon}) \equiv \frac{0.077\mu_{\alpha}(\theta,\dot{\varepsilon})}{1-\upsilon_{\alpha}} \tag{6-29}$$

$$s_{o,\beta}(\theta,\dot{\varepsilon}) \equiv \frac{0.077\mu_{\beta}(\theta,\dot{\varepsilon})}{1-\upsilon_{\beta}} \tag{6-30}$$

Here, only the shear resistance s_α in the α-process evolve to a preferred state with plastic straining:

$$\dot{s}_{\alpha} = h_{\alpha}\left(1-\frac{s_{\alpha}}{s_{ss,\alpha}}\right)\dot{\gamma}_{\alpha}^{p} \tag{6-31}$$

where h_α is the softening slope and $s_{ss,\alpha}$ is the shear resistance at its "preferred state". This internal variable s_i is both temperature- and rate-dependent, which allows us to capture the rate/temperature dependence of the yield stress through mimicking the rate/temperature dependence of shear modulus, and the evolution of s_i in the α-process also enables us to access the strain softening phenomenon. Further details of the model may be found in Mulliken (2006) [11].

At yield point, the total stress ($\sigma_{y,total}$) of polymer can be described as the sum of the α-process (Eq. (6-33)) and the β-process (Eq. (6-34)):

$$\sigma_{y,total} = \sigma_{y,\alpha} + \sigma_{y,\beta} \tag{6-32}$$

$$\sigma_{y,\alpha} = \frac{\sqrt{3}k\theta(s_{o,\alpha} + \alpha_{p,\alpha} p)}{\Delta G_\alpha}\left(\ln\frac{\sqrt{3}\dot{\varepsilon}}{\dot{\gamma}^p_{o,\alpha}} + \frac{\Delta G_\alpha}{k\theta}\right) \tag{6-33}$$

$$\sigma_{y,\beta} = \frac{\sqrt{3}k\theta(s_{o,\beta} + \alpha_{p,\beta} p)}{\Delta G_\beta}\sinh^{-1}\left[\frac{\sqrt{3}\dot{\varepsilon}}{\dot{\gamma}^p_{o,\beta}}\exp\left(\frac{\Delta G_\beta}{k\theta}\right)\right] \tag{6-34}$$

where $\dot{\varepsilon} = \frac{1}{\sqrt{3}}\dot{\gamma}^p$ is the axial strain rate. Eq. (6-33) and (6-34) are obtained through rearranging Eq. (6-28) and Eq (6-27), respectively.

6.2. Results

6.2.1. DMA Analytical Prediction

In association with the DMA data, analytical techniques have been developed to predict the contribution of the restricted β-motions to the overall deformation resistance under strain rate conditions well beyond the scope of the DMA apparatus. These techniques are based on an analytical decomposition of the storage modulus into α- and β-contributions, using clues in both the loss modulus and storage modulus curves. Figure 6-2 shows an example of a decomposed PVC storage modulus and its corresponding α- and β-components.

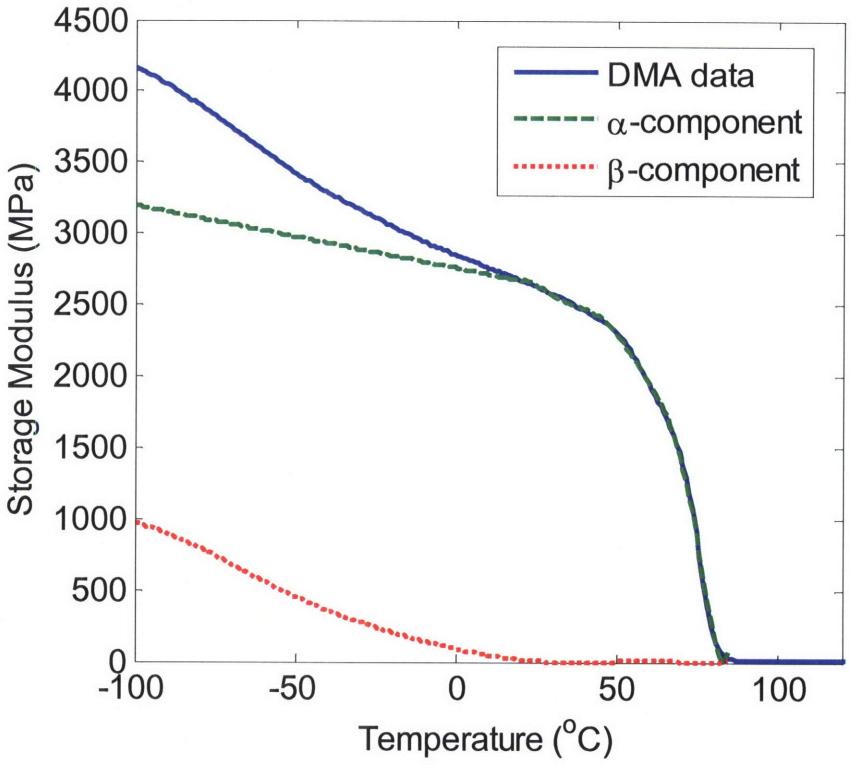

Figure 6-2. Analytical break-down of PVC storage modulus into the α- and β-components.

The α- and β-components are then taken to shift with increasing strain rate, according to the rate-dependence characterized in DMA, and thus the entire modulus curve may be reconstructed for any strain rate of interest. The analytical decomposition of the PVC storage modulus data is given in Figure 6-3, along with the shifted α- and β-contributions at a moderate strain rate (5/s) and at a high strain rate (5000/s). Based on the analytical results, the β-component becomes significant at room temperature when the strain rate is above approximately 1/s, where the PVC β-motions are expected to require stress-assisted activation in order to enable plastic flow. Therefore, above the "1/s" transition rates, according to the DMA analytical prediction, PVC is expected to exhibit an increase in the rate-sensitivity of deformation resistance. Such prediction is consistent with the yield stress results observed in compression testing shown in Figure 3-9a.

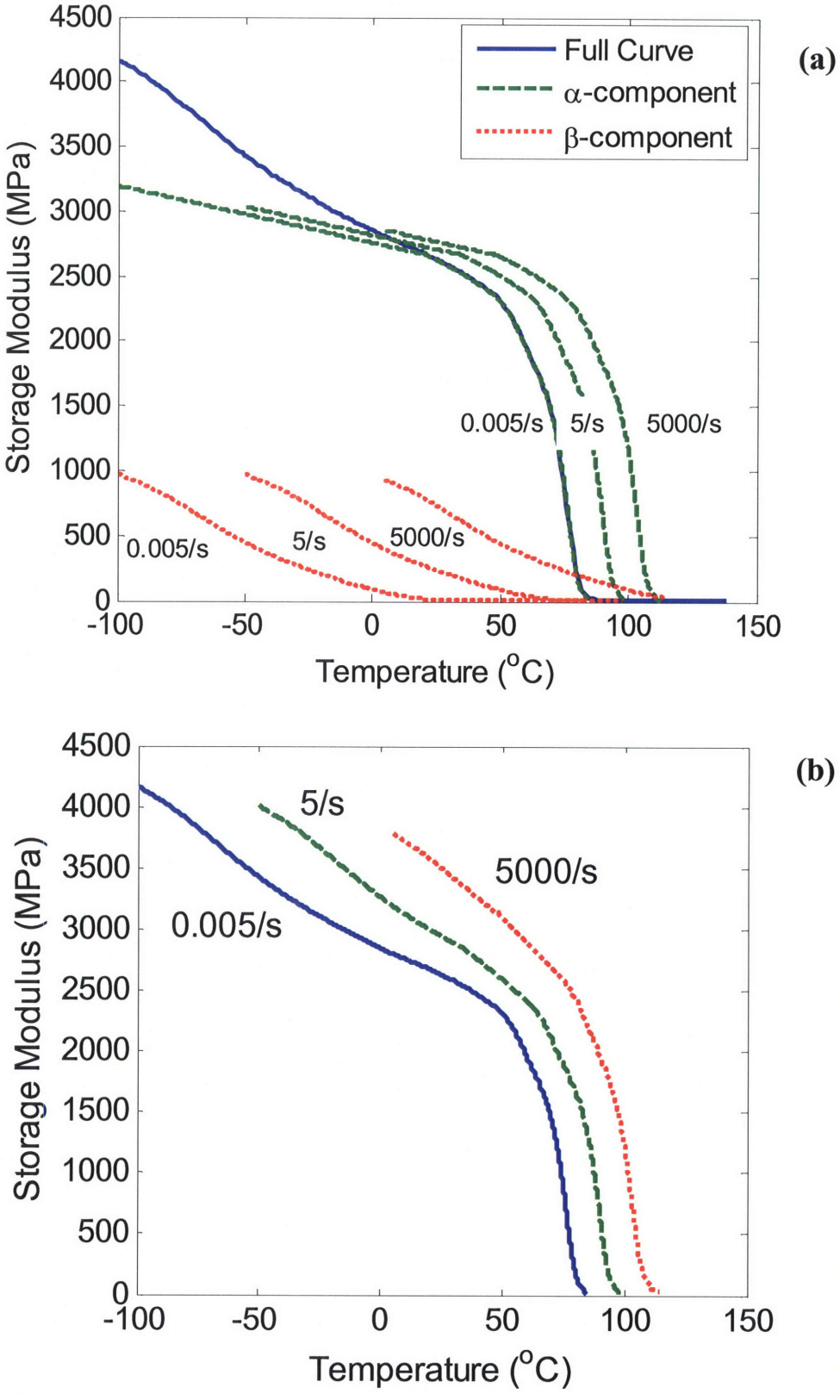

Figure 6-3. Shifting of decomposed α- and β- components (a) and recombined total contributions (b), at three strain rates: $5x10^{-3}$/s, 5/s, and $5x10^{3}$/s.

6.2.2. Yield Stress Model Prediction

Figure 6-4 shows the model prediction of PVC yield stress in compression as a function of the strain rate compared to the experimental compression data. Individual contributions of the α- and β-processes to the yield stress at different strain rates are shown in the figure, and the total model prediction is the sum of the α- and β-components. Noting that the model parameters, including the activation energy and preexponential factor for both the α- and β-processes, were fitted merely using the low and high rate compression data collected at MIT (without the moderate rate regime data from Purdue). The model is seen to capture the strong transition in rate sensitivity of the PVC as one transitions from low rates to very high rates. The moderate rate compression data also confirms that the model is able to predict the gradual transition accurately. Note that the α-contribution alone exhibits a gradual, small change in slope with strain rate, but this does not capture the dramatic difference in rate sensitivity observed at high rates. The models show that as the strain rate is increased, the β-motion requires stress-assisted activation, particularly as the strain rate approaches and exceeds 100/s. The need for stress activation of the β-motions at high rate is responsible for the increased rate sensitivity of yield seen at high rates. The rate-dependent yield stress at different temperatures can also be predicted by this model, and the results are shown in Figure 6-5.

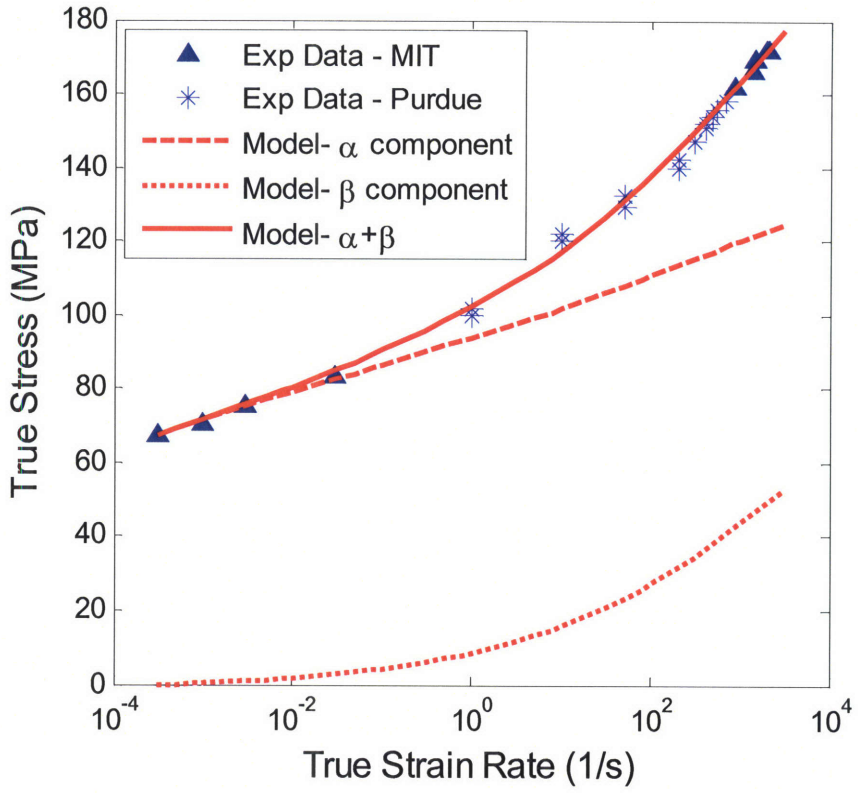

Figure 6-4. Model prediction of PVC yield stress as a function strain rate.

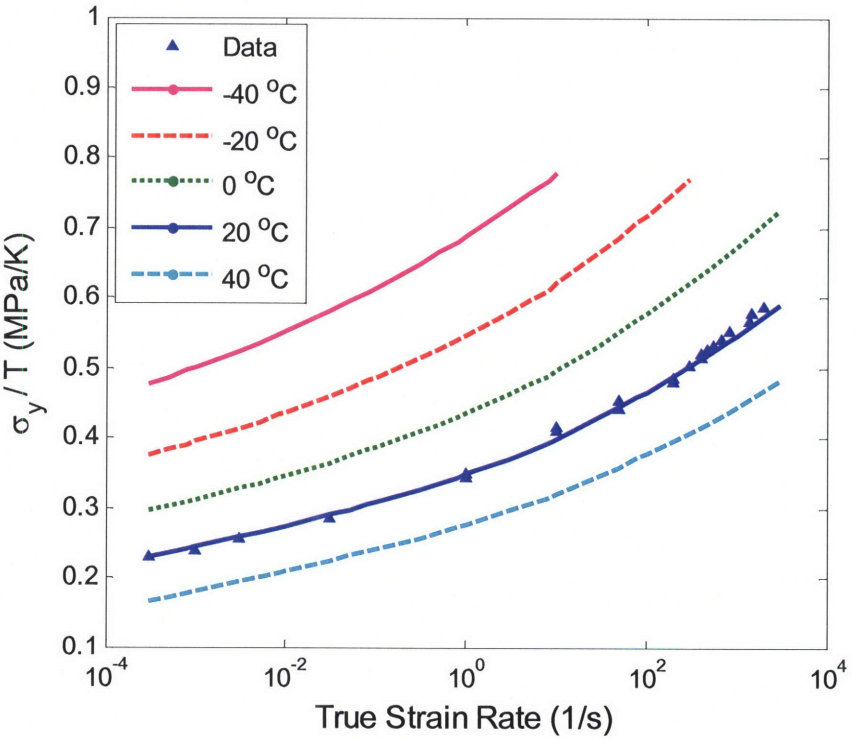

Figure 6-5. Model predictions of normalized yield stress of PVC as a function of strain rate at various temperatures.

Figure 6-6 and Figure 6-7 show the total model predictions as well as the isolated β-contributions plotted together with the compression yield data for the PVC/mPOSS and the PVC/DOP compounds. Table 6-1 includes the model parameters of both the α- and β-processes calculated from the experimental data. The α-process activation energy (ΔG_α) is ~4 times that of the β-process (ΔG_β), which is consistent with the values obtained from the DMA data. The model is seen to capture the transition in rate sensitivity of the yield stress and the increase in rate sensitivity is attributed to the β-component. In the PVC/mPOSS blends (Figure 6-6), the model finds the β-process to require stress-assisted activation at a slightly higher strain rate with increasing POSS content. Such prediction is consistent with the DMA data, in which the β-transition temperature was found to decrease slightly when the methacryl-POSS is added. In the PVC/mPOSS blends, the β-contribution results in the change in rate sensitivity of yield at high strain rates giving as much as a 40 MPa increase in yield stress over that of the α-contribution alone.

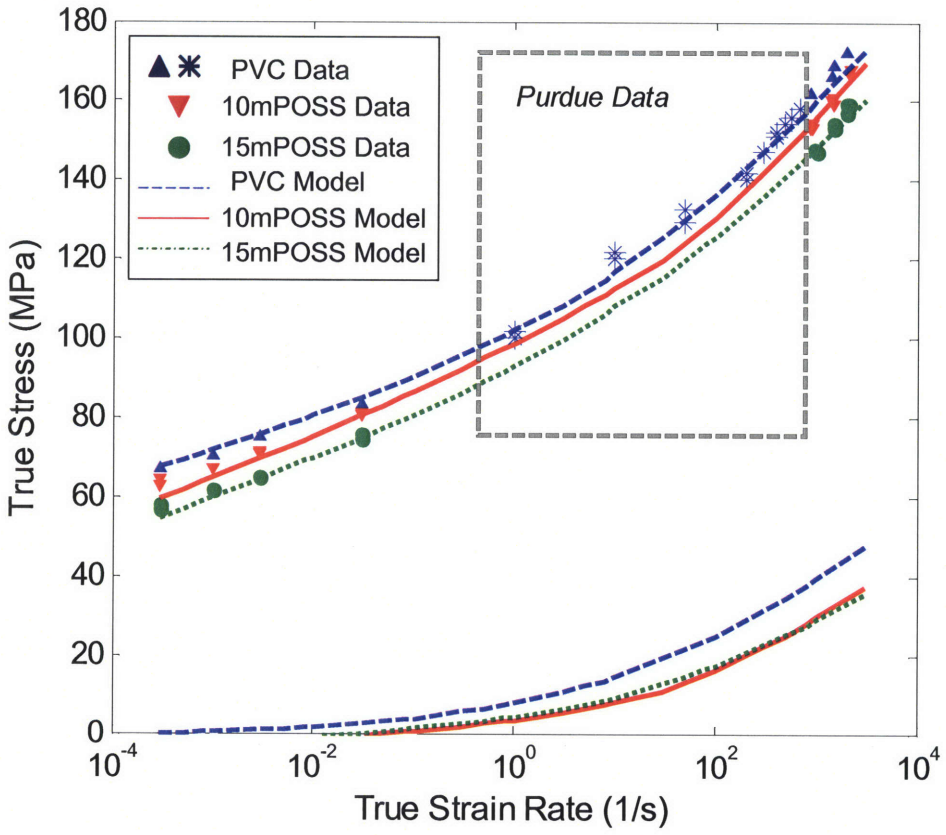

Figure 6-6. Yield stress as a function of strain rate for PVC/mPOSS blends: model prediction vs. experimental data.

In the 15 and 20 wt% DOP/PVC compounds (Figure 6-7), the β-contribution is fully restricted below the glass transition and thus does not manifest itself as a distinct additional contribution at specific temperatures or strain rates. Therefore, yield is modeled as a single lumped activated process. The model shows that the rate sensitivity of yield is fully captured using a single activation approach for the PVC/DOP compounds. In particular, for the 20 wt% DOP blend, the rate sensitivity of yield, as one moves from the low to the high strain rate regime, is because the material transitions from being in a rubbery regime of response at the low rate to a glassy regime of response at the high rate. Hence, the transition in rate sensitivity of yield is fully predictable as a single lumped stress-activated event for PVC/DOP compounds, in stark contrast to the PVC and PVC/mPOSS compounds.

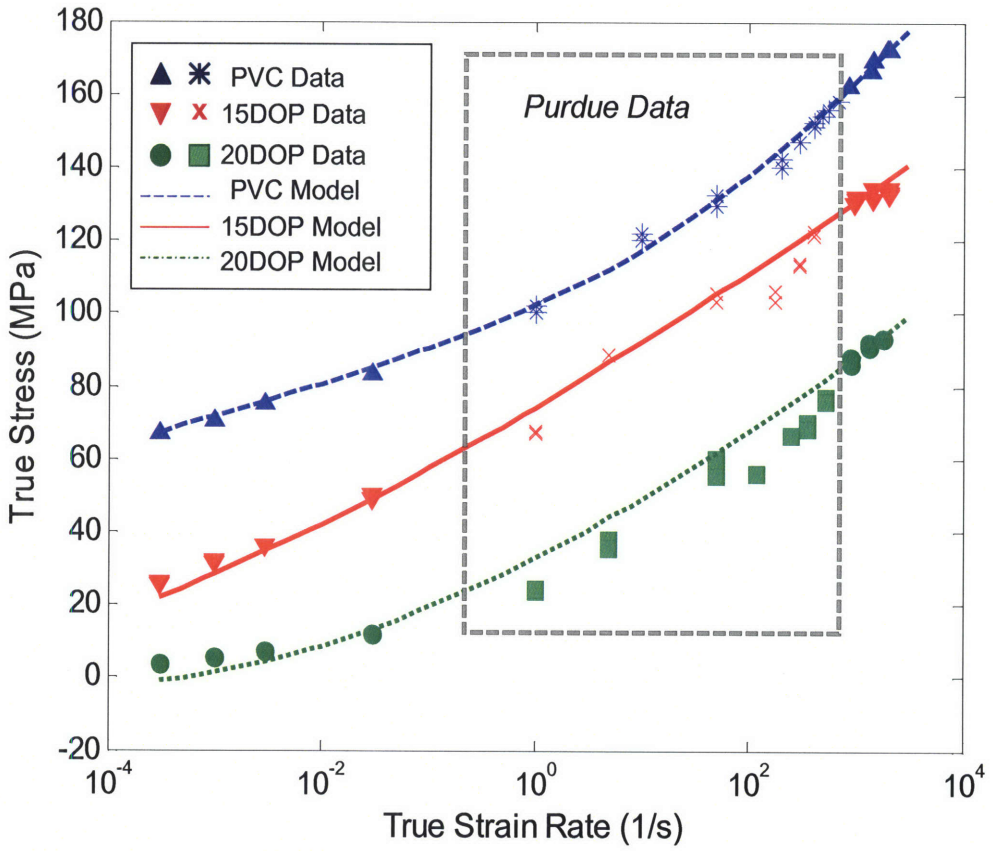

Figure 6-7. Yield stress as a function of strain rate for PVC/DOP blends: model prediction vs. experimental data.

Table 6-1. Model Parameters for the PVC/mPOSS and the PVC/DOP

	ΔG_α [J]	ΔG_β [J]	$\dot{\gamma}^p_{o,\alpha}$ [s^{-1}]	$\dot{\gamma}^p_{o,\beta}$ [s^{-1}]
PVC	$3.10x10^{-19}$	$9.19x10^{-20}$	$9.97x10^{18}$	$8.21x10^{6}$
10mPOSS	$2.62x10^{-19}$	$7.06x10^{-20}$	$2.33x10^{15}$	$3.85x10^{5}$
15mPOSS	$2.39x10^{-19}$	$6.88x10^{-20}$	$5.09x10^{13}$	$1.07x10^{5}$
15DOP	$1.37x10^{-19}$	-	$6.92x10^{8}$	-
20DOP	$1.11x10^{-19}$	-	$9.27x10^{9}$	-
40DOP[7]	$1.07x10^{-20}$	-	$4.45x10^{3}$	-

6.2.3. True Stress-True Strain Curves Model Prediction

In fitting the constitutive model to the stress-strain behavior of PVC compounds, Matlab files developed by Mulliken and Boyce [3,4] for PC and PMMA was modified and implemented. For PVC and PVC/mPOSS materials, two elastic-viscoplastic molecular processes, α and β, are employed. The PVC and PVC/10 wt% mPOSS model predictions are given in Figure 6-8 and Figure 6-9, respectively. At the low rates, where only the α-component requires stress-assisted activation and the deformation is isothermal, the model predictions agree with the experimental curves. The model predicts the dramatic increase in stress associated with high-rate deformation, by accounting for the deformation resistance associated with restricted β-motions. Without this consideration, in the case of PVC, the model would under-predict the yield stress at 1400/s by almost 50 MPa. The inset of Figure 6-8 shows the model predicted temperature changes in PVC during deformation at high rates. At 1400/s, the predicted temperature increases approximately 15 °C at 0.3 strain. Without considering the rise in temperature and updating the material properties in the model, the flow stress at high rate would be over-predicted, as shown in Figure 6-10.

---

[7] Backward process is important for PVC/40 wt% DOP since the stress is low. Therefore, the full Eq. (2) was considered for fitting.

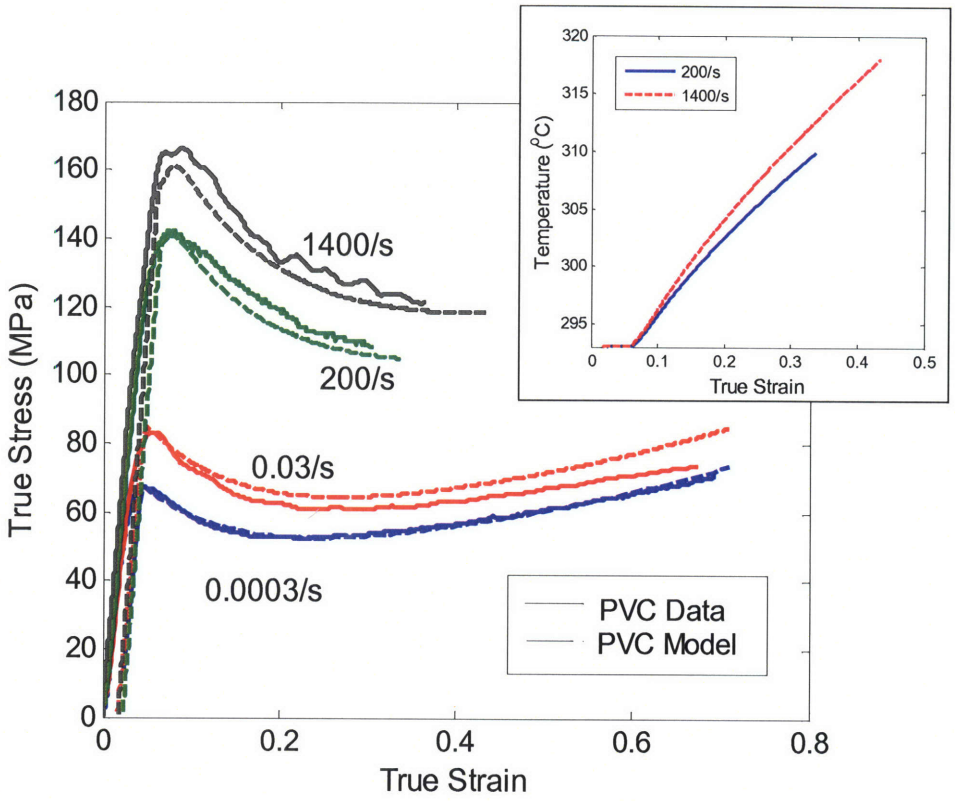

Figure 6-8. PVC true stress-true strain behavior in uniaxial compression: model (thin, dashed lines) vs. experiment (solid lines). Inset figure showing the predicted temperature rise at 200/s and 1400/s.

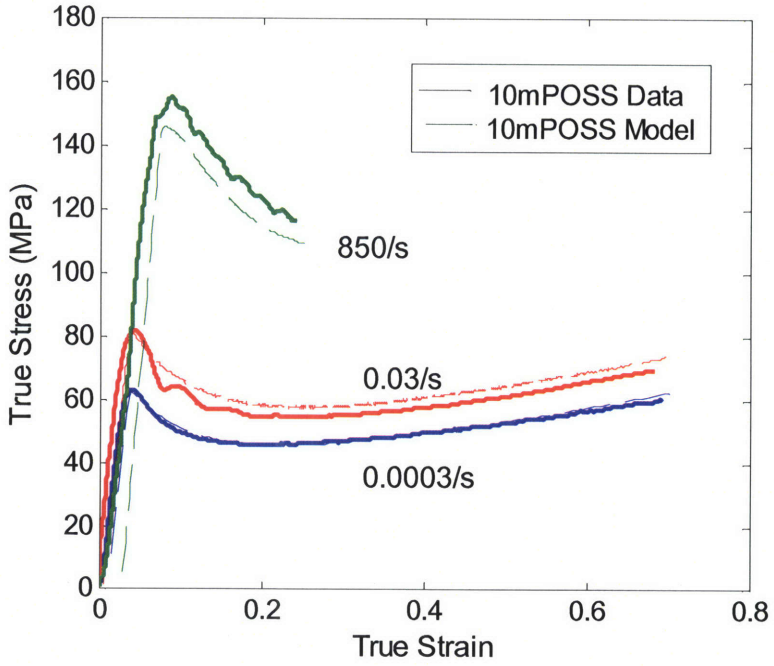

Figure 6-9. PVC/10 wt% mPOSS true stress-true strain behavior in uniaxial compression: model (thin, dashed lines) vs. experiment (solid lines).

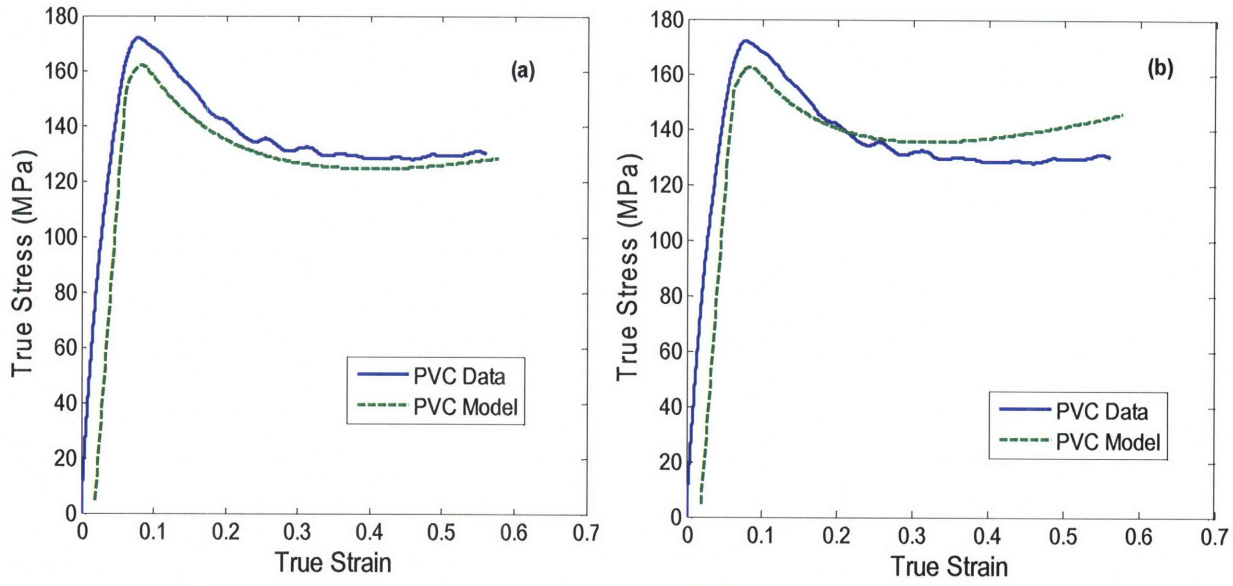

Figure 6-10. PVC data and model prediction at a strain rate of 1400/s: including adiabatic heating (a) and without adiabatic heating (b).

Figure 6-11 shows the model prediction and experimental results of the PVC/20 wt% DOP true stress- true strain behavior. In this case, the model accounts for only a single lumped α- process since the β-motions are fully restricted. The model is shown to also capture the rubbery-to-glassy transition of the PVC/20 wt% DOP blend stress-strain behavior over low to high strain rates. The model parameters used to capture the material behaviors of PVC, PVC/10 wt% mPOSS and PVC/20 wt% DOP are given in Table 6-2, Table 6-3, and, Table 6-4respectively.

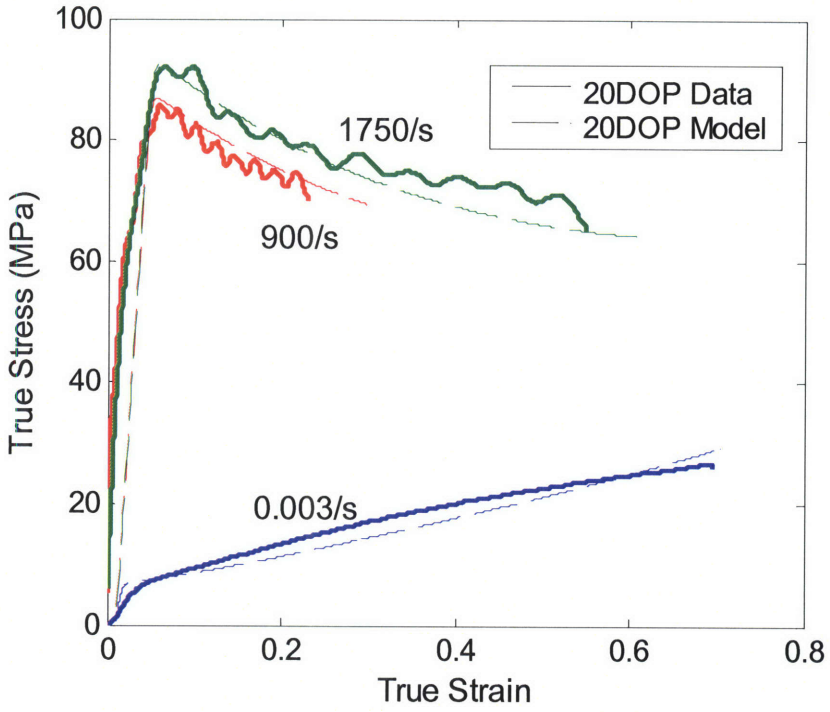

Figure 6-11. PVC/20 wt% DOP stress-strain behavior in uniaxial compression, model (thin, dashed lines) vs. experiment (thick, solid lines).

Table 6-2. Constitutive model parameters for PVC, as defined in ref. [3].

Elasticity		**Viscoplasticity**		**Strain Hardening**	
$E_\alpha(\dot{\varepsilon},\theta)$	DMA data	$\dot{\gamma}^p_{o,\alpha}$ [s^{-1}]	9.97×10^{18}	$\sqrt{N}$	2.9
$E_\beta(\dot{\varepsilon},\theta)$	DMA data	$\dot{\gamma}^p_{o,\beta}$ [s^{-1}]	8.21×10^{6}	C_R [MPa]	13.0
κ_α [MPa]	2550	ΔG_α [J]	3.10×10^{-19}	**Adiabatic Heating**	
Pressure Dependence		ΔG_β [J]	9.19×10^{-20}	C_p [J/kg/°C]	1400
α_α	0.22*	h_α [MPa]	450		
α_β	0.22*	s_{ss}/s_o	0.53		

* As determined by the pressure-dependent PVC yield data in ref. [19].

Table 6-3. Constitutive model parameters for PVC/10 wt% POSS, as defined in ref. [3].

Elasticity		Viscoplasticity		Strain Hardening	
$E_\alpha(\dot{\varepsilon},\theta)$	DMA data	$\dot{\gamma}^p_{o,\alpha}$ [s^{-1}]	1.03×10^{14}	$\sqrt{N}$	3.75
$E_\beta(\dot{\varepsilon},\theta)$	DMA data	$\dot{\gamma}^p_{o,\beta}$ [s^{-1}]	3.85×10^{5}	C_R [MPa]	11.5
κ_α [MPa]	2550	ΔG_α [J]	2.42×10^{-19}	**Adiabatic Heating**	
Pressure Dependence		ΔG_β [J]	6.06×10^{-20}	C_p [J/kg/°C]	1400
α_α	0.22*	h_α [MPa]	525		
α_β	0.22*	s_{ss}/s_o	0.53		

* As determined by the pressure-dependent PVC yield data in ref. [19].

Table 6-4. Constitutive model parameters for PVC/20 wt% DOP, as defined in ref. [3].

Elasticity		Viscoplasticity		Strain Hardening	
$E_\alpha(\dot{\varepsilon},\theta)$	DMA data	$\dot{\gamma}^p_{o,\alpha}$ [s^{-1}]	9.3×10^{9}	$\sqrt{N}$	4.0
κ_α [MPa]	2300	ΔG_α [J]	1.26×10^{-19}	C_R [MPa]	10.5
Pressure Dependence		h_α [MPa]	200	**Adiabatic Heating**	
α	0.22*	s_{ss}/s_o	0.57	C_p [J/kg/°C]	1400

* As determined by the pressure-dependent PVC yield data in ref. [19].

6.2.4. Scaling of Constitutive Model Parameters

PVC/mPOSS. Model parameters ΔG_i and $\dot{\gamma}^p_{o,i}$ (i=α, β) of PVC, PVC/10 wt% mPOSS and PVC/15 wt% mPOSS (see Table 6-1. Model Parameters for the PVC/mPOSS and the PVC/DOP) were plotted as a function of POSS content, as shown in Figure 6-12. The addition of POSS lowers the activation energy (ΔG_i) and the preexponential factor ($\dot{\gamma}^p_{o,i}$) for both α- and β-processes since POSS is a plasticizer for PVC. Model parameters of 10 and 15 wt% POSS were extrapolated to the point where no POSS is added, and the results were compared to the fitted

PVC model parameters. The extrapolated ΔG_α value at 0 wt% POSS added was seen to be identical with the fitted ΔG_α of neat PVC, while the extrapolated values of ΔG_β, $\dot{\gamma}^p_{o,\alpha}$ and $\dot{\gamma}^p_{o,\beta}$ were slightly below the fitted values of neat PVC. Overall, the scaling for model parameters holds fairly well for the PVC/mPOSS blends.

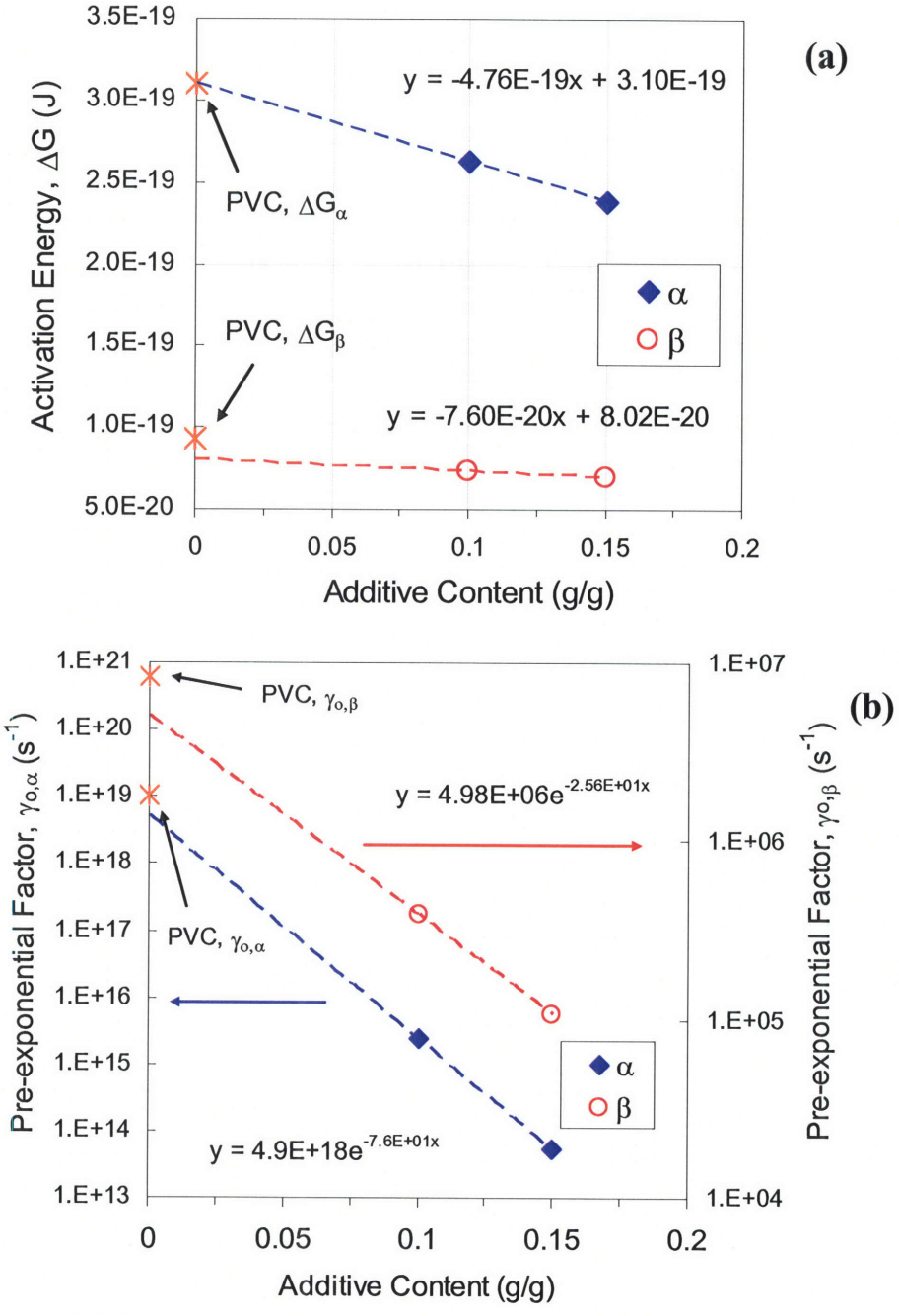

Figure 6-12. Model parameters of PVC/mPOSS as a function of POSS content: activation energy, ΔG_i (a) and preexponential factor, $\dot{\gamma}^p_{o,i}$ (b).

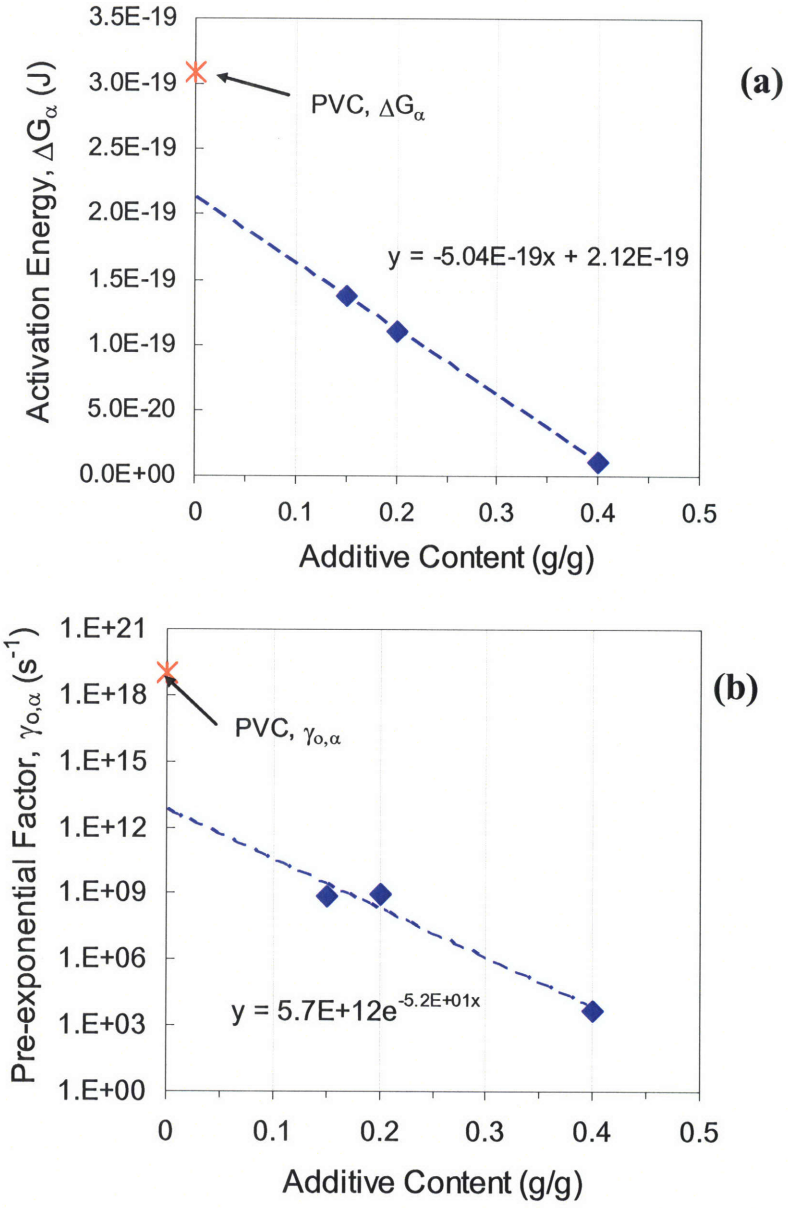

Figure 6-13. Model parameters of PVC/DOP as a function of DOP content: activation energy, ΔG_α (a) and preexponential factor, $\dot{\gamma}^p_{o,\alpha}$ (b).

PVC/DOP. Figure 6-13 shows the model parameters of PVC/DOP compounds as a function of the DOP content (g/g). Both the activation energy ΔG_α and the preexponential factor $\dot{\gamma}^p_{o,\alpha}$ decrease with increasing DOP content due to the plasticizing effect. However, the extrapolated parameter values at 0 wt% DOP content are significantly lower than the fitted values. Note that the PVC/DOP blends with DOP above 15 wt% were modeled as a single activated lumped α-

process due to the restricted β-motions, while the neat PVC was fitted with both the α- and β-processes. Hence, the activation energy (ΔG_α) and preexponential factor ($\dot{\gamma}^p_{o,\alpha}$) of PVC/high DOP compounds include an inseparable β-contribution, which would explain the under-prediction of the extrapolated values.

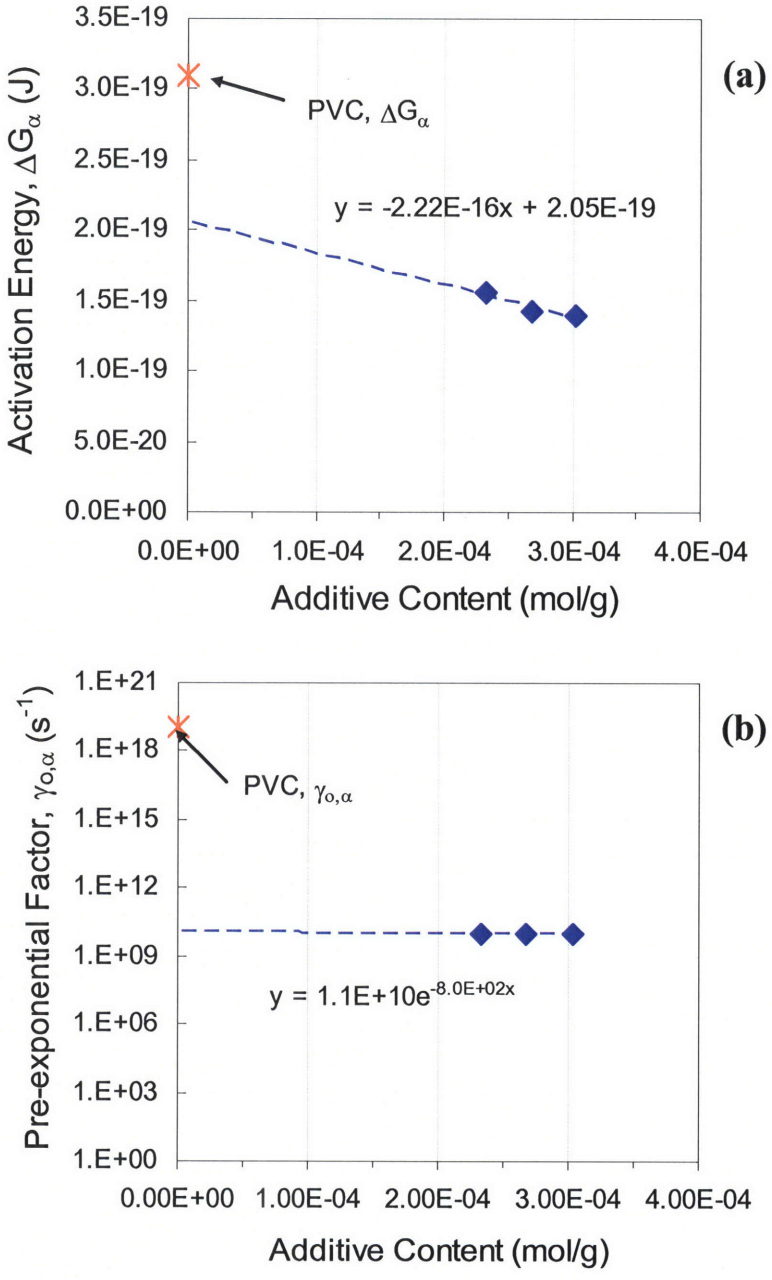

Figure 6-14. Model parameters of PVC/mPOSS/5 wt% DOP as a function of additive content (mol/g): activation energy, ΔG_α (a) and preexponential factor, $\dot{\gamma}^p_{o,\alpha}$ (b).

PVC/mPOSS/5 wt% DOP. Ternary PVC blends with 5 wt% DOP were also fitted to the constitutive model. The values of model parameters are included in Appendices Table A-1. Since the β-peaks were barely recognizable in the PVC/mPOSS/5 wt% DOP blends, the materials were modeled as one single activated α-process. Figure 6-14 shows the model parameters as a function of additive contents on the basis of molar amount plasticizer in per gram material. Again both the activation energy (ΔG_α) and preexponential factor ($\dot{\gamma}_{o,\alpha}^{p}$) decreases with increasing additive content. However, the parameter extrapolations to no plasticizer added were much lower when compared to the neat PVC fitted values, especially in the case of $\dot{\gamma}_{o,\alpha}^{p}$.

6.3. Conclusions

A constitutive model developed by Mulliken and Boyce [3,4] for finite strain deformation behavior of amorphous polymers was used to predict the rate-dependent yield and stress-strain behavior of the PVC compounds. In the case of PVC and PVC/mPOSS blends, both α and β processes were employed following a Ree-Eyring form of model. The two-process model captures the stress activation of the α-motions to govern the rate sensitivity of yield at low strain rates; at higher strain rates, the β-motions also require stress activation to enable plastic flow and hence provide the observed increase in rate sensitivity of yield at high rates. The model is also able to predict the post-yield thermal softening due to adiabatic heating at high strain rates. In contrast, the β-motions are suppressed over the entire glassy regime of the PVC/high DOP content materials and the PVC/mPOSS/5 wt% DOP compounds. Therefore, the rate-dependent yielding is captured by a single lumped activated process (α). The apparent increase in rate sensitivity of the PVC/DOP blends is then naturally captured by the model as a result of transitioning through the rubbery-leathery-glassy regimes at different strain rates.

The scaling of fitted model parameters was evaluated for three sets of materials: PVC/mPOSS, PVC/DOP, and PVC/mPOSS/5 wt% DOP. The activation energies and preexponential factors were found to decrease with increasing additive content in all cases due to the plasticizing effect. The scaling holds for the α and β activation energy and preexponential factor of PVC/mPOSS blends. When the parameters were scaled back to 0 wt% POSS added, the extrapolated values

agreed with the fitted parameter values of the neat PVC. In the case of PVC/DOP and PVC/mPOSS/5 wt% DOP compounds, the extrapolated values of parameters are significantly lower than the fitted PVC parameter values. Since PVC/DOP and PVC/mPOSS/5 wt% DOP blends were modeled as a single activated process, the inseparable β-contribution might be the cause of discrepancy between the scaled back and fitted neat PVC parameter values.

6.4. References

1. Soong, S. Y.; Cohen, R. E.; Boyce, M. C.; Mulliken, A. D., "Rate-Dependent Deformation Behavior of POSS-Filled and Plasticized Poly(vinyl chloride)", *Macromolecules* **2006**, *39*, 2900-2908.

2. Mulliken, A. D.; Soong, S. Y.; Boyce, M. C.; Cohen, R. E., "High-Rate Thermomechanical Behavior of Poly(vinyl chloride) and Plasticized Poly(vinyl chloride)", *J. Phys. IV France* **2006**, *134*, 217-223.

3. Mulliken, A. D.; Boyce, M. C., "Mechanics of the Rate-Dependent Elastic-Plastic Deformation of Glassy Polymers from Low to High Strain Rates", *Int. J. Solids Struct.* **2006**, *43*, 1331-1356.

4. Mulliken, A. D.; Boyce, M. C. *SEM X International Congress and Exposition on Experimental and Applied Mechanics* **2004**, Paper No 197.

5. Arruda, E. M.; Boyce, M. C., "Evolution of Plastic Anisotropy in Amorphous Polymers During Finite Straining", *Int. J. Plasticity* **1993**, *9*, 697-720.

6. Arruda, E. M.; Boyce, M. C.; Jayachandran, R., "Effects of Strain Rate, Temperature and Thermomechanical Coupling on the Finite Strain Deformation of Glassy Polymers", *Mech. Mater.* **1995**, *19*, 193-212.

7. Arruda, E. M.; Boyce, M. C., "A Three-Dimensional Constitutive Model of the Large Stretch Behavior of Rubber Elastic Materials", *J. Mech. Phys. Solids* **1993**, *41*, 389-412.

8. Boyce, M. C.; Arruda, E. M.; Jayachandran, R., "The Large Strain Compression, Tension, and Simple Shear of Polycarbonate", *Polym. Eng. Sci.* **1994**, *34*, 716-725.

9. Boyce, M. C.; Parks, D. M.; Argon, A. S., "Large Inelastic Deformation of Glassy Polymers. Part I: Rate Dependent Constitutive Model", *Mech. Mater.* **1988**, *7*, 15-33.

10. Mulliken, A. D., "Low to High Strain Rate Deformation of Amorphous Polymers: Experiments and Modeling", Master Thesis, Massachusetts Institute of Technology, Cambridge, MA, **2004**.

11. Mulliken, A. D., "Mechanics of Amorphous Polymers and Polymer Nanocomposites during High Rate Deformation", PhD Thesis, Massachusetts Institute of Technology, Cambridge, MA, **2006**.

12. Bergstrom, J.; Boyce, M. C., "Constitutive Modeling of the Large Strain Time-Dependent Behavior of Elastomers", *J. Mech. Phys. Solids* **1998**, *46*, 931-954.

13. Bergstrom, J.; Boyce, M. C., "Large Strain Time-Dependent Behavior of Filled Elastomers", *Mech. Mater.* **2000**, *32*, 627-644.

14. Boyce, M. C.; Socrate, S.; Llana, P., "Constitutive Model for the Finite Deformation Stress-Strain Behavior of Poly(ethylene terephthalate) above the Glass Transition", *Polymer* **2000**, *41*, 2183-2201.

15. Boyce, M. C.; Kear, K.; Socrate, S.; Shaw, K., "Deformation of Thermoplastic Vulcanizates", *J. Mech. Phys. Solids* **2001**, *49*, 1073-1098.

16. Kroner, E., "Allgemeine Kontinuumstheorie der Versetzungen und Eigenspannungen", *Archive for Rational Mech. and Analy.* **1960**, *4*, 273-334.

17. Lee, E., "Elastic-Plastic Deformation at Finite Strains", *ASME J. Appl. Mech.* **1969**, *36*,

18. Argon, A. S., "A Theory of the Low-Temperature Plastic Deformation of Glassy Polymers", *Philos. Mag.* **1973**, *28*, 839-865.

19. Pae, K. D.; Bhateja, S. K., "The Effect of Hydrostatic Pressure on the Mechanical Behavior of Polymers", *J. Macromol. Sci.-Revs. Macromol. Chem.* **1975**, *C13*, 1-75.

Chapter 7: Concluding Remarks

7.1. Summary of Accomplishment

The aim of this thesis is to investigate the rate-dependent deformation behavior of polymer nanocomposites and establish understandings of the influence of nanoparticles on the rate-sensitive mechanical properties of polymer. POSS was selected as the nanofiller for PVC due to its hybrid structure and large selection of functional groups. Methacryl-POSS was successfully incorporated into PVC through a melt-blending process using a lab-scale twin-screw extruder, and various uniform binary (PVC/mPOSS and PVC/DOP) and ternary (PVC/mPOSS/DOP) blends were produced. It was found that methacryl-POSS can be incorporated into PVC and result in homogeneous and transparent nanocomposites up to 15 wt% POSS added. Being a cage mixture, methacryl-POSS does not form crystalline structure at room temperature and was found to plasticize PVC regardless of the rigid silica cage center. The rate-dependent yield and postyield behavior of various PVC compounds were examined in uniaxial compression testing. Utilizing four different mechanical testing equipments, we were able to characterize the materials over seven decades of strain rates, ranging from 10^{-4}/s to nearly 4000/s. Transitions in the rate sensitivity of yield were observed in many blends; such behavior was explained and attributed to either the need for stress-assisted activation of β-motions at high strain rates or the rubbery-to-glassy transition in the α-regime, depending on the material.

The rate-dependent stress-strain behavior of the PVC compounds was modeled using the Mullken and Boyce constitutive model. The two-process Mulliken and Boyce model was developed for amorphous glassy polymers and was shown to capture the rate-dependent yield and postyield behavior of polycarbonate (PC) and poly(methyl methacrylate) (PMMA). We were able to expand the use of this model to fit the stress-strain behavior of our homogenous polymer nanocomposite/blend systems. Different strategies were applied in order to model various PVC compounds. In the case of glassy PVC blends, both the α- and β-processes were employed and the model was shown to be able to capture the transition in rate dependence of yield through triggering the β-process. The two-process model was modified to a single lumped process (α) model for the heavily plasticized and antiplasticized PVC blends. In both cases, the model was

shown to capture the rate-sensitivity transition in yield and the large deformation stress-strain behavior over a wide range of strain rate of all the materials of interest.

When considered as a plasticizer for PVC, methacryl-POSS offers unique attributes compared to the conventional smaller molecule plasticizers, such as DOP. Methacryl-POSS does not result in antiplasticization due to the larger molecular size and its bulky, quasi-spherical geometry. Furthermore, POSS molecule is more stable and less volatile in nature than conventional low molecular weight plasticizers. However, the miscibility limit (15 wt%) precludes the use of methacryl-POSS alone as a satisfactory plasticizer for PVC. Further exploring the idea of using POSS as a plasticizer for PVC, we discovered that the addition of a small amount of DOP increases the miscibility of methacryl-POSS in PVC substantially, and we demonstrated that the ternary compounds exhibit desirable ductile behavior in tension. We also established a linear relationship between the T_gs of various binary and ternary PVC compounds and the plasticizer content on the molar basis, which can be used to anticipate the T_g of other homogeneous binary and ternary blends. The POSS/DOP-plasticized PVC also demonstrated considerably different mechanical behavior in low rate compression and tensile experiments when compared to the DOP-plasticized PVC which has the same T_g. Such findings reveal the possibility of using POSS to engineer the material properties of plasticized PVC compounds.

The effects of thermomechanical history and strain rate on antiplasticization in slightly plasticized PVC were further investigated. We showed that inelastic straining and quenching treatment erased the antiplasticization. Both inelastic straining and quenching are known to increasing local free volume, which liberates the β-motions. As a result, the erasure of antiplasticization was observed. We found that antiplasticization is more significant at low rate and it gradually disappears with increasing strain rate. Such finding is consistent with our interpretation of the relationship between rate sensitivity transition and local β-relaxation.

7.2. Future Work

7.2.1. POSS as a Plasticizer for PVC

PVC/mPOSS/DOP ternary systems were investigated to evaluate the potential of using methacryl-POSS as a novel plasticizer. The miscibility of various PVC/mPOSS/DOP compositions was mapped on a ternary diagram, as shown in Figure 7-1. Although adding DOP increases the amount of methacryl-POSS that can be incorporated into PVC, the maximum amount of POSS that can be added into the compound is restricted by the melt blending process. At a processing temperature of 180 °C, when a large enough portion of the mixture fed to extruder is methacryl-POSS, the interspacing of the POSS molecules becomes much smaller where the reactive vinyl groups on the cage corners starts to polymerize and crosslink throughout the extruder chamber. The polymerization of POSS immediately increases the torque in the extruder and hence terminates the melt blending process. For instance, the immiscibility of the blend with a composition of PVC/mPOSS/DOP=50/30/20 is due to processing difficulty.

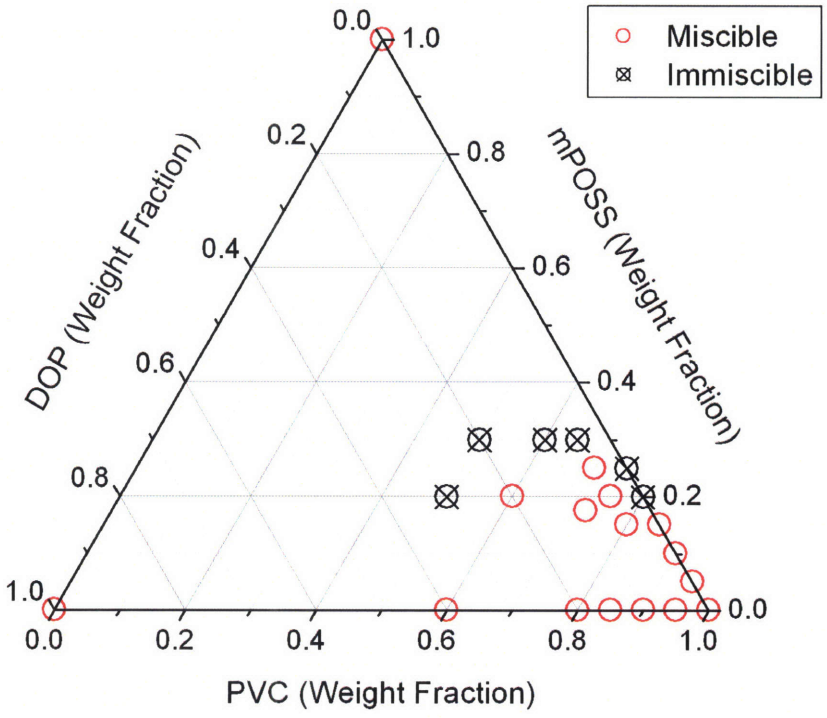

Figure 7-1. Ternary diagram of the miscibility in PVC/mPOSS/DOP system.

Figure 7-2 shows examples of immiscible blends due to the polymerization during processing and the nature of PVC/mPOSS systems. There are possible solutions which may resolve this processing issue. Alternative blending methods may be chosen to avoid the high temperature involved in melt blending process, such as solvent casting. However, melt-blending is more time efficient and inexpensive from the manufacturing point of view.

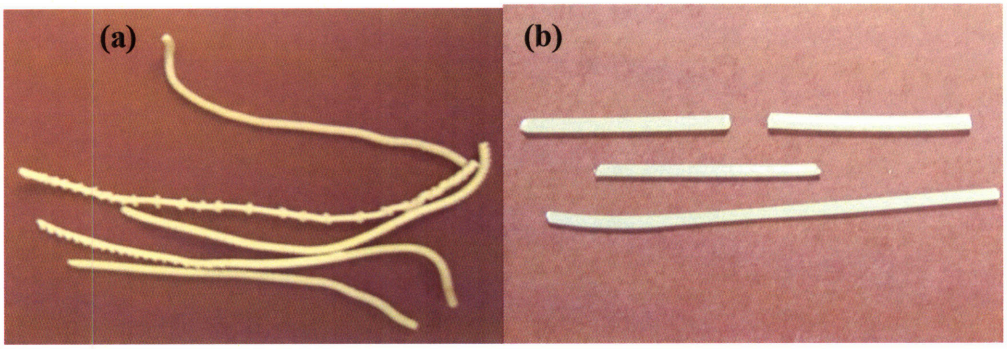

Figure 7-2. Pictures of polymer strands from extruder: PVC/mPOSS/DOP=50/30/20 (a) and PVC/mPOSS=80/20.

The stability test conducted in the vacuum oven mentioned in Chapter 4 did not show any preference in the mPOSS/DOP-plasticized PVC over the conventional DOP-plasticized PVC. The oven test only recorded the total weight loss at the end of the two-week period; no information on the progress of plasticizer weight loss was available. More sophisticated thermal analysis can be accomplished by thermogravimetric analysis (TGA). Figure 7-3 shows the preliminary TGA data, comparing the weight change of PVC, 85 wt% PVC/15 wt% DOP, and 72.5 wt% PVC/17.5 wt% mPOSS/10 wt% DOP as a function of temperature at a 4 ^{o}C/min ramping rate. Note the later two blends have the same T_g. It was seen that the mPOSS/DOP-plasticized PVC showed a more gradual decrease in weight when compared to 15 wt% DOP blend due to the existence of POSS. By changing the temperature profiles given to the samples, TGA may be able to reveal substantial differences between the thermal properties of mPOSS/DOP-plasticized and DOP-plasticized PVC.

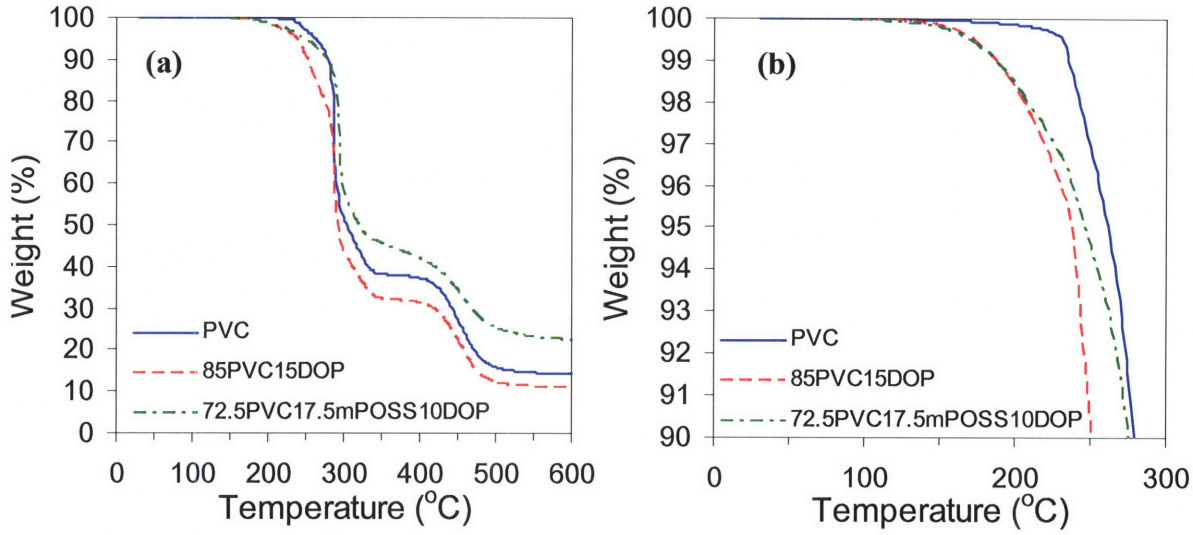

Figure 7-3. TGA results for PVC, 85 wt% PVC/15 wt% DOP, and 72.5 wt% PVC/17.5 wt% mPOSS/10 wt% DOP: full temperature range (a) and zoomed-in temperature range (b).

In the future, the idea of using POSS as a plasticizer for either PVC or other brittle polymers may be explored through designing the functional groups on cage corners. POSS is shown to be able to plasticize polymers with unique attributes when the system is miscible. Characteristics of a good POSS candidate for this application include: 1. being a cage mixture, which prevents POSS molecules crystallizing in the polymer matrix; 2. having long functional groups at the corners, which increases the polymer free volume more efficiently; 3. having functional groups that help establish good interactions between the POSS molecules and the surrounding polymer matrix, which further increases the miscibility of the system; and 4. having non-reactive functional groups, which averts any unwanted cross-linking reaction and undesirable deterioration of material property .

7.2.2. Rate-Dependent Mechanical Behavior of Polymer Nanocomposites

The transition observed in the rate dependence of yield has been related to the secondary transitions in polymer. Incorporating nanoparticles into polymer matrix may potentially influence the local molecular motion of polymer and thus affect the high rate/low temperature mechanical behavior of the material. Interestingly, POSS has been found to affect the rate-dependent mechanical properties differently in various polymer/POSS systems. In the case of

PVC/methacryl-POSS studied in this thesis, the addition of methacryl-POSS reduced both the α- and β-transition temperatures, and no significant influence on the local β-motions was identified. As a result, the rate dependence in yield behavior of methacryl-POSS filled PVC appeared to be similar to the neat PVC. Mulliken et al. [1] studied PC/trisilanophenyl-POSS nanocomposite system, and trisilanophenyl-POSS was shown to have very little effect on the α-regime while liberating the local β-motions of PC. Consequently, trisilanophenyl-POSS showed nearly no influence in the yield stress of PC at low strain rate while reducing the deformation resistance in the high rate regime significantly. Future work may focus on understanding how POSS or other nanoparticles alter the local molecular motion of a polymer. Such understanding would be very informative for designing polymer nanocomposites with applications in high rate or low temperature in the future.

7.2.3. Antiplasticization

Antiplasticization has been observed in many commonly used polymers like PVC, PC and PMMA. Alterations in the mechanical properties such as increases in modulus and yield stress and decreases in impact strength and elongation due to antiplasticization may be undesirable [2]. Other property changes such as reductions in molecular mobility and gas permeability may also be unattractive [3-5]. In Chapter 5 we demonstrated that quenching and elastic straining can erase the antiplasticization effect in yield behavior of slightly plasticized PVC. The time-scale of this erasure through thermomechanical history may be an interest for future study. Furthermore, the influence of thermomechanical history on other property alterations due to antiplasticization may worth investigating. Understanding how thermal treatments and mechanical history influence the antiplasticization effect may potentially enable us to utilize "antiplasticization" to our advantage in engineering future polymer/low molecular weight plasticizer systems.

7.3. References

1. Mulliken, A. D.; Boyce, M. C., "Polycarbonate and a Polycarbonate-POSS Nanocomposite at High Rates of Deformation", J. Eng. Mater. Technol. 2006, 128, 545-550.

2. Jackson Jr., W. J.; Caldwell, J. R., "Antiplasticization. III. Characteristics and Properties of Antiplasticizable Polymers", J. Appl. Polym. Sci. 1967, 11, 227-244.

3. Maeda, Y.; Paul, D. R., "Effect of Antiplasticization on Gas Sorption and Transport. III. Free Volume Interpretation", J. Polym. Sci.: Part B: Polym. Phys. 1987, 25, 1005-1016.

4. Maeda, Y.; Paul, D. R., "Effect of Antiplasticization on Gas Sorption and Transport. I. Polysulfone", J. Polym. Sci.: Part B: Polym. Phys. 1987, 25, 957-980.

5. Vidotti, S. E.; Chinellato, A. C.; Hu, G.-H.; Pessan, L. A., "Effects of Low Molar Mass Additives on the Molecular Mobility and Transport Properties of Polysulfone", J. Appl. Polym. Sci. 2006, 101, 825-832.

Appendices

A.1. Supplementary DMA Data

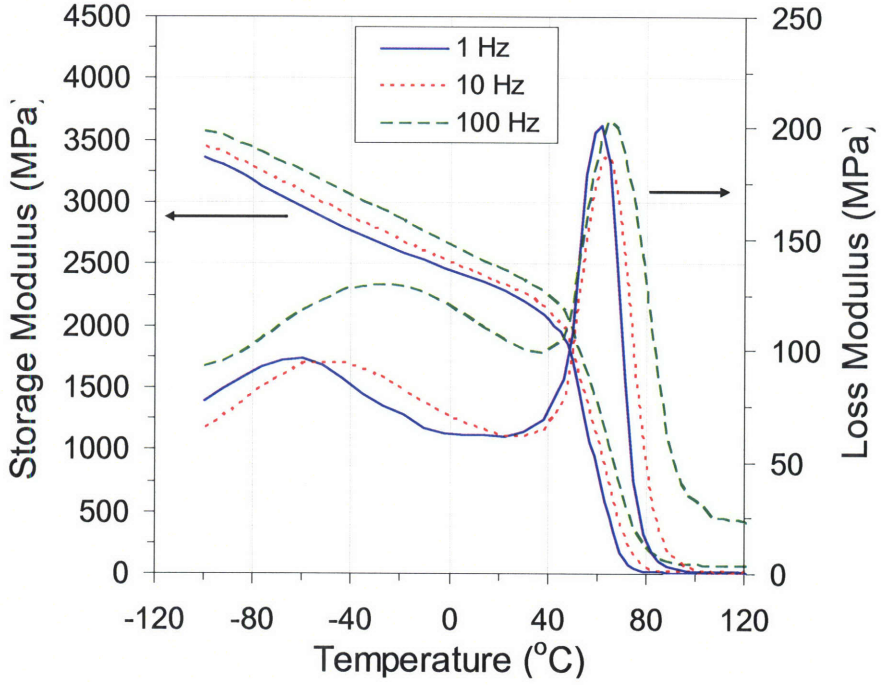

Figure A - 1. Shifting of storage and loss modulus: PVC/10 wt% mPOSS.

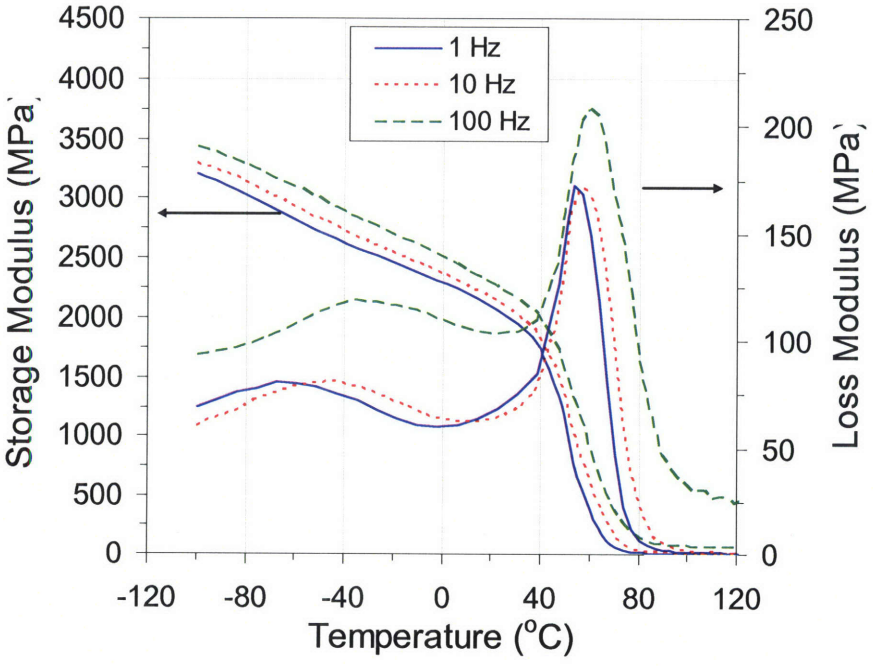

Figure A - 2. Shifting of storage and loss modulus: PVC/15 wt% mPOSS.

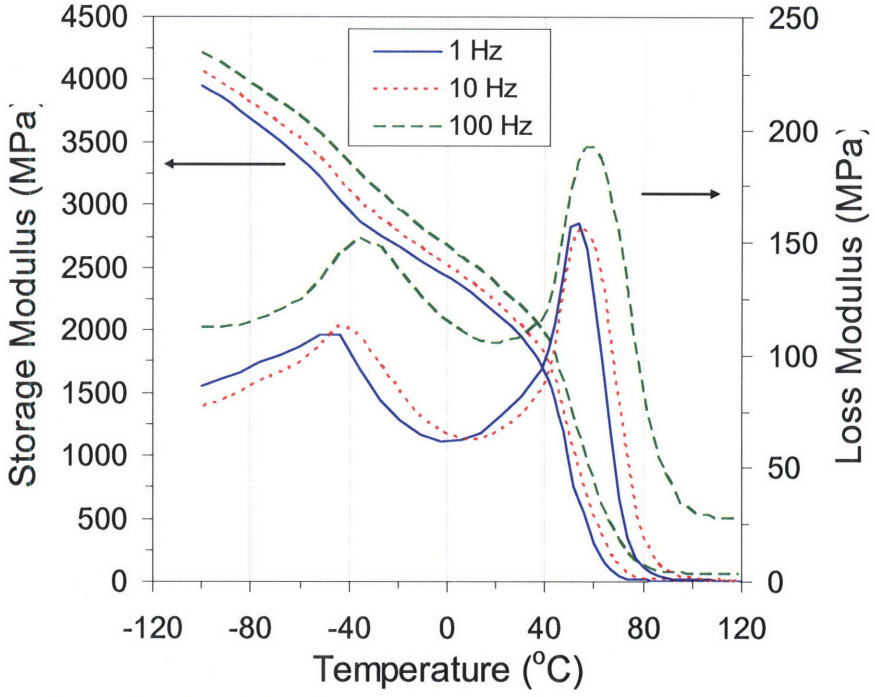

Figure A - 3. Shifting of storage and loss modulus: PVC/20 wt% mPOSS.

A.2. Supplementary Compression Testing Data

5.2.1. Strain Rate in High Rate Compression Testing

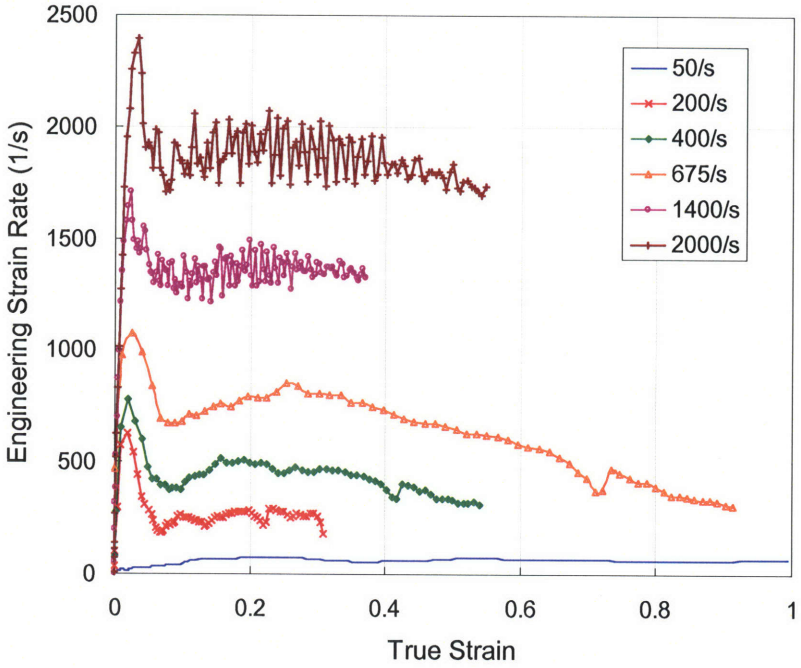

Figure A - 4. Engineering strain rates as a function of true strain for PVC in high rate compression testing.

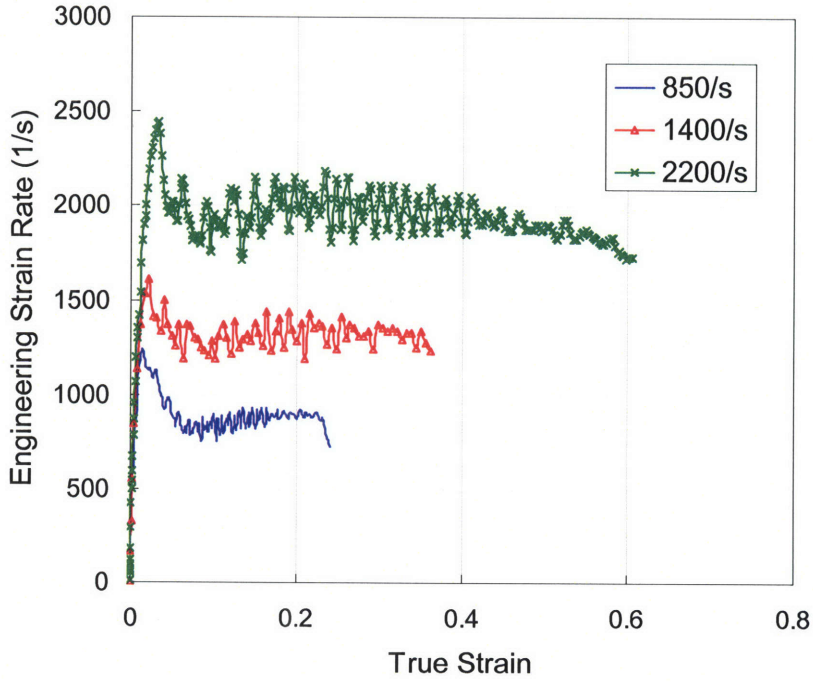

Figure A - 5. Engineering strain rate as a function of true strain for PVC/10 wt% mPOSS in high rate compression testing.

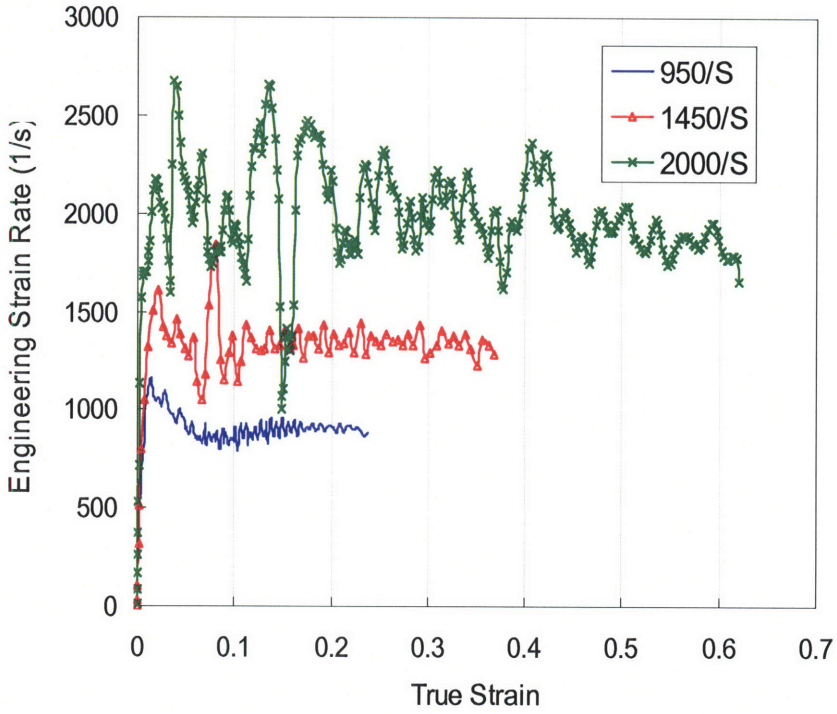

Figure A - 6. Engineering strain rate as a function true strain for PVC/15 wt% mPOSS in high rate compression testing.

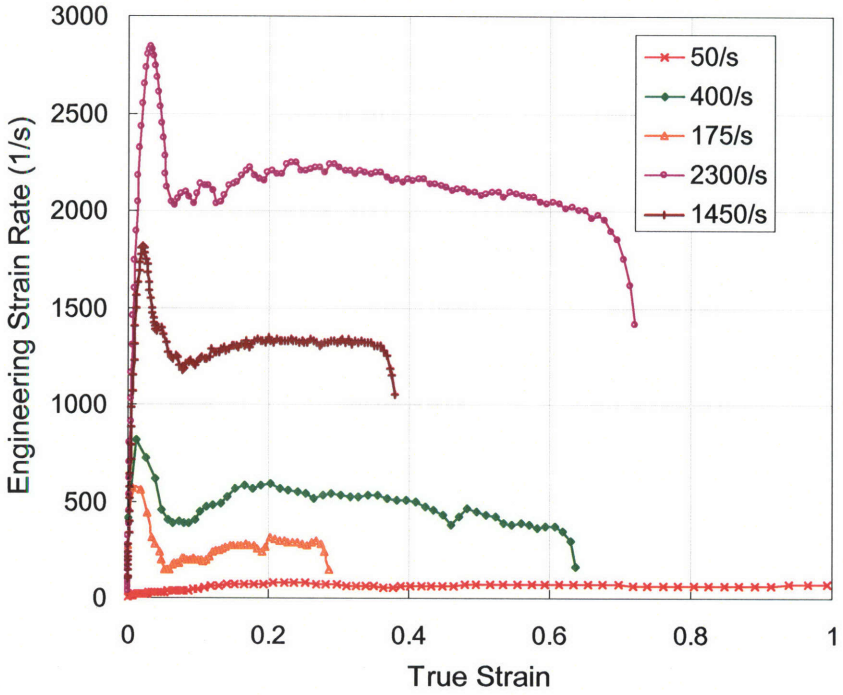

Figure A - 7. Engineering strain rate as a function of true stress for PVC/5 wt% DOP in high rate compression testing.

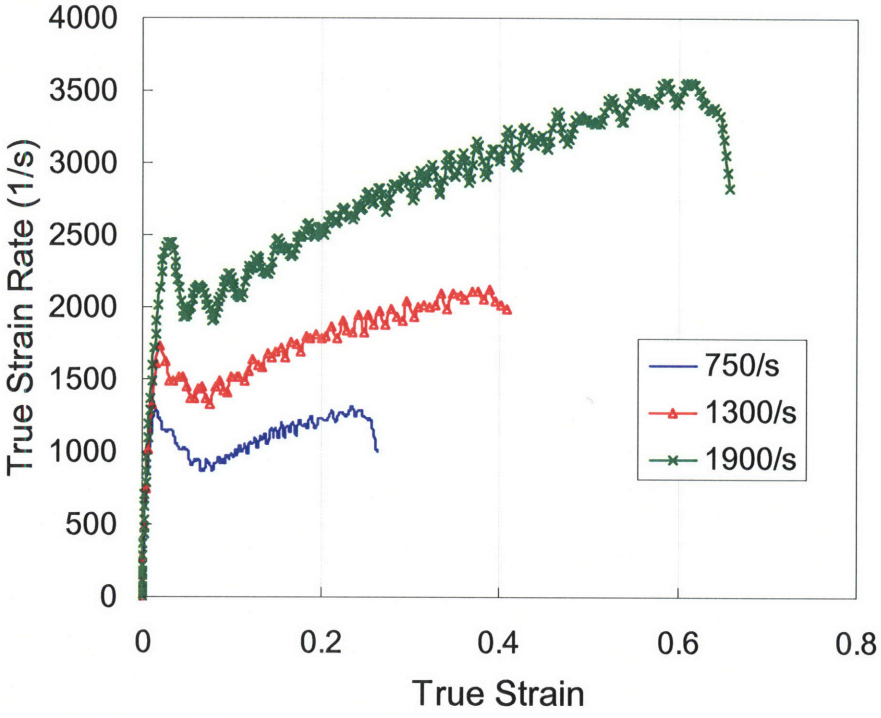

Figure A - 8. True strain rate as a function of true strain for PVC/10 wt% DOP in high rate compression testing.

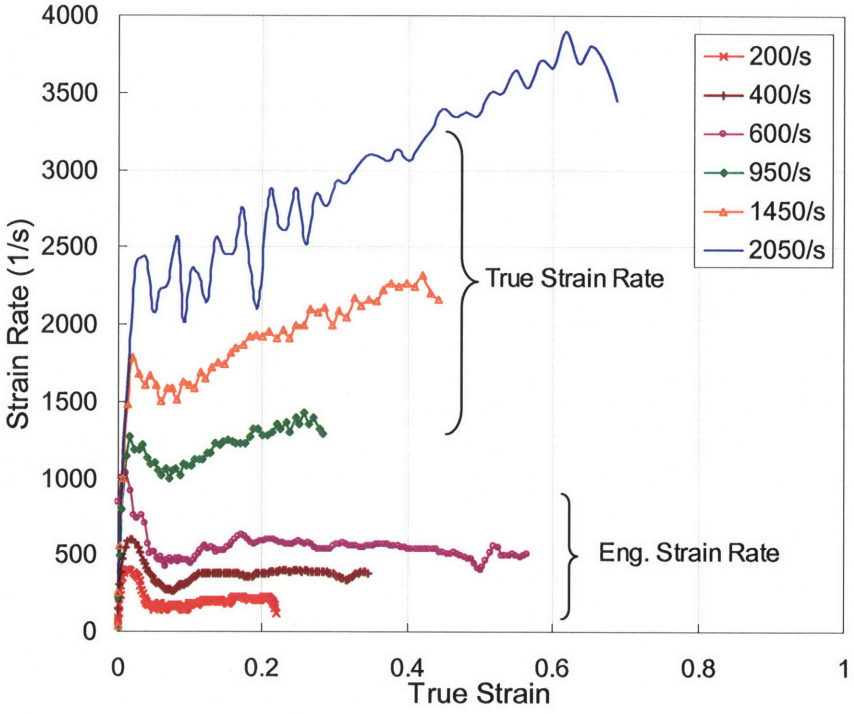

Figure A - 9. Strain rate as a function of true strain for PVC/15 wt% DOP in high rate compression testing.

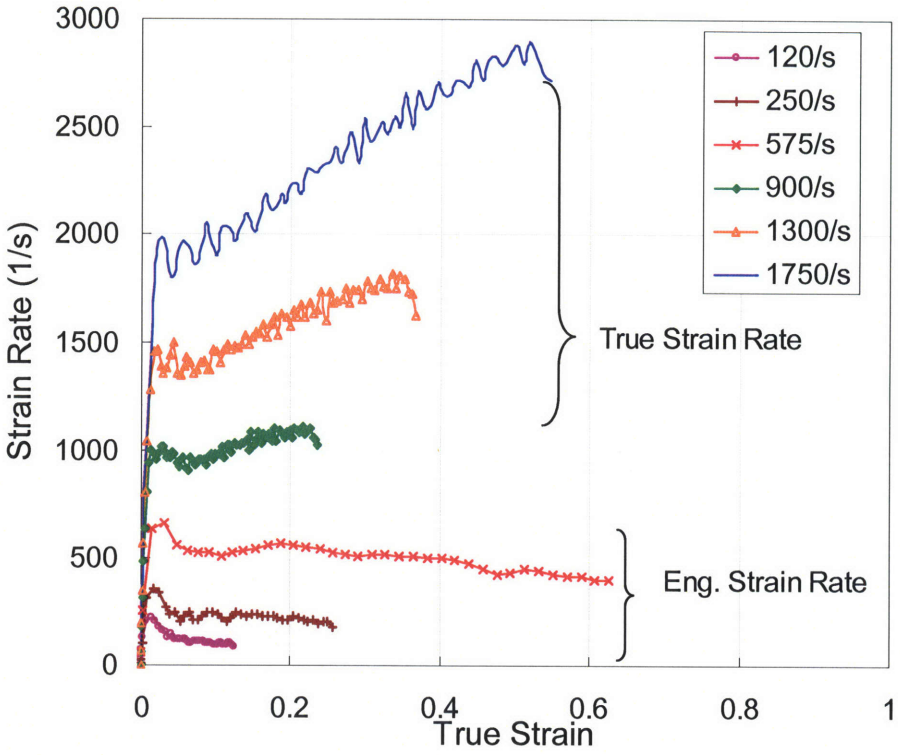

Figure A - 10. Strain rate as a function of true strain for PVC/20 wt% DOP in high rate compression testing.

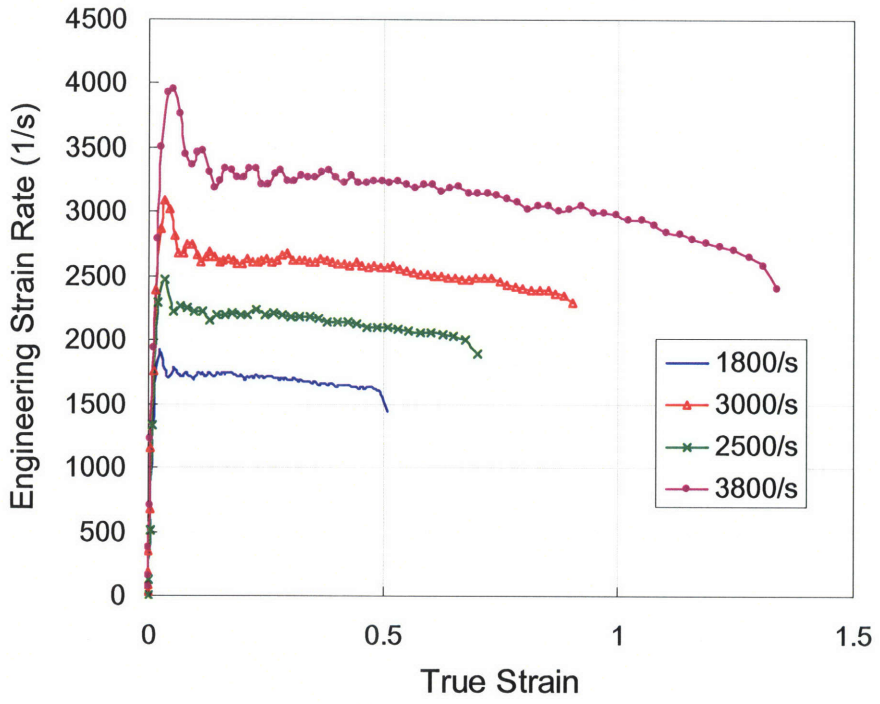

Figure A - 11. Engineering strain rate as a function of true strain for PVC/40 wt% DOP in high rate compression testing.

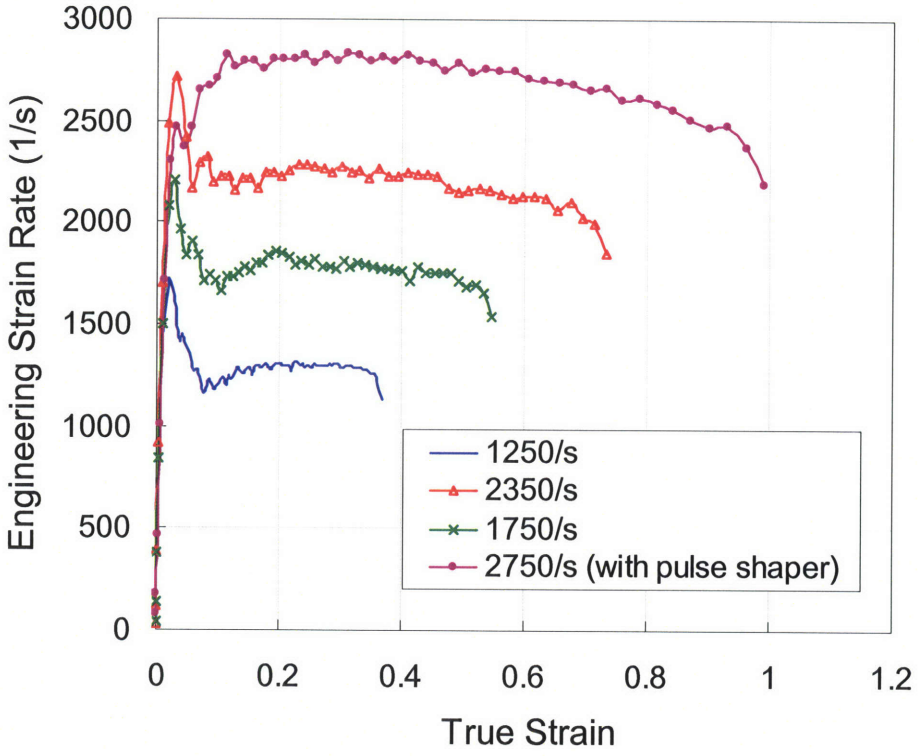

Figure A - 12. Engineering strain rate as a function of true strain for 80 wt% PVC/15 wt% mPOSS/5 wt% DOP in high rate compression testing.

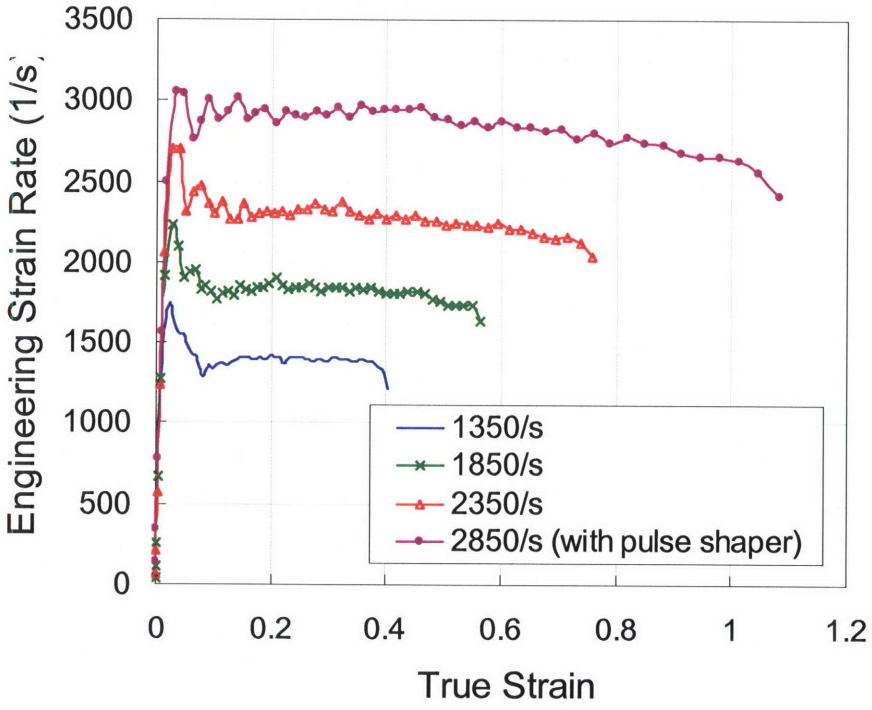

Figure A - 13. Engineering strain rate as a function of true strain for 75 wt% PVC/20 wt% mPOSS/5 wt% DOP in high rate compression testing.

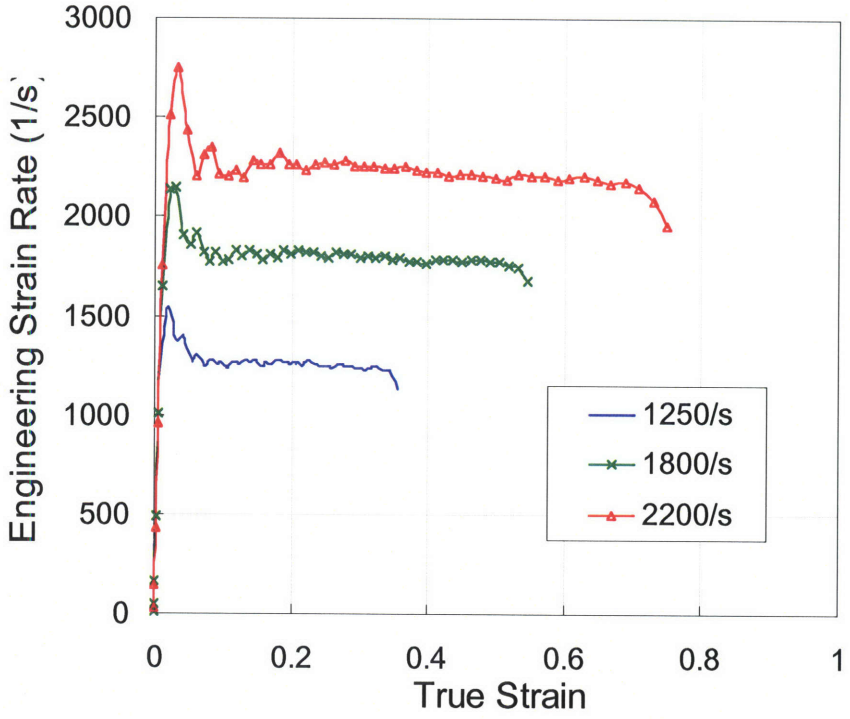

Figure A - 14. Engineering strain rate as a function of true strain for 70 wt% PVC/25 wt% mPOSS/5 wt% DOP in high rate compression testing.

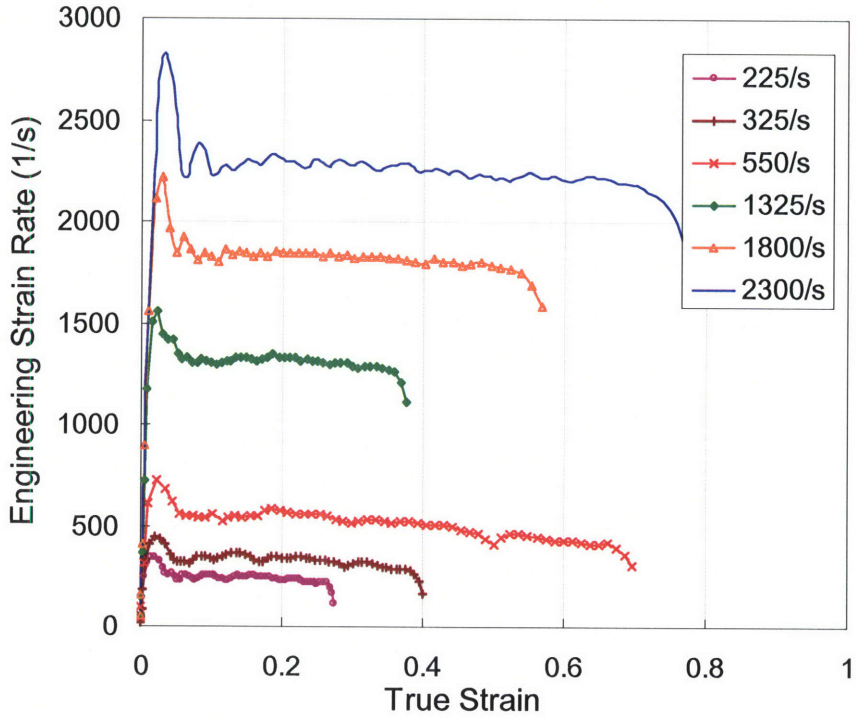

Figure A - 15. Engineering strain rate as a function of true strain for 72.5 wt% PVC/17.5 wt% mPOSS/10 wt% DOP in high rate compression testing.

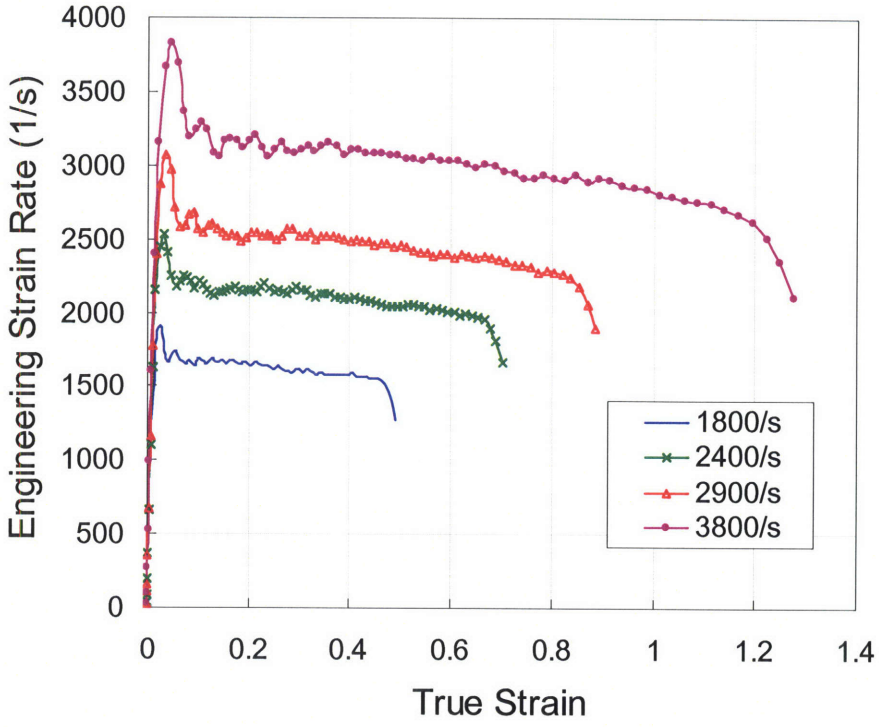

Figure A - 16. Engineering strain rate as a function of true strain for 60 wt% PVC/20 wt% mPOSS/20 wt% DOP in high rate compression testing.

5.2.2. Stress-Strain Behavior of Various PVC Compounds in Uniaxial Compression Testing

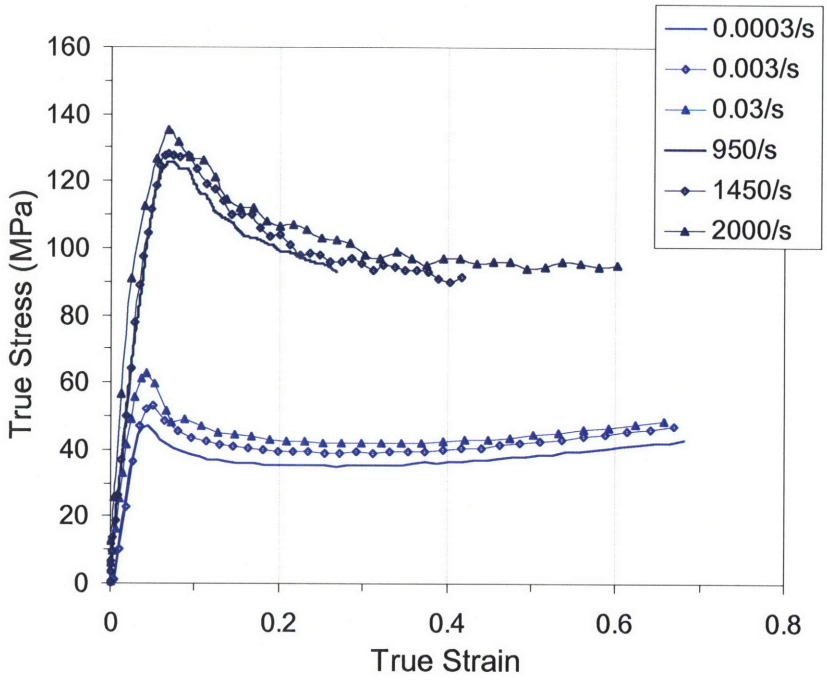

Figure A - 17. True stress-true strain curves of PVC/10 wt% mPOSS under different strain rates in uniaxial compression testing.

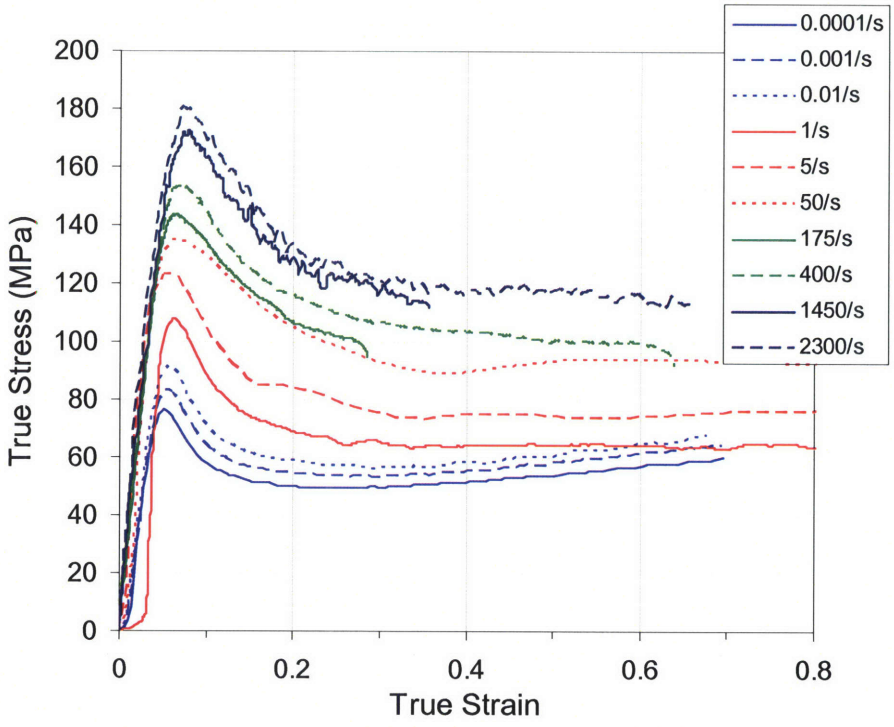

Figure A - 18. True stress-true strain curves of PVC/5 wt% DOP under different strain rates in uniaxial compression testing.

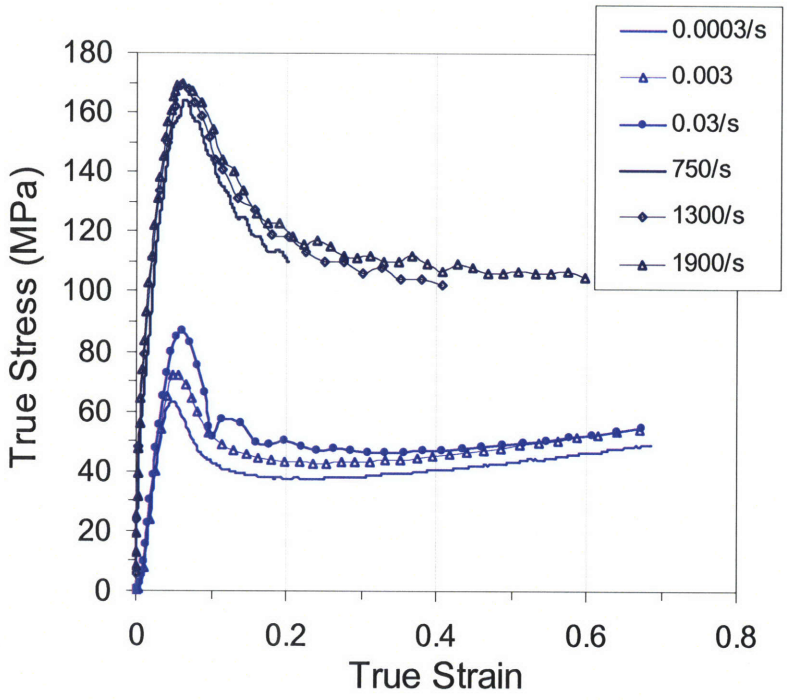

Figure A - 19. True stress-true strain curves of PVC/10 wt% DOP under different strain rates in uniaxial compression testing.

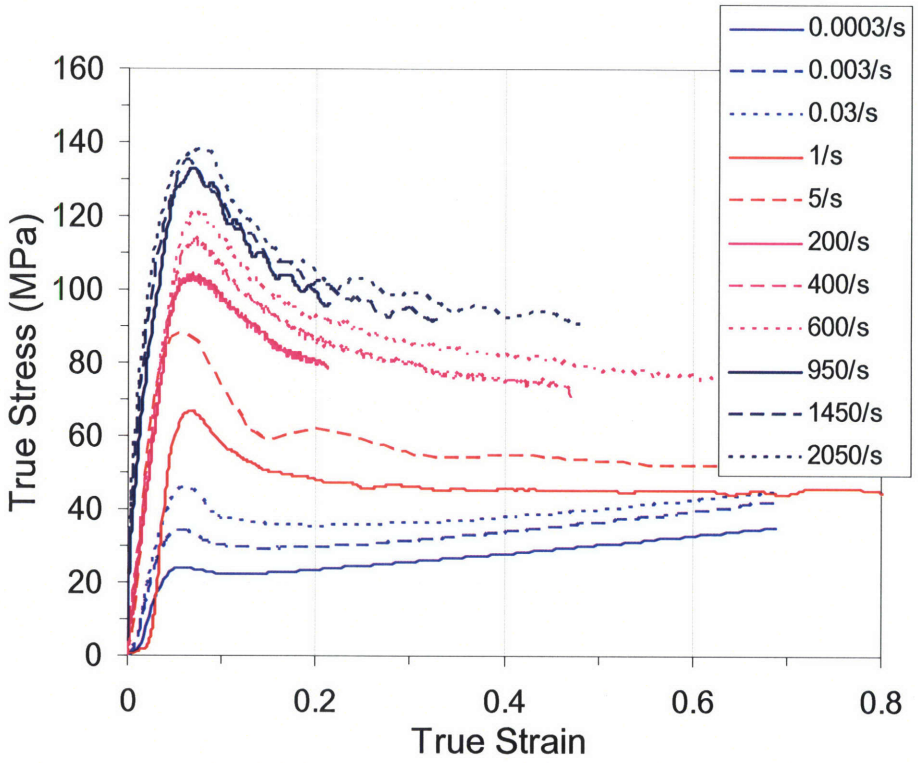

Figure A - 20. True stress-true strain curves of PVC/15 wt% DOP under different strain rates in uniaxial compression testing.

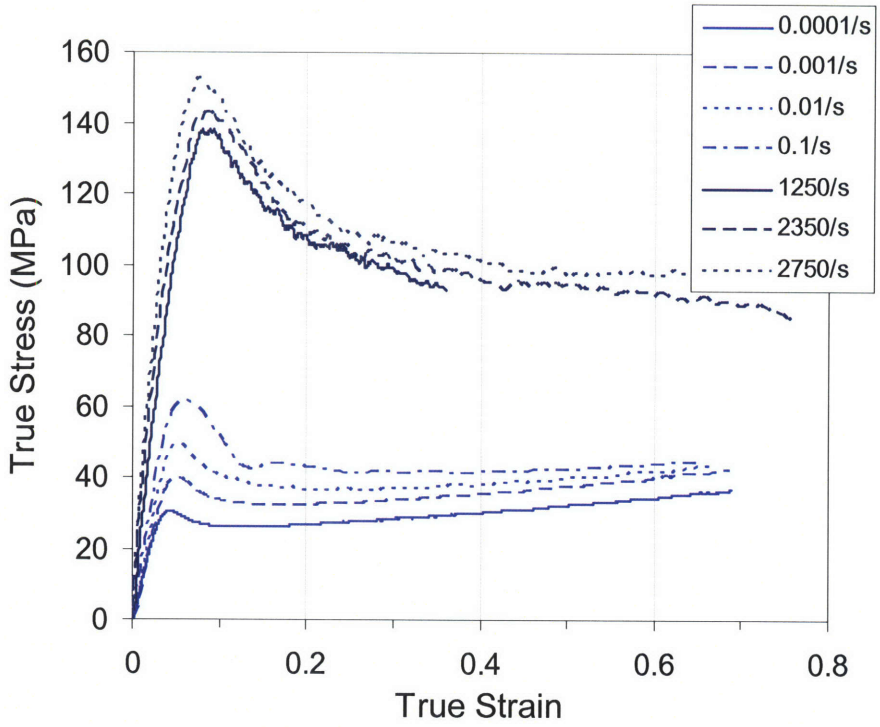

Figure A - 21. True stress-true strain curves of 80 wt% PVC/15 wt% mPOSS/5 wt% DOP under different strain rates in uniaxial compression testing.

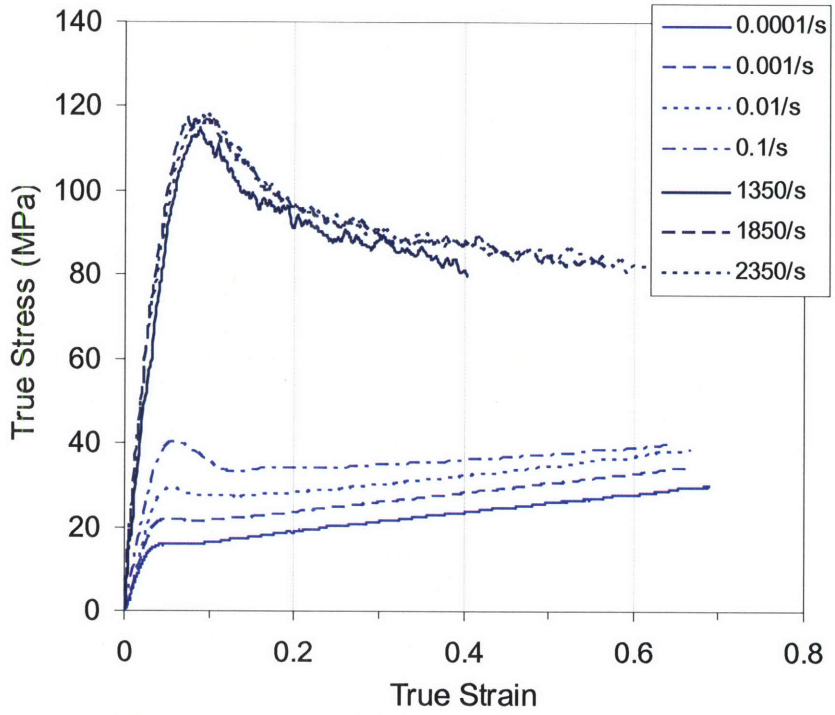

Figure A - 22. True stress-true strain curves of 75 wt% PVC/20 wt% mPOSS/5 wt% DOP under different strain rates in uniaxial compression testing.

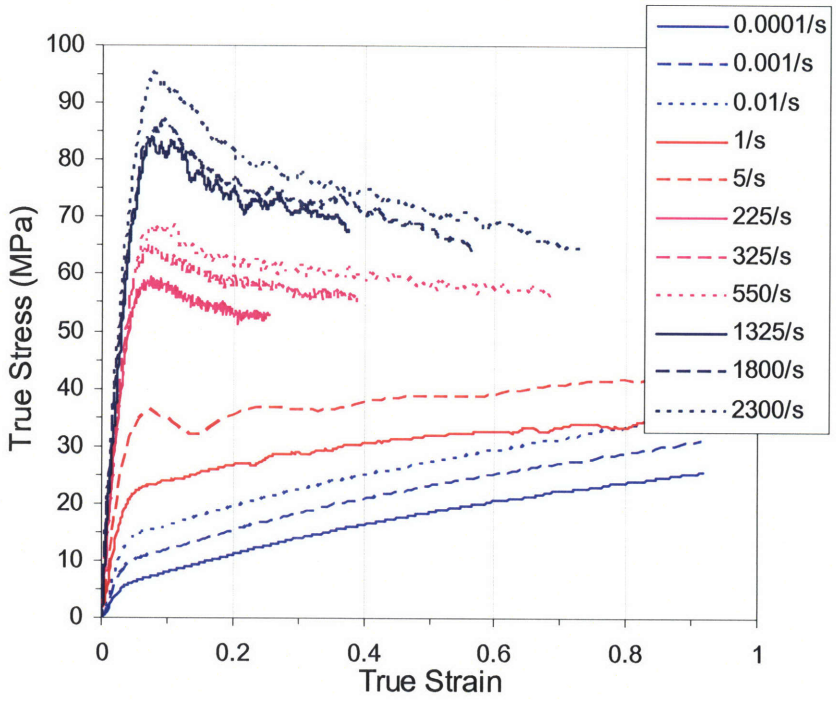

Figure A - 23. True stress-true strain curves of 72.55 wt% PVC/17.5 wt% mPOSS/10 wt% DOP under different strain rates in uniaxial compression testing.

A.3. Supplementary Modeling Results

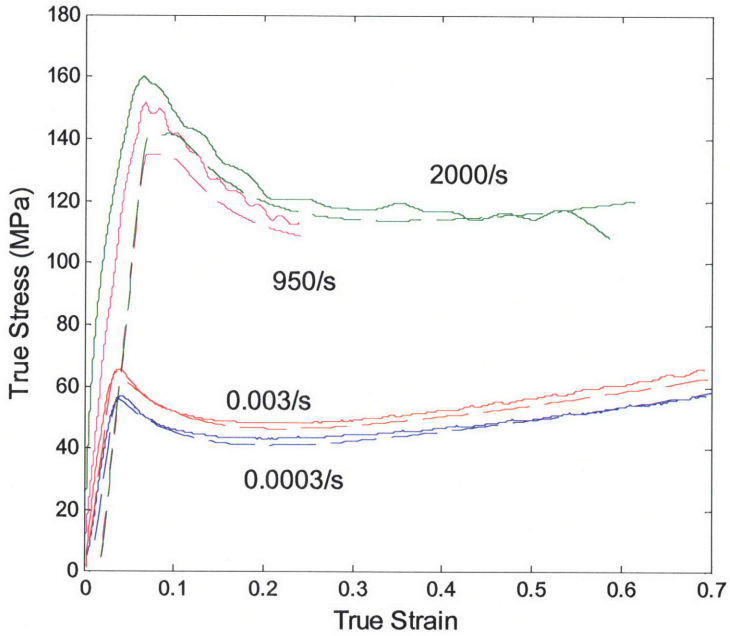

Figure A - 24. PVC/15 wt% mPOSS true stress-true strain behavior in uniaxial compression: model (thin, dashed lines) vs. experiment (solid lines).

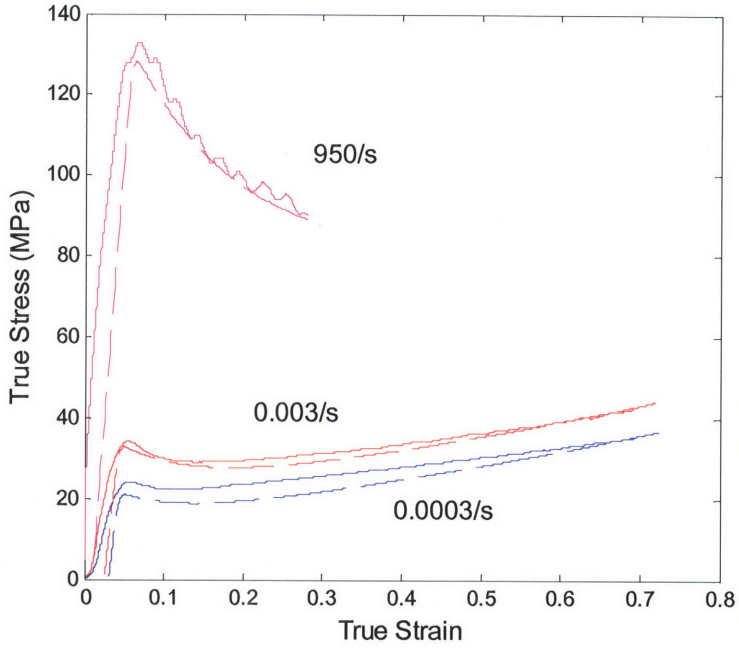

Figure A - 25. PVC/15 wt% DOP true stress-true strain behavior in uniaxial compression: model (thin, dashed lines) vs. experiment (solid lines).

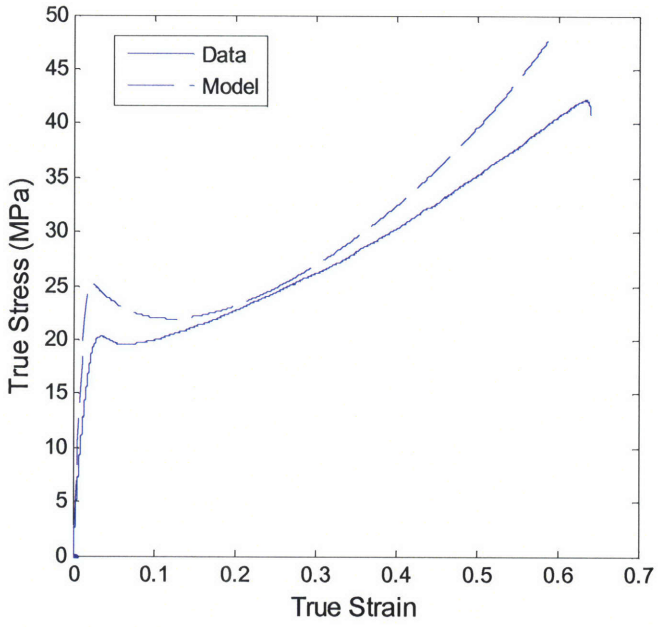

Figure A - 26. PVC/15 wt% DOP true stress-true stain curves in uniaxial tension: model (thin, dashed lines) vs. experiment (solid lines).

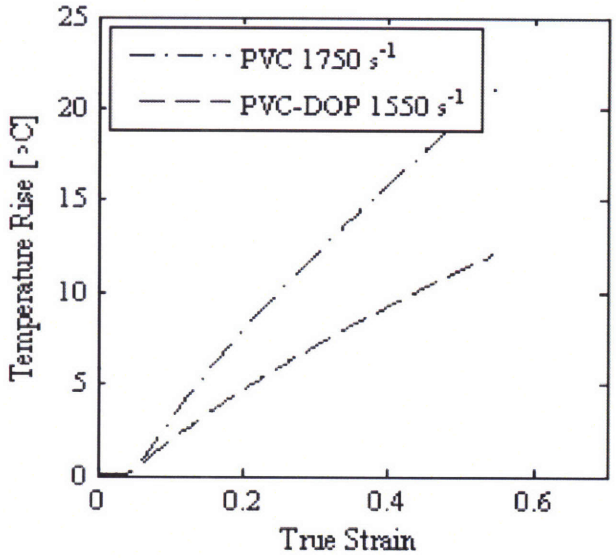

Figure A - 27. PVC and PVC/20 wt% DOP model-predicted temperature rise at high rates.

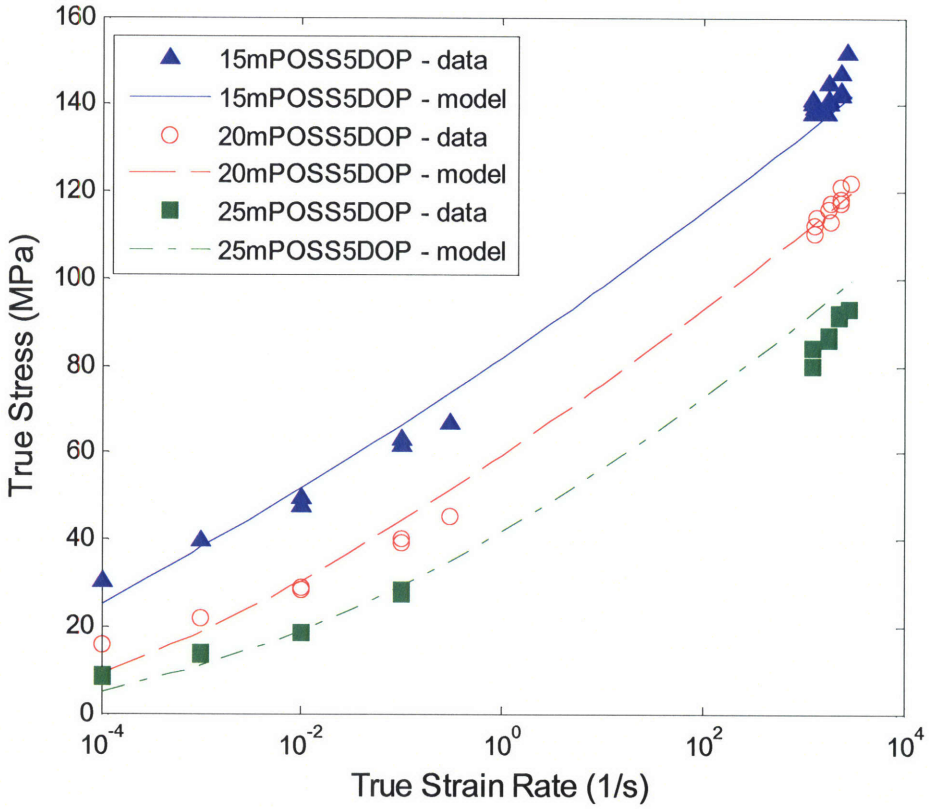

Figure A - 28. Yield stress as a function of strain rate for PVC/mPOSS/5 wt% DOP: model prediction vs. experimental data.

Table A - 1. Model parameters for PVC/mPOSS/5 wt% DOP.

	ΔG_α [J]	$\dot{\gamma}^{p}_{o,\alpha}$ [s^{-1}]
15mPOSS5DOP	$1.55x10^{-19}$	$9.07x10^{9}$
20mPOSS5DOP	$1.42x10^{-19}$	$8.85x10^{9}$
25mPOSS5DOP	$1.40x^{-19}$	$8.58x10^{9}$